Energy Research and Development Division
FINAL REPORT

POWER GENERATION USING ADVANCED THERMOCHEMICAL GASIFICATION OF BIOMASS

Prepared for: California Energy Commission
Prepared by: University of California San Diego

MARCH 2012
CEC-500-2013-107

PREPARED BY:

Primary Author(s):
Dr. Robert Cattolica
Dr. Reinhard Seiser

University of California San Diego
Department of Mechanical and
Aerospace Engineering
9500 Gilman Dr MC0411
La Jolla, CA 92093-0411

Contract Number: CEC-PIER-07-002

Prepared for:

California Energy Commission

Rizaldo Aldas, Ph.D.
Project Manager

Linda Spiegel
Office Manager
Energy Generation Research

Laurie ten Hope
Deputy Director
ENERGY RESEARCH & DEVELOPMENT DIVISION

Robert P. Oglesby
Executive Director

DISCLAIMER

This report was prepared as the result of work sponsored by the California Energy Commission. It does not necessarily represent the views of the Energy Commission, its employees or the State of California. The Energy Commission, the State of California, its employees, contractors and subcontractors make no warranty, express or implied, and assume no legal liability for the information in this report; nor does any party represent that the uses of this information will not infringe upon privately owned rights. This report has not been approved or disapproved by the California Energy Commission nor has the California Energy Commission passed upon the accuracy or adequacy of the information in this report.

ACKNOWLEDGEMENTS

This research was performed by a research team from the University of California to include faculty, staff, and students from the San Diego, Davis, and Berkeley campuses. West Biofuels, LLC (San Rafael, CA) provided equipment, materials, engineering and staff support, and the use of the Woodland Biomass Research Center in Woodland, CA to conduct this research in the amount of $1,070,000. Dr. Rizaldo Aldas provided guidance on this contract CEC-PIER-07-002 ($499,857) from the California Energy Commission to conduct this research. This report was prepared with input from the following personnel:

University of California San Diego:	Dr. Robert Cattolica
	Dr. Reinhard Seiser
University of California Davis	Dr. Bryan Jenkins
	Dr. Chang-hsien Liao
	Patrick Fitzgerald
	Kevin Copley
	Rob Williams
	Zach McCaffery
University of California Berkeley	Dr. Robert Dibble
	Dr. J-Y Chen
	Andrew Van Blarigan
West Biofuels, LLC	Dr. Mathew Summers
	Brandon Bruning

PREFACE

The California Energy Commission Energy Research and Development Division supports public interest energy research and development that will help improve the quality of life in California by bringing environmentally safe, affordable, and reliable energy services and products to the marketplace.

The Energy Research and Development Division conducts public interest research, development, and demonstration (RD&D) projects to benefit California.

The Energy Research and Development Division strives to conduct the most promising public interest energy research by partnering with RD&D entities, including individuals, businesses, utilities, and public or private research institutions.

Energy Research and Development Division funding efforts are focused on the following RD&D program areas:

- Buildings End-Use Energy Efficiency
- Energy Innovations Small Grants
- Energy-Related Environmental Research
- Energy Systems Integration
- Environmentally Preferred Advanced Generation
- Industrial/Agricultural/Water End-Use Energy Efficiency
- Renewable Energy Technologies
- Transportation

This Final Report is for the Power Generation Using Advanced Thermochemical Gasification of Biomass project (contract number CEC-PIER-07-002, grant number UCSD-18744A) conducted by University of California San Diego The information from this project contributes to Energy Research and Development Division's Energy-Related Environmental Research Program.

For more information about the Energy Research and Development Division, please visit the Energy Commission's website at www.energy.ca.gov/research/ or contact the Energy Commission at 916-327-1551.

ABSTRACT

This bioenergy demonstration project focused on renewable power production from high quality producer gas generated from forest wood waste using advanced thermochemical gasification with a dual fluidized-bed gasifier operating near atmospheric pressure with air. The five ton per day gasification facility at the Woodland Biomass Research Center was provided by West Biofuels, LLC. The University of California (San Diego, Berkeley, and Davis) conducted laboratory research and pilot-scale power generation studies with a spark ignition engine/generator (100 kilowatt hour equivalent) provided by West Biofuels to investigate research and development issues related to gasifier operation, producer gas cleanup, engine performance and exhaust emission cleanup, power generation, and producer gas combustion properties. An evaluation of the commercial development of this renewable power technology and recommendations for future development are also provided in addition to the technical and scientific results from this study.

TABLE OF CONTENTS

Acknowledgements ii

PREFACE iii

ABSTRACT iv

TABLE OF CONTENTS v

LIST OF FIGURES xi

LIST OF TABLES xviii

EXECUTIVE SUMMARY 1

Introduction 1

Project Purpose 1

Project Results 2

Benefits to California 7

Chapter 1: Introduction 9

Chapter 2: Task 2.1 Producer Gas Purification System Design and Testing 12

2.1 Task 2.1.1 Design Review of Gas Scrubbing and Purification 12

2.1.1 Gasifier Types 12

2.1.2 Tar Quantity Dependence on Gasifier Type 13

2.1.3 Gas Quality Requirements 13

2.2 Gas Cleaning Strategies 13

2.3 System Design 15

2.3.1 System Schematic 16

2.3.2 Gasifier Design 16

2.3.3 Particulate Removal 17

2.3.4 Cyclone 17

2.3.5 Barrier Filters 18

2.3.6 Tar Removal 18

2.3.7 Scrubber Design 19

2.4 Conclusions 20

Chapter 3: Task 2.1.2 Fabricate laboratory scale prototype gas purification system 22

3.1 Laboratory Scale Gasifier 22

3.2 Hot Gas Filter 24

3.3 Wet Scrubber 25

3.4 Thermal Oxidizer 27

3.5 Summary 30

Chapter 4: Task 2.1.3 Test Plan for Prototype Gas Purification System 31

4.1 Hansen Solubility Parameters 33

4.2 Test Methods 35

4.2.1 EU Method 35

4.2.2 Soxhlet Extraction 36

4.2.3 Gravimetric Tar Mass 37

4.2.4 Solid-phase Adsorption 37

4.2.5 Gas Chromatographic Analysis 38

4.3 Experimental Plan 38

Chapter 5: Task 2.1.4 Test the prototype gas purification system 40

5.1 Test Run on 6/13/2012 40

5.1.1 Feedstock 40

5.1.2 Bed Material 42

5.1.3 Tar Sampling 42

5.1.4 Results 42

5.1.5 Tar sampling 43

5.1.6 Composition of tar by GC/MS 45

5.2 Conclusions 48

Chapter 6: Task 2.1.5 Pilot gas purification system design 49

6.1 Gas Cleaning Design at West Biofuels 49

6.1.1 Initial gas cleaning system configuration 50

6.1.2 Current gas cleaning system configuration 51

6.1.3 Recommended gas cleaning system configuration 53
6.1.4 Conclusions 53
Chapter 7: Task 2.1.6 Pilot Gas Purification Monitoring Plan 55
7.1 Tar and PM 56
7.2 Gas Purification System 57
7.2.1 System Monitoring 59
7.2.2 Tar Sampling 62
7.3 Monitoring Plan Objectives 62
Chapter 8: Task 2.1.7 Monitoring Pilot Gas Purification System Performance 64
8.1 Fluidization 67
8.2 Temperature 67
8.3 Steam 68
8.4 Syngas Quality 69
8.5 Biodiesel 70
8.6 Partial Oxidation 70
8.7 Bed Material 71
8.8 Feedstock 71
8.9 Conclusions 71
Chapter 9: Task 2.2 Producer Gas SI Engine/Exhaust Gas Cleanup 73
9.1 Task 2.2.1 Simulation of gasifier syngas from a Methanol reformer 73
9.2 Gas Phase Methanol Reformer, T>1200K 74
9.3 Catalytic Methanol Reformer T~400C 74
9.4 Catalytic Methanol Reformer 3 Way Catalyst T~600C 77
Chapter 10: Task 2.2.2 Design Review for Exhaust Gas Cleanup System 78
10.1 Catalyst Selection 78
10.1.1 Stoichiometric Design 78
10.1.2 Rich/lean dual catalyst 78
10.2 Catalyst Operating Considerations 79

10.3 Catalyst Feedback Control 79
Chapter 11: Task 2.2.3 Fuel Air Ratio Controller for Engine 80
11.1 Design Criteria 80
11.2 Hardware Selection 80
11.3 Software and Controls 81
Chapter 12: Task 2.2.4 Fabricate Exhaust Clean-up System for Engine 85
12.1 Engine Exhaust Assembly 85
12.2 Installation of Sensors 87
12.3 Initial Exhaust System Test 88
Chapter 13: Task 2.2.5 Exhaust Gas Clean-up System Performance Tests 89
13.1 Propane Emissions 89
13.2 Flow Rate Effect 89
13.3 Producer Gas Results 90
Chapter 14: Task 2.3 Power Generation from Gasification of Wood Waste. 95
14.1 Task 2.3.1 Selection/Acquisition of 100 kW Generator Set 95
14.2 Engine Selection 95
14.3 Engine Setup 97
Chapter 15: Task 2.3.2 Installation of a 100 kW Generator Set on Research Reactor 99
15.1 Preparations for Engine Installation 99
15.1.1 Final Engine Installation 102
15.2 Engine Testing with Propane 103
Chapter 16: Task 2.3.3 Engine Parameter/Emissions Instrumentation 105
16.1 Control Equipment for Engine Operation 105
16.2 Additional Instrumentation on Engine 108
16.3 Variable Loadbank 110
16.4 Exhaust Emissions Sampling 110
16.5 Testing of Engine Control and Instrumentation 112
16.5.1 Two Independent Air Throttle Valves 112

16.5.2 One Air Throttle Valve for both Engine Banks 113

Chapter 17: Task 2.3.4 Exhaust Cleanup System 115

17.1 Installation of Catalyst on Slip-stream 115

17.2 Catalyst Testing on Propane 116

17.3 Catalyst Testing on Producer Gas 118

Chapter 18: Task 2.3.5 Engine/Power Performance Monitoring 120

18.1 Initial Testing on Propane 120

18.2 Producer Gas Production 121

18.3 Engine Performance on Producer Gas 123

18.3.1 First test on producer gas 123

18.3.2 Rich/lean dual catalyst 126

18.3.3 High H_2/CO ratio producer gas with three-way catalyst 127

18.3.4 Performance summary for gasifier and engine 129

Chapter 19: Task 2.4 Combustion Properties and Chemical Mechanism for Producer Gas ... 131

19.1 Task 2.4.1 Autoignition/Extinction Properties of Producer Gas 131

19.2 Experimental 131

19.2.1 Critical conditions of extinction 133

19.2.2 Critical conditions of autoignition 133

19.3 Numerical procedure 134

19.4 Results 134

19.4.1 Critical conditions of extinction 134

19.4.2 Critical conditions of autoignition 136

19.5 Conclusions 138

Chapter 20: Task 2.4.2 Chemical Mechanisms for Producer Gas 139

20.1 Numerical Computations 139

20.2 Results and Discussion 140

Chapter 21: Task 2.4.3 Computational Prediction of Laminar Burning Velocity 141

21.1 Numerical Computations 141

21.2 Results and Discussion 141
21.2.1 Influence of Hydrogen 142
21.2.2 Influence of Carbon Monoxide 145
Chapter 22: Task 2.4.4 Reduced Chemical Kinetic Mechanism for Producer Gas 149
22.1 Skeletal Chemical Kinetic Mechanism 149
22.2 Reduced Chemical Kinetic Mechanism 153
22.3 Further Improvements 156
Chapter 23: Task 2.5 Technology Transfer Activities 159
23.1 Industrial and Government Presentations 159
23.1.1 Presentations at Academic Institutions 160
23.1.2 Annual Program Review 161
23.1.3 Presentations at Professional Engineering Meetings 164
23.2 Undergraduate and Graduate Research Projects 164
Chapter 24: Task 2.6 Production Readiness Plan. 167
24.1 Production Processes 167
24.2 Production Facilities and Key Suppliers 171
24.3 Production Costs and Investment 173
24.4 Implementation Plan 175
Chapter 25: Summary and Recommendations 178
25.1 Task 2.1 Producer Gas Purification System Design and Testing 178
25.2 Task 2.2 Producer Gas SI Engine/Exhaust Gas Cleanup. 178
25.3 Task 2.3 Power Generation from the Gasification of Wood Waste. 179
25.4 Task 2.4 Combustion Properties and Chemical Mechanism for Producer Gas 179
25.5 Task 2.5 Technology Transfer Activities 179
25.6 Task 2.6 Production Readiness Plan 179
25.6.1 Technical Performance Objectives 180
25.6.2 Economic Performance Objectives: 182
25.7 Benefits to California 183

REFERENCES **186**

LIST OF FIGURES

Figure ES-1: Sensitivity of project returns to power prices and waste heat prices. 6

Figure ES-2: Sensitivity of project returns to feedstock costs with no waste heat sales. 7

Figure 1: Process Schematic of the 5 Ton-Per-Day Dual-Fluidized Bed Biomass Gasification System with Engine Generator 9

Figure 2: Schematic of the Core of the Dual-Fluidized-Bed Gasification Process 10

Figure 3: Gasification and purification system schematic 16

Figure 4: Separation efficiency of fabric filter, ESP, Venturi, wash tower, and cyclone (adapted from Hasler et al, 1999) 18

Figure 5: Conceptual schematic of scrubber system (Proll et al, 2005) 19

Figure 6: Fluidized bed gasifier schematic 23

Figure 7: Laboratory scale gasifier and purification system 23

Figure 8: Zone heaters and controllers on main fluidized bed reactor 24

Figure 9: Gasifier and control panel 24

Figure 10: Hot gas filter schematic (dimensions: inches) 25

Figure 11: Hot gas filter installed 25

Figure 12: Scrubber layout 26

Figure 13: Scrubber tanks 27

Figure 14: Scrubber tanks and the lower section of the scrubber. 27

Figure 15: Thermal Oxidizer General Layout 28

Figure 16: Thermal Oxidizer, clockwise from upper left: Strapped to shipping crate, "Tilt-up", Transport to lab, Positioned in lab 28

Figure 17: Operational Thermal Oxidizer 29

Figure 18: Gasifier system 29

Figure 19: Temperature trends during initial trial run of the gasifier and thermal oxidizer 30

Figure 20: Schematic of laboratory scale gasifier and clean-up system 32

Figure 21: Modules of the EU sampling train 36

Figure 22: Soxhlet extraction apparatus 36

Figure 23: Impinger train 37

Figure 24: Rotovap 37

Figure 25: System schematic for test run on 6/13/2012 41
Figure 26: Upper (left) and lower (right) impingers 42
Figure 27: Temperature histories of the system during test at 6/13/2012 43
Figure 28: GC/MS chromatogram of liquid sample from impinger #1. 46
Figure 29: GC/MS analysis of collected impinger liquids using EPA610 standard (concentrations on log scale). 47
Figure 30: Dual reactor allothermal gasifier schematic (Boerrigter et al., 2006) 49
Figure 31: Initial Gas Cleaning Configuration 50
Figure 32: Typical Pall ring used in random packings (Ningbo T.C.I. Co., LTD) 51
Figure 33: Current Gas Cleaning Configuration 52
Figure 34: Drop out tank and gas filters 52
Figure 35: Example for Recommended Gas Cleaning Configuration 53
Figure 36: Directional flow and inlet ports of the dual fluidized bed reactor 58
Figure 37: West Biofuels dual-fluidized bed gasifier and purification system. 59
Figure 38: Thermocouple, pressure transducer, and flow meter locations within the system. 60
Figure 39: Gas sampling locations at West Biofuels 61
Figure 40: Dual bed reactor and gas cleaning system on 4/8/2010 65
Figure 41: Pressure at bottom of gasifier reactor 67
Figure 42: Indicator of tar concentration 68
Figure 43: Tar species concentrations measured before scrubber on 9/22/2011 69
Figure 44: GC sample of producer gas after charcoal filter (major species) 69
Figure 45: Gross Heating Value 70
Figure 46: Reactor temperature in and above the bed on 3/29/2011 70
Figure 47: GC sample of producer gas after charcoal filter (minor species) 71
Figure 48: Kinetics of methanol reforming at 1200 K 74
Figure 49: Schematic of Methanol Reformer using a Catalyst Bed for copper based and 3 way catalyst. 75
Figure 50: Rich/Lean exhaust clean-up concept: A system capable of running the rich/lean system would require 3 catalyst: a TWC running rich followed by air injection and then an ammonia selective catalyst and a CO and HC oxidation catalyst 79
Figure 51: Response of the controller modeled in Simulink to a ramp input – the controller showed a good ability to adapt to such a change 82

Figure 52: Response of the controller modeled in Simulink to a step change – without lookup tables or fuel data the system takes time to respond to a large, rapid change. 83

Figure 53: The final feedback-controller design implemented into labview. 83

Figure 54: The labview models response to some sample scenarios. 84

Figure 55: Engine intake and exhaust design. 85

Figure 56: The engine before the installation of the catalyst and flapper plate. 86

Figure 57: The engine exhaust with catalyst installed. 86

Figure 58: The flapper plate can be seen in this picture in a mostly-open state. 87

Figure 59: CO and NOx levels after the three way catalyst vs. the oxygen concentration. 89

Figure 60: Emission levels exiting the three way catalyst for several different flow rates, indicated by the 'flapper position. It can be seen that the catalyst has an ideal operating flow rate. 90

Figure 61: Ammonia is produced in the first catalyst (shown in purple), and is subsequently converted back to NOx in the lean catalyst (shown in red) at a rate of over 90% 91

Figure 62: A system capable of running the rich/lean system would require 3 catalyst: a TWC running rich followed by air injection and then an ammonia selective catalyst and a CO and HC oxidation catalyst 92

Figure 63: An overview of the system operating with two catalysts in series with no air injection 93

Figure 64: NO_X and CO exhaust emission cleanup performance. 94

Figure 65: Waukesha H-2475G engine at the Woodland Biomass Research Center 96

Figure 66: Test run of engine on propane in September 2009. 97

Figure 67: Concrete pad reinforcement with rebar before pouring, October 2009. 97

Figure 68: Concrete pad with engine, October 2009 98

Figure 69: Schematic Illustration of the Pilot Plant with engine location (shown as orange box). Gas sampling lines (shown in green) transport gas samples from the engine exhaust and other locations to the measuring instruments (shown as blue boxes). 99

Figure 70: Concrete pad reinforced with steel is used to support the engine generator set. 100

Figure 71: Preparation for Concrete Area around Engine Pad 100

Figure 72: Construction of Roof above Engine-Generator-Set 101

Figure 73: Schematic Illustration of Engine Control 101

Figure 74: Pressure-relief valve vents excess gas to a safety flare if the pressure rises above atmospheric 102

Figure 75: Fuel filters in the background in the middle of the photograph. A radiator/fan assembly is installed for cooling the engine coolant (shown on the right). 103

Figure 76: Engine-generator-set installed on concrete pad with electrical enclosures protecting various electrical and electronic components. 103

Figure 77: Power Output during Testing on Propane output from Eaton power meter showing 3-phase power of 107 kW (271 V and 132 A). 104

Figure 78: Schematic of SI-engine with Control System 105

Figure 79: Woodard Model F-Series with integrated actuator 106

Figure 80: Bosch Universal Exhaust Gas Oxygen (UEGO) Sensor Unit LSU4.2 106

Figure 81: Waukesha engine exhaust system with custom flanges and straight exhaust tubes with installation of exhaust gas oxygen sensors (shown with black cable). 108

Figure 82: Waukesha engine-intake manifold with governor throttle and throttle-position sensor; the throttle above the governor throttle is a manual throttle used for low loads 109

Figure 83: Plot of engine governor position measurement with LabView during simultaneous operation of Woodard air intake control valves; when air-valves close sufficiently, the governor throttle is fully open. 109

Figure 84: Variable loadbank for testing of the engine control system; the left photograph shows the backside of the loadbank with the cooling fans. The right photograph shows the control end with breaker panel and optional manual control switches 110

Figure 85: Catalytic Converter and Gas Sampling Probes The left photograph shows the adjustable exhaust cap on the end of the main exhaust tubes to create necessary back pressure. The right photograph shows the catalyst and two gas sampling lines. 111

Figure 86: Sample Lines Piping and Instrumentation 111

Figure 87: Horiba Gas Analyzer: gas analyzer during operation on left. The right photograph shows the gas analyzer in its enclosure, the water trap, and the heated gas sampling lines. 112

Figure 88: Single Engine Bank control of air fuel ratio (Lambda) of the two 4-cylinder banks of the Waukesha engine with and without automatic control with LabView Software 113

Figure 89: New engine inlet configuration with combined intake manifold for both engine banks 114

Figure 90: Drawing showing the catalyst system: two catalysts (in purple) are mounted in series on a slip stream off one of the engine banks. 115

Figure 91: Exhaust of engine showing tube with two insulated (in white) catalysts. The adjustable flapper valve at the end of the exhaust is used to force the exhaust through the catalyst. 116

Figure 92: Emissions using Propane: CO and NOx concentration as a function of O2 concentration in the exhaust from a 120 kW engine generator operating on propane. 117

Figure 93: CO and NOx concentrations and exhaust temperatures over time with three different flow rates through the catalyst were evaluated by restricting the flapper position on the main exhaust pipe. 118

Figure 94: Emissions using Producer Gas as Fuel NOx and CO concentration as a function of O2 concentration in the exhaust from a 120 kW engine generator operating on producer gas from the gasification of wood 119

Figure 95: Schematic of SI-engine configuration during testing with two possible fuel inlets: the lower inlet is the original configuration with propane flowing through the carburetor. The upper inlet is for producer gas or propane and they mix with an accurately controlled air stream. 120

Figure 96: Air valve positions versus time; both valves meter into the same mixing chamber, so it is only necessary to oscillate one valve. 121

Figure 97: NOx and CO Emissions during testing on propane with dithering 121

Figure 98: Producer gas composition measured by gas chromatograph. The gas for fluidization was recycle gas at the top of the gasifier and the exhaust of a propane/air burner at the bottom of the gasifier. 122

Figure 99: Producer gas composition with steam operation measured by gas chromatograph. The gas for fluidization was recycle gas at the top of the gasifier and steam at the bottom of the gasifier. 122

Figure 100: Air throttle valve position versus time with engine generator operation on producer gas 123

Figure 101: Probability distribution of the relative fuel/air ratio (lambda) during engine/generator operation 124

Figure 102: Post-catalyst NOx vs. CO emissions from producer gas runs with improved results with purple plus-shaped symbols. 125

Figure 103: Post-catalyst CO and NOx vs. O2 in exhaust with ideal operating point at just rich of stoichiometric. 125

Figure 104: CAD model of the dual catalyst design for rich/lean operation with air injection in between the two catalysts. 126

Figure 105: Ammonia production in Rich/Lean Catalyst System. Ammonia is produced in the firscatalyst (shown in purple) and is subsequently converted back to NOx in the lean catalyst (shown in red) at a rate of over 90% 127

Figure 106: Design of rich/lean 3-Catalyst capable of running the rich/lean system would require 3 catalysts: a TWC running rich followed by air injection and then an ammonia selective catalyst and a CO and HC oxidation catalyst 128

Figure 107: Dual stoichiometric catalyst design with two catalysts in series with no air injection; while some NOx passes beyond the first catalyst, almost no NOx is observed after the second catalyst; Negative O2 values result from extrapolation of the lambda signal from the lean side. 128

Figure 108: Optimized emissions control with an average of less than 8 ppm NOx and CO... 129

Figure 109: Schematic of the counterflow configuration employed in the experimental and numerical studies. 132

Figure 110: The strain rate at extinction, $a_{2,e}$ as a function of the mass fraction of fuel, $Y_{F,1}$ in the fuel stream. The symbols represent experimental data and the lines are best fits to the data.... 135

Figure 111: The strain rate at extinction, $a_{2,e}$ as a function of the mass fraction of producer gas, $Y_{PG,1}$ in the fuel stream, with $Y_{CH4,1} = 0$. 135

Figure 112: The strain rate at extinction, $a_{2,e}$ as a function of the mass fraction of fuel in the fuel stream, $Y_{F,1}$ with the mole fraction of producer gas maintained at a constant value of 25%. 136

Figure 113: The strain rate at extinction, $a_{2,e}$ as a function of the mass fraction of producer gas in the fuel stream, $Y_{PG,1}$. The experimental data was obtained at constant values of ξ_{st} =0.4, and T_{st} = 1800 K. 137

Figure 114: The temperature of air at autoignition, $T_{2,I}$, as a function of the strain rate, $a_{2,I}$ for producer gas. 137

Figure 115: The temperature of air at autoignition, $T_{2,I}$, as a function of the mass fraction of producer gas in the fuel stream, $Y_{PG,1}$, at a fixed value of the strain rate. $a_2 = 250\ s^{-1}$.The symbols represent experimental data and the line is a best fit to the data. 138

Figure 116: The temperature of air at autoignition, $T_{2,I}$, as a function of the strain rate, $a_{2,I}$ for producer gas and a comparison with numerical computations employing the San Diego Mechanism. 140

Figure 117: The temperature of air at autoignition, $T_{2,I}$, as a function of the mass fraction of producer gas in the fuel stream, $Y_{PG,1}$, at a fixed value of the strain rate. $a_2 = 250\ s^{-1}$.The symbols represent experimental data and the line is a best fit to the data. 140

Figure 118: The burning velocity s_L as a function of the mass fraction of hydrogen for various values of T_c. The calculation were performed at $Y_{CO,u} = 0$, and equivalence ratio, $\varphi = 1.0$. 142

Figure 119: Structure of methane flame CH_4, O_2, CO, H_2, H, CO_2, H_2O, and temperature T, as a function of distance. The calculation were performed at $T_c = 2300$ K, $Y_{CO,u} = Y_{H2,u} = 0$, and equivalence ratio, $\varphi = 1.0$. 143

Figure 120: Net reaction rates production of CH_4, O_2, CO, H_2, H, CO_2, H_2O, and temperature T as a function of distance. The calculation were performed at $T_c = 2300$ K, $Y_{CO,u} = Y_{H2,u} = 0$, and equivalence ratio, $\varphi = 1.0$. 143

Figure 121: Structure of methane flame with hydrogen addition for CH_4, O_2, CO, H_2, H, CO_2, H_2O, and temperature, T, as a function of distance. The calculation were performed at $T_c = 2300$ K, $Y_{CO,u} = 0$, $\alpha = 0.625$ and equivalence ratio, $\varphi = 1.0$. 144

Figure 122: Net reaction rates for production of CH_4, O_2, CO, H_2, H, CO_2, H_2O, and temperature, T, as a function of distance. The calculations were performed at $T_c = 2300$ K, $Y_{CO,u} = 0$, $\alpha = 0.625$ and equivalence ratio, $\varphi = 1.0$. 144

Figure 123: Structure of methane flame with hydrogen addition for CH_4, O_2, CO, H_2, H, CO_2, H_2O, and temperature T as a function of distance. The calculation were performed at T_c = 2300 K, $Y_{CO,u}$ = 0, α = 6.25 and equivalence ratio, φ = 1.0. 145

Figure 124: Profiles of net rates of production of CH_4, O_2, CO, H_2, H, CO_2, H_2O, and temperature T as a function of distance. The calculation were performed at T_c = 2300K, $Y_{CO,u}$ = 0, α = 6.25 and equivalence ratio, φ = 1.0. 145

Figure 125: The burning velocity s_L as a function of the mass fraction of carbon monoxide for various values of T_c. The calculation were performed at $Y_{H2,u}$ = 0, and equivalence ratio, φ = 1.0. 146

Figure 126: Structure of methane flame with CO addition profiles of CH_4, O_2, CO, H_2, H, CO_2, H_2O, and temperature T as a function of distance. The calculation were performed at Tc = 2300K, $Y_{H2,u}$ = 0, β = 8.25 and equivalence ratio, φ = 1.0. 146

Figure 127: Reaction rate profiles of net rates of production of CH_4, O_2, CO, H_2, H, CO_2, H_2O, and temperature T as a function of distance. The calculation were performed at Tc = 2300K, $Y_{H2,u}$ = 0, β = 8.25 and equivalence ratio, φ = 1.0. 147

Figure 128: Structure of methane flame with CO addition profiles of CH_4, O_2, CO, H_2, H, CO_2, H_2O, and temperature T as a function of distance. The calculation were performed at Tc = 2300K, $Y_{H2,u}$ = 0, β = 82.5 and equivalence ratio, φ = 1.0. 147

Figure 129: Reaction rate profiles of CH_4, O_2, CO, H_2, H, CO_2, H_2O, and temperature T as a function of distance. The calculation were performed at T_c = 2300K, $Y_{H2,u}$ = 0, β = 8.25 and equivalence ratio, φ = 1.0. 148

Figure 130: Extinction of producer gas / air flames; the producer gas stream is diluted with nitrogen. The symbols show experimental data, the lines show the results of numerical computations. 151

Figure 131: Extinction of methane / air flames; the methane stream is diluted with nitrogen; the symbols show experimental data, the lines show the results of numerical computations. 151

Figure 132: Extinction measurements of flames of mixtures of producer gas and methane; the fuel stream contains 20vol% producer gas and varying amounts of methane and the balance is nitrogen. 152

Figure 133: Extinction characteristic of mixtures of producer gas and methane; the symbols show experimental data, the lines show the results of numerical computations. 153

Figure 134: Extinction measurements of producer gas / air flames; the producer gas stream is diluted with nitrogen. 155

Figure 135: Extinction measurements of methane / air flames; the methane stream is diluted with nitrogen. 155

Figure 136: Extinction measurements of flames of mixtures of producer gas and methane; the fuel stream contains 20vol% producer gas and varying amounts of methane with the balance nitrogen. 156

Figure 137: Extinction characteristic of mixtures of producer gas and methane; the symbols show experimental data, the lines show the results of numerical computations. 156

Figure 138: Extinction experiments using methane as fuel. The lines show comparisons to numerical computations using the San Diego Mechanism and one in which the rate of $CH_4+M \rightarrow CH_3+H+M$ was increased by a factor 1.5. 157

Figure 139: Extinction experiments using a mixture of producer gas (25vol%) and methane as fuel; the lines show comparisons to numerical computations using the San Diego Mechanism and one in which the rate of $CH_4+M \rightarrow CH_3+H+M$ was increased by a factor 1.5. 158

Figure 140: Extinction experiments using producer gas as fuel. The lines show comparisons to numerical computations using the San Diego Mechanism and one in which the rate of $CH_4+M \rightarrow CH_3+H+M$ was increased by a factor 1.5. 158

Figure 141*:* Steps in the Biomass Combined Heat and Power system using a DFB Gasifier 167

Figure 142: Schematic of (a) Gussing Renewable Energy America fast circulating fluidize bed (FCFB) gasifier and (b) West Biofuels' (DFB) dual fluidized bed gasifier. 169

Figure 143: Gasifier and engine availability history for Gussing BCHP operations 2002-2011 .. 169

Figure 144: Rendering of commercial BCHP facility supplied by West Biofuels and Gussing Renewable Energy America 171

Figure 145: Sensitivity of project returns to power prices and waste heat prices. 183

Figure 146: Sensitivity of project returns to feedstock costs with no waste heat sales 183

Figure 147: Gross annual biomass production in California and feedstock amount estimated to be available for sustainable use for renewable energy.[6] BDT = bone dry tons. 184

LIST OF TABLES

Table 1: Tar in raw gas by gasifier class (Milne, Evans et al. 1998),(Morf 2001) 13

Table 2: End use gas quality requirements 13

Table 3: Advantages and challenges of different gasifying agents, gasifier design, and gasifier operation (adapted from Wang et al, 2008) 14

Table 4: Summary of biomass gasification "success stories" (adapted from Hofbauer and Knoef, 2005) 15

Table 5: Dispersion, polar, hydrogen bonding solubility parameters, and molar volume (adapted from Hansen, 2007). 34

Table 6: Calculated correlations between tar compounds and solvents 34

Table 7: GC/MS Instrument Parameters 38

Table 8: Volitile solids, ash, ultimate analysis, HHV, volatile matter, and fixed carbon measurements on a dry basis 40

Table 9: Measured weight (g) of impingers, solvent, and collected liquids. 44

Table 10: Weights (g) of solvent and tar aliquots before and after air drying 45

Table 11: Analysis of the liquid from impingers 1, 2, 3 and 5+6 47

Table 12: End use gas quality requirements 55

Table 13: Proximate analysis of biomass materials (% dry fuel) (Jenkins et al, 1998) 56

Table 14: List of chemical compounds identified and quantified using Agilent 3000 MicroGC. 61

Table 15: Summary of gasifier runs between 6/16/2010 and 2/17/2011 65

Table 16: Summary of gasifier runs between 3/29/2011 and 11/17/2011 66

Table 17: Power needed to heat methanol up to 300 deg C at different engine speeds 76

Table 18: Power needed to heat methanol up to temperatures at engine speed = 600 RPM 76

Table 19: Producer gas composition from gasification of wood waste. 95

Table 20: Engine specifications for Waukesha H-2475G 96

Table 21: Oxygen calibration of four Bosch UEGO sensors model LSU4.2. 107

Table 22: Exhaust emissions (after catalyst) from a 120 kW engine generator operating on producer gas from the gasification of wood; 119

Table 23: First engine operation on producer gas gas on December 1, 2010; the temperatures are measured in the exhaust of the two engine banks. 123

Table 24: Gasifier biomass input and producer gas production. 130

Table 25: Summary of engine performance and emissions. 130

Table 26: Skeletal chemical kinetic mechanism derived from the San Diego Mechanism for the combustion of producer gas (Version sd20111122skel14r) 150

Table 27: Industrial and Government Presentations 159

Table 28: Invited Presentations/Seminars at Academic Institutions 160

Table 29: UC Discovery/West Biofuels/CEC Technology Review Meeting – UC San Diego, UC Davis, and UC Berkeley, Sept 18-19, 2008. 161

Table 30: UC Discovery/West Biofuels/CEC Technology Review Meeting, UC San Diego – UC Berkeley – UC Davis October 22nd-23rd, 2009 162

Table 31: UC Discovery/West Biofuels Program Review Meeting UC San Diego - UC Berkeley - UC Davis, October 28th-29th, 2010. 162

Table 32: UC/CEC Program Review Meeting Tuesday, June 7, 2011 163

Table 33: UC Discovery/WestBiofuels/CEC Program Review Meeting UC San Diego – UC Berkeley – UC Davis, October 12, 2011 164

Table 34: Undergraduate Student Training and Research 165

Table 35: Graduate Student Training and Research 166

Table 36: Producer gas properties from West Biofuels' (DFB) Dual Fluidized Bed Gasifier and from Gussing Renewable Energy's Fast Circulating Fluidized Bed (FCFB) Gasifier 170

Table 37: Tar species before and after gas cleaning system. 181

Table 38: Engine operating parameters and emissions. 182

Table 39: Electricity and heat that can be produced from California biomass feedstock.[6] BDT = bone dry tons, CHP = combined heat and power, TWh = terawatt-hour, MWe = megawatt electric. 184

Table 40: Biomass production of heat and power and the displacement of natural gas and associated carbon dioxide. 185

EXECUTIVE SUMMARY

Introduction

In California, total power production capacity is currently 67,500 megawatts (MW) with less than one percent (478 MW) produced solely from wood waste. These wood waste power production facilities are based on direct combustion with steam cycle electric power generation and use a fraction of the potential 25 million tons per year of available forest wood waste biomass. Modern wood waste power production technology uses thermochemical gasification of wood waste to generate a producer gas for subsequent direct combustion. The producer gas is primarily composed of carbon monoxide (CO), hydrogen (H_2), methane (CH_4), and carbon dioxide (CO_2). Using advanced thermochemical gasification directed towards the production of high value-added products such as transportation fuel or chemicals provides the opportunity to improve the economics of power co-generation using waste wood and processing residues.

Project Purpose

The overall goal of this project was to successfully demonstrate that power could be generated from forest wood waste using an advanced thermochemical gasification process. Research and development issues related to technological hurdles and scientific baseline knowledge in the areas of gasifier operation, producer gas combustion properties, producer gas cleanup, engine performance and emissions, emission cleanup, and engineering simulation tools were investigated. This project also addressed the PIER goal of improving the environmental and public health costs/risk of California's electricity.

The following technical tasks to accomplish the project goals and to determine the potential of advanced thermochemical conversion of biomass for power production were addressed:

- Producer gas purification system design and testing.
- Producer gas spark-ignited (SI) engine/exhaust gas cleanup.
- Power generation from the gasification of wood waste.
- Combustion properties and chemical mechanism for producer gas.
- Technology transfer activities.
- Production readiness plan.

Both technical and economic objectives were evaluated based on the performance of the advanced biomass gasification power system developed in this project.

The technical performance objectives were:

- Achieving minimum gasification efficiency of 75 percent on a low heating value (LHV) basis using an advanced thermochemical gasification process.
- Tar/contaminant gas cleaning of producer gas with a minimum efficiency of 96 percent.
- Using an internal combustion engine fueled by producer gas to achieve a minimum thermodynamic efficiency of 30 percent.
- Internal combustion engine exhaust cleanup below the Yolo County Air Quality Management District (AQMD) Stationary Source Prohibitory Rule 2.32 limits for the

emissions regulation of nitrogen oxides (NOx) and CO. The limit for NOx is 2.1 pounds per megawatt hour (MWh) and the limit for CO is 42.5 pounds per MWh.

The economic performance objectives were:

- A capital cost below $1500 per kilowatt (kW) at a production scale of 100 units.
- Operating costs below $0.06/kWh including variable feedstock cost.

Project Results

The researchers developed an advanced thermochemical gasification system for processing up to five tons per day of biomass using a dual-fluidized bed gasifier, operating near atmospheric pressure with air, generating high quality producer gas for power production at 100 kilowatt electricity (kWe).

The methodology used to accomplish the research tasks is discussed below.

For the producer gas purification system design and testing task, a design review was conducted to evaluate gas scrubbing and purification systems for the removal of tars and contaminants in the producer gas generated from biomass gasification. A laboratory system and a pilot system for the West Biofuels gasifier were constructed. The laboratory gas cleaning system was designed primarily to remove particulate matter (PM) and tar. Particles larger than 20 microns were removed by cyclonic separation. A barrier filter removed particles greater than one micron. A packed-bed wet scrubber was designed to allow operation with different liquid solvents at variable flow rates for tar removal. The scrubber contained a large reservoir for collecting condensables and for steam gasification. The laboratory system was constructed but delays in the installation and approval of a thermal oxidizer required for fire safety systems at UC Davis prevented all but preliminary testing. The pilot gas purification system for the West Biofuels gasifier at the Woodland Biomass Research Center (WBRC) was built and tested continuously over the duration of the project with additional units added to improve gas cleaning. The final configuration consisted of two packed beds with water scrubbing followed by a charcoal filter to reduce the condensable tars with drop tanks and filters provide ahead of the SI engine/generator.

The recommended gas cleaning design included a PM removal system specifically designed for the system gas flow and temperature and consisting of a cyclone followed by a ceramic candle filter module. The design also included a chilled solvent packed-bed scrubber for final drying and light tar removal. As with the initial design, it was recommended that the first packed bed scrubber use an organic solvent (e.g., biodiesel) to better enable disposal through the combustor.

The producer gas SI engine/exhaust gas cleanup task was originally intended to use a laboratory engine at UC Berkeley and synthetic produce gas produced from reforming methanol to develop and test a fuel/air ratio controller and exhaust gas cleanup system. UC Berkeley required additional time and funds to replace and update the equipment, which would have had a negative effect on the progress of tests on the generator set at the Woodland site. It was concluded that this task could be effectively performed on the Waukesha Engine

Generator at the Woodland Biomass Research site operating on producer gas from the West Biofuels gasifier.

A fuel/air ratio controller for engine operation based on throttling the air to the Waukesha engine was developed in conjunction with the installation of three-way automotive catalyst technology. Both lambda sensors and direct nitric oxide sensors were used in both single and dual catalyst configurations to successfully remove NOx and CO from the engine emissions to meet the Yolo County AQMD Rule 2.32 for emissions.

For the power generation from the gasification of wood waste task, a Waukeshar H-2475G engine/generator set capable of 200 kWe when operated on natural gas was installed at the WBRC to operate on producer gas from the West Biofuels dual fluidized-bed gasifer. The engine generator was expected to generate 100-150 kWe when operated on producer gas from the gasification of wood. Power from the system was routed to a programmable load bank (1.4 to 140 kWe) that could be used from agricultural processing. The West Biofuels gasification facility is an intermittent technology demonstration facility that cannot be operated continuously. The lack of a net-metering program for biomass power generation with the local utility (Pacific Gas and Electric Company) precluded a grid connection. The engine/generator was extensively instrumented and the exhaust emission was monitored with both an Environmental Protection Agency (EPA) approved continuous emission analyzer and more advanced gas chromatography (GC) and Fourier transform infrared spectroscopy (FTIR) gas analysis instruments. Power generation from the gasification of wood waste with the West Biofuels gasifier was demonstrated at the 100 kWe level with both NOx and CO levels below eight parts per million (ppm) using three-way catalyst technology adapted to the system Future engine/generator system designs should focus on lean burn engines to increase efficiency and power specific emissions. Lean burn engine exhaust provides the opportunity to evaluate other emission control technologies such as selective catalytic reduction (SCR) using urea injection.

For the combustion properties and chemical mechanism for producer gas task, an advanced chemical kinetic mechanism (43 species and 470 reactions) for the combustion of producer gas was developed and validated on laboratory experiments to predict auto-ignition, extinction properties, and laminar burning velocities for producer gas with varying composition. A skeletal chemical kinetic mechanism (15 species and 18 reactions) and a reduced chemical kinetic mechanism with five global reactions were also developed for use in direct engine simulation codes to predict performance and combustion emission.

Industry, government, educational institutions, and the professional engineering community were provided with information on the performance of the biomass energy system to fulfill the technology transfer task. This information was communicated through presentations to these entities and through written publications. In addition, undergraduates, graduate students, and post-doctoral scholars were exposed to critical issues associated with biomass energy production through associated research projects through the University of California educational function.

This research and demonstration project at the WBRC demonstrated that synthetic gas produced from biomass gasification can be used in conventional spark-ignited engines by implementing gas cleanup technology and a successful engine control strategy for ultra-low emissions. The production readiness plan task involved plans to bring this technology to the marketplace. The entire package of a biomass gasifier, gas conditioning, and low-emissions engine generator will be commercialized together as a biomass combined heat and power (BCHP) system. West Biofuels, the commercial partner of UC San Diego on this project, has been working on implementing BCHP technology in California and North America. West Biofuels has teamed with companies with commercially proven technologies for each step of the process to become established in the marketplace and attract conventional investment and project financing. Previous studies by West Biofuels and the University of California project team showed that at an installed cost of $3.5-5.0 million per MW, the BCHP system could a cost effective form of power generation for many biomass energy projects in California and North America. The economics of any commercial project are dependent on project specific costs (feedstock, expendables, labor, etc.) and project specific returns (displaced power, displaced heat, value of ash, etc.). The analysis showed that a number of feasible projects were possible in this target cost range. Internal analysis by West Biofuels showed that the BCHP system could be supplied for this cost with a modest technology license fee of 10 percent included in the cost. A new demonstration plant at WBRC incorporating technologies developed in this project was scheduled to begin construction in 2012 and commissioned in 2013 in partnership with Gussing Renewable Energy American, with matching funds from West Biofuels and the University of California. Primary funding for the project is from the California Energy Commission Emerging Technology Demonstration Grant Program II (PON-11-501).

The technical performance objective results are described below.

The first technical objective was achieving minimum gasification efficiency of 75 percent on a LHV basis using an advanced thermochemical gasification process. A biomass rate of three wet tons per day using wood pellets produced 68 standard cubic feet per minute (scfm) of producer gas. The LHV of the gas was 52 percent of the lower heating value in the biomass. Sixty-nine percent of the biomass energy could be converted to producer gas if all volatiles could be converted to producer gas. The results were lower for two reasons. First, some of the gas was oxidized with oxygen above the fluidized bed to increase the temperature and reduce the tar content. Therefore, some of the gas was converted into CO_2 and water (H_2O) and the energy content was lowered. Without this step, 58 percent of the biomass would have been converted to producer gas. Second, oxygen (O_2) and air entered into the gasifier from the combustor through the downcomer connected to the regeneration section of the gasifier. At the same time, not all of the volatile fraction of the biomass might have been converted and some was moved over to the combustor. This explained the remaining difference between the 58 percent and 69 percent conversion rates. Since the gasification process in general only converts the volatile fraction of the carbon in the biomass the maximum conversion for the wood biomass could only be 69 percent. The remaining 31 percent of the energy was not lost. The energy in the fixed carbon was used in the combustion regenerator to produce the necessary heat for the endothermic gasification process and could be recovered as waste heat. This process has been

demonstrated in an integrated co-gen gasification system to contribute to an overall energy utilization of 80 percent.

The second technical objective was tar/contaminant gas cleaning of producer gas with a minimum efficiency of 96 percent. The measured reduction in tar species was 76 percent using the gas scrubbing and cleaning system developed for the West Biofuels gasification system. Additional technical approaches were being developed to improve the performance of tar removal. These approaches included higher operating temperature for the gasification process, catalytic bed materials, organic scrubbing liquids instead of water, and a regenerative catalytic reformer system developed by the National Renewable Energy Laboratory. This system could remove tars by 99 percent for power production and also provided the potential for using catalytic synthesis of the producer gas to produce fuel and chemicals.

The third technical objective was using an internal combustion engine fueled by producer gas a minimum thermodynamic efficiency of 30 percent. The gasifier integrated with the SI engine/generator was operated over a power range from 40 to 100 kWe with different gasifier operating conditions. It was necessary to operate the gasifier at three tons per day instead of the maximum five tons per day to minimize tar production and exhaust emissions. The efficiency obtained was 16 percent since only about 40 percent of the capacity of the engine was used due to throttling of the gas and a large parasitic load of almost 60 kW. With full load the efficiency could be expected to be 25 to 30 percent. To obtain better efficiency either a smaller engine matched to the lower volumetric output of the current gasifier or improved energy content of the producer gas from the gasification process to better match the engine is required. In future development both improved producer gas properties and a lean burn engine would provide higher efficiency.

The fourth technical objective was that internal combustion engine exhaust cleanup would be below the Yolo County Air Quality Management District (AQMD) Stationary Source Prohibitory Rule 2.32 limits for NOx and CO. The limit for NOx is 2.1 pounds per megawatt hour (MWh) and the limit for CO is 42.5 pounds per MWh. At optimized operating conditions the SI engine used to generate electrical power produced eight ppm of NO and CO with emission control adapted from automotive catalyst technology developed in this project. The emission levels corresponded to 0.16 pounds per megawatt hour (lb/MWh) for NO and 0.15 lb/MWhr for CO. These levels were well below the Yolo county requirements for small power production and approached the generally more restrictive California Air Resources Board (CARB) and Regional Air District Standards for non-attainment districts. Both improved engine efficiency and better operating characteristics of the gasification process should provide sufficient improvement for the emission control technology to meet the higher CARB standards.

The economic performance objective results are described below.

The first economic performance objective was achieving a capital cost below $1500/kW at a production scale of 100 units. This objective did not seem attainable with the current gasification technology and market. It is expected that to become established in the marketplace and attract conventional investment and project financing, a commercial entity such as West Biofuels teamed with companies with commercially proven technologies for each step of the

process could produce a BCHP system for many biomass energy projects in California and North America at an installed cost of $3.5-$5.0 million per MW. This cost could be reduced with larger scale production, but typically power projects of this type are not produced in an assembly line production system. A more realistic cost approaching $3 million per MW at large scale production may be attainable. The expected cost of $3.5-$5.0 million per MW should be economically viable given increased renewable power standards, higher retail power costs, and greenhouse gas cap and trade policy in California.

The second economic performance objective was achieving operating costs below $.06 per kWh including variable feedstock cost. The economic performance of a three MWe gasification co-generation power plant with a capital cost of $2..9 million per MWe and a feedstock cost of $2 per ton is shown in Figure 1. The critical element in the feasibility of an operating cost of $0.06/kWh was the value of the recoverable waste heat sales, which were tied to the cost of natural gas. The breakeven point in terms of the net present value of the project for a natural price of $4.5 million British thermal units (Btu) was $79/MWh or $0.079 kWh. The value of the waste heat at $4.5 million Btu was worth $0.03 kWh, so without waste sales the breakeven price of the power sales would need to be $0.109/kWh. The effect of feedstock cost (shown in Figure 2) was important but not as critical as capital costs, plant scale, and the value of the waste heat. The effect on the cost of electrical sales changed by about $0.034/kWh as the feedstock cost changed from $0 to $20 per ton. Based on this analysis, a target price of below $0.6/kWh was only reachable with the inclusion of waste heat sales.

Figure ES-1: Sensitivity of project returns to power prices and waste heat prices.

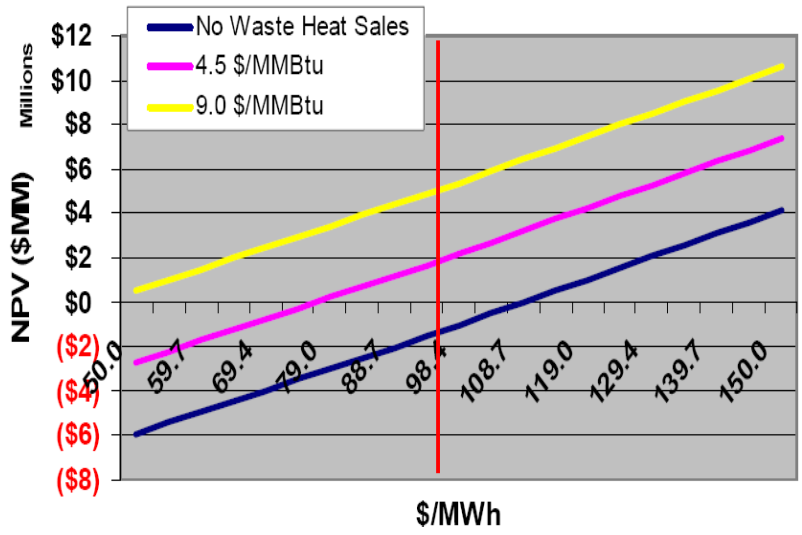

Figure ES-2: Sensitivity of project returns to feedstock costs with no waste heat sales.

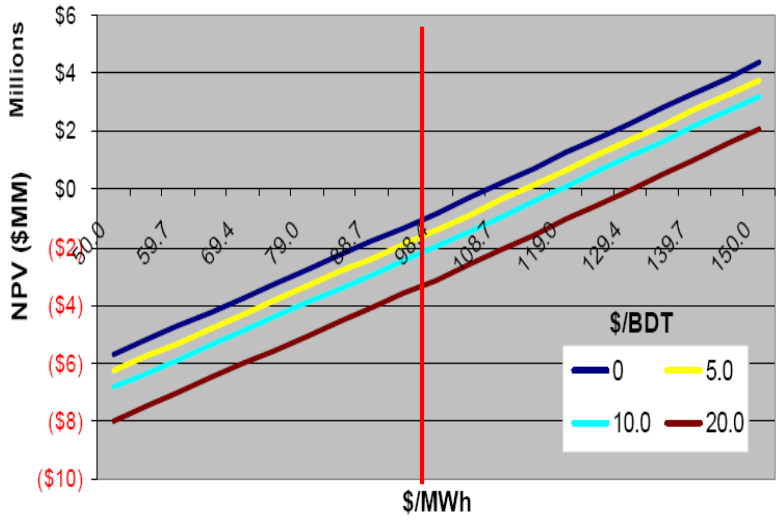

Benefits to California

Power generation from renewable sources such as biomass which are "carbon neutral" will lower greenhouse gas emissions from power generation compared to natural gas powered production. Combined heat and power production from biomass could displace natural gas for power and heat production and eliminate the corresponding greenhouse gas emissions. Using less natural gas and fossil fuels would help California meet its Renewable Portfolio Standards objectives and would reduce greenhouse gases that contribute to climate change and other air emissions that cause air pollution.

Chapter 1: INTRODUCTION

Problem Statement: In California, total power production capacity is currently 67,500 MW with less than one per cent (478 MW) produced solely from wood waste. These wood waste power production facilities are based on direct combustion with steam cycle electric power generation and use a fraction of the potential 25 million tons/year of available forest wood waste biomass. Modern wood waste power production technology uses thermochemical gasification of wood waste to generate a producer gas (primarily CO, H_2, and CH_4, and CO_2) for subsequent direct combustion. Using advanced thermochemical gasification directed towards the production of a high value added products such as transportation fuel or chemicals, provides the opportunity to improve the economics of the co-generation of power using waste wood/processing residues.

The University of California (San Diego, Berkeley, Davis) in collaboration with West Biofuels, LLC has developed an advanced thermochemical gasification and engine/power generation system for processing up to 5 tons/day of biomass using a dual-fluidized bed gasifier, operating near atmospheric pressure with air, generating high quality producer gas and is illustrated in Fig 1. The focus of this research, development and demonstration project is power production using the gas from the advanced West Biofuels biomass gasification system.

Figure 1: Process Schematic of the 5 Ton-Per-Day Dual-Fluidized Bed Biomass Gasification System with Engine Generator

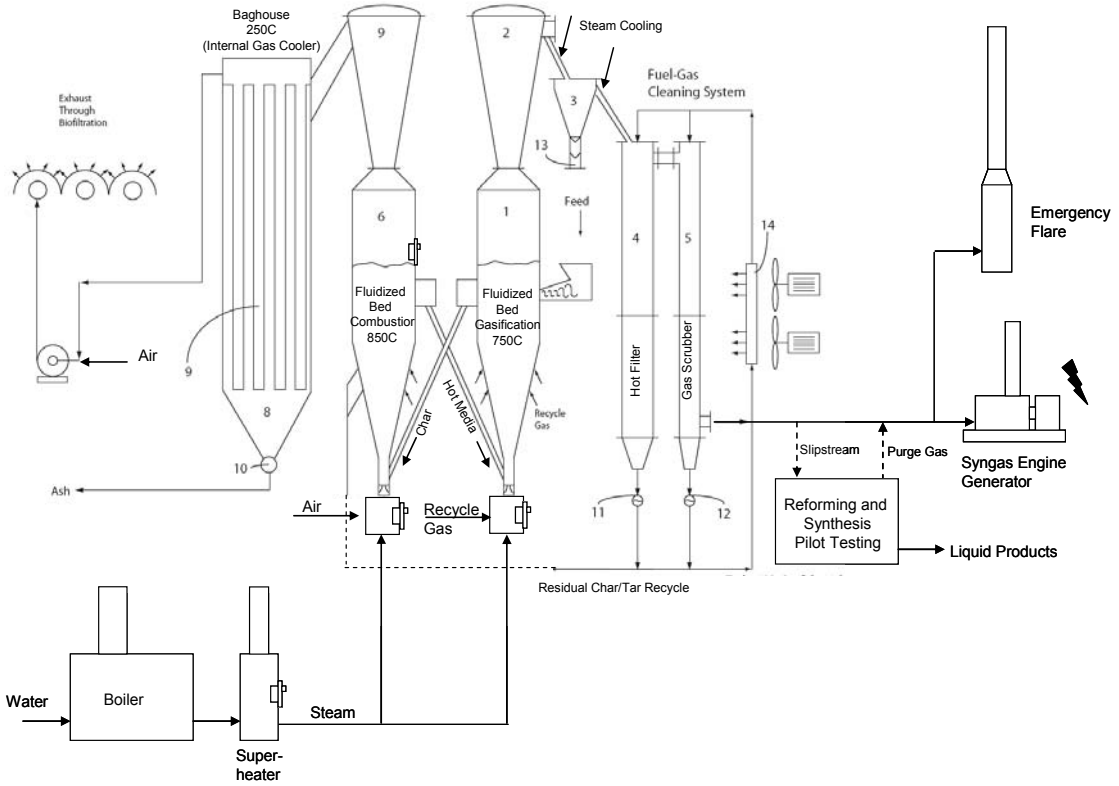

Description of project: In the conversion of biomass to a fuel gas, a thermochemical conversion process is used in which the hydrocarbons and fixed carbon from a biomass source are combined with water at a high temperature (steam) in a gasification reactor to generate producer gas which is composed primarily of CO, H_2, CH_4, and CO_2 with some water and higher-order hydrocarbons. This process can be accomplished with a variety of gasifier designs. The West Biofuels gasifier design is based on a dual-fluidized-bed gasification process, which is the state of the art for the thermochemcial conversion of biomass to producer gas for energy production. In this design, 70 percent of the energy in the biomass is converted into product gas and the remaining 30 percent provides heat for gasification and other processes as shown in Fig. 2.

Figure 2: Schematic of the Core of the Dual-Fluidized-Bed Gasification Process

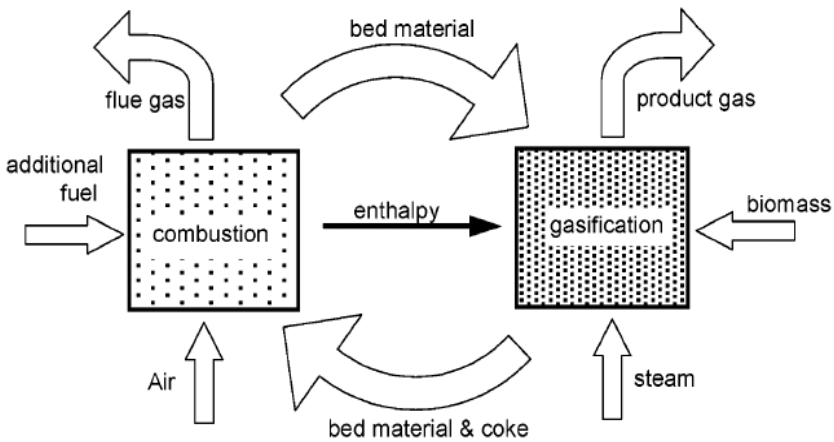

The West Biofuels system is designed to generate high-quality producer gas that can be converted to syngas (H_2, CO) for the production of transportation fuel such as alcohol which is in high demand in California (1 Billion gal/year) for gasoline blending, and is mostly imported to the state (97 percent), or for production of chemicals such as ammonia for fertilizer. The use of producer gas for power production is the goal of this project. Research and development for fuels and chemicals production is a longer-term objective.

Overall Project Goals: The overall goal of this project is to successfully demonstrate generation of power from forest wood waste using the West Biofuels advanced thermochemical gasification process In this project, research and development issues related to technological hurdles and scientific baseline knowledge in areas of gasifier operation, producer gas combustion properties, producer gas cleanup, engine performance and emissions, emission cleanup, and engineering simulation tools are investigated. This project also addresses the PIER goal of improving the environmental and public health costs/risk of California's electricity

Technical Performance Objectives: This research and development project to demonstrate renewable power from forest wood waste/residues with advanced thermochemical gasification has the following technical performance objectives:

1) Achieve minimum gasification efficiency of 75 percent on a LHV basis using an advanced thermochemical gasification process

2) Tar/contaminant gas cleaning of producer gas with a minimum efficiency of 96 percent.

3) Using an internal combustion engine fueled by producer gas a minimum thermodynamic efficiency of 30 percent.

4) Internal combustion engine exhaust cleanup will be below the Yolo County AQMD RULE 2.32 for the emissions regulation for NOx (2.1 lbs/MW-Hr) and CO (42.5 lbs/MW-Hr).

Economic Performance Objectives: The West Biofuels 5 ton/day gasification system to produce 100 kW of power is not considered to be a commercial unit at this scale. The technical performance and economic analysis of the proposed system will yield information for estimating the size of a system that will produce the minimum capital cost and operating cost to meet the following economic objectives:

1) A capital cost below $1500/kW at a production scale of 100 units.

2) Operating costs below $0.06/kW-Hr to include variable feedstock cost.

Technical Tasks: To accomplish the project goals and to determine the potential of advanced thermochemical conversion of biomass for power production to meet the technical and economic objectives of the project, the following technical tasks were addressed and presented in this report.

Task 2.1 Producer Gas Purification System Design and Testing
Task 2.2 Laboratory Producer Gas SI Engine/Exhaust Gas Cleanup.
Task 2.3 Power Generation from the Gasification of Wood Waste.
Task 2.4 Combustion Properties and Chemical Mechanism for Producer Gas
Task 2.5 Technology Transfer Activities
Task 2.6 Production Readiness Plan

Chapter 2:
Task 2.1 Producer Gas Purification System Design and Testing

2.1 Task 2.1.1 Design Review of Gas Scrubbing and Purification

Gasification is the conversion of carbonaceous material into fuel gases. It is accomplished via partial oxidation of the feedstock using insufficient air or oxygen with or without steam. The product gas, or syngas, is principally CO, H_2, methane, and lighter hydrocarbons, H_2O, particulate matter (PM), tar, alkali vapors, nitrogen and sulfur compounds, and depending on the process used, can contain significant amounts of CO_2 and N_2, the latter mostly from air. Product gas can be used directly for heat production or burned in prime movers for electricity generation. The combustion of gasification-derived fuel gases generates the same categories of products as direct combustion of solids, but pollution control and conversion efficiencies may be improved. The product gas from biomass gasification can be further processed to produce hydrogen or a range of liquid fuels including methanol, ethanol, mixed alcohols and gasoline- or diesel-range hydrocarbons.

Task 2.1.1 presents the design review for a laboratory-scale biomass gasification reactor and gas cleaning system. The purpose of the system is to provide a test platform for conducting experiments under a wide variety of operating conditions including various types of solid biomass feedstock, reacting agents, flow rates, and temperatures. The gas cleaning system is designed to remove tars and particulate matter from the product gas. Included in this report are a review of available technologies and a detailed design analysis including thermodynamic and performance analysis of the recommended system.

2.1.1 Gasifier Types

Gasifier types include *fixed bed* (updraft or downdraft), *fluidized* or "bubbling" bed, *circulating fluidized bed,* and *entrained flow*. The units can operate at atmospheric or higher pressure. The gasification medium is generally air, oxygen, steam, or a combination of these. Indirectly heated and dual-bed configurations are also utilized.

The *fixed bed* gasifiers are usually small batch or continuously-fed devices in which the fuel bed is held stationary while the reaction front passes through it, or the bed can move through reaction or mechanical displacement. *Fluidized bed* reactors contain a bed of relatively small particles of inorganic material (often sand or small diameter ceramic beads or gravel). The bed is 'fluidized' by blowing hot oxidant up from the bottom. In a *circulating fluidized bed,* the bed material flows up with the fluidizing gas and is carried over into a reinjection system after some type of gas/particle separation stage (i.e., a cyclone or disengagement zone). *Entrained flow* gasifiers have high gas velocities and high material throughput. Consequently, time for reaction is short which requires the feedstock to be of very small particle size, a liquid, or liquid slurry. High temperature (>1250 °C) is generated from combustion in oxygen that melts the ash (sometimes called slagging gasifier) and requires reactor cooling. Little to no tar is formed as the feedstock is essentially completely converted to H_2, CO, CO_2, and H_2O.

2.1.2 Tar Quantity Dependence on Gasifier Type

Tar traditionally describes the organic material from gasification that condenses under operating conditions in transfer lines, inlet devices, and other surfaces and generally limiting or degrading performance of the device using the producer gas (boiler, engine, etc.) In general, downdraft gasifiers produce relatively low tar, updraft gasifiers produce high-tar gas with fluid bed and entrained flow gasifiers falling somewhere between the two (Table 1).

Table 1: Tar in raw gas by gasifier class (Milne, Evans et al. 1998),(Morf 2001)

	Fixed Bed		Fluidized Bed		
	Updraft (counter current)	Downdraft (cocurrent)	Bubbling	Circulating	Entrained
Mean tar content (g Nm^{-3})	50	1	12	8	10
Range of tar (g Nm^{-3})	1-160	0.01-6	1 - 150	1 – 150	2 - 30

2.1.3 Gas Quality Requirements

Gas cleaning to remove tars, PM, sulfur and nitrogen compounds, acid gases and other impurities from biomass producer gas is usually necessary before utilization. The degree of gas cleaning depends on the application (Table 2).

Table 2: End use gas quality requirements

Impurity	Units	Reciprocating Engine	Gas Turbines	Chemical and F-T synthesis
Particles	mg/ Nm3	<50	<30	<0.02
Particle size	μm	<10	<5	-
Tar	mg/ Nm3	<100	0.5-5 (or below dewpoint)	below dewpoint
Alkali metals	-	-	0.24 mg/Nm3	< 10 ppbV
HCL +HBr + HF	-	-	-	< 10 ppbV
NH3 + HCN	-	-	-	< 1 ppmV
H2S + COS + CS2	-	-	-	< 1 ppmV
class 2 (hetero atoms)		-	-	< 1 ppmV

Sources: (Stassen 1993; Milne, Evans et al. 1998; Bergman, van Paasen et al. 2003)

2.2 Gas Cleaning Strategies

Particulate matter and tar reduction technologies can be broadly divided into two categories: treatments during gasification and gas cleaning or conditioning after gasification. Treatments inside a gasifier for tar reduction include gasifier design and operation and use of bed additives/catalysts. Wang et al. reviewed the advantages and challenges for different gasifier types and operating conditions, summarized in Table 3 (Wang et al, 2008).

Table 3: Advantages and challenges of different gasifying agents, gasifier design, and gasifier operation (adapted from Wang et al, 2008)

	Advantages	Challenges
gasifying agent		
Air	partial combustion for heat supply moderate char and tar content	low heating value (3-6 MJ Nm^{-3}) large amounts of N_2 in syngas (> 50% by vol.) difficult determination of equivalence ratio (ER) (0.2 - 0.4)
Oxygen	high heating value syngas (6-12 MJ Nm^{-3}) medium to low tar content	requires air separation plant
Steam	high heating value syngas (10-15 MJ Nm^{-3}) H_2 rich syngas (e.g. > 50% by vol.)	requires indirect or external heat high tar content
carbon dioxide	high heating value syngas high H_2 and CO, low CO_2	requires indirect or external heat high tar content requires source of CO_2
gasifier design		
fixed bed	simple design tolerant of higher moisture biomass favorable economics on small scale	long residence time/low throughput non-uniform temperature distribution high char and/or tar content low efficiency low productivity (~5GJ m^{-2} h^{-1})
fluidized bed	short residence time high throughput (20-30 GJ m^{-2} h^{-1}) uniform temperature distribution low char and/or tar content reduced ash problems	high PM favorable economics on medium to large scale
entrained flow	high throughput utilized in coal/petcoke conversion can use liquid feeds	requires small fuel particle size
Gasifier operation		
Higher temperature	decrease tar production decreased methane in syngas increased carbon conversion increased heating value of syngas	decrease energy efficiency increased ash problems
Higher pressure	low char and tar content no compression required during utilization	limited design and operational experience higher costs for small scale
Higher ER	low char and tar content	decreased heating value of syngas

Gasifier design can have a major influence on the amount of tar produced in the product gas, as shown in Table 1. Updraft gasifiers produce on typically between 50 – 100 g/Nm^3, fludized bed gasifiers about 10 g/Nm^3, and downdraft gasifiers about 1 g/Nm^3.

In an updraft gasifier, biomass is fed from the top, and air is fed from the bottom. The temperature is hottest close to the grate where the oxygen meets the char. Gas continues travel upwards through cooler temperature areas within the gasifier and to the exit. The temperature profile from grate to gas exit is decreasing. Since the tar generated in the 200-500°C region only continues to cool, the updraft gasifier design leads to large tar production (50-100 g/Nm^3).

In a downdraft gasifier, both gas and biomass travel downward. As the gas travels downward, the temperature profile increases to a maximum and then reduces again. During the temperature ascent primary tar is produced in the 200-500°C region. As gas temperatures continue to rise above 500°C, primary tar begins to rearrange forming more non-condensable gases (including CO_2, CO, H_2O) and heavier secondary and tertiary tars (Evans and Milne, 1997). Tar and oxygen are in contact at high temperature and thus have the opportunity to burn and be converted to non-condensable gaseous products. Thus the downdraft gasifier has the lowest tar production (~1 g/Nm^3) (Basu, 2010).

The fluidized bed gasifier (bubbling or circulating) design allows a high degree of mixing. This has the effect of allowing both fresh biomass and char to come in contact with oxygen that enters from the bottom. Temperatures tend to be more moderate, and oxygen concentration is lower in the upper portion of the gasifier. Thus, tar generation in a fluidized bed gasifier is between that produced by updraft and downdraft gasifiers; averaging about 10 g/Nm^3 (Basu, 2010).

2.3 System Design

"Success stories"

Table 4 summarizes five biomass gasifier power plants and lists the major gas cleaning components installed. The facilities at Vermont and Varnamo, Sweden were demonstration projects that no longer operate as originally configured. The most common similarities in the five purification systems are the use of a cyclone, filter (fabric, ceramic, or metal), and scrubber/water tower.

Table 4: Summary of biomass gasification "success stories" (adapted from Hofbauer and Knoef, 2005)

	Greve-in-Chanti, Italy	Güssing, Austria	Harboore, Denmark	Varnamo, Sweden	Vermont Battelle /SilvaGas
Gasifier Type	CFB	Indirect FICFB	Updraft	pressurized CFB	indirect CFB
Fuel power	30 MW	8 MW	5 MW	18 MW	44 MW
Heat power	N/A	4.5 MWth	3.4 MWth	9 MWth	N/A
Electrical power	6.7 MWe	2 MW	up to 1.4 MWe	6 MWe	8-9 MWe

Fuel	RDF (60% paper, 40% plastic)	Wood/ Woodchips	Woodchips	woodchips, bark, straw, RFD	wood/ woodchips
Application	Gas fired to boiler	CHP, gas engines and boilers	CHP, engines, Boilers	CHP, gas turbine	medium BTU gas
Cyclones	Yes, two.	Yes	No	Yes	Yes
Filters	Ceramic	Fabric	No	ceramic/metal	No
Scrubbers	No	Biodiesel	No	No	Water
Other	Acid gas/dechlorination		water tower, ESP		ESP

2.3.1 System Schematic

The gasification and gas cleaning system being designed presently consists of five components: fluidized bed gasifier, cyclone separator, gas cooler, filter, and scrubber. The primary goal of the cleaning system is removal of PM and tars (Fig. 3).

Figure 3: Gasification and purification system schematic

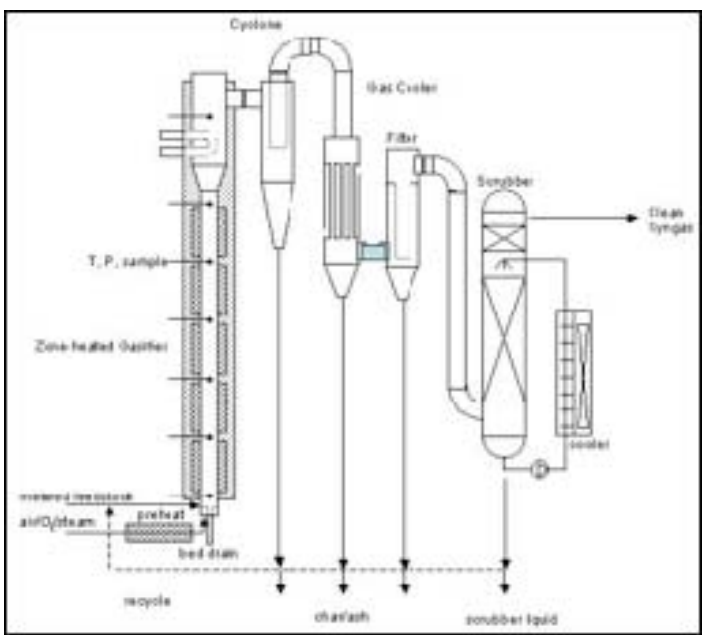

2.3.2 Gasifier Design

A bubbling fluidized-bed-type gasifier was selected for the design. The reaction zone is heated externally through the wall by three 4.6 kW circumferential electric heaters. In operation, hot air, steam, or other oxidants can be injected through the distributor system at the base of the reactor to fluidize the bed. With the reactor at the prescribed temperature, biomass fuel is

injected via an auger-type feeding system located just above the distributor plate. The present distributor is a multi-hole bubble-cap design, although different distributor designs can be accommodated depending of performance of the present design.

Estimating Minimum Fluidization Velocity

Minimum air fluidization velocity is the minimum air velocity required to fluidize the bed material. Minimum fluidizing velocity is calculated to be 0.115 m/s, however the gasifier will be more typically operating between velocities of 0.6 and 1 m/s for optimum heat transfer.

Estimating Syngas Flow Rate using Air as an Oxidant

Assuming a wood fuel (48 percent carbon, 45 percent oxygen, 5 percent hydrogen by mass), the syngas flow rate is estimated to be approximately 25 m^3/h.

Estimating Steam Flow Rates

For steam gasification, literature suggests typical steam-to-biomass (S/B) ratios between 0.5 and 1.7 (by mass). Based on the fuel rates reported in the literature, a range of possible steam flow rates into the present gasifier between 1.0 and 22.4 kg/h, although for most fuels and S/B ratios, 10 kg/h is sufficient.

2.3.3 Particulate Removal

Particulate matter refers to solid-phase particles entrained in the raw product gas stream exiting the gasifier. Particulate matter can be composed of the ash derived from mineral matter in the feedstock, unconverted biomass in the form of char, and material from the gasifier bed. Circulating and bubbling fluidized bed gasifiers typically produce high PM loading requiring particle removal from the gas stream. The primary source of fly ash PM is the mineral matter in the biomass feedstock, some of which becomes entrained in the product gas. The concentration of ash in the product gas depends on reactor design and operation as well as the mineral content of the biomass feedstock (Opdal, 2006).

The most common technologies to remove PM include; cyclonic separators, barrier filters, electrostatic precipitators (ESP) and wet scrubbers. Due to their physical size and cost, electrostatic precipitators are usually suited to large-scale systems, and aren't considered in the present system. Figure 4 shows a plot of the estimated separation efficiency versus particle size for several particulate removal systems.

2.3.4 Cyclone

Cyclone separators direct the gas flow into a circular path, enhancing the centrifugal force to remove particles from the stream. In this system, a cyclone will be used as a pre-cleaner for larger particle removal. It will be placed upstream of the gas filter and wet scrubber components. The cyclone is expected to remove nearly 100 percent of particles larger than 20 microns.

Figure 4: Separation efficiency of fabric filter, ESP, Venturi, wash tower, and cyclone (adapted from Hasler et al, 1999)

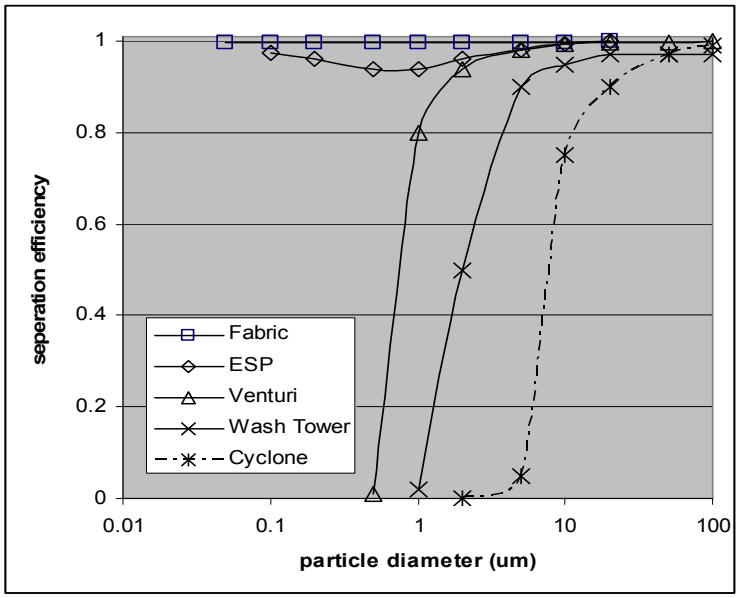

2.3.5 Barrier Filters

Barrier filters encompass a range of porous materials, including fabric, metal, and ceramic. These filters allow gases to pass through but prevent particles above a certain size. Typically this gas cleaning technique can remove particles with diameters in the range 0.5 – 100 µm (Knoef, 2005). It is in theory possible to design a filter to remove particles of almost any size, but a pressure drop increases as both the pore size and filter cake permeability decreases. Barrier filters are most effective in removing dry particles and less suitable for stickier, moist contaminants (Knoef, 2005).

Mechanical methods for gas cleaning such as bag house filtering, scrubbing, and EPS typically can only operate at low temperatures. Operational temperatures for fabric filters are lower (<350°C) than for metal or ceramic candle filters (<600°C). Problems occur in barrier filters of all types if tar condensation blocks the filter. Filters may need to be periodically shaken or back flushed with clean syngas or nitrogen to remove particle accumulation. Hasler and Nussbaumer observed that a 90 percent particle removal was easier to achieve than a 90 percent tar removal using the mechanical methods (Hasler et al, 1999).

2.3.6 Tar Removal

Tars foul equipment downstream of the gasifier, coat surfaces, and enter pores of filters; generally clogging things. They are considered by many to be the major obstacle for future utilization of biomass gasification (Bergmann et al, 2002). The two basic approaches for tar removal are physical removal of tar using techniques similar to particle removal, and catalytic and thermal tar cracking.

Thermal tar cracking involves heating the product gas to near 1300°C. At high temperature, tars will crack into simpler molecules with lower dew points. The main disadvantage of this process is the expensive equipment involved, increased soot production, reduced heating value of the product gas and/or lower thermal efficiency.

Catalytic tar cracking offers a lower temperature alternative to thermal cracking, typically operating near 800-900°C instead of 1200-1300°C. Alkali metals, non-metallic oxides, and supported metallic oxides are catalyst materials that have been applied in biomass gasification systems. Alkali salts are mixed directly with the biomass as it is fed into the gasifier and causes enhanced char formation. However, poorer carbon conversion, increased ash content, and the fact that the added alkali metals are difficult to recover make alkali metals unattractive gasification catalysts for commercial use.

2.3.7 Scrubber Design

In the present system, tar removal will be accomplished primarily by the scrubber, which is designed following the example of Güssing, Austria. The Güssing scrubber system consists of a packed tower using structured packings, rapeseed oil methyl ester (RME) solvent sprayers, and an aerosol trap. The scrubber in Güssing reaches tar separation efficiencies of about 98 percent for tars detectable with gravimetric methods. The water-phase condensate captured in the scrubber is evaporated and fed into the gasifer. A significant advantage of this process is in avoiding wastewater problem.

In the present design, gas flows upward counter-current to a descending liquid solvent. The center section of the scrubber contains a bed of 5/8-inch stainless steel, random-packings. The random packings increase the gas-liquid contact area, thus increasing mass transfer. Total height of the scrubber is 105 inches.

Figure 5: Conceptual schematic of scrubber system (Proll et al, 2005)

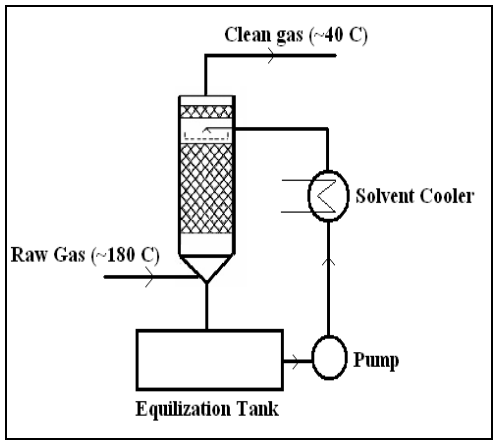

The packed bed has a diameter of 6.4 inches (6-inch schedule 10 pipe) and has a height of 6 feet. A low resistance gas injection plate supports the packed bed. Above the packed bed is a nozzle that sprays solvent and a demister to prevent solvent entrainment. At the gas inlet and exit are temperature and pressure probes ports for the data acquisition system. The packed bed can be easily removed for cleaning via a 3.5″ pipe flange near the gas inlet. All tower internals, externals, piping, pumps, and sumps are made of 316 stainless steel for corrosion resistance.

Liquid solvent is pumped from the sump to the nozzle at a variable rate between 2 and 10 gpm. The sump contains two baffles to separate solvent, settled contaminants, and condensed water

vapor. The sump is designed to accommodate 8 hours of gasifier operation at a 20 kg/h steam rate.

Packing material

Due to the planned scrubber's operating range of 10 to 45 gpm/ft^2 and the corrosiveness of the fluids involved, corrosive resistant metal random packings were selected.

Liquid Holdup

Liquid holdup is the liquid present in the void spaces of the packing. Reasonable liquid holdup is necessary for good mass transfer and efficient tower operation. High liquid holdup increases column pressure drop, the weight of the packings, the support load at the bottom of the packing, and the column drainage time. Most importantly, high holdup can lead to excessive fouling and degradation. We estimate a 6-inch diameter, 2-meter tall packed bed of 1-inch Pall rings will hold-up a maximum of 1.8 L of RME.

Theoretical Stages

Using an equilibrium distillation calculation, we estimate six theoretical stages are required. Industry empirical rules of thumb suggest minimum packed bed height should be 6 feet.

Pressure drop

Amistco calculated, using their AHPP 15 packing (copy of stainless steel IMTP) with properties of syngas and biodiesel solvent, a pressure drop of 0.02 in WC/ft (16.7 Pa/m)

2.4 Conclusions

A gasification and purification system has been designed with the following guidelines:

- Laboratory scale design
- Atmospheric pressure
- Use scalable technologies; i.e. select technologies that will be appropriate for current design and for larger scale projects.
- Low cost. With an eye towards larger scale implementations, technologies were selected that would allow the system to eventually operate profitably.
- Particulate matter and tar removal. End-use applications will require low concentrations of tar and particulate matter.
- Flexible – allow wide variety of operating conditions (e.g. different feedstock, reacting agents, temperature control, modular system that allows gas cleaning units to be added/removed/interchanged).

A fluidized-bed type gasifier was selected in the design process for its ability to generate high-energy, high throughput product gas with low tar and PM generation, favorable economic scale-up for medium/large projects, and reduced ash problems. As a laboratory tool, the gasifier is capable of operating under a wide array of operating conditions: variable feedstock, variable gasifying agent, temperature control, with various temperature/pressure monitoring/gas sampling access points.

The gas cleaning system was designed primarily to remove particulate matter and tar. Particles larger than 20 microns are removed by cyclonic separation. A barrier filter removes particles greater than 1 micron. For tar removal, a packed-bed wet scrubber was designed to allow operation with different liquid solvents at variable flow rate. The scrubber contains a large reservoir for collection of condensables for steam gasification. Overall, the designed system will allow a wide spectrum of thermodynamic biomass conversion experiments to be conducted.

For additional details on this task see McCaffrey, Z., Williams, R., and Jenkins, B., 2012. *Task 2.1.1 Design Review of Gas Scrubbing and Purification*. California Energy Commission. Publication number: CEC-PIER-2007-002.

Chapter 3:
Task 2.1.2 Fabricate laboratory scale prototype gas purification system

The goal of Task 2.1.2 was to fabricate a gas purification system based on the outcomes of Task 2.1.1. Further, the task objectives specified that the laboratory-scale purification system would be deployed on the UC Davis laboratory scale internally-recirculating atmospheric fluidized bed reactor for preliminary testing, and would include options for batch or continuous recycling of scrubber effluents to the gasification reactor.

The design, fabrication, and installation of the laboratory scale fluidized bed reactor and purification system was completed with an estimated capacity of process 16 Nm^3 of gas per hour (25°C, 1 atm).

3.1 Laboratory Scale Gasifier

The gasifier was designed as an internally-recirculating fluidized bed reactor. The primary reactor diameter is 96 mm, expanding to 197 mm diameter in the disengagement zone as shown in Fig. 6. Overall height is 3 m. The reactor is zone-heated using 3 heater groups, 0.5 m in length. Each heater group (composed of two semi cylindrical heaters) is rated for 4.6 kW (208 V single phase, 22 A). Actual current draw is approximately 20.5 A for each heater group (about 93 percent of rating). The disengagement zone may also be heated depending on the extent of heat loss in the upper stages of the reactor. Six temperature and pressure access ports are spaced vertically along the gasifier, plus access ports at the top of the gasifier that allow thermocouples, pressure taps, gas sampling and other sampling equipment to be inserted to any depth. In operation, hot air, steam, or other oxidants can be injected through the distributor system at the base of the reactor to fluidize the bed. With the reactor at the prescribed temperature, biomass fuel is injected via an auger-type feeding system located just above the distributor plate. Fuel is fed into the reactor using a belt feeder system driven by a variable speed stepper motor. The feeder can supply feedstock over a range of 0.3 to 2 g/s. The fuel feeder and hopper are lightly pressurized using a small amount of nitrogen (~5 L min^{-1}) to prevent back-flow of reaction products into the fuel feeder. The distributor is a multi-hole bubble-cap design, although different distributor designs can be accommodated depending of performance of the present design. The gasifier is rated at a design raw gas flow rate of 16 Nm^3 per hour (25°C, 1 atm) for the range of feedstock feed rates indicated above. This flow range was used in designing the downstream gas conditioning equipment.

The installation of the laboratory scale gasifier is shown in Fig. 7 with details of zone heaters shown in Fig. 8 and gasifier control in Fig. 9.

Figure 6: Fluidized bed gasifier schematic

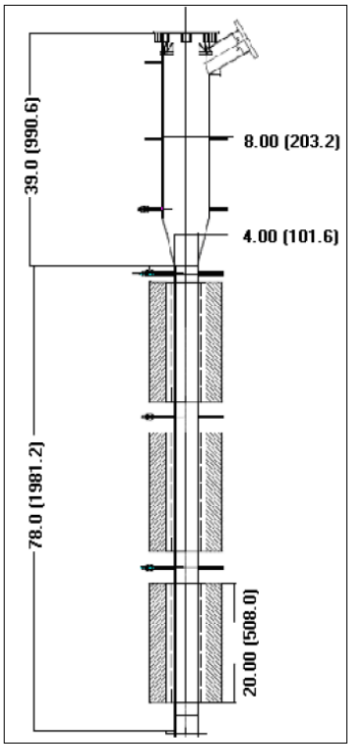

Figure 7: Laboratory scale gasifier and purification system

Figure 8: Zone heaters and controllers on main fluidized bed reactor

Figure 9: Gasifier and control panel

3.2 Hot Gas Filter

A hot gas filter is positioned after the gasifier and before the scrubber to remove solid materials entrained in the raw gas stream. The filter element is a porous (5 micron), ceramic candle filter manufactured by Glosfume (U.K.). The filter has the following dimensions: 1000 mm length, 55 mm OD, and 38 mm ID as shown in Fig. 10. The filter housing is mounted horizontally and contains ports for temperature and pressure measurements, and a port for back-pulse capability to allow cleaning of the filter during operation as shown in Fig. 11.

Figure 10: Hot gas filter schematic (dimensions: inches)

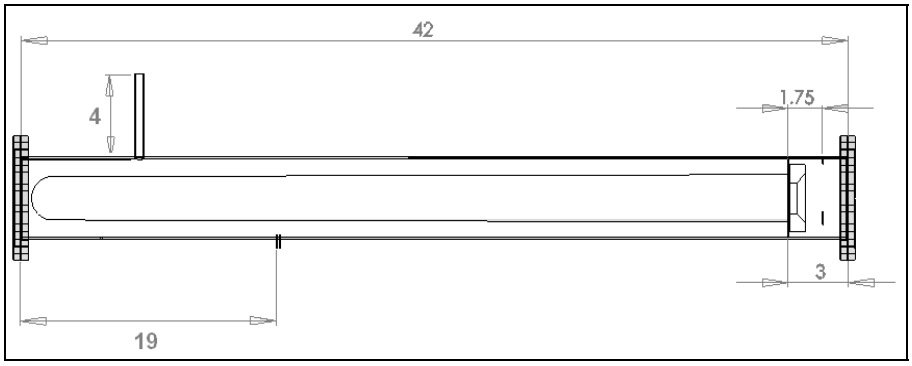

Figure 11: Hot gas filter installed

3.3 Wet Scrubber

Design criteria for the wet scrubber are detailed in the interim report for Task 2.1.1. Tar removal will be accomplished primarily in the scrubber with expected separation efficiency to reach as high as 98 percent. In addition, the temperature reduction will cause most of the steam to condense here. The condensate will contain water soluble trace components like NH_3 and HCl. The scrubber packed bed has a diameter of 163 mm (6.4 in) and a height of 1.8 m (6 feet). Scrubber system overall height is approximately 3.7 m (12 ft). The solvent spray nozzle and demister is located above the packed bed. All scrubber internals, externals, piping, pumps, are made of 316 stainless steel. The sump tanks and secondary containment are made of mild steel

In the scrubber, liquid flows countercurrent to the upward flowing gas through a 6-foot tall packed bed of 15 mm (0.6 in) diameter stainless steel metal, random packings (Amistco High Performance Packings, Alvin, Texas) as shown in Fig. 12.

Figure 12: Scrubber layout

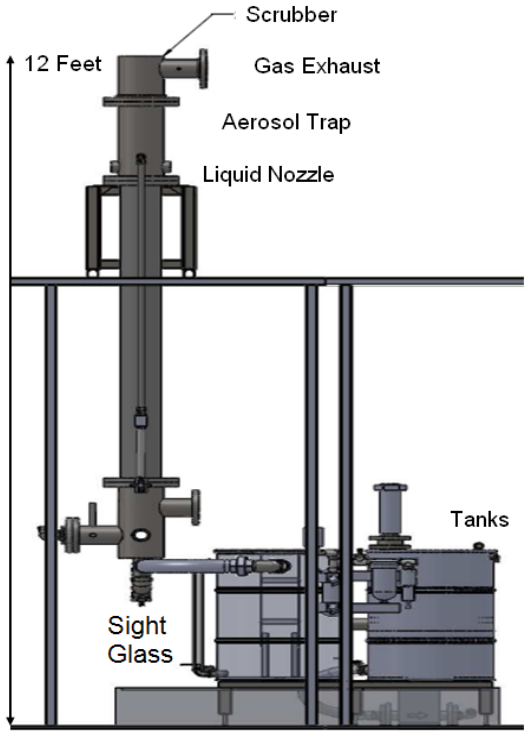

After passing through the scrubber tower, liquid solvent returns to the equalization tanks via a J-trap. A 100-mesh screen filter is positioned before the liquid exits the tanks to the pump to prevent damage to the pump. A multi-stage centrifugal stainless steel pump pressurizes the solvent through a 10 μm cartridge filter, shell and tube heat exchanger, needle valve, and turbine flow meter, with solvent returning through the nozzle above the packed bed. Solvent flow rate can be controlled between 1 and 10 gallons per minute (4 – 38 L min^{-1}). The equalization tank consists of two 30-gallon steel drums connected at top and bottom (Fig. 13). The lower connection equalizes liquid volume between the tanks, and the upper connection equalizes gas pressure.

The scrubber tanks act as a reservoir for the solvent and collected liquids (Fig. 14). Liquid entering the tanks must pass through a set of baffles and a 100-mesh screen before flowing through the solvent pump. The tanks contain knock-out baffles, a level indicator, a 100-mesh screen filter, and burst disc for pressure relief. After passing through the tanks, solvent then flows from the pump through pressure relief valve, filter, heat exchanger, flow control valve, and finally nozzle above the packed bed.

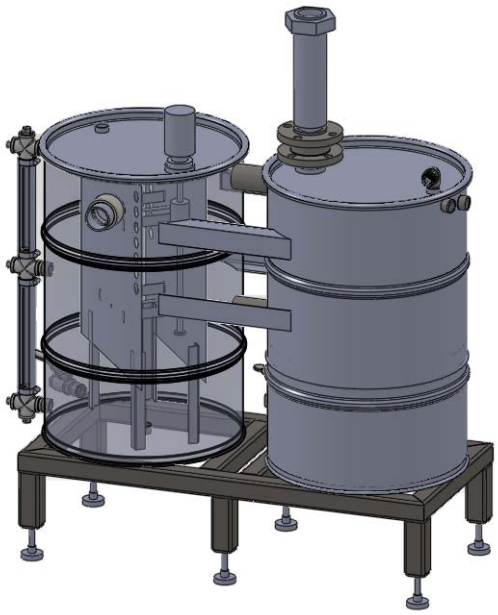

Figure 13: Scrubber tanks

Figure 14: Scrubber tanks and the lower section of the scrubber.

3.4 Thermal Oxidizer

The purpose of the thermal oxidizer is to combust all gaseous products to ensure hazardous air pollutants and any volatile organic compounds generated are destroyed before being exhausted out of the building. General layout of the thermal oxidizer is shown in Fig. 15. The direct-fired, natural gas thermal oxidizer arrived early January 2012 and has been installed and tested. The firing box operates at a nominal temperature of 620°C (1150°F), and maximum temperature of 700°C (1300°F). Figure 16 shows arrival crate and positioning in lab. Figure 17 shows fully installed and operational thermal oxidizer (hood and exhaust ducting, power supply, product gas inlet line, etc.). The overall gasifier system appears in Fig. 18.

During the week of March 26th, 2012, the system was successfully demonstrated in the presence of UCD Fire Department personnel (see reactor temperature trends in Fig. 19) and the system was approved for operation.

Figure 15: Thermal Oxidizer General Layout

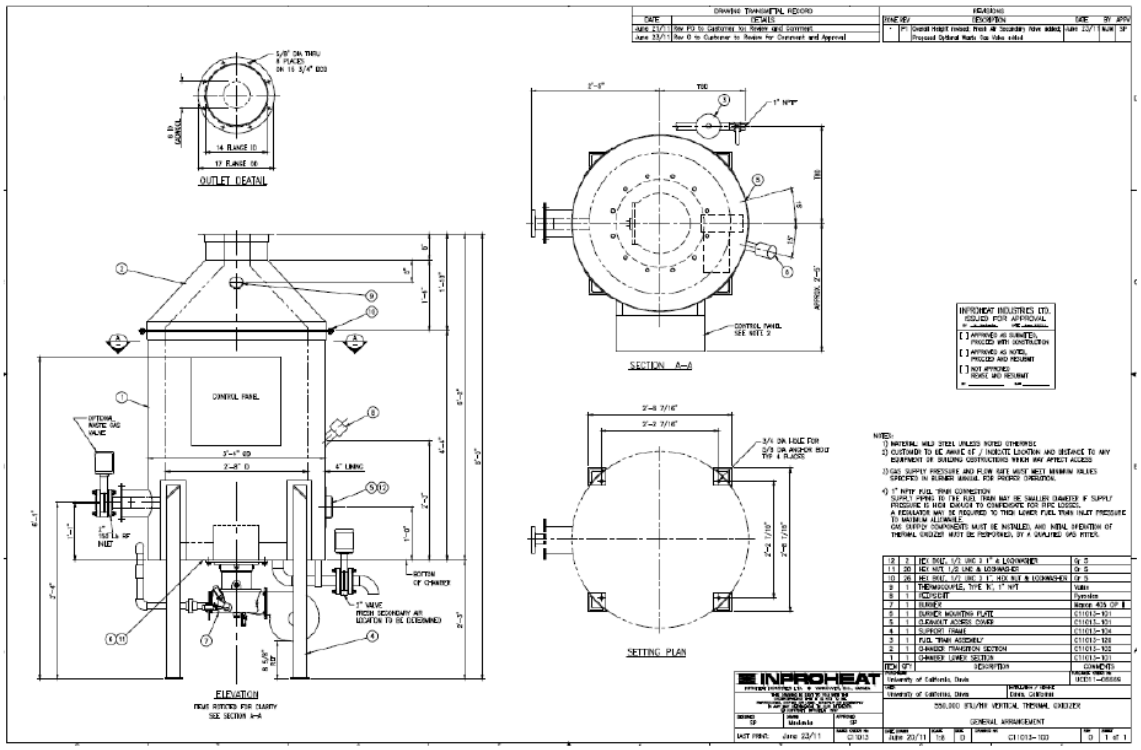

Figure 16: Thermal Oxidizer, clockwise from upper left: Strapped to shipping crate, "Tilt-up", Transport to lab, Positioned in lab

Figure 17: Operational Thermal Oxidizer	Figure 18: Gasifier system

Figure 19: Temperature trends during initial trial run of the gasifier and thermal oxidizer

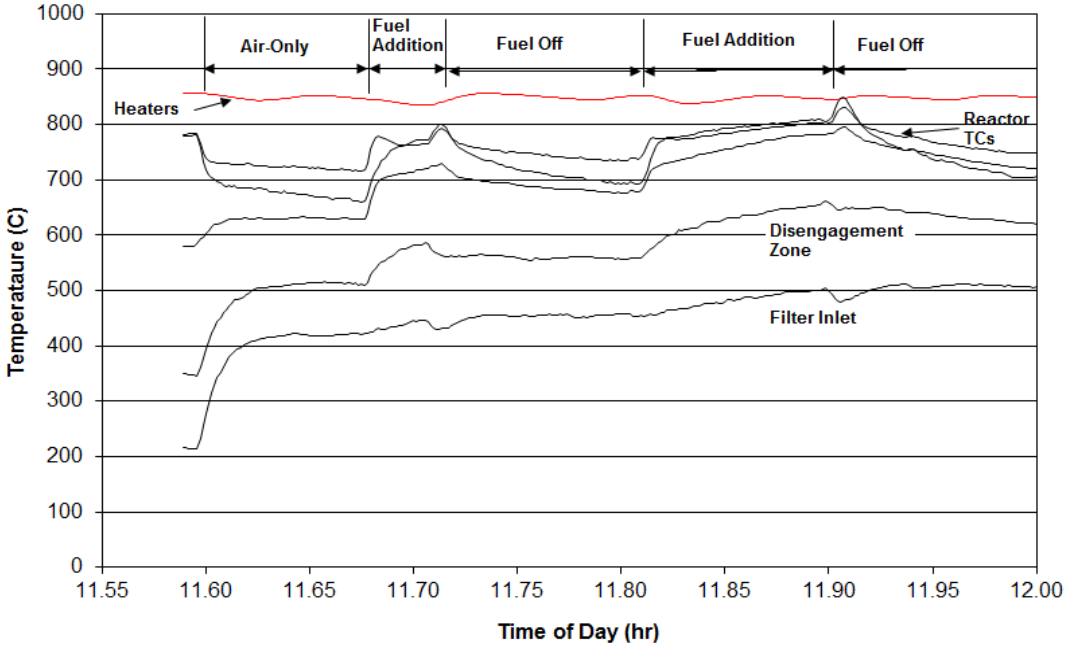

3.5 Summary

The design, fabrication, and installation of the laboratory scale fluidized bed reactor and purification system was completed following the design criteria established in Task 2.1.1. This temperature controlled, internally-recirculating reactor is designed to conduct fundamental thermal conversion studies. The purification system includes a hot-gas filter and advanced liquid scrubber. The system is capable of operating across a range of feedstock and feed rates (0.3 to 2 g/s), pretreatment processes, cleaning processes, different levels of filtration, and reacting agent combinations. The reactor and purification system has an estimated capacity of process 16 Nm^3 of gas per hour (25°C, 1 atm).

Chapter 4:
Task 2.1.3 Test Plan for Prototype Gas Purification System

Removal of tars is critical to the design and operation of biomass gasification systems as syngas utilization processing equipment (e.g. internal combustion engines, gas turbines, fuel cells, and liquid fuel synthesis reactors) have a low tolerance for tar. Capturing and disposing of tar is expensive due to equipment costs, high hazardous waste disposal costs where direct uses cannot be found, and system energy losses incurred. By capturing tar prior to gas utilization and recycling to the gasifier, higher efficiency may be obtained while avoiding disposal issues. While a number of studies make use of a wet scrubber for tar and other contaminant removal, no published studies have thoroughly investigated optimization of a scrubber system used for tar removal in a recycling gasification system.

The goal of the task was to prepare a comprehensive plan for evaluating the prototype gas purification system performance. The specific objectives are:

- Tar capture: evaluate the impact that scrubber solvent has on tar removal efficiency.
    - Select scrubber solvents that minimize both tar dew-point and total concentration in the cleaned syngas using Hansen Solubility Parameters (HSP) theory.
    - Experimentally evaluate solubility in selected solvents using slip-stream of raw syngas from laboratory reactor and bubbling through impingers of solvent.
    - Experimentally evaluate tar removal efficiency using laboratory gasifier and scrubber system.
- Tar destruction: evaluate the impact of gasifying tar + solvent on gas composition and tar concentration exiting the gasifier.
    - Experimentally measure the gas composition and tar concentration exiting the gasifier with and without recycled tar + solvent.

The results will provide a better understanding of tar collection and recycle using a packed-bed wet scrubber, and will provide information for designing tar management systems for biomass gasification.

Gasification experiments will be performed using the Biomass Laboratory gasification and clean-up system, which consists of a fluidized-bed gasifier, hot gas ceramic filter, and packed-bed wet scrubber (Fig. 20). In addition, a thermal oxidizer is used to combust all produced gases before being exhausted from the building. Initially, tests will be conducted to establish stable, reproducible steady-state operating conditions and to measure gas composition and tar content of the syngas. Gas composition will be measured using online mass spectrometry, and tar will be measured using a modified EU tar sampling protocol via slip-stream sampling (CEN/TS, 2006). Tar compounds will be identified and quantified using GC/MS/FID analysis using standards.

After tar concentrations of the syngas have been measured, solvents will be selected using Hansen's solubility parameters (HSP). HSP is a theory that predicts solubility between solvent and solute based on the similarity of the dispersion, polarity, and hydrogen-bonding solubility parameters. Hansen's HSP Handbook (Hansen, 2007) reports the solubility parameters for over 1100 solvents and additional solvent and solute HSP parameters can be calculated theoretically or measured experimentally. Correlations between potential solvents and measured solutes can then be calculated. Solvents that HSP predict to be well suited to dissolving tar compounds will be tested using impinger experiments to verify solubility. Further safety and material properties review will be performed prior to using any of the selected solvents in the scrubber. Tar measurements using the impinger method will allow testing of the solvent effectiveness on a syngas slip-stream at lower material and disposal costs and in less time than the pilot-scale experiments to come later.

Figure 20: Schematic of laboratory scale gasifier and clean-up system

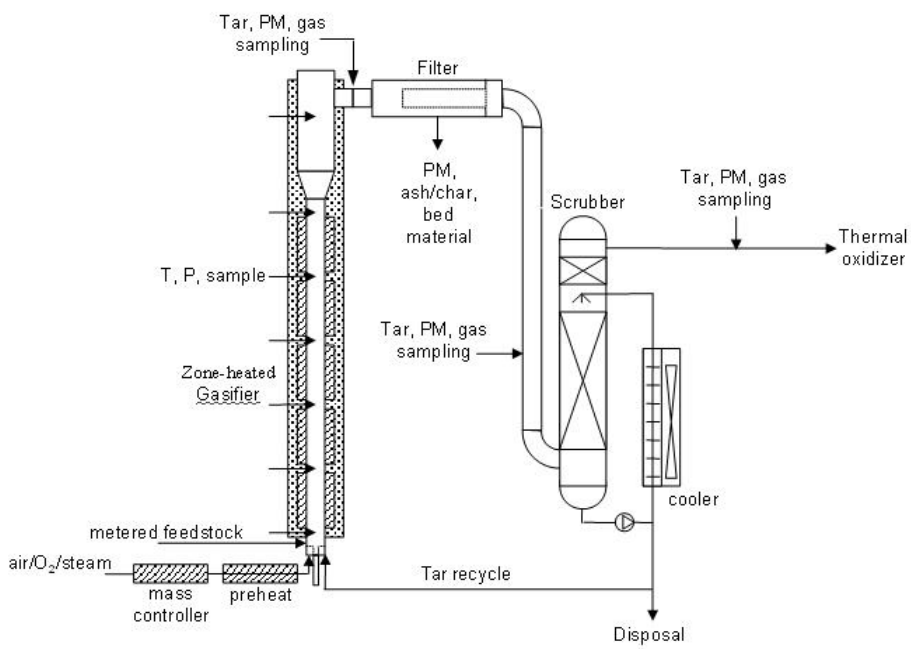

Once an appropriate scrubber solvent has been selected and tested via slip-stream, the full system can be operated with scrubber and new solvent. Operating without recycling, the scrubber tar removal efficiency will be determined using the selected solvent. Finally, the full system will be tested using recycled tar as partial feedstock into the gasifier. Tar in solution with solvent will be added to the gasifier bed using a roller pump and injection through the central vertical riser that also serves intermittently as the bed drain. Feed rate can be adjusted, either continuously or in batches, to match overall steady-state operation with a specified scrubber blow-down rate (with tar disposal as needed).

The goal of this project is to investigate the full tar-removing capability of a gas scrubber system used in a tar management system for biomass gasification. Recycling tars back into the gasifier increases utilization of energy content of the feedstock and avoids or reduces the waste disposal issues required of tar compounds. Emphasis will be on tar capturing using a packed-bed wet

scrubber, determination of a solvent that effectively dissolves the multi-component compounds constituting tar, and the effect recycling tar has on the producer gas composition and tar concentration. For this work, the principal feedstock will be woodchips. Gasification experiments will be conducted using the laboratory-scale fluidized-bed reactor in the Biomass Laboratory at the University of California, Davis. This temperature-controlled, internally-recirculating reactor is used to conduct fundamental conversion studies. Full energy and material balances will be completed around the gasifier and the downstream gas purification components (filter and scrubber). On-line process gas mass spectrometry and ga-chromatography/mass spectrometry will be used to analyze syngas quality.

4.1 Hansen Solubility Parameters

Hansen solubility parameters (HSP) have been used to predict solubility especially in the area of polymers (Levin and Redelius, 2008; Lindvig et al, 2002; Segarceanu and Leca, 1997). If solubility parameters can be used to predict solubility for tar compounds, this could facilitate selection of an appropriate solvent to be used within the packed bed wet scrubber for tar removal. However, most solubility parameters are developed for single-component materials, it is not completely evident that solubility parameters are appropriate for describing the solubility of mixed tars.

Theory: A material becomes dissolved in a solvent if the free energy of the process is zero or negative as described by

$$\Delta G = \Delta H - T\Delta S \qquad (1)$$

where ΔG is the free energy, ΔH is the enthalpy of mixing, T is absolute temperature, and ΔS is the change in entropy. Hildebrand described this enthalpy or heat of mixing as

$$\Delta H = \Phi_1\Phi_2 V ((\Delta E_1/ V_1)^{1/2} - (\Delta E_2/ V_2)^{1/2})^2 \qquad (2)$$

where ΔH is the heat of mixing, V is total volume, ΔE_x is the molar energy of vaporization of component x, V_x is the molar volume of component x, and Φ_x is the volume fraction of component x in the solution (Hildebrand et al. 1970). The term $(\Delta E/V)^{1/2}$ is called the solubility parameter, ζ. The heat of mixing two materials is dependent on the difference between their solubility parameters squared, $(\zeta_1 - \zeta_2)^2$. If the solubility parameters are not identical, the term $(\zeta_1 - \zeta_2)^2$will have a positive value which will cause the energy term ΔH to oppose the entropy term. If ΔH is equal to or less than $T\Delta S$, the dissolution will occur. Hansen states that the entropy of mixing, ΔS, can be assumed positive for practical approaches to using the solubility parameters (Hansen and Beerbower, 1971).

Hansen proposed a more complicated solubility parameter that includes the interactions of dipole and hydrogen bonding. For solvents and materials with strong polarity and hydrogen bonding components, dissolution is not predictable by a dispersion solubility parameter alone. Solubility is maximized when the three components for the solvent and material being dissolved are as similar as possible. Hansen defines the overall solubility parameter, ζ, as

$$\zeta^2 = \zeta_D^2 + \zeta_P^2 + \zeta_H^2 \qquad (3)$$

where the D, P, and H subscripts refer to the dispersive, polar, and hydrogen-bonding forces, respectively. While a statistical thermodynamic method exists for calculating the three solubility parameters, in practice, empirical based methods are more often used. Table A.1 in Hansen

(Hansen, 2007) contains a table of dispersion, polarity, and hydrogen bonding parameters for over 1100 solvents, most of which have been calculated using empirical formulas.

Table 5: Dispersion, polar, hydrogen bonding solubility parameters, and molar volume (adapted from Hansen, 2007).

	D	P	H	MV
acetone	15.5	10.4	7	74
ethanol	15.8	8.8	19.4	58.5
2-propanol	15.8	6.1	16.4	76.8
water	15.5	16	42.3	18
acetonitrile	15.3	18	6.1	52.6
hydrogen peroxide	15.5	12.2	42.7	23.2
acetic acid	14.5	8	13.5	57.1
xylene	17.6	1	3.1	123.3
furfural	18.6	14.9	5.1	83.2
gylerol	17.4	12.1	29.3	73.3
Benzene	18.4	0	2	89.4
Napthalene	19.2	2	5.9	111.5
phenol	18	5.9	13.8	207.5
bi-phenyl	19.7	1	2	155.1
toluene	18	1.4	2	106.8
xylene	17.6	1	3.1	123.3
Methyl benzoate	18.9	8.2	4.7	124.9

Once the solubility parameters are known for potential solvents and compounds to be dissolved, an HSP correlation can be computed.

$$Ra^2 = 4(\zeta_{D1} - \zeta_{D2})^2 + (\zeta_{P1} - \zeta_{P2})^2 + (\zeta_{H1} - \zeta_{H2})^2 \qquad (4)$$

Ra is called a modified difference between the HSP for a solvent (1) and a compound to be dissolved (2). An example of using Hansen's Solubility Parameters follows. Table 5 lists the solubility parameters for 10 potential solvents and 7 tar compounds. Table 6 shows the calculated correlation (Ra) for each pair, and an average value for the solvent. The lower the average Ra value, the better the solvent is. Results of the computation show that the solvents are (from best to worst): xylene, acetone, furfural, 2-propanol, acetic acid, ethanol, acetonitrile, glycerol, hydrogen peroxide (H_2O_2), water. Further safety and material properties review and small scale testing will need to be performed prior to using any of the selected solvents in the scrubber. Potential candidate solvents will be tested using an impinger train capture on a gas slipstream prior to being added to the scrubber for full system testing.

Table 6: Calculated correlations between tar compounds and solvents

	acetone	ethanol	2-propanol	water	acetonitrile	H2O2	acetic acid	xylene	furfural	glycerol
Benzene	12.92	20.18	16.48	43.75	19.47	42.88	16.03	2.18	15.22	29.93
Napthalene	11.25	16.57	13.16	39.7	17.8	38.9	13.5	4.37	12.98	25.74
phenol	9.57	7.69	5.11	30.65	15.33	30	7.31	11.8	12.57	16.74
bi-phenyl	13.56	20.6	17.15	43.81	19.58	43.04	17.01	4.34	14.41	29.83
toluene	11.45	19.41	15.77	43.15	17.93	42.4	14.99	1.42	13.9	29.35
xylene	11.01	18.43	14.69	42.18	17.87	41.37	13.99	0	14.18	28.46
Methyl benzoate	7.51	15.97	13.41	39	12.24	38.81	12.45	7.82	6.74	25.09
Average	11.04	16.98	13.68	40.32	17.17	39.63	13.61	4.56	12.86	26.45

4.2 Test Methods

Tar sampling will performed before and after the scrubber using two methods: 1) an impinger train with an organic solvent (isopropanol) as a trapping solution following the EU standard, and 2) with solid phase adsorption (SPA) technology. The tar-suspended liquids recovered using the EU method are analyzed for tar compounds by gas chromatography (GC) mass spectrometry (MS) and gravimetric methods. GC analysis can provide information about tar composition and concentration but is not suitable for compounds with boiling points above 275°C. Thus the GC method will be used to analyze the lighter tar compounds and gravimetric measurement will be used for quantifying the total tars captured.

4.2.1 EU Method

The EU tar standard method involves isokinetic sampling of the gas stream, a heated filter for particle collection, an impinger train with solvent (isopropanol), volumetric dry gas meter, temperature sensors, and pump. Utilizing standard methods is good practice for reproducibility and improves ability to compare results and performance across different research groups and reactor systems. However, the method's disadvantages include a large number of components, labor-intensive setup and tar recovery and extraction, and the long sampling period (typically between 30 and 60 minutes). The long sampling period leads to limited information about transients.

Design of an EU method tar sampling apparatus has been done based on the EU tar standard (CEN/TS, 2006). Example of a standard tar sampling train is shown in Fig. 21. Components include:

4.2.1.1 Gas probe (Module 1)

- Gas flow through sampling train should be limited to between 0.1 m^3/h and 0.6 m^3/h
- Pre-conditioning (Module 1)
- Isokinetic sampling requires appropriate nozzle or probe tip facing into the gas stream. If only gas phase components are to be sampled, then isokinetic sampling is not required and the probe tip can be oriented perpendicular to gas flow and/or a filter can be placed at the probe tip. Gas is heated and the probe contains a valve for shutoff for the case of a pressurized gas line.

4.2.1.2 Particle Collection (Module 2)

- Heated filter is heated to 100-125°C for updraft gasifier, 300-350°C for downdraft, fluidized bed, and entrained flow gasifiers.

4.2.1.3 Tar collection (Module 3)

- Train of seven impingers -- impingers 1 through 4 are “warm” and impingers 5 and 6 are “cold”. Impingers 1, 5, and 6 contain frits or glass beads (bead diameter = 6mm). Impingers 1 through 5 contain isopropanol solvent. Impinger 6 is without any initial liquid. The “warm” impingers will be maintained between 35 and 40°C and the two “cold” impingers will be maintained between -15 and -20°C. The “warm” impinger’s temperature is maintained by immersing the impingers in a heated water bath using an immersion heater, and the “cold” impinger temperature is maintained using an ice-salt-water bath. Impinger 7

contains desiccant. (Fig. 23)

4.2.1.4 Volume Registration (Module 4)

- Gas pump
- Flow rate and total volume measurement and control
- Ventilation

Figure 21: Modules of the EU sampling train

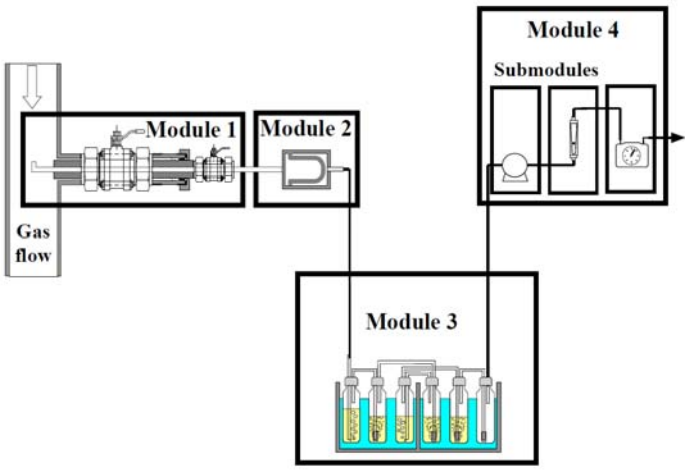

Figure 22: Soxhlet extraction apparatus

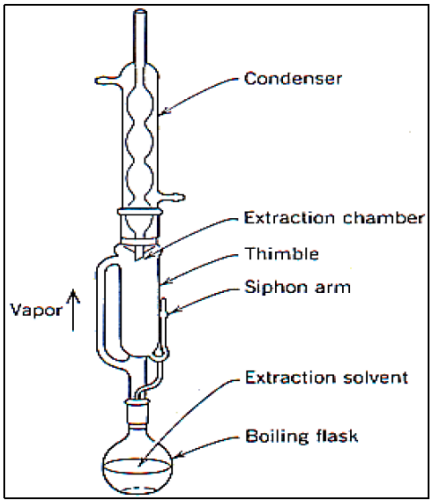

4.2.2 Soxhlet Extraction

After sampling, the particle filter from the impinger train is weighed and then placed in the Soxhlet chamber of the Soxhlet apparatus for tar extraction shown in Fig 20. The boiling flask is three-quarters filled with isopropanol and heated to low rolling boil. Isopropanol vapor travels to the extraction chamber and condenses against the cool surface of the condenser. Solvent fills the extraction chamber until liquid level within the extraction chamber reaches sufficient height

to be siphoned (with extracted tars) back to the boiling flask. The apparatus is cycled until droplets of isopropanol coming off the filter are clear (approximately 6 hours). The collected solvent and tars are then added to the impinger liquids for analysis. The "wet" filter is dried in the hood and then in an oven at 105°C and re-weighed. The difference in weight between the dried, final filter and the original clean filter is the particulate matter.

4.2.3 Gravimetric Tar Mass

Total mass of tar is determined gravimetrically using a rotary evaporator (rotovap), desiccator and a scale. The EU tar standard specifies the rotovap should be operated using a water bath of 55 C and a vacuum pressure of 10 kPa (absolute). Sample liquid is weighed, and then placed in the rotovap shown in Fig. 24. After the liquid is evaporated, 20 mL of ethanol is added to the tar flask and the rotovap is run again. Following evaporation of the ethanol, the tar flask is placed in a desiccator overnight and then the tar is re-weighed.

Figure 23: Impinger train

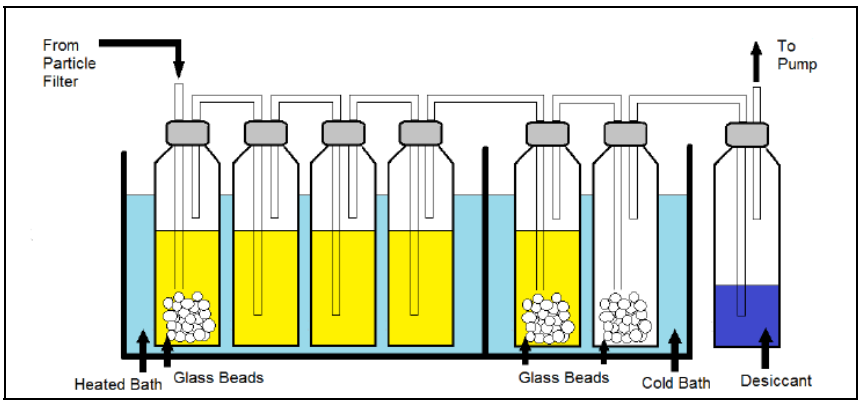

Figure 24: Rotovap

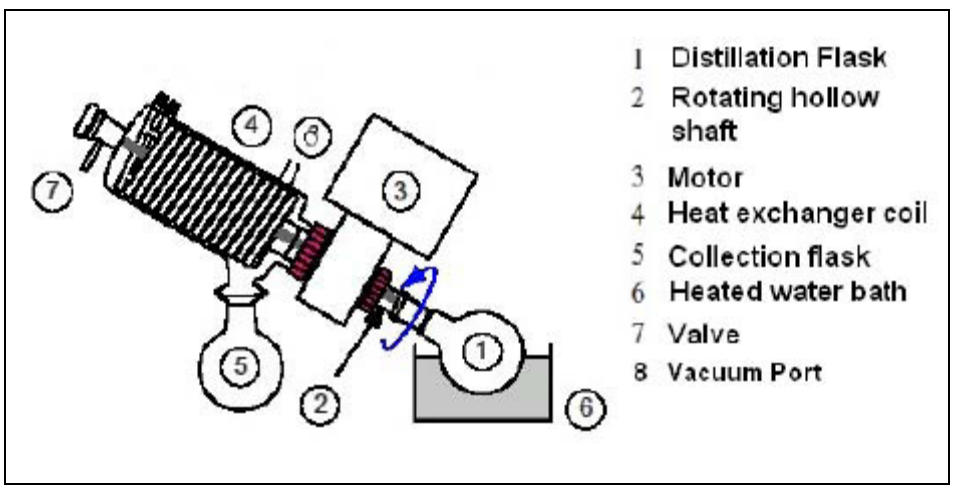

4.2.4 Solid-phase Adsorption

In preparation before sampling, each column (Alltech Extract Clean(tm) Amino 500mg, 4mL) has Methylene Chloride (DCM) run through them, then they are dried quickly, capped, and put

into large disposable centrifuge tubes for storage. To sample, the procedure follows that of Brage (1997). Tar extraction is a simple procedure involving eluotropic solvent desorption. Aromatics are eluted with 1.5 mL DCM. Phenols are eluted with 1 mL of isopropanol-DCM (1:1 v/v) followed by 500 μL IPA for a 500 mg column. Fractions are collected in auto-sampler vials (1.8 mL) and closed with a hole-cap with PTFE-silicone septa. In addition the phenols are derivatized by addition of 50 μL of BSTFA and allowed to react for 1 hour prior to GC analysis.

4.2.5 Gas Chromatographic Analysis

The tar-trapping solution was analyzed using GC/MS (Agilent 6850/5975C) equipped with an HP5MS capillary column. For the EU Method, tar samples are to be analyzed using the following program. Column temperature program consisted of 1) hold @ 55°C for 4 min 2) ramp at 10°C/min to 75°C and 3) ramp at 20°C/min to 250°C. Other parameters are shown in Table 7.

Table 7: GC/MS Instrument Parameters

Injector split	20:1
Inlet temperature	280°C
Auxiliary line temperature	240°C
Injector volume	1 μL
Column flow (Helium)	0.8 mL/min

For the solid phase adsorption method, the column temperature program consists of 1) initial temperature of 150°C (no hold), 2) ramp at 1°C/min to 250°C.

4.3 Experimental Plan

Tests to be conducted include syngas characterization, solvent selection, gasification without recycle, gasification with recycle, plus element and mass balance for the complete system. All of the experimental tests will be conducted in triplicate. Initial tests will develop a procedure for steady-state operation of the gasifier, filter, and scrubber. Tests involving recycle treatments will be performed by injecting a tar-substitute/solvent solution using a roller pump into the gasifier. The tar substitute will be comprised of the highest concentration tar compounds found in the tests without recycle. Many of these chemicals are hazardous and carcinogenic. Proper precautions will be taken, including development of safe operating and accident procedures prior to operation and consultation with University Environmental Health and Safety personnel. These procedures will be continually updated throughout the project.

Experiment #1: Tar solubility and effect of recycle

A slip-stream of syngas sampled after the hot gas filter will be bubbled through impingers of solvent. This experiment has two treatments: solvent (4 levels), recycle (2 levels: with recycle, without recycle). Four solvents will be selected using HSP theory. Each solvent will be tested using the impinger method. Because capture of tar using the slipstream method will not provide enough tar for recycling to the gasifier, recycle treatments will be accomplished using a 'tar substitute' in solvent solution. The tar substitute will be comprised of the highest concentration tar compounds found in the tests without recycle. From the literature, tar concentration in sampled gas exiting the gasifier is expected to be about 15 g/Nm^3 (Table 1) (Cui et al, 2010). Tar solution will be added to the gasifier bed using a roller pump and injection

through the central vertical tube. Total gravimetric tar and tar compound concentrations of the samples captured in the impingers will be measured by using EU method and GCMS with standards, respectively.

Total # of tests = 4 x 2 x (triplicate) = 24

Time required to complete experiment = approximately 2 months

Experiment #2: Scrubber tar removal efficiency

Gasifier, hot gas filter, and scrubber will used in this experiment. Tar concentration before and after scrubber will be measured using EU and SPA methods. This experiment has two variables: solvent (2 levels: water and best solvent from Experiment #1), and recycle (2 levels: with recycle and without recycle). Total gravimetric tar and tar compound concentrations will be measured using the EU method, SPA, and GCMS with standards, respectively.

Total # of tests = 2 x 2 x (triplicate) = 12

Time required to complete experiment = approximately 2 months

Experiment #3: Feedstock effect

Gasifier, hot gas filter, and scrubber will used in this experiment. Tar concentration before and after scrubber will be measured using EU and SPA methods. This experiment has two variables: solvent (2 levels: water and best solvent from Experiment #1), and feedstock (3 levels). Total gravimetric tar and tar compound concentrations will be measured using the EU method, SPA, and GCMS with standards, respectively.

Total # of tests = 2 x 3 x (triplicate) = 18

Time required to complete experiment = approximately 2 months

Experiment #4: Full system mass and energy balance

Full system mass will be conducted once in triplicate. Proximate, ultimate and elemental analysis of the feedstock, ICPMS analysis of solids (bed material before and after test and filter dust, solids with the scrubber), GCMS analysis of scrubber solvent, and gas analysis (inline MS) and tar composition (EU method, SPA, GCMS) will be conducted. Energy balance requires calorimetry of feedstock samples and estimation of heat transfer.

Total # of tests = 1 x (triplicate) = 3

Time required to complete experiment = approximately 1.5 months

Chapter 5:
Task 2.1.4 Test the prototype gas purification system

The goal of this task was to test the performance of the prototype gas purification system following the test plan of Task 2.1.3. The test plan could not be completed on schedule due to extensive laboratory retrofit required by the campus fire department to meet new fire regulations implemented after project initiation. Additional equipment was added to the laboratory to meet new fire safety requirements including: a thermal oxidizer for destruction of the product gas, a combustible gas alarm system for facility and fire department notification, and a central control system with emergency shutdown. The laboratory as shown in Fig. 7 was re-authorized for operation in April 2012 allowing for an initial test of the gasifier, including temperature profiles and tar content of the product gas, as reported here.

5.1 Test Run on 6/13/2012

Objective of the test run on 6/13/2012 was to measure the tar concentration of the product gas. Figure 25 shows a schematic of the system configuration. The gasifier was operated using air (100 L/min, 250 °C) and Douglas fir woodchips (4.9 kg/h, 30°C, 9 percent moisture content on a wet basis). External zone heaters for the gasifier were set to 900°C with temperature within the heated section of the reactor between 725 and 850°C (Fig. 27). The reactor operated in gasification mode for about 45 minutes during which tar samples were collected for further analysis.

5.1.1 Feedstock

Douglas fir wood chips were obtained from Mallard Creek Inc., Rocklin, California in November 2008 from Douglas fir trees harvested on the western slopes of the Sierra Nevada between Chico and Grass Valley, California. The trees were debarked and delimbed prior to chipping. Immediately after collection, the Douglas fir chips were air-dried under cover in room conditions (22°C – 25°C, 40 – 50 percent relative humidity) to reduce moisture content below 10 percent wet basis. The Douglas fir was analyzed for volatile solids, ash content, ultimate analysis (C-H-N-S), higher heating values (HHV), volatile matter, and fixed carbon (Table 8). Prior to analysis, biomass samples were knife-milled (Pulverisette 19, Fritsch, Germany) through a 2-mm screen. Milled samples were stored dry at room temperature (22°C) in air-tight plastic bags for up to 7 to 10 days prior to analysis.

Table 8: Volitile solids, ash, ultimate analysis, HHV, volatile matter, and fixed carbon measurements on a dry basis

Ash content	0.2	% dry matter
Volatile matter	83.8	% dry matter
Fixed carbon	16.0	% dry matter
HHV	19.86	MJ/kg dry material
Carbon	50.0	% dry basis
Nitrogen	0.4	% dry basis
Hydrogen	6.1	% dry basis
Sulfur	n.d.	

Ash	0.2	% dry basis
Oxygen*	43.3	% dry basis
Volatile solids	9	mg/g dry
Ash	1.3	mg/g dry

*by difference.

Figure 25: System schematic for test run on 6/13/2012

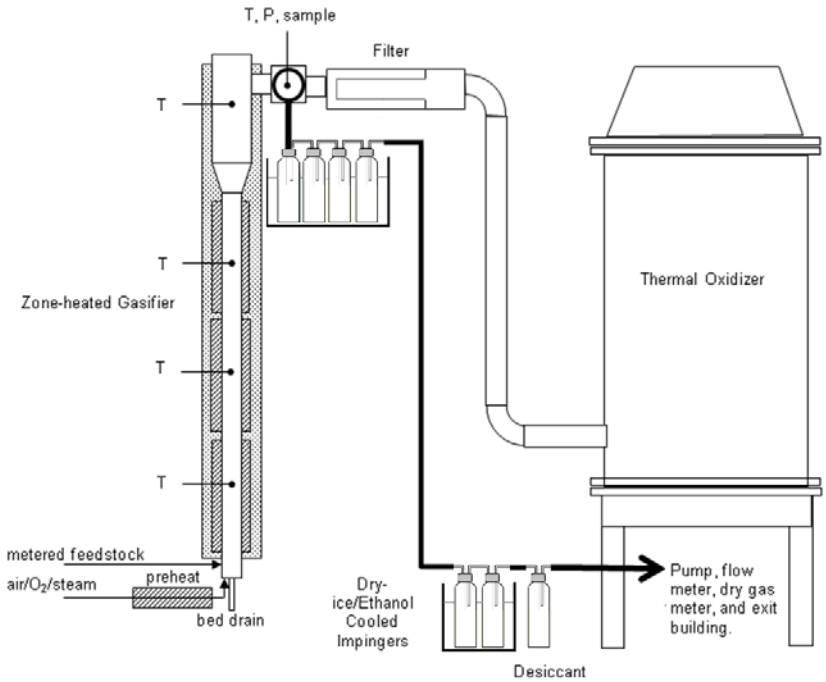

Volatile solids and ash of the Douglas fir were determined by loss-on-ignition of oven dried samples in an air-muffle furnace (Fisher Model 750-58, Fisher Scientific, Pittsburgh, PA) at 575°C for 3 hours (ASTM E1755). Higher heating value (HHV) was determined by adiabatic constant volume (bomb) calorimetry (IKA C5003 Control and IKA C5001 Cooling System, Staufen, Germany) according to ASTM D5865. Volatile matter and fixed carbon of each sample were determined in accordance with ASTM D3175. In this study, the inorganic fraction is classified as ash due to the method used to determine the mass fraction, and the residual fraction is classified as volatile solids. The carbon, hydrogen, and nitrogen contents are determined with infrared spectroscopic or thermal conductivity cells (ASTM D-5373) using a LECO TrueSpec CHN Elemental Determinator. The typical uncertainty is 0.5-1 percent RSD and lower limit of detection 25-100 ppm. The sulfur content is similarly determined using infrared spectroscopy (ASTM D-4239) using a LECO TruSpec Sulfur add-on module with a typical uncertainty of 1 percent RSD and a lower limit of detection of 5 ppm. The oxygen contents are estimated by difference to 100 percent, adding the C, N, S, H, ash, and moisture contents.

5.1.2 Bed Material

NARCO Investocast 60 grain was used as the bed material. This grain had a mean particle size of 210 µm. Slumped bed depth was approximately 9.6 cm (3.8 inches) or one reactor diameter. Bed pressure drop is indicative of bed agglomeration, as a more rapid or sudden decline in pressure drop than that normally observed through elutriation implies agglomeration and channeling in the bed (Meister et al., 2005). The initial mass of bed media was 1 kg.

5.1.3 Tar Sampling

Tar was sampled exiting the gasifier before the hot gas filter using a sintered metal filtering probe positioned intersecting and perpendicular to the centerline of the primary gasifier exit duct. Gas collected through the probe was pulled (5-6 L/min) through a series of seven impingers: three with isopropanol solvent plus one empty (dry) in a water-ice bath (~0°C) close to the sampling point (upper impingers), two impingers with isopropanol solvent and one with silica gel dessicant in a dry ice-ethanol bath on the floor at -50°C (Figure 26). After the impingers the sampling gas passed through pump, flowmeter, dry gas meter, and building exhaust.

Figure 26: Upper (left) and lower (right) impingers

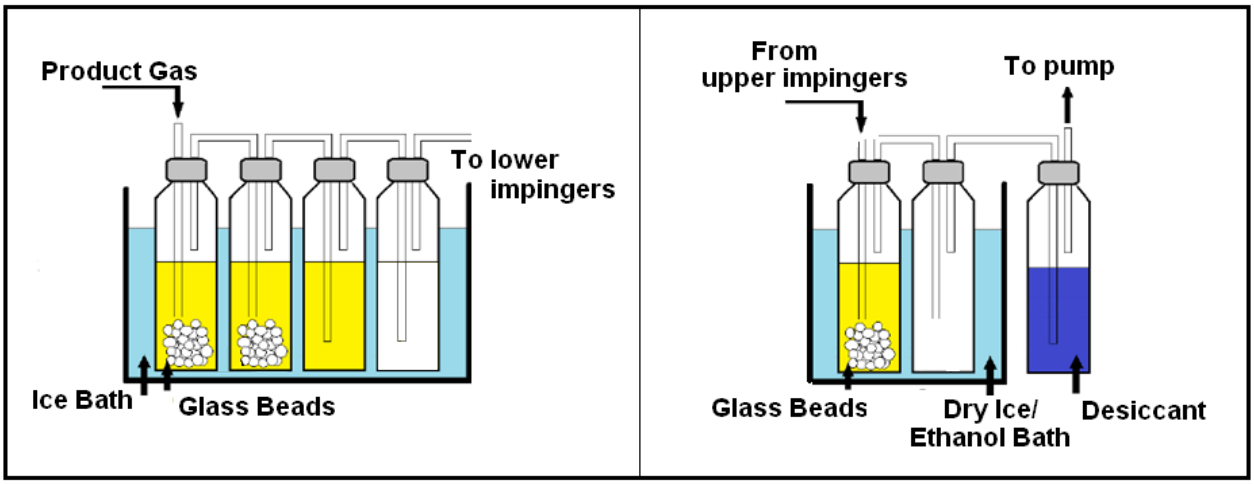

5.1.4 Results

Reactor heaters, lower, middle, and upper reactor, disengagement zone, filter inlet and thermal oxidizer temperatures are shown in Fig. 27. After 12 minutes, biomass was added to the reactor at a rate to ensure complete combustion. Fuel feed rate was then increased to 4.9 kg/h in gasification mode beginning at 20 minutes. At 25 minutes gas sampling was started, continuing through 65 minutes to termination. Fuel feed was stopped at 70 minutes and the heaters were shut off and the system allowed to cool down.

Figure 27: Temperature histories of the system during test at 6/13/2012

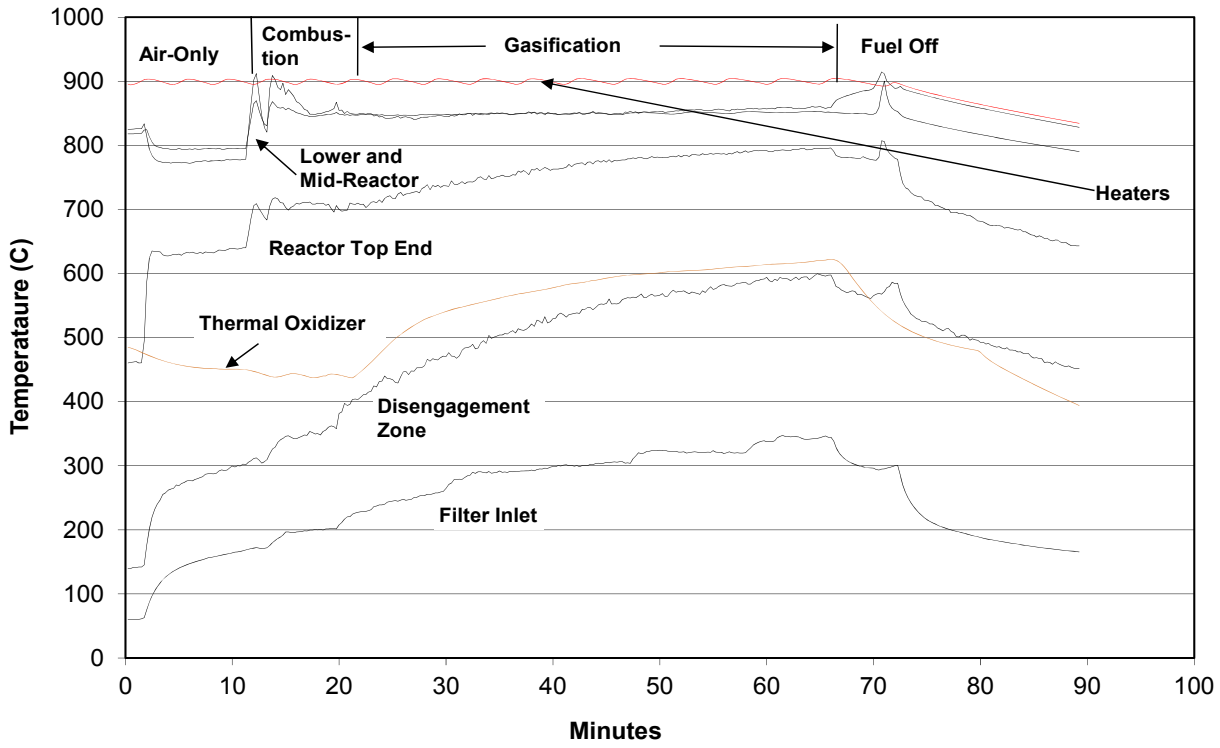

Due to concern for the hot gas filter becoming clogged, gas sampling could not wait for the disengagement zone and hot gas filter to reach a steady-state temperature. Lower reactor temperatures are about 50 degrees cooler than heater settings. Reactor temperature at the transition to the disengagement zone is between 100 and 200 degrees cooler than the heaters. Gas in the disengagement zone is about 250 degrees cooler than peak reactor temperature approaching steady state, and almost 500 degrees cooler prior to feedstock addition.

5.1.5 Tar sampling

Table 9 shows the mass balance (in grams) of the impingers for the tar sampling experiment. 'w/o Solvent' is the weight of the empty impinger without solvent. For impingers with glass beads, this weight includes the weight of the beads. For impinger #7, the desiccant is included in the without-solvent weight. 'w/Solvent' is the weight of the impinger with solvent if added prior to tar sampling. Impingers #4 (empty) and #7 (desiccant) do not have solvent added. 'Final" weight is the resulting weight of the impinger after tar sampling. "Delta' is the difference between "Final" and "w/Solvent", and indicates how much mass was accumulated through tar sampling in each impinger. Overall, 40.9 grams of liquid was accumulated in the impinger train, corresponding to 180.9 g/Nm^3 (0.23 m^3 of gas was sampled over 44 minutes at an average temperature of 25°C corrected to normal temperature and pressure conditions). Final weight includes solids (particulate matter and char), water, and other condensables (including tars).

Table 9: Measured weight (g) of impingers, solvent, and collected liquids.

Impinger	w/o Solvent	w/ Solvent	Final	Delta	Initial solvent wt.
1 W B S	1058.9	1183.7	1198.3	14.6	124.8
2 W B S	1023.7	1133.7	1140.1	6.4	110.0
3 W S	540.0	794.0	795.2	1.2	254.0
4 W (empty)	613.6	613.6	613.9	0.3	0.0
5 E B S	1048.8	1167.9	1174.2	6.3	119.1
6 E S	497.8	752.4	753.5	1.1	254.6
7 D	949.3	949.3	960.3	11.0	0.0
			TOTAL (g)	40.9	862.5
			g/Nm^3	180.9	
W = ice-water, E=dry ice/ethanol, B = beads, S=solvent, D=desiccant					

Gravimetric tar is measured by filtering the collected tars and allowing volatiles to evaporate overnight in the fume hood. Remaining material is considered tar. Table 10 shows the results of taking 3 aliquots (A, B, C) of collected impinger sample per solvent in aluminum cups, setting the cups in the hood overnight, and weighing the change in mass. The results show that remaining tar is about 1 percent of initial mixture for impinger #1, and about 0.1 percent of initial mixture for impinger #2. Impingers #3 and #5+6 have no measurable amount of tar using this method. Total gravimetric tar of the product gas is 8.6 g/Nm^3; with 93 percent of the gravimetric tar being collected in impinger #1 and the remaining gravimetric tar being collected almost entirely in impinger #2.

Table 10: Weights (g) of solvent and tar aliquots before and after air drying

Impinger		A	B	C	average	sd
1	Empty cup	2.05	2.06	2.06	2.06	5.77E-03
	Cup + used solvent	22.29	19.56	19.92	20.59	1.48E+00
	After air drying	2.31	2.29	2.29	2.30	1.15E-02
	Tar	0.26	0.23	0.23	0.24	1.73E-02
	tar fraction	1.28E-02	1.31E-02	1.29E-02	1.30E-02	1.63E-04
2	Empty cup	2.07	2.09	2	2.05	4.73E-02
	cup + used solvent	34.94	31.23	30.83	32.33	2.27E+00
	After air drying	2.11	2.09	2.06	2.09	2.52E-02
	Tar	0.04	0	0.06	0.03	3.06E-02
	tar fraction	1.22E-03	0.00E+00	2.08E-03	1.10E-03	1.05E-03
3	Empty cup	2.03	2.07	2.02	2.04	2.65E-02
	Cup + used solvent	36.2	34.27	31.48	33.98	2.37E+00
	After air drying	2.03	2.07	2.02	2.04	2.65E-02
	Tar	0	0	0	0.00	0.00E+00
4	Not enough liquid	nd	nd	nd	nd	nd
5+6	Empty Cup	2.04	2.01	2	2.02	2.08E-02
	cup + used solvent	35.17	32.42	32.31	33.30	1.62E+00
	After air drying	2.04	2.01	2	2.02	2.08E-02
	tar	0	0	0	0.00	0.00E+00

5.1.6 Composition of tar by GC/MS

The tar-trapping solution was analyzed using GC/MS (Agilent 6850/5975C) equipped with a capillary column (HP5MS) with the following settings: injector split 20:1, inlet temperature 310°C, auxiliary line temperature 310°C, injector volume 1 µL, column flow (helium) 0.8 mL/min. Column temperature program consisted of 5 steps:

1. ramp from 150 to 167°C at rate of 1°C/min
2. ramp from 167 to 180°C at rate of 10°C/min
3. ramp from 180 to 185°C at rate of 1°C/min
4. ramp from 185 to 205°C at rate of 10°C/min
5. ramp from 205 to 265°C at rate of 1°C/min

Samples from impingers #1, #2, #3, and a mix from impingers #5 and #6 were filtered using 0.2 µm syringe filters (Sun SRI Titan2, 42213-NP) and injected into the GC/MS. Sample from impinger #1 was first diluted 1:1 with isopropanol. The EPA Method 610 PAH Mix (Supelco, 4S-8743) standard containing 16 tar compounds was analyzed at the same time for identification and quantification of the tar species included in the standard. Figure 28 shows the chromatogram produced from a sample of impinger #1. One hundred forty-one peaks were observed and 15 of the 16 EPA610 standard tar compounds were identified in the impinger #1 sample.

Figure 28: GC/MS chromatogram of liquid sample from impinger #1.

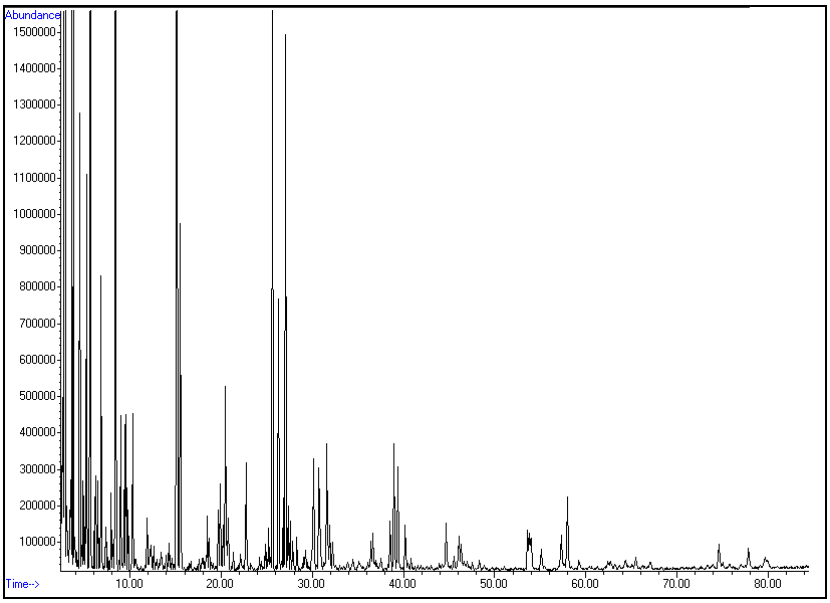

Table 11 shows the results of the GC/MS analysis for impingers #1, #2, #3 and #5+6. The tar compounds in the samples have been identified and quantified using the EPA610 PAH external standard. The concentration of 16 analytes is calculated by multiplying the relative response factor of the analyte in the sample with the known concentration in the standard. Impinger #1 contains 90 percent of the tar collected in all impingers (6655.2 mg/m^3 captured out of total 7392.6 mg/m^3 collected in all impingers combined). 59 percent of the mass of tars collected in impinger #1 are comprised of the compounds present in the EPA610 standard. Impinger #2 collected 7 percent of the total mass of tar (544.6 mg/m^3 captured out of the total 7392.6 mg/m^3). Impingers #5+6 collected 2.3 percent and impinger #3 collected 0.7 percent of the total mass of tar. Overall, naphthalene accounts for 32 percent of the total tar collected. The larger amount of tar collected in impingers #5+6 compared to impinger #3 is due to the lower solvent temperature. Figure 29 shows the concentration of each analyte collected in impinger #1, #2, #3, #5+6, and total of all impingers on a log scale.

Table 11: Analysis of the liquid from impingers 1, 2, 3 and 5+6

	Impinger 1	Impinger 2	Impinger 3	Impinger 5+6	Total
Naphthalene, mg/Nm^3	2328.3	55.7	0.0	0.0	2384.0
Acenaphthylene, mg/Nm^3	42.0	52.3	4.4	4.7	103.3
Acenaphthene, mg/Nm^3	0.0	0.0	0.0	0.0	0.0
Fluorene, mg/Nm^3	302.8	29.2	0.0	4.5	336.4
Antracene, mg/Nm^3	428.6	43.0	2.2	7.2	481.1
Phenanthrene, mg/Nm^3	164.8	17.3	0.0	0.0	182.1
Fluoranthene, mg/Nm^3	174.0	19.8	2.0	9.5	205.3
Pyrene, mg/Nm^3	178.3	24.2	0.9	0.0	203.4
Benz[a]anthracene, mg/Nm^3	65.8	6.3	0.0	0.0	72.1
Chrysene, mg/Nm^3	60.7	5.9	0.0	0.0	66.6
Benzo[b]fluranthene, mg/Nm^3	38.5	3.8	0.0	0.0	42.3
Benzo[k]fluroanthene, mg/Nm^3	43.0	4.5	0.0	0.0	47.5
Benzo[a]pyrene, mg/Nm^3	55.0	6.1	0.0	0.0	61.1
Benzo[ghi]perlyene, mg/Nm^3	48.2	4.8	0.0	0.0	53.0
Indeno91,2,3-cd]pyrene, mg/Nm^3	2.3	0.0	0.0	0.0	2.3
Dibenz[a,h]anthracene, mg/Nm^3	22.0	2.9	0.0	0.0	24.9
Total (standards), mg/Nm^3	3954.3	275.8	9.6	25.8	4265.6
Total unknown, mg/Nm^3	2700.8	268.8	8.2	149.2	3127.1
% known	59.4	50.6	53.7	14.8	57.7
# of compounds	143.4	89.5	9.2	21.4	
				Total Tar (known + unknown), mg/Nm^3	7392.6

Figure 29: GC/MS analysis of collected impinger liquids using EPA610 standard (concentrations on log scale).

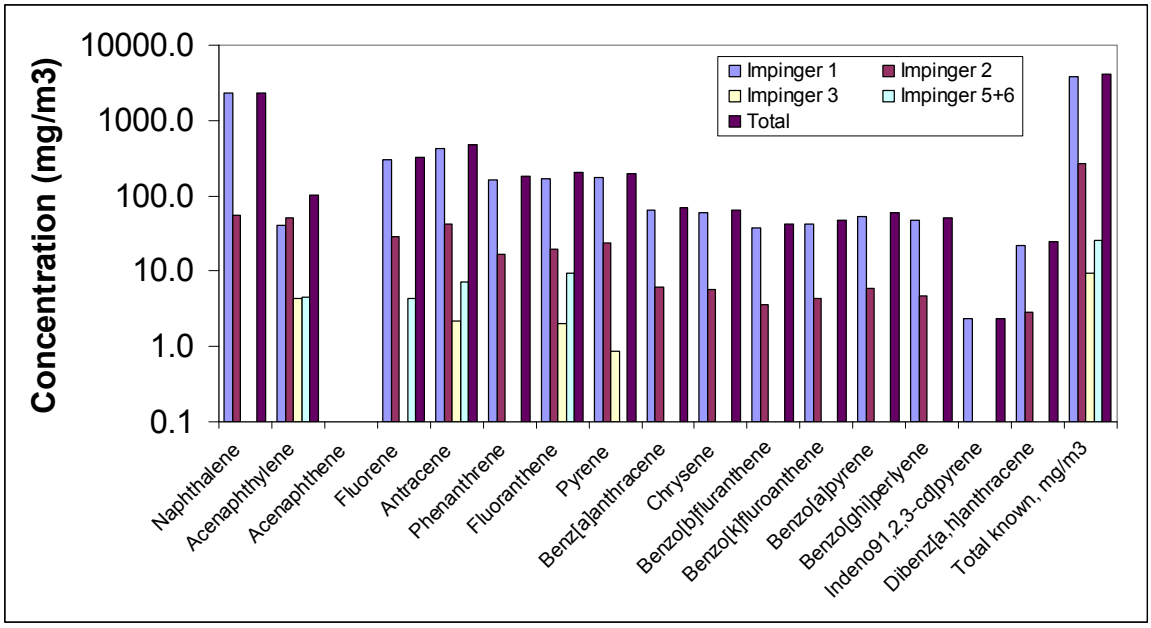

5.2 Conclusions

The laboratory scale gasifier was run successfully using air and Douglas fir woodchips at reactor temperatures between 725 and 850°C. Tar was sampled during the run using cold impingers and gravimetric tar concentration was measured using air dry method to be 8.6 g/Nm^3. Using GC/MS to analyze the collected tar samples, tar concentration of 16 compounds could be measured using an external standard. The mass of the identified compounds made up 58 percent of the total tar mass, and the mass of naphthalene made up 32 percent of the total tar collected. The results of this test form a baseline for assessing the performance of new operating conditions and future gas purification testing.

Chapter 6:
Task 2.1.5 Pilot gas purification system design

West Biofuels, LLC has designed, built and installed an allothermal gasifier based on a design by Kunii (i.e., dual fluid bed reactors, including the allothermal gasifier and a combustor which circulate bed media between them for heat transfer to the gasifier and char transfer to the combustor). Figure 30 is a simple schematic of the dual fluidized-bed allothermal gasifier.

Figure 30: Dual reactor allothermal gasifier schematic (Boerrigter et al., 2006)

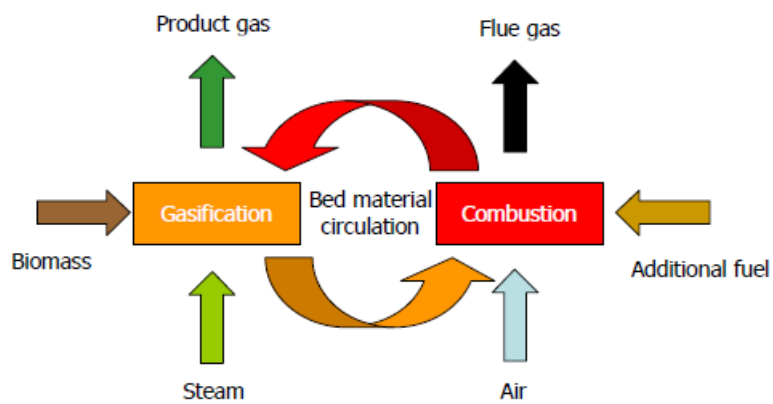

The product gas is principally CO, H_2, CH_4, lighter hydrocarbons, H_2O, CO_2, particulate matter (PM), tar, alkali vapors, nitrogen and sulfur compounds. Product gas from autothermal air-blown gasification usually contains significant amounts of CO_2 and N_2. Gasification processes also produce liquids (tars, oils, and other condensates) and solids (char, ash) from solid feedstocks.

Gas cleaning to remove tars, PM, sulfur and nitrogen compounds, acid gases and other impurities from biomass producer gas is usually necessary before utilization. The degree of gas cleaning depends on the application. Direct firing of producer gas may require little or no gas cleaning or conditioning while converting synthesis gas into liquid products, for example through a Fischer-Tropsch (FT) process, requires robust cleaning and possibly conditioning/reforming or shifting. Gas quality requirements for use in rotating or reciprocating internal combustion (IC) engines is less stringent than FT applications but more than direct firing in boilers or heaters.

6.1 Gas Cleaning Design at West Biofuels

At the beginning of this project, discussions were held with West Biofuels about the pilot reactor gas cleaning system. However, the pilot project had been in place for some time with private funding and the gasifier and gas cleaning system designs were, for the most part settled with many components already fabricated and installed, so not all recommendations for system design were incorporated.

6.1.1 Initial gas cleaning system configuration

The initial gasifier and gas cleaning system is shown schematically in Fig. 31. On the right are the two fluidized bed reactors, the gasifier and the combustor, connected by bed circulation tubes that cross each other as they move material from one reactor to the other.

Combustion exhaust gas flows out the right-most portion of Fig. 31 and into an exhaust gas cleanup apparatus (not shown) that includes a bag house for particulate matter (PM) control. The product gas cleaning system is the left portion of the figure and consists of a flow-reversing impingement or "knockout" vessel, two packed-bed liquid scrubbers.

The product gas flows from the top of the gasifier reactor into the cone-shaped particle "knockout" vessel. The knockout vessel is not a cyclone but has a vertical interior baffle to force gas flow down into the vessel before reversing direction to travel to the gas exit near the top. Gravity and the gas flow reversal cause larger particles to disengage from the flow and collect on the bottom where they are removed. After the knockout vessel, gas flows to the bottom of the first liquid scrubber. The scrubbers are loaded with random packings of Pall rings (Pall Corporation, Port Washington, NY, Fig. 32).

Figure 31: Initial Gas Cleaning Configuration

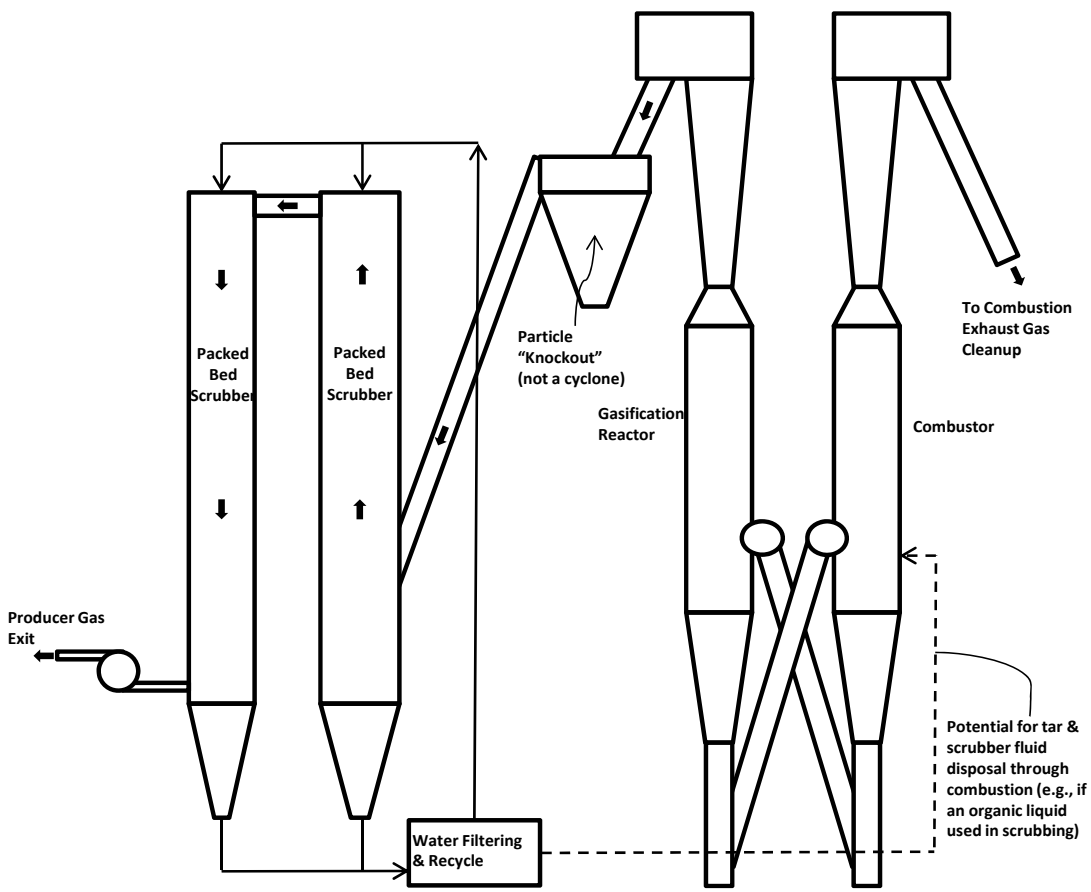

Figure 32: Typical Pall ring used in random packings (Ningbo T.C.I. Co., LTD).

The Pall rings provide a large surface area for the gas-liquid interface over which mass transfer can occur. The product gas flows upward through the first scrubber while scrubber liquid trickles down through the packing (counter-current gas-liquid flow). In the initial design, gas exited the top of the first scrubber and entered the top of the second scrubber and flowed downward with the scrubber liquid (co-current).The gas exited the bottom of the second packed bed scrubber, was pumped through a fan and exited the building to a flare or engine.

Liquid leaving the scrubbers is collected, filtered and returned to the top of the scrubbers. Initial plans called for using organic liquids, such as biodiesel, for the scrubber solvent and then recycling sludge and tar saturated liquid to the combustor reactor for disposal and energy. This has not yet been implemented because the combination of hot product gas and flammable scrubbing liquid require further safety measures.

6.1.2 Current gas cleaning system configuration

After experience with operating the gasifier system, several modifications have been made to the gas cleaning system (Fig. 33). In the current gas cleaning configuration, the PM knockout cone was removed and replaced with a straight section of refractory lined (internally insulated) pipe. The knockout was removed because it was not refractory lined and became too hot during operation. Because the insulated new section of pipe did not extend all the way to the scrubber, water injection was added to the non-insulated pipe section leading into the scrubber to keep the metal at a safe temperature (Fig. 33). Gas piping was reconfigured to place the second packed bed scrubber in counter-current flow like the first scrubber. A charcoal filter was added after the second packed-bed liquid scrubber (Fig. 33) to absorb some of the lighter tar compounds that were not removed in the scrubbers.

Finally, a heat exchanger was added for cooling scrubber liquid before it is pumped back to the top of the scrubbers. Incoming gas temperature was generally higher after removing the particle knockout vessel and insulating a portion of the scrubber inlet pipe which led to increased liquid temperature and vapor pressure during operation.

The overall height of the scrubbers is 7.4 m. The first scrubber has an internal diameter (ID) of 0.9 m and the second scrubber 0.7 m. The charcoal filter is 1.9 m long and 0.38 m diameter.

Additional clean-up devices were added before the gas entered the Waukesha spark-ignition (SI) engine. A tube–in-shell heat exchanger was added in which the producer gas is cooled to near ambient temperature condensing some remaining tars and water vapor. An aerosol "knock-out" tank follows (0.6 m diameter by 1.6 m tall. Finally, the gas is passed through fabric

filter elements (approximately 100 micron) in 0.46 m diameter by 1.8 m tall filter housings (Fig. 34)

Figure 33: Current Gas Cleaning Configuration

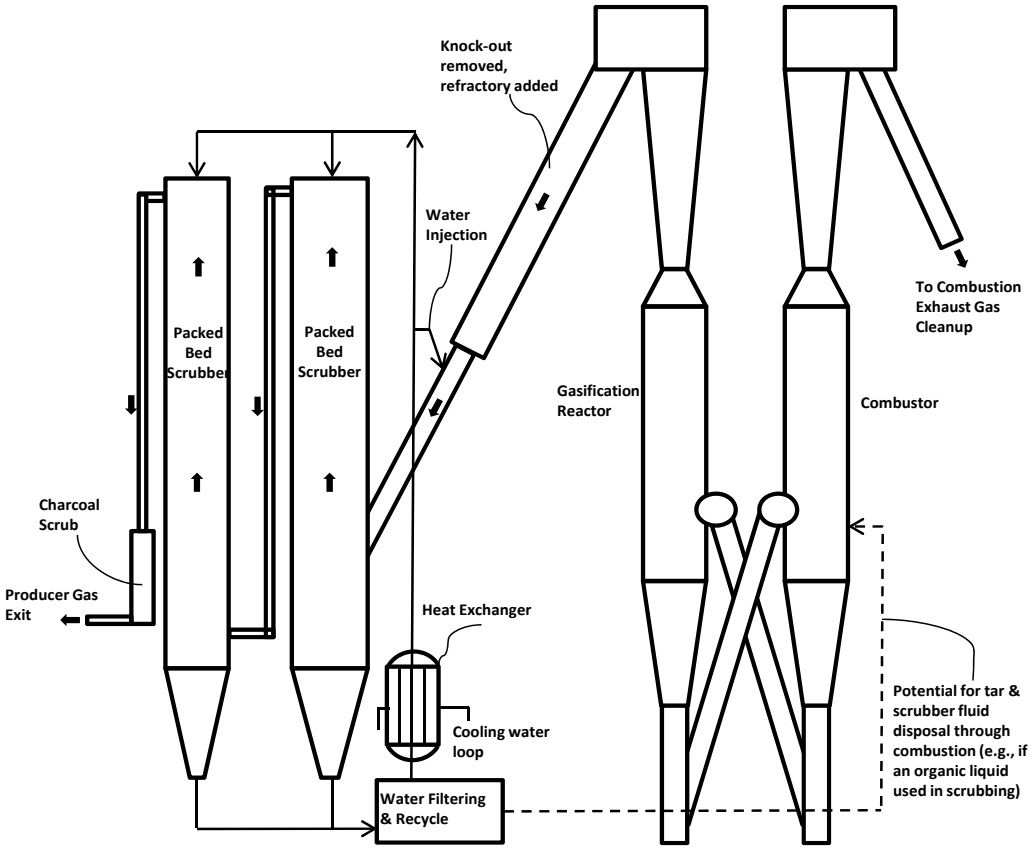

Figure 34: Drop out tank and gas filters

6.1.3 Recommended gas cleaning system configuration

The recommended gas cleaning configuration included devices for PM removal, an initial packed bed scrubber using biodiesel (or other organic liquid) as the solvent followed by a scrubber using chilled water as the solvent. Also included was cooling for the biodiesel solvent and sludge/saturated organic solvent disposal in the combustor (Fig. 35).

The components for reducing PM in the gas flow include a refractory lined cyclone with particle return to the gasifier (or potentially to the combustor side, if pressure and flows could be balanced). The cyclone which removes larger particles, would be followed by a hot gas filter composed of a number of ceramic "candle" filters (Fig. 35). Improving PM removal before the gas is subject to liquid scrubbing, reduces problems with scrubber liquid handling, sludge production and, likely improves scrubber effectiveness.

The chilled-water packed-bed scrubber is to reduce gas temperature to further remove water vapor and lighter tars. The saturated liquid from this system would need onsite treatment and possibly disposal of the concentrate if it cannot be dewatered sufficiently for disposal through the combustor.

Figure 35: Example for Recommended Gas Cleaning Configuration

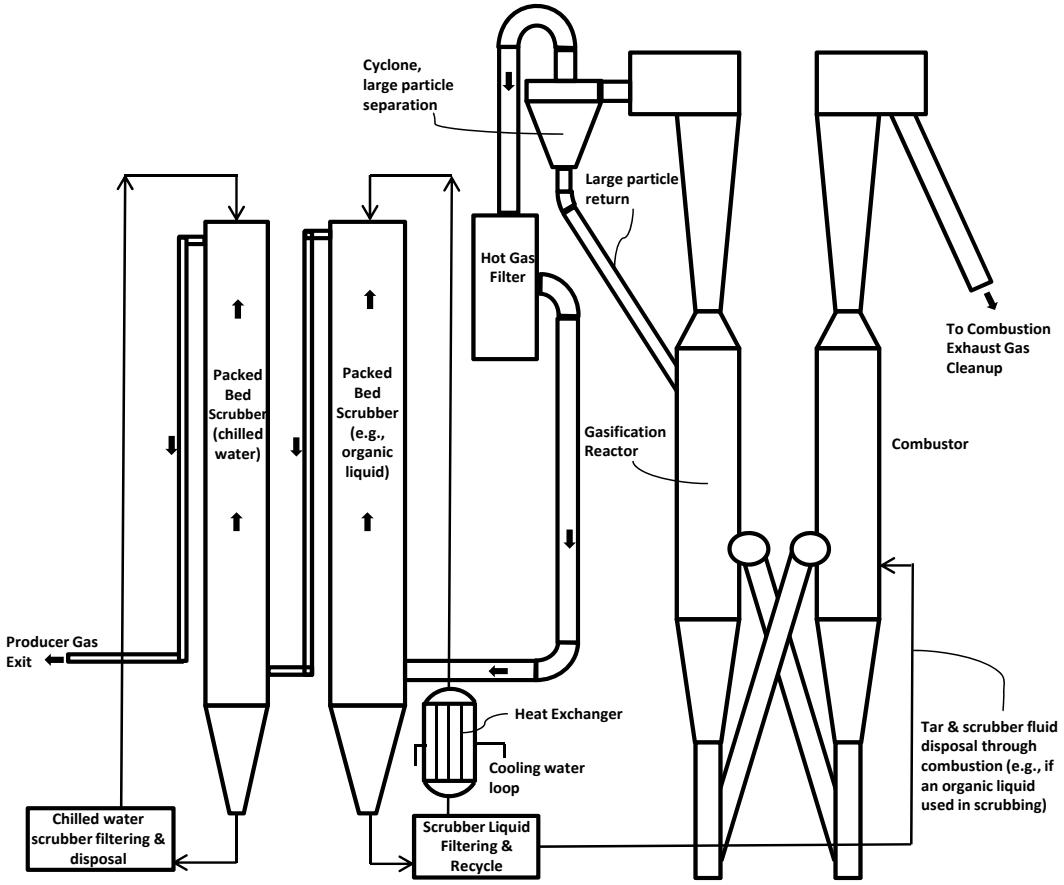

6.1.4 Conclusions

The gas cleaning system for the West Biofuels pilot plant has evolved from the initial installation including removal of the partially effective PM knockout device, thereby forcing all

PM removal to occur in the liquid scrubbers leading to significant sludge/slurry production in the scrubber circuit. Addition of scrubber liquid cooling and enhanced filtering/sludge removal, rearranging flow of the second packed-bed scrubber, and addition of a charcoal based scrubber have been implemented to improve overall effectiveness.

A recommended gas cleaning design includes a PM removal system specifically designed for the system gas flow and temperature and consisting of a cyclone followed by a ceramic candle filter module. Also included is a chilled solvent packed-bed scrubber for final drying and light tar removal. As with the initial design, the first packed bed scrubber is recommended to use an organic solvent (e.g., biodiesel) to better enable disposal through the combustor.

Chapter 7:
Task 2.1.6 Pilot Gas Purification Monitoring Plan

Gasification is a thermochemical process that converts carbonaceous material into gaseous fuel by partial oxidation. The product gas in its crude, unprocessed form is principally composed of CO, H_2, CH_4, lighter hydrocarbons, H_2O, particulate matter (PM), tar, alkali vapors, nitrogen and sulfur compounds, and depending on the process used, can contain significant amounts of CO_2 and N_2. The combustion of gasification derived fuel gases generates the same categories of products as direct combustion of solids, but pollution control and conversion efficiencies may be improved. Direct firing of producer or synthesis gas may require little or no gas cleaning or conditioning. Converting synthesis gas into liquid products, for example through a Fischer-Tropsch (FT) process, requires robust cleaning and possibly conditioning, shifting, or other upgrading. Gas cleaning requirements for firing in reciprocating or rotating internal combustion (IC) engines is less stringent than FT applications but more than direct firing in boilers or heaters. Table 12 shows syngas quality requirements for several end-use applications.

Table 12: End use gas quality requirements

Impurity	Units	Reciprocating Engine	Gas Turbines	Chemical and F-T synthesis
Particles	mg/Nm3	<50	<30	<0.02
Particle size	µm	<10	<5	-
Tar	mg/Nm3	<100	0.5-5 (or below dewpoint)	below dewpoint
Alkali metals	-	-	0.24 mg/Nm3	< 10 ppbV

Sources: (Stassen 1993; Milne, Evans et al. 1998; Bergman, van Paasen et al. 2003)

One of the biggest problems in biomass gasification is tar removal (Devi, 2003; Kiel, 2002; Milne et al, 1998, Scahill 2009, Bergmann et al, 2002). While a precise definition of tar is lacking, tar generally contains a complex mixture of condensable hydrocarbons including single-ring to 5-ring aromatic compounds with other oxygen-containing hydrocarbons and complex polycyclic aromatic hydrocarbons. Tar compounds are formed as vapors at gasifier reaction temperatures but begin to condense below 400°C. The condensed tars will be present as deposits on the walls of the piping, interior surfaces of the appliance, and as an aerosol in the gas. Tars are troublesome as they reduce engine life, foul catalysts, clog valves and cause multiple problems in the downstream utilization of the product gas. Tars can embody a significant fraction of energy in the product gas stream that would be unavailable for syngas conversion to fuels or chemicals (unless the tar is reformed or its production is minimized by reactor design and operation).

Gas monitoring is a critical component of a research facility studying the effects that feedstock, operating conditions, and bed materials have on gas quality and composition. To monitor the effects of system changes and varying operating conditions, this report documents the instrumentation necessary to measure the pilot plant gas purification system performance.

7.1 Tar and PM

The primary purpose of West Biofuel's pilot gas purification system is the removal of tars and solids from the product gas stream. Tars foul equipment downstream of the gasifier, coat surfaces, and enter pores of filters; and clog or plug flow passages. The two basic approaches for tar removal are physical removal of tar using techniques similar to particle removal, and catalytic and thermal tar cracking.

Particulate matter refers to both liquid and solid-phase particles entrained in a gas stream. Particulate matter can be composed of the inorganic matter in the feedstock, unconverted biomass (including char), condensed liquid droplets suspended in the gas stream and, in the case of fluidized bed reactors, material from the gasifier bed. Circulating and bubbling fluidized-bed gasifiers typically produce high PM loading requiring particle removal from the gas stream (Stevens, 2001). Removal of particulate matter is critical to preserving the downstream gas cleaning components and/or the appliance from fouling or early failure (Boerrigter, 2005). The proximate analysis of selected biomass feedstock is shown in Table 13. Mineral matter from soil due to feedstock handling (adventitious material) may also contribute to ash based PM in the product gas (Stevens, 2001).

Char is another source of PM and is formed when feedstock is incompletely gasified. These particles can exit the gasifier before becoming completely gasified, particularly in gasifiers with turbulent beds. As partially converted biomass, char also contributes to lower conversion efficiencies but in some cases may be deliberately produced as a biochar product for the purposes of carbon sequestration, soil amendment, or other applications. Collection of char and re-injection into the gasifier can increase overall gasification efficiency. Refer to Task Report 2.1.1 for more details on tar, PM, and removal strategies.

Table 13: Proximate analysis of biomass materials (% dry fuel) (Jenkins et al, 1998)

	fixed carbon	volatile matter	Ash
alfalfa stems	15.81	78.92	5.27
wheat straw	17.71	75.27	7.02
rice hulls	16.22	63.52	20.26
rice straw	15.86	65.47	18.67
switch grass	14.34	76.69	8.97
sugar cane bagasse	11.95	85.61	2.44
willow wood	16.07	82.22	1.71
hybrid poplar	12.49	84.81	2.7

*Fixed carbon computed as difference between 100 percent and percent volatile matter and ash

7.2 Gas Purification System

The gas purification system may begin as far upstream as with the feedstock production or pretreatment, but generally begins in the gasifier. As discussed above, PM and tar generation is reduced when using a clean, low-ash feedstock and proper operating conditions are maintained. Use of steam and recycled product gas for fluidization reduces nitrogen dilution and the use of steam also increases hydrogen production. The operating procedure for the West Biofuel gasifier targets a steady-state temperature between 820 and 850°C for efficient gas production and reduced tar generation. Additionally, use of oxygen injection above the gasifier bed (partial oxidation) aids in immediate tar destruction as tar compounds are converted to permanent gases.

Figure 36 shows the locations of inlet ports to the West Biofuels dual fluidized-bed reactor and flow direction of gas and recirculating bed-material streams. Gasification occurs in the left reactor by mixing biomass and steam to a hot fluidized bed of inert bed material. Product gas is produced during the process and exits the top of the reactor with the steam. Gravity moves bed material and char from the gasifier reactor through the crossover arm to the combustor fluidized-bed reactor. The fluidized-bed reactor (right reactor in Fig. 36) uses blown air to combust char and heat the bed material. The exit stream from the combustor side of the reactor is principally carbon dioxide, water, and ash, although other products typically produced by combustion are also present. There is a second gravity fed crossover arm to return hot bed material to the gasifier side. The recirculating action of the bed material and the char is the key to the operation of the dual fluidized bed reactor. Due to separation of combustion and gasification processes, the dual fluidized-bed gasifier has the advantage of producing a higher calorific product gas that is relatively free of diluting nitrogen gas.

The gasifier reactor has a bottom steam port, recycle gas port in the cone section, and oxygen/steam port in the top section of the reactor. This system allows a lot of flexibility in fluidizing the dual-bed reactor, including studying the effects of steam gasification, recycling product gas for reduced steam and nitrogen fluidization, and secondary injection of oxygen/air above the gasifier bed (partial oxidation). Steam gasification has the benefit of increasing the heating value and H_2-content of a product gas compared to air-blown gasification. However, tar content in the produced gas is likely to also increase (Gil et al, 1999). Partial oxidation above the gasifier bed should reduce tar concentration exiting the gasifier. The flexibility of re-injecting product gas into the gasifier reactor reduces the need for using as much steam, reducing the required steam pressure and size of the boiler, as well as reducing the condensate collected in the scrubber that would need disposal.

Figure 36: Directional flow and inlet ports of the dual fluidized bed reactor

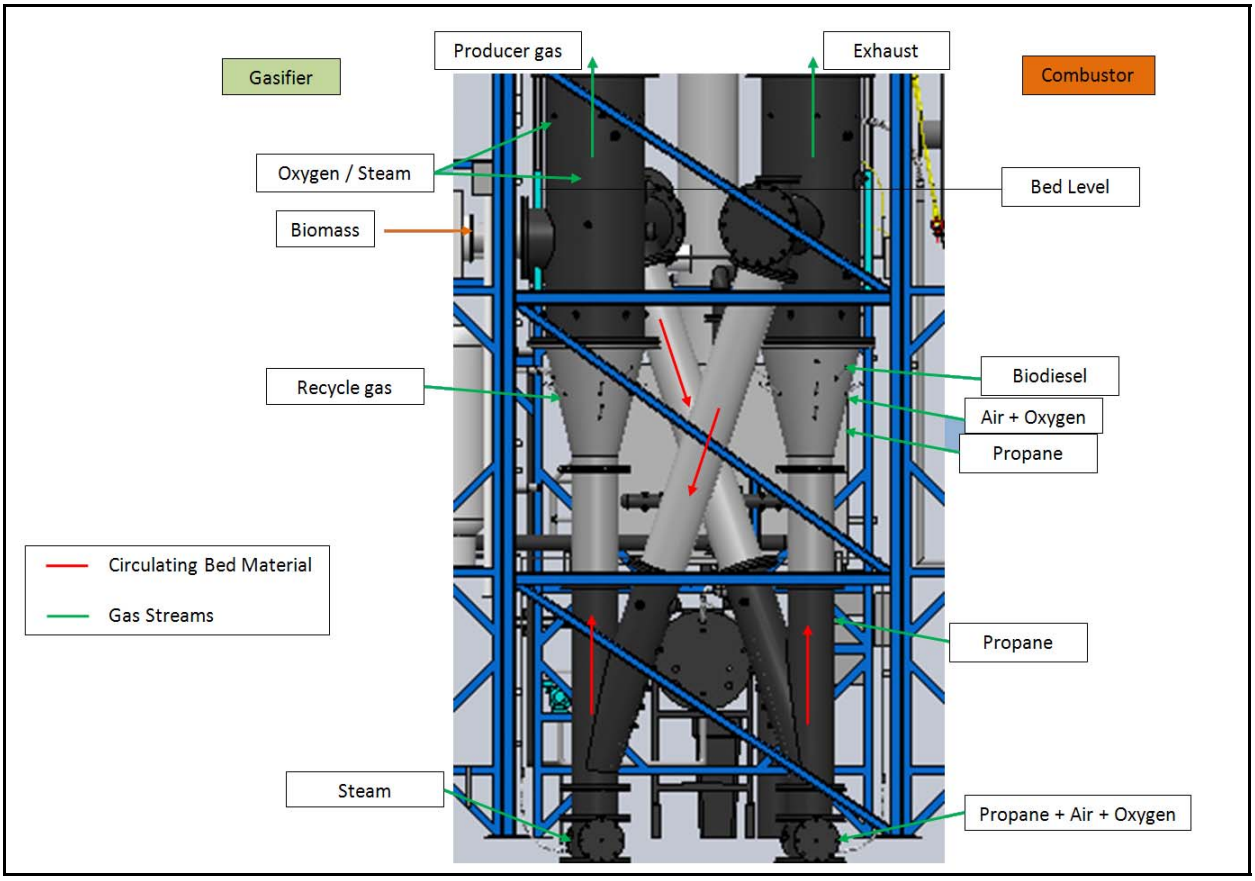

The right-side combustor reactor has a bottom port for propane, air, and oxygen; a lower section port for propane; and ports in the cone section for propane, air and oxygen, and biodiesel. The main purpose of the combustor is to heat the bed material to ensure gasification processes are maintained at a controlled temperature. In addition, biodiesel can be used to aid in the heating of the reactors. In the future, the water used in the wet scrubbers may be replaced with biodiesel as biodiesel may have better tar absorbency properties. Once the used biodiesel becomes saturated with tar it can be recycled for destruction within the combustor reactor. Using biodiesel instead of water as the solvent in the wet scrubbers will eliminate a wastewater problem.

West Biofuel's gas purification system attempts to remove tar and particulate matter using physical techniques. The purification system consists of two water scrubbers, a charcoal filter, a gas cooler heat-exchanger, a knock-out tank, and filter chamber. Product gas travels through each component of the cleaning system before entering the engine (Fig. 37). Details of the gas cleaning system are described in the Task 2.1.5 report.

Figure 37: West Biofuels dual-fluidized bed gasifier and purification system.

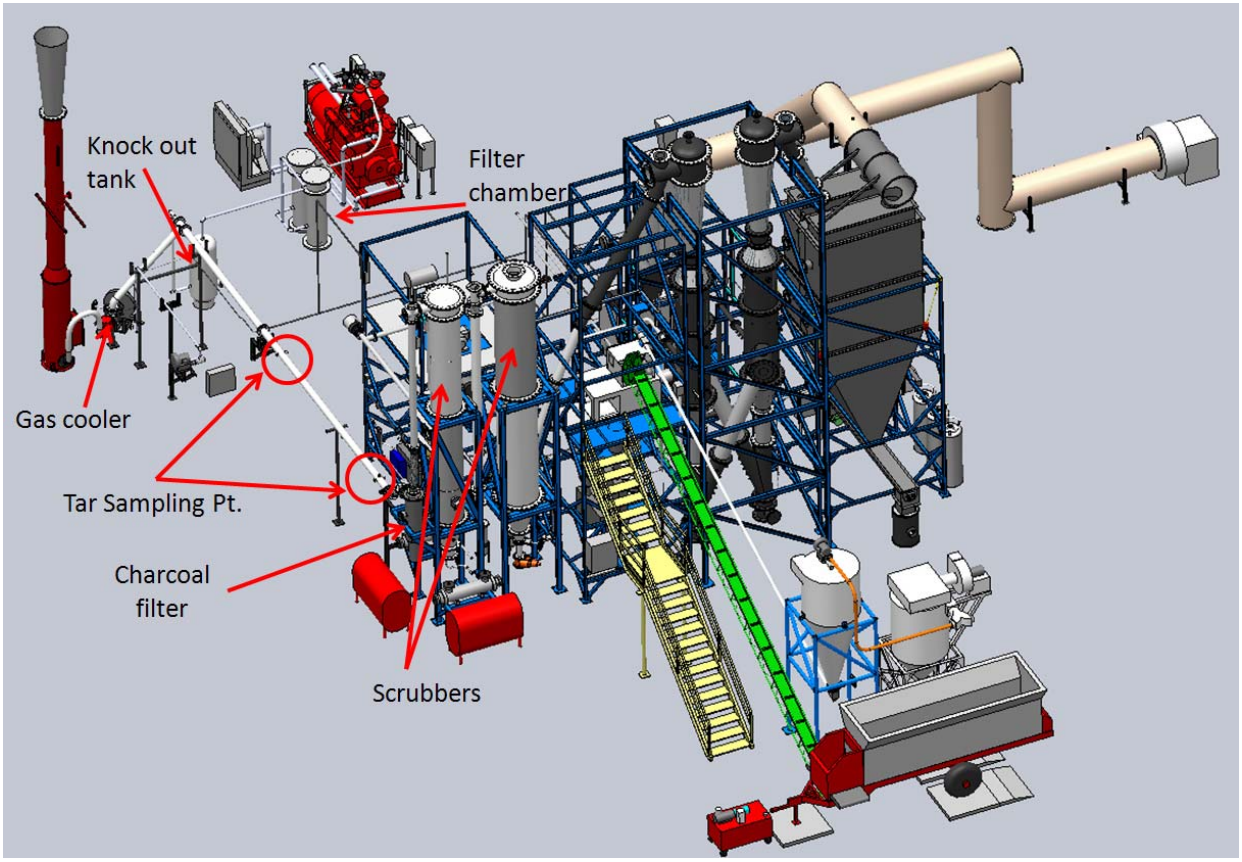

7.2.1 System Monitoring

Gasification products are a function of biomass feedstock composition and flow rate, reacting agent types and flow rates, temperature, pressure, and residence time. All of these parameters vary spatially and temporally throughout the system. A monitoring system is necessary to ensure processes operate within design boundaries and equipment is maintained within specifications. Temperature, pressure, and flows are measured through the system (Fig. 38).

Gases are monitored continuously at the exit of the charcoal filter using both Fourier transform infrared spectroscopy (FTIR) and gas chromatography (GC) systems. The FTIR gas analyzer broadcasts an infrared beam of variable frequencies and measures the spectrum absorbed by the gas stream. Each compound produces a unique infrared absorption spectrum. In addition, the size of the peaks in the spectrum is a direct indication of the amount of material present. The infrared absorption spectrum obtained can be used to identify and quantify the material present. West Biofuels uses a MKS MultiGas 2030 FTIR instrument (MKS Instruments, Andover, MA) to measure CO_2, H_2O, CO, CH_4, and NO species.

Gas chromatography is a separation technology that uses both a mobile phase and a stationary phase. The mobile phase is usually an inert carrier gas, for example helium. The stationary phase is a microscopic layer of liquid or polymer on an inert solid support. The exact stationary phase is selected based on the compounds being analyzed. The gaseous analytes interact to varying degrees with the stationary phase in the column. This separates the compounds causing them to elute at different times. The column is placed within an oven where the

temperature and therefore retention time of the analytes can be controlled. After compounds have been separated using the GC, identification and quantification is performed using a detector (e.g. mass spectrometer (MS), thermal conductivity detector (TCD), or flame ionization detector (FID)). An Agilent 3000 MicroGC (Agilent Technologies, Santa Clara, CA) is used to identify and quantify the compounds listed in Table 14. A gas sample from the gas sampling system (Fig. 39) can be analyzed every 15 minutes using the GC.

Figure 38: Thermocouple, pressure transducer, and flow meter locations within the system.

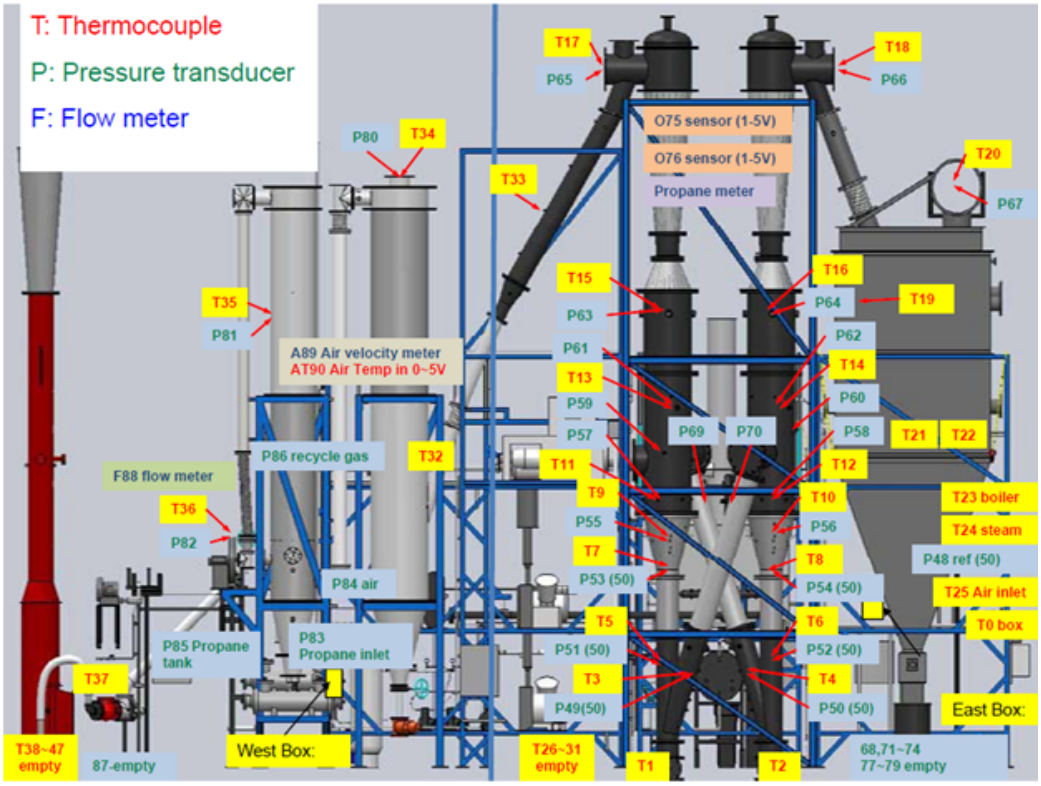

Figure 39: Gas sampling locations at West Biofuels

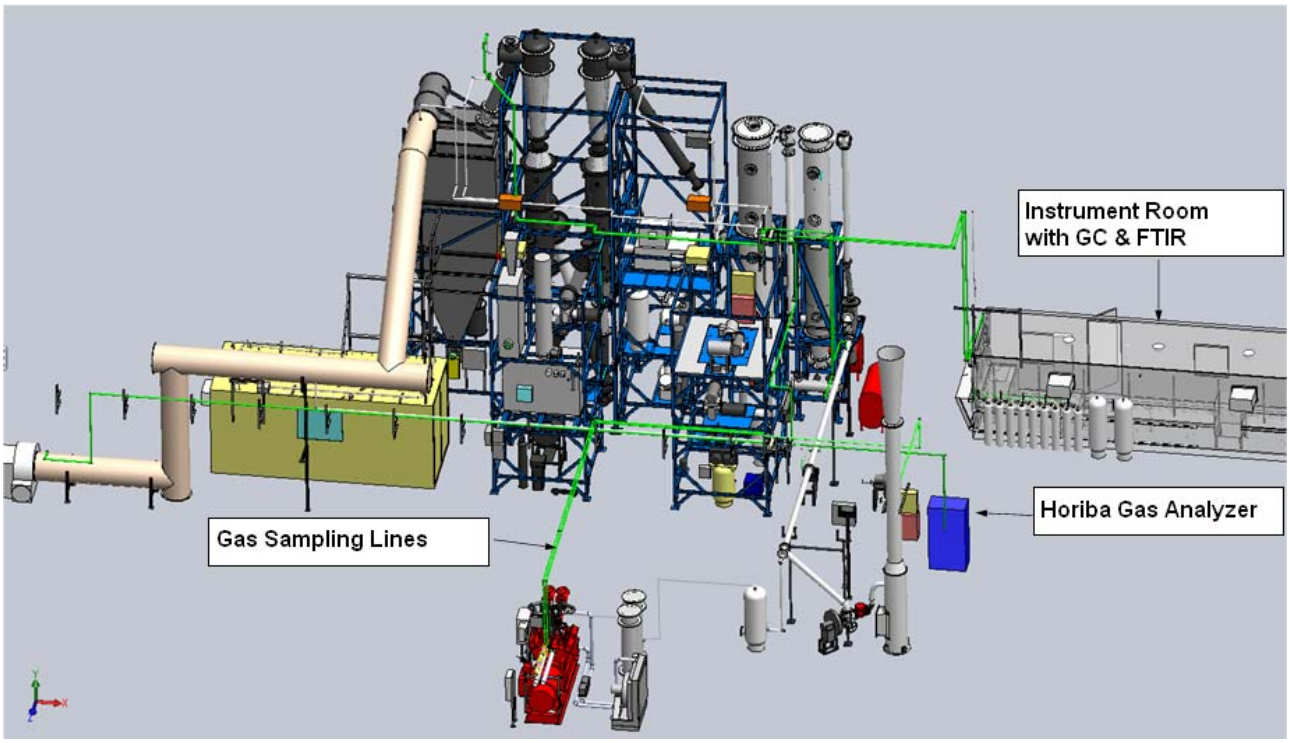

Table 14: List of chemical compounds identified and quantified using Agilent 3000 MicroGC

1	Neon + Helium	17	Propadiene	33	Cyclopentene
2	Hydrogen	18	Propyne	34	Hexene
3	Oxygen	19	Methanol	35	Hexane
4	Nitrogen	20	Acetaldehyde	36	Isobutanol
5	Methane	21	Butene	37	Butanol
6	Carbon Monoxide	22	Butadiene	38	Benzene
7	Carbon Dioxide	23	Butane	39	Heptene
8	Ethylene	24	Propionaldehyde	40	Heptane
9	Ethane	25	Acetone	41	Toluene
10	Acetylene	26	Ethanol	42	Xylene
11	Formaldehyde	27	Acetone	43	Styrene
12	Ethylene + Acetylene	28	Isopropanol	44	Octene

13	Hydrogen Sulfide	29	Propionaldehyde	45	Octane
14	Water	30	Pentene	46	Nonene
15	Propylene	31	Cyclopentadiene	47	Decane
16	Propane	32	Propanol		

7.2.2 Tar Sampling

Brage, et al. (1997) has developed an efficient method of tar sampling that can considerably reduce sample time compared to conventional cold trapping methods (e.g. EU method). Brage's method is suitable for intermittent trapping of tar compounds ranging from benzene to coronene. The faster sampling step allows collection of one to three samples per minute, compared with one or two samples per hour using conventional cold trapping techniques, allowing for observation of transient changes in tar concentrations.

Procedures for tar sampling using the impinger method and for using solid phase adsorption cartridges are detailed in Task report 2.1.3. Until correlations between solid phase adsorption tar concentrations and impinger cold trappings can be established, tar samples are collected using both tar sampling methods before and after the scrubber systems, as the scrubbers are the primary tar removal system. In addition, solid phase absorption methods can be used to estimate tar removal effectiveness of the charcoal filter, the knock-out tank, and the filter chambers.

Steady-state operation of the dual-bed reactor will be determined by monitoring reactor temperatures and gas composition sampled after the charcoal filter using the FTIR gas analyzer. Once steady-state has been reached, EU tar sampling can begin. During the 1 hour sampling time for the EU method, at least 2 or 3 SPE samples will be taken at each sampling location (i.e. before scrubber, after scrubber/before charcoal filter, and after charcoal filter). In addition, the GC gas analyzer will sample gas after the charcoal filter. After all SPE, GC, and EU samples have been collected, the gasifier and purification systems can be adjusted to new operating conditions. Once steady-state operation is regained, new samples can be taken. In this way multiple experiments can be conducted during a single run.

7.3 Monitoring Plan Objectives

The goal of this task is to develop a test plan for monitoring the performance of the pilot gas purification system over a range of gasification conditions. The main objective of the gasification and purification system is to develop a steady state, energy rich, low tar concentration, low PM content synthesis gas for electricity generated by an internal combustion engine. The specific objectives are to:

1) Identify conditions necessary for dual-bed fluidization that avoid excess slugging and loss of bed material.
2) Identify start up procedure and operating conditions to generate sufficient heat for efficient gasification (~850°C).
3) Identify gasifier and purification system conditions that lead to a low tar, low PM product gas.
4) Identify operating conditions that lead to an energy-rich syngas.
5) Identify operating conditions for use with tar-laden biodiesel recycle

    a. Initial testing with clean biodiesel
6) Test injection of air/oxygen above the gasifier bed for tar reduction effects (i.e. partial oxidation)
7) Identify operating conditions for steam gasification
    a. Initial testing with steam-recycled gas mixtures
8) Test use of catalytic bed materials for tar reduction
9) Test other feedstocks

Task 2.1.7 will report each run's improvement towards the above objectives in addition to the resulting gas composition, tar content, energy content of the gas, and if the engine was able to run on the gas produced.

Chapter 8:
Task 2.1.7 Monitoring Pilot Gas Purification System Performance

The goal of this task was to monitor the performance of the pilot gas purification system over a range of gasification conditions. Ideally, the result of the work produces a steady-state, energy-rich, low tar-concentration, low PM-content synthesis gas for electricity generation using an internal combustion engine. Following the monitoring plan created in Task 2.1.6, this report presents findings in accomplishing the following objectives:

1. Identify conditions necessary for dual-bed fluidization that avoid excess slugging and loss of bed material.
2. Identify start up procedure and operating conditions to generate sufficient heat for efficient gasification (~850 C).
3. Identify gasifier and purification system conditions that lead to a low tar, low PM product gas.
4. Identify operating conditions that lead to an energy-rich syngas.
5. Identify operating conditions for use with tar-laden biodiesel recycle
    - Initial testing with clean biodiesel
6. Test injection of air/oxygen above the gasifier bed for tar reduction effects (i.e. partial oxidation)
7. Identify operating conditions for steam gasification
    - Initial testing with steam-recycled gas mixtures
8. Test use of catalytic bed materials for tar reduction
9. Test other feedstocks

The pilot gas purification system described in Task 2.1.5 was developed and evaluated through gasification experiments performed using the West Biofuel's 5-ton per day gasification and clean-up system, which initially consisted of a dual fluidized-bed gasifier and two packed-bed water scrubbers (Fig. 40). The gas stream exiting the clean-up system is fed to the inlet of the engine and flare system for electricity generation and destruction. Initially, tests were focused on optimizing operating parameters for efficient fluidization and providing enough heat to the system to ensure high conversion efficiency and low tar generation. Later tests attempted to improve product gas energy content and reduce tar entering the engine. The main mechanism for improving energy content of the product gas was to reduce N_2 content in the gas by fluidizing the dual bed reactor with syngas and steam. Gas and tar composition was measured using the equipment and analytical techniques described in Task 2.1.6.

Figure 40: Dual bed reactor and gas cleaning system on 4/8/2010

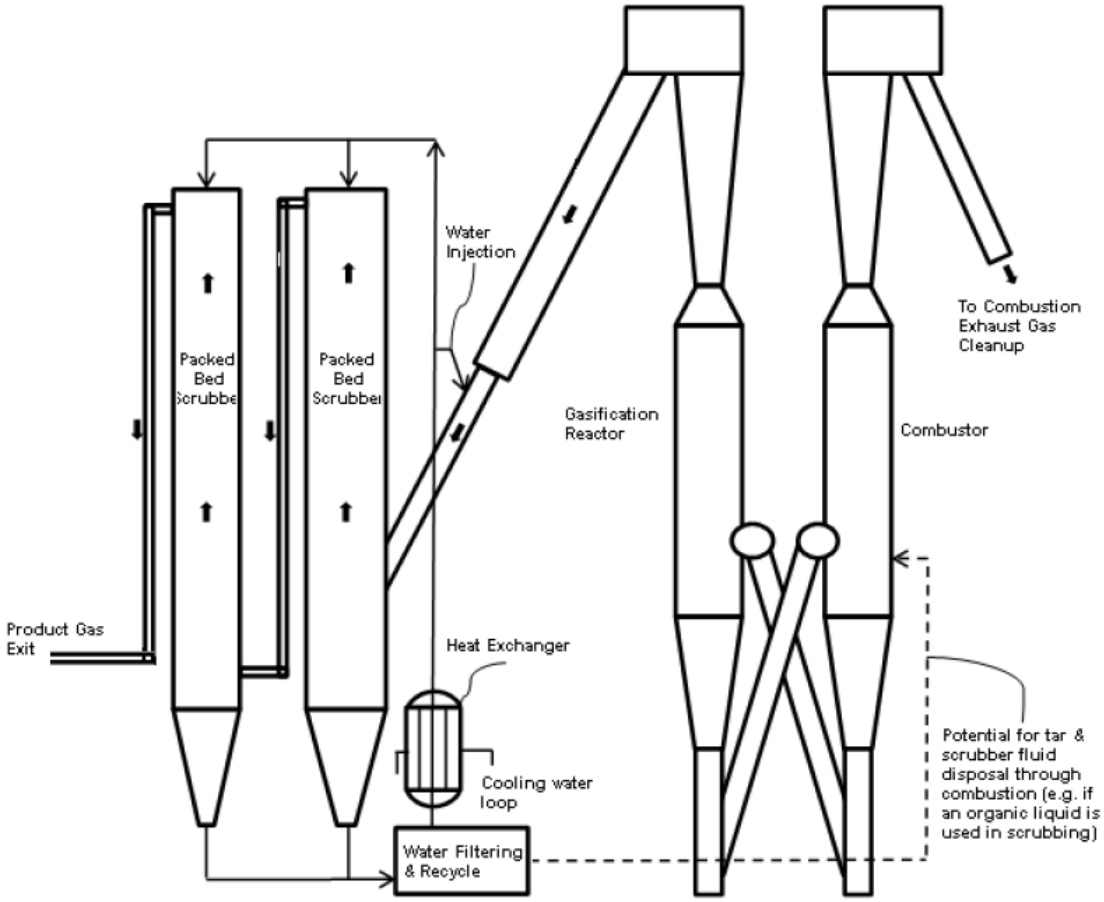

Table 15 presents a summary of the early test run dates, system improvements, and performance and presents a summary of the later runs where gas sampling and tar analysis were used to assess system performance of different operating conditions.

Table 15: Summary of gasifier runs between 6/16/2010 and 2/17/2011

Date	Test Objectives	Notes
Improvements: added O_2 sensors, propane flow meter, air flow meter, gas sampling system improvements		
4-8-2010	1	**Result:** cold flow test
6-16-2010	1, 2	Tall nozzles broke
6-30-2010	1, 2	Startup @ 450°C

7-14-2010	1, 2	Startup @ 550°C. O_2 sensor broke.
8-03-2010	1, 2, 8	Startup @ 650°C. Bed material blown out.
Improvements: Improved gas sampling, added charcoal + propane on startup, added valve on scrubber for solids removal, added knock-out tank and 2 producer gas filters.		
9-30-2010	1, 2, 8	Startup @ 700°C. **Cone broke.**
Improvements: new mild steel cones. Recycle product gas for fluidization.		
11-10-2010	1, 2, 4	Startup @ 740°C, 620-675°C on recycle. N_2 concentration of product gas = 50%
12-01-2010	1, 2, 4	Startup @ 760°C, 620-675°C on recycle gas. Extra O_2 used on combustor side → N_2 = 36%
Improvements: new O2 injectors added to combustor to allow increase biomass feedrate.		
1-26-2011	1, 2, 3, 4	Gas sampling system online. Startup @ 825°C, 710-750°C on recycle gas.
Improvements: new mild steel downcomers, added more propane inlets on combuster. Increase biomass feedrate.		
2-17-2011	1,2,3,4,6	Startup @ 825, 710- 750°C on recycle gas

Table 16: Summary of gasifier runs between 3/29/2011 and 11/17/2011

Date	Test Objectives	Propane consumed (scf)	Charcoal/ Feedstock Consumed (lbs)	Notes
3-29-2011	1,2,3,4,6	5020	420/571	Startup 850°C, 820°C on recycle gas, partial oxidation. Lowest tar concentration.
4-20-2011	1,2,3,4,6,7	5135	0/1449	Startup 850°C. Gasification using steam at 825°C. Recycle gas into bottom.
5-11-2011	1,2,3,4,6,7	5509	0/1813	Startup 875°C. Gasification using recycle gas at 825°C. Steam into bottom. Highest heating value product gas.
7-18-2011	1,2,3,4,5,6,7	4125	0/1004	Startup 875°C. Gasification using recycle gas at 825°C. Steam into bottom (test 1) and into top (test 2). High biomass feed rate.
9-22-2011	1,2,3,4,5,6,7	6194	ND/1028	Startup 875°C. Gasification using recycle gas at 865°C. Reached 820°C while steam into bottom. Low biomass feed rate
11-17-2011	1,2,3,4,5,6,7, 9	5805	ND/824	Almond hogwood. Steam gasification @ 800°C

8.1 Fluidization

Reactor fluidization testing was performed using air, combinations of air and recycle-gas, and combinations of steam and recycle-gas. Steam as a reacting agent in gasification is advantageous as it can be removed by condensation resulting in a higher energy content gas and the increased hydrogen concentration resulting from the enhanced water-gas shift reaction. However the use of steam also increased the generation of tars and the boiler was not capable of fluidizing both reactors entirely on steam alone. Therefore, experiments were conducted with supplemental air and recycle gas in combination with maximum steam.

Figure 41: Pressure at bottom of gasifier reactor

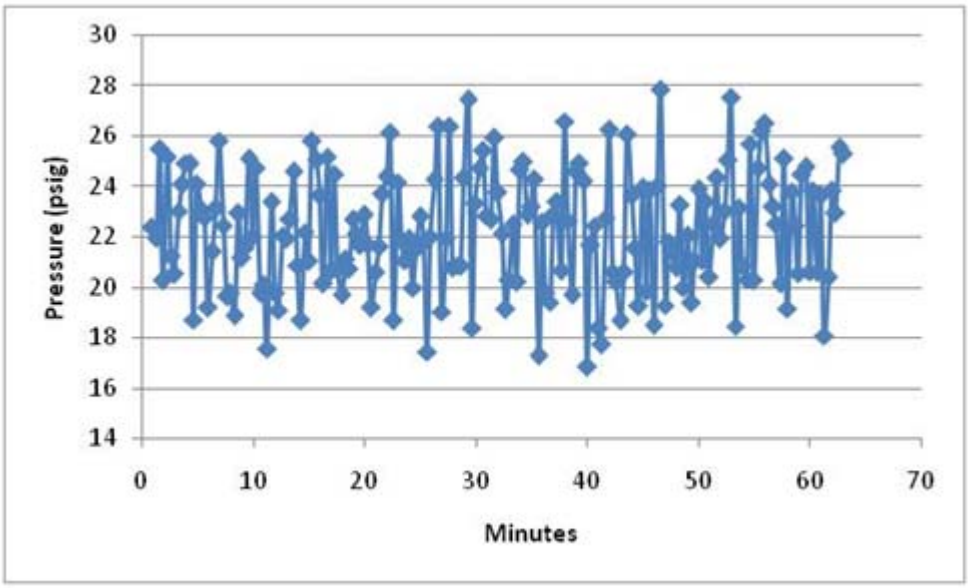

Pressure fluctuations throughout the system were a persistent problem. Figure 41 shows a typical pressure profile during gasification process near the bottom of the gasifier reactor. The unsteady operation of the gasifier reactor causes non-uniform residence time of product gases and solids. This in turn caused non-steady results in tar sampling measurements with short sampling period and also made engine operation difficult. Future modification of the reactor design will alleviate this problem.

8.2 Temperature

Gasifier reactor temperature plays an important role in tar formation and also in tar decomposition, thus influencing both the total tar content and the tar composition. The maximum temperature is crucial during the formation of secondary and tertiary aromatic and polyaromatic tar species (Milne and Evans, 1998). Therefore, a significant effort was made in order to maximize reactor temperature. Propane, oxygen and biodiesel ports were added in multiple locations to increase the heat addition by combustion to the reactors. New reinforced cones and downcomers were manufactured to withstand the higher temperature requirements. Tables 15 and 16 show the increase in reactor temperature due to reactor modification over the course of the project. Reactor temperature during gasification improved from 450°C on 6/30/2010 to 875°C on 9/22/2011.

8.3 Steam

Gasification with steam generates higher heating value product gas but also more tar. The test runs generating the two highest hydrogen concentrations (5/11/2011 and 9/22/2011) were generated using steam, however the strongest predictor of heating value of the product gas was methane concentration. Methane gross heating value (37.7 MJ/Nm3) is more three times hydrogen heating value (12.1 MJ/Nm3) on a volumetric basis. Methane made up a relatively small portion of the total product gas composition at between 5-10 percent, and hydrogen was between 10-20 percent of the total composition.

Figure 43 shows that use of steam generated equal or greater tar than air mixtures. April, 20, 2011 was the first run with steam, and also was the highest measurement of toluene and styrene using the GC online gas analyzer. Test run on 9/22/2011 gives the best indication of the effect of steam on tar concentration as fluidization was switched during the run from air-recycle to air-steam (Fig. 42). Other parameters were held as constant as possible; however the switch to steam reduced the reactor temperature from 850 to 800°C. Figure 43 shows that naphthalene is present in the highest concentration of any tar species, making up greater than 50 percent of total tar. Switching from air-recycle to steam-recycle had the largest impact on naphthalene as well; increasing from 537 to 1053 mg/m^3. The increase in naphthalene makes up 89 percent of increase in total tar.

Figure 42: Indicator of tar concentration

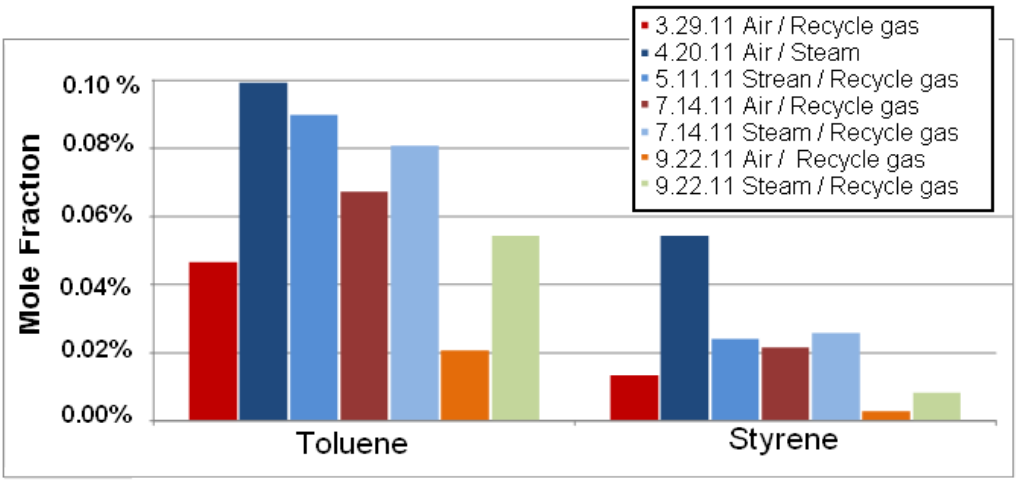

Figure 43: Tar species concentrations measured before scrubber on 9/22/2011

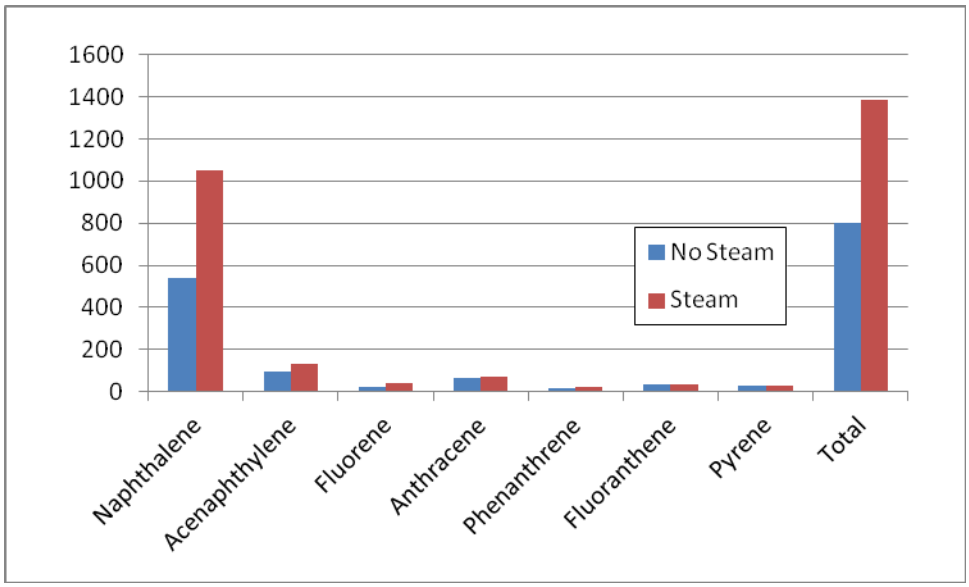

8.4 Syngas Quality

Figure 44 shows the major species of the product gas for test runs between 3/29/2011 and 11/17/2011. Test runs with air resulted in higher nitrogen (>33 percent mole fraction) and lower hydrogen (<15 percent mole fraction) and methane content (<7 percent mole fraction) in the gas. Oxygen mole fraction was near zero for all runs, which is typical of gasification reaction. Figure 45 shows the gross heating value of the product gas. Using steam-recycle gas to fluidize the reactor generated the highest heating value gas.

Figure 44: GC sample of producer gas after charcoal filter (major species)

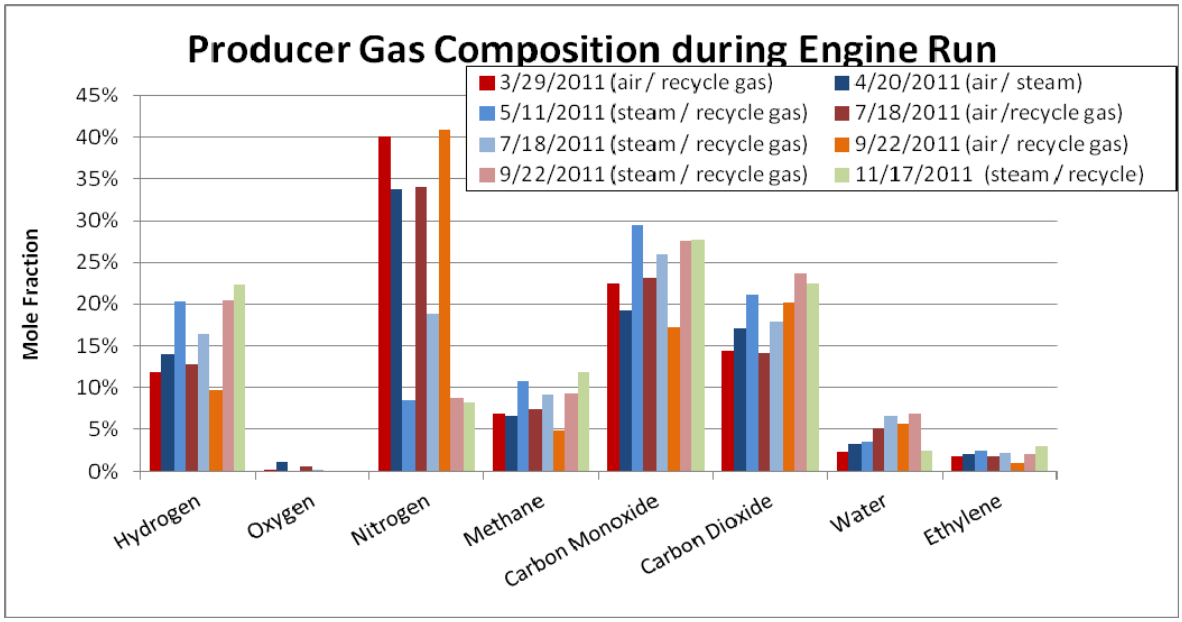

Figure 45: Gross Heating Value

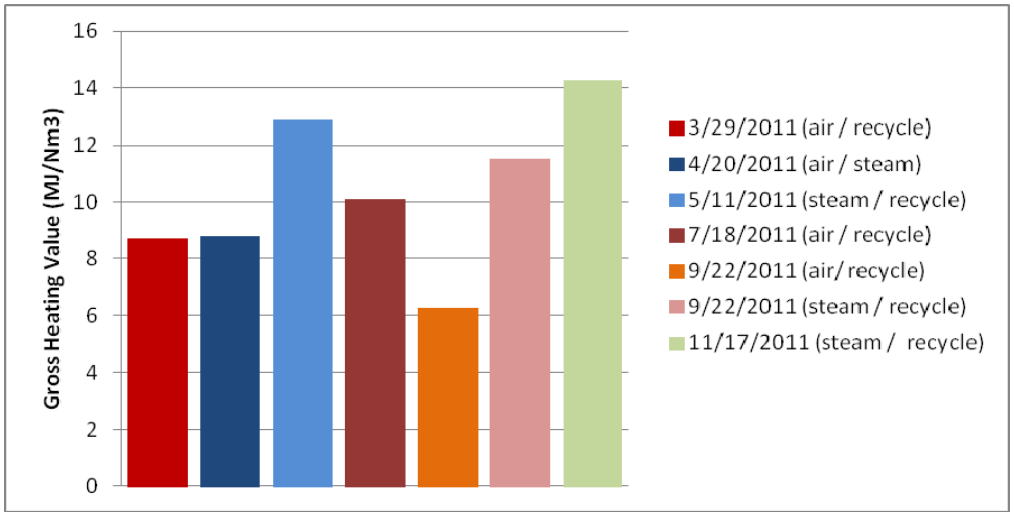

8.5 Biodiesel

Initial tests performed at West Biofuels successfully demonstrated that the infrastructure for pumping used solvent into the combustor during operation worked and provided the benefit of additional heat. In future operation, biodiesel is expected to be used as the scrubber solvent and later recycled after becoming saturated in the combustor reactor for tar destruction to provide heat. In this way tars will be more efficiently removed from the product gas and the wastewater problem will be eliminated. Use of biodiesel as a scrubber solvent at West Biofuels has not yet been implemented because of the concern for the possibility of the biodiesel igniting.

8.6 Partial Oxidation

Partial oxidation did not have a significant effect on tar destruction. Temperature above the bed (Figure 46) did not achieve sufficiently high levels to have significant effect.

Figure 46: Reactor temperature in and above the bed on 3/29/2011

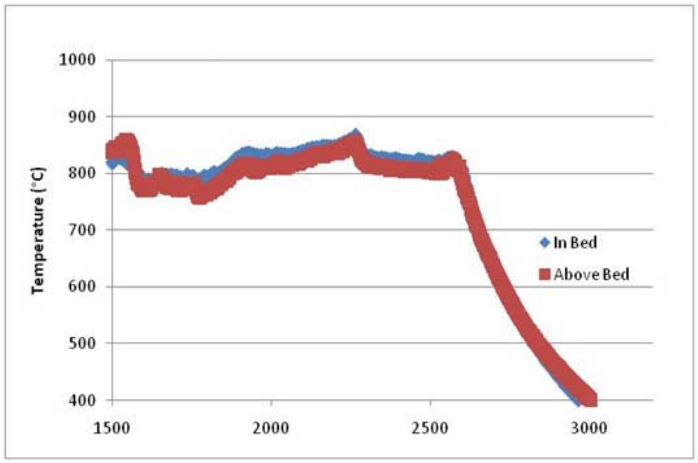

8.7 Bed Material

Two bed materials were tested: Carbo Econoprop 40/70 and Carbo HSP 30/60. After some difficulty with loss of material during fluidization using the lighter Econoprop, the bed material was replaced using the HSP 30/60. Neither bed material had much of a catalytic effect on tar reduction.

8.8 Feedstock

For all tests prior to the test run on 11/17/2011 wood pellets were used as the feedstock. Proximate, ultimate, higher heating value of the wood pellets was measured using ASTM standards. On 11/17/2011 hogwood chips were tested. Major and minor species are shown in Figures 44 and 47, respectively. There was no significant difference between the major species generated by gasifying the almond hogwood and the major species generated by gasifying the wood pellets on 9/22/2011.

Figure 47: GC sample of producer gas after charcoal filter (minor species)

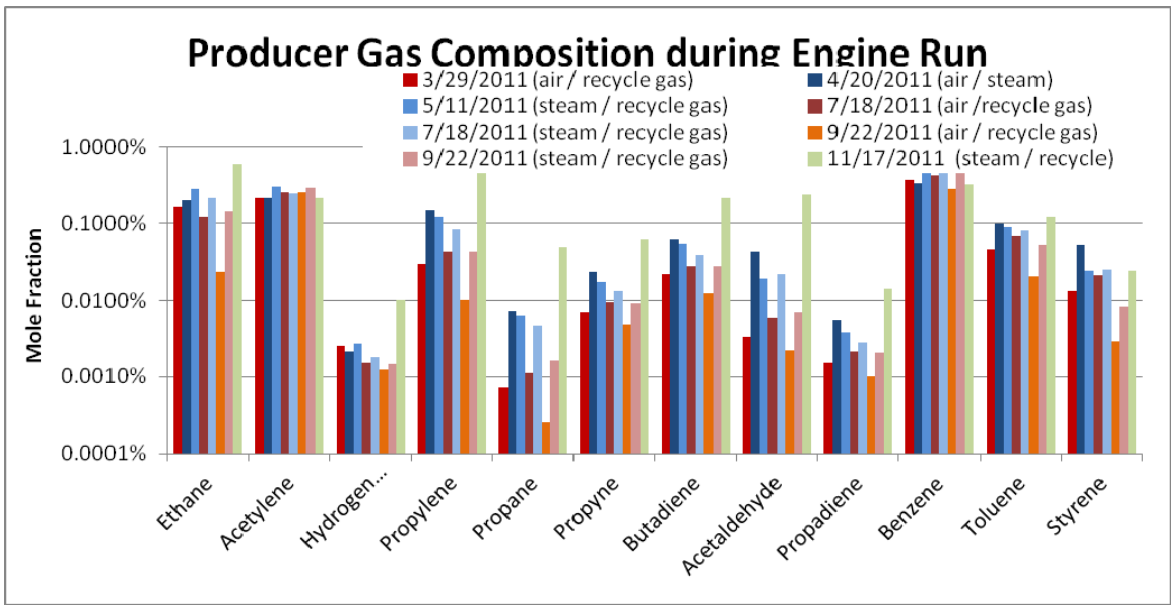

Detailed discussion of the critical operating parameter in the operation of the dual fluidized bed gasifier and gas clean can be found in McCaffrey, Z., Seiser, R., Fitzgerald, P., Liao, C., Williams, R., Cattolica, R. and Jenkins, B., 2012.*Task 2.1.7 – Monitoring Pilot Gas Purification System Performance*.California Energy Commission. Publication number: CEC-PIER-2007-002.

8.9 Conclusions

Performance for the dual-bed reactor and purification system at West Biofuels, LLC was monitored for a range of gasification conditions. The dual-bed reactor was operated using mixes of air, recycled product gas, and steam for fluidization. Reactor improvements were made to allow reactor temperature during gasification up to 865°C. Clean biodiesel was introduced into the combustor reactor for heat addition and for demonstrating that recycled tar-laden biodiesel can be recycled. Secondary-air was introduced above the gasifier reactor in order to generate a hot region above the bed for tar destruction. Unfortunately no significant

difference in tar concentration was noticed. Two different bed materials and two feedstock, wood pellets and hogwood chips, were tested. The main conclusions that can be drawn from the study are that using a steam-recycle mixture for fluidization had a positive effect on generating a higher heating value gas, however it also generated a higher tar concentration. Pressure swings generated in the reactor made engine operation difficult. Future research will focus on reducing the pressure swings and further tar concentration reduction.

Chapter 9:
Task 2.2 Producer Gas SI Engine/Exhaust Gas Cleanup

The University of California (San Diego, Berkeley, and Davis) and West Biofuels, LLC are jointly operating the Woodland Biomass Research Center (WBRC) in Woodland, California. Here, they are developing a dual fluidized-bed gasifier that is capable of converting woody biomass and agricultural feedstocks into producer gas. West Biofuels, LLC has built a pilot scale plant gasifier at the WBRC that is capable of converting 4 tons(dry)/day of biomass. Researcher from the University of California are analyzing the performance of the gasifier and measuring the producer gas composition.

The team at the WBRC has installed a Waukesha H-2475G SI-engine that is capable of generating 100 kW of electricity from the producer gas. The following chapters describe the details of engine emissions tests.

Task 2.2.1 develops a methanol reformer that creates a stream of hydrogen and carbon monoxide for research tests on the Berkeley (CFR) research engine. Tasks 2.2.2 to 2.2.5 to develop and test a fuel/air ratio controller and exhaust gas cleanup system were originally planned to be accomplish with the CFR engine at the University of California at Berkeley. It was determined that the equipment available on the CRF engine at UC Berkeley to set up the fuel/air ratio controller was too unstable for satisfactory development and testing of the system. To replace and update the equipment would require additional time and funds which would have a negative effect on the progress of tests on the generator set at the Woodland site. It was concluded that the tasks (2.2.2 to 2.2.5) could be effectively performed on the Wakeshua Engine Generator at the Woodland Biomass Research site to accomplish the objectives of those tasks.

9.1 Task 2.2.1 Simulation of gasifier syngas from a Methanol reformer

In Task 2.2.1 three methanol reactor designs were developed and tested The methanol reformer built for this project, is documented in detail in a Master of Engineering Thesis at the University of California, Berkeley, Department of Mechanical Engineering (Boyce , 2010). Here, the salient features of the results of the research conducted in support of Task 2.2.1. The goal was to produce from methanol, readily available, a stream of syngas (CO and H2) for subsequent combustion research in a spark ignited engine. In the long term, the spark ignited engine would be fueled by syngas from wood. It was originally assumed that syngas from gasification of wood would take time to develop, and therefore it was decided to create syngas from methanol so that tests could be run on the UC Berkeley research engine with syngas while the wood to syngas reactor was under construction. The development of the methanol to syngas reactor proceeded at the same rate as the wood to syngas reactor, and in time, the methanol reactor that was developed, was not needed as the wood to gas reactor came on stream Providing sufficient gas for testing and the development of emission controls strategies,

9.2 Gas Phase Methanol Reformer, T>1200K

Figure 48: Kinetics of methanol reforming at 1200 K

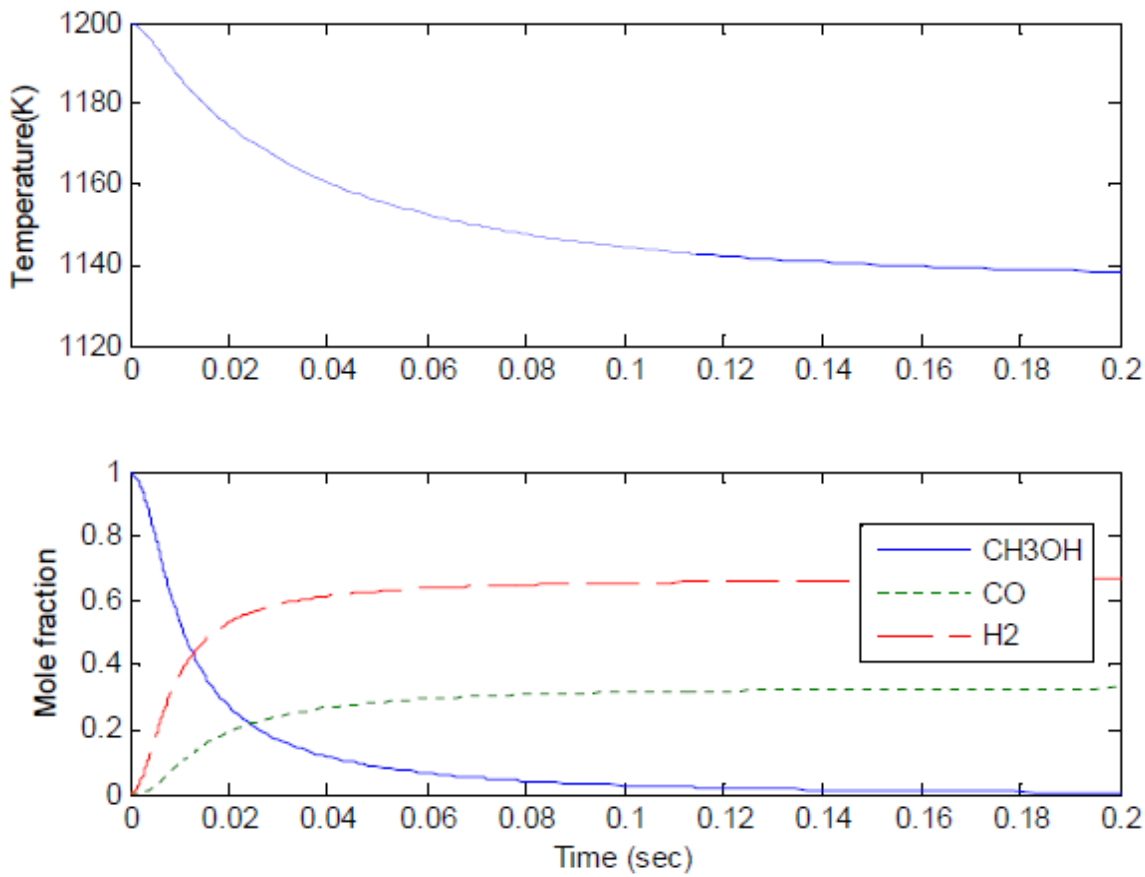

In Figure 1, the kinetics of the gas phase reforming of methanol at 1200 K is presented (Warnatz J, Maas U, Dibble RW (2006)) The are two graphs, one showing the change in temperature over time, and the other showing the reactant (methanol) gradually being converted to products. The temperature vs. time is interesting because it shows that the reaction is endothermic (which is expected from calculating the change in enthalpy). The methanol kinetics at a lower temperature, 800 K requires a longer time to react. At 900 K (627° C), the reaction takes about 62 minutes to proceed to 99 percent completion. However, at 1500 K, the reaction takes only 2 ms to achieve 99 percent completion. A flow reactor was constructed of stainless steel 1/4 inch tubing that was coiled inside of a flame tube fueled by premixed natural gas with air combustors. The hot (glowing red) stainless steel easily converted the methanol to CO and H_2. The hot CO and H_2 from methanol reforming were cooled in a heat exchanger. The gas was then ready to be delivered to the engine.

9.3 Catalytic Methanol Reformer T~400C

The gas phase methanol reforming system (Fig. 2) demonstrated with a stainless steel tube operating at high temperature worked well. From a research point of view, this simple system used a turbulent premixed methane flame to heat the stainless steel tube. To lower the

temperature required to reform the methanol a catalyst bed (was employed as described in this section and in following sections. This design contains two stages of in-line heaters, followed by a pipe filled with copper based catalysts (from BASF). The methanol injection was achieved through a standard automobile fuel injector manufactured by Bosch. The fuel injector was pulsed (standard automotive fuel injector) with a pulse generator and solid state relay.

Figure 49: Schematic of Methanol Reformer using a Catalyst Bed for copper based and 3 way catalyst.

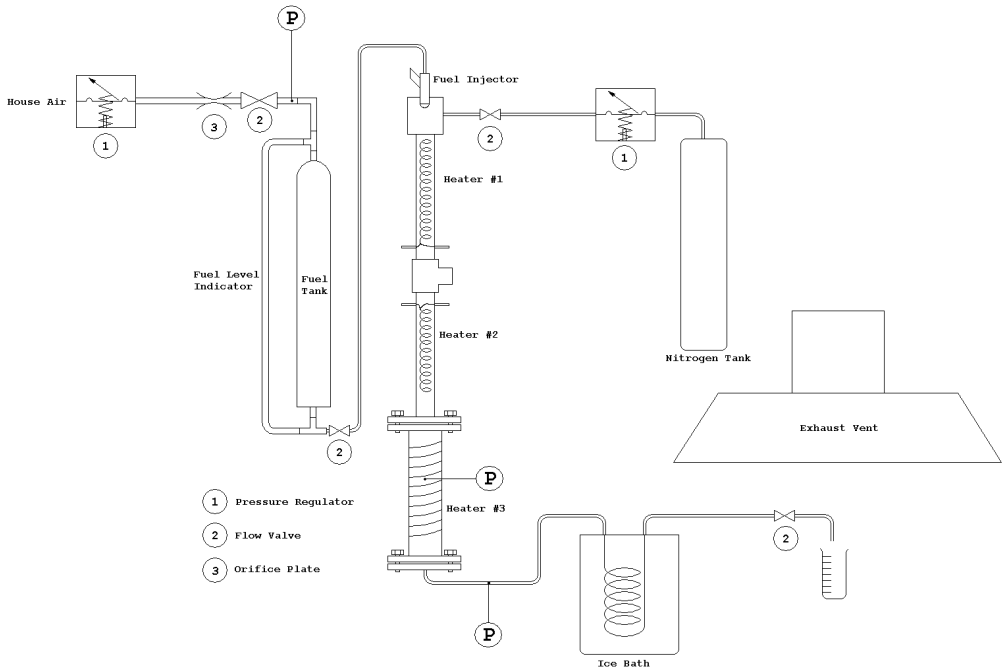

Methanol has a boiling point of 65°C and its enthalpy of vaporization is 1168 kJ/kg. This is a relatively high value for its heat of vaporization. As a comparison, the enthalpy of vaporization of ethanol is 841 kJ/kg, and methane is 510 kJ/kg, and water's is 2260 kJ/kg (one of the highest, due to the molecules' strong polarity). Methanol's high enthalpy of vaporization means that a significant portion of the heat input will go to this process. In Table 1, the power required for the vaporization into gas phase for the CFR engine (a 0.6 Liter single cylinder engine at U C Berkeley) at different engine speeds is presented in Table 1. In Table 2 the power input for the CFR engine at 600 RPM is shown. This means that a constant mass flow rate of methanol (or its reformed products) at 574 mg/s if the engine is to be operated stoichiometrically.

Table 17: Power needed to heat methanol up to 300 deg C at different engine speeds

	25 C to 65 C		65 C to 300 C	
RPM	sensible heat, W	heat of vaporization, W	sensible heat, W	Total heat input, kW
600	32	671	248	0.95
900	49	1006	371	1.43
1200	65	1342	495	1.90
1500	81	1677	619	2.38
1800	97	2012	743	2.85

Table 18: Power needed to heat methanol up to temperatures at engine speed = 600 RPM

Temp (C)	Power (kW)
300	0.95
400	1.06
500	1.16
600	1.34
700	1.53
800	1.66
900	1.88
1000	2.02
1100	2.27

Tables 1 and 2 show the rate of heat needed in order to heat methanol to the temperatures shown. Table 1 shows heat input as a function of CFR engine RPM, and Table 2 shows the heat input required to get methanol up to the shown temperature at CFR engine speeds of 600 RPM.

As described previously, the heating is achieved through two stages of electric heaters. Both heaters have a resistance in the range of 8 Ω. Therefore, if they're being supplied with the maximum value of 15 amps, the power rate for each heater will be approximately 1.8 kW, for a total of 3.6 kW that can go into the methanol stream. This is more than enough with the CFR running at 600 RPM. There are two routes that can be taken to reform methanol with this design.

The use of copper catalysts limits the high temperature significantly. The catalyst beads are active in the range of 200-400°C. Note, that temperatures above this range put the catalyst in danger of being destroyed. This was actually confirmed during one of our experiments when the catalyst bed reached 450° C, and the beads became inactive. However, when running the reformer with the 3-way catalyst, higher temperatures are an advantage. The 3- way catalyst is much less sensitive to temperatures above 300° C, as the experimental data shows. Still, there is enough power with the electric heaters to get the methanol stream up to temperatures appropriate for the 3-way catalyst. The two catalysts being considered for the methanol reformer were the copper based catalyst from BASF and the affordable 3-way catalyst from an automobile

The catalyst that was used in the methanol reformer was a copper based catalyst from BASF (2 kilogram, gratis). This catalyst was selected after some communication with a BASF representative. The representative sent the lab two 1 liter samples of a copper based catalyst. The catalyst sent was designed for the steam reformation of methanol. After some investigation, it was found that most methanol is produced from natural gas. This natural gas is heated with water to produce carbon monoxide and hydrogen. At this point, the carbon monoxide and hydrogen are put under high pressures and moderate temperatures, and a copper catalyst to produce methanol. It was decided that attempting this reaction at atmospheric pressure, with the same copper based catalyst, would reverse this reaction into carbon monoxide and hydrogen. Since the reaction favors the fewer moles at high pressure (one mole of methanol vs 3 moles of carbon monoxide and hydrogen), it would make sense that more moles are favored at lower pressures. The literature that comes with the catalyst claims that a residence time of 0.72 s is typical for this catalyst, but that residence times as low as 0.09 s have shown to reform methanol. The findings of the experiments performed show that residence times need to be slightly longer to successfully reform methanol.

9.4 Catalytic Methanol Reformer 3 Way Catalyst T~600C

A standard 3-way catalyst consists of platinum, palladium, and rhodium. The 3-way catalyst is designed to remove NO, CO and unburned HCs from the exhaust of a spark ignited or diesel engine. The reaction that removes NO works by reducing this molecule and forming N_2 and O_2, the reaction that removes CO oxidizes it by turning it into CO_2, and unburned hydrocarbons are also oxidized into carbon dioxide and water. A catalyst works by changing the activation energy of specific reactions, but not all reactions. Previous research detailing methanol reformation in a palladium catalyst by Shiozaki (1999), gave a reason to attempt these tests. The evidence from the tests done with the 3-way catalyst shows that it does indeed induce the reformation of methanol. In view of the lower cost of the automotive catalyst, we would recommend the 3 way catalyst for the reformation of methanol

Chapter 10:
Task 2.2.2 Design Review for Exhaust Gas Cleanup System

10.1 Catalyst Selection

The SAE research literature was review to evaluate different options for cleaning up internal combustion engines operating under different conditions

10.1.1 Stoichiometric Design

The project's details and goals were discussed with Richard MaClaughry of Umicore, a major catalyst producing company. For a small system it was determined a stoichiometric burn engine with three-way catalyst clean-up would be the most affordable. It was determined initial testing should be performed passing a slipstream through a stock 1-liter catalyst with 9:1 palladium to rhodium loading. The palladium is primarily responsible for reforming unburned hydrocarbons and carbon monoxide. The rhodium is the material which promotes of the majority of the NOx reduction. The results of these slipstream tests will be used as a starting point for choosing the ideal catalyst for our operation. A great deal of information was discussed and obtained from Umicore in determining which catalyst should be used and what control strategy should be applied. However, this information was confidential, and thus is not presented in this public report.

Three-way catalysts operate best near their maximum allowed temperature of approximately 850°C. In automotive applications this must be carefully considered to prevent overheating of the catalyst which leads to accelerated deterioration. For an engine running on landfill gas the cylinder charge is reduced due to the large volume of the fuel (as opposed to propane, gasoline, or either natural gas). This results in an exhaust stream which rarely exceeds 600°C, and thus it was determined the catalyst should be mounted close to the exhaust manifold with good thermal insulation.

10.1.2 Rich/lean dual catalyst

In this design concept two catalysts were mounted in the exhaust in series with ports for air injection in between. The system was designed to allow one catalyst to run rich, removing NOx, and the second to run lean, removing CO and hydrocarbons. Because each catalyst needs to be only rich or lean, and not precisely at stoichiometric, the design should be highly robust with very little emissions slip. In order to achieve such a system some efficiency must be sacrificed. Extra fuel must be present in the exhaust to convert NOx in the first catalyst, while air must be compressed for injection between the two catalysts.

It was determined that running the first three-way catalyst under such conditions resulted in the formation of ammonia. This same phenomenon has been observed in the lab at UC Berkeley, and has been briefly discussed in the literature. The formation of ammonia is a major hurdle to the system, as ammonia cannot be directly vented, and when burned with oxygen it tends to form NO. Ammonia is oxidized in three main ways:

$$2\ NH_3 + 3/2\ O_2 \rightarrow N_2 + 3\ H_2O + 151\ \text{kcal} \quad (1)$$

$$2\ NH_3 + 2\ O_2 \rightarrow N_2O + 3\ H_2O + 132\ kcal \quad (2)$$
$$2\ NH_3 + 5/2\ O_2 \rightarrow 2\ NO + 3\ H_2O + 108\ kcal \quad (3)$$

Under normal TWC conditions reaction 3 is favored over 90 percent. Due to this issue a two catalyst system is not feasible for robust emissions cleanup. However, certain catalytic wash coats have been found to favor reaction 1 as much as 95 percent. With such a catalyst in place the system could be feasible, but would require 3 catalyst in series to first convert the NOx, then to react any ammonia via reaction 1 above, and finally to oxidize CO and hydrocarbons. A possible system design is shown in Fig 3.

Figure 50: Rich/Lean exhaust clean-up concept: A system capable of running the rich/lean system would require 3 catalyst: a TWC running rich followed by air injection and then an ammonia selective catalyst and a CO and HC oxidation catalyst

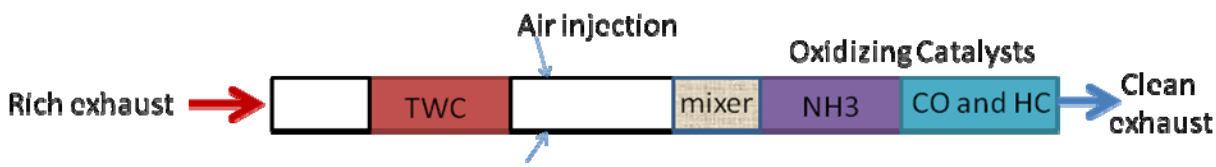

This design was evaluated, but considered to be too complex, with only minor advantages over the traditional three-way catalyst system.

10.2 Catalyst Operating Considerations

Based on the literature review it was determined that catalysts perform best at reducing NOx when the air fuel ration is oscillated around stoichiometric with approximately a 1 Hz frequency. To improve the robustness of the cleanup system the engine controls will be designed such as to allow variation of both the frequency and the magnitude of the oscillations. A Simulink model was created to simulate a possible controller of the engine including valve flow characteristics, simple combustion chemistry, and feedback control

10.3 Catalyst Feedback Control

Typical narrow band sensors were originally considered as they are highly standardized and provide an indication of whether the engine is running rich or lean. Unfortunately such devices have very rapid response curves and quickly saturate, so the magnitude of the richness/leanness of the exhaust cannot be determined. Also, these devices are quite sensitive to both pressure and temperature, varying linearly with pressure differential and exponentially with temperature, making them somewhat unreliable. A superior device for measuring lambda is the Universal Exhaust Gas Oxygen Sensor (UEG.O sensor). These devices, more commonly known as wideband lambda sensors, use an ion pump to control the oxygen content of a small chamber exposed to the exhaust only through an orifice. The advantage of these devices is that they provide a nearly linear output over a wide range of lambdas, have no pressure dependence, and less than a linear temperature dependence.

Chapter 11:
Task 2.2.3 Fuel Air Ratio Controller for Engine

11.1 Design Criteria

Gas and air fuel ratio delivery designs were reviewed. Originally work had been completed assuming excess fuel would be produced at all times and thus the fuel would be metered to control stoichiometry. This approach was abandoned since it is necessary to use all of the fuel provided at all times to prevent flaring and the associated emissions. The design approach will meter only the air and let the fuel be delivered un-throttled Metering the air is a reasonable approach because the volumetric flow rate of both the air and the fuel are on the same order of magnitude. Several approaches were reviewed for accurate metering. One option was to have a large port that was always open and a second valve that could be fine-tuned until the amount of air balanced the amount of fuel. It was determined that this system would not be effective for wide fluctuations of the fuel and as such was not a desired solution. A second method is to meter the fuel through high pressure injection. This had the advantage of highly understood control and more fine control of the actual injection, but the energy to compress the fuel for injection would be on the order of 10-15 percent of the total work output of the engine.

For power generation system to function using air throttling rather than fuel throttling it is necessary for the generator to be capable of absorbing varying amounts of energy automatically. A load bank was thus built which utilized electronic switching, allowing the engine controller to adjust the load to match the power output.

It was determined that catalysts perform best at reducing NOx when the air fuel ration is oscillated around stoichiometric with approximately a 1 Hz frequency. To improve the robustness of the cleanup system the engine controls will be designed such as to allow variation of both the frequency and the magnitude of the oscillations. A Simulink model was created to simulate a possible controller of the engine including valve flow characteristics, simple combustion chemistry, and feedback control. It was found that the most robust system was a simple PI controller tuned for the specific engine. Look up tables and advanced feedback controllers were determined to add too many instabilities for a system with unknown fuel energy density and are not necessary as transient situations are minimal.

11.2 Hardware Selection

The performance and characteristics of throttling valves was researched. Testing was performed on an electronic Bosch throttle body designed for motorcycles. Results indicated that these valves require highly complex external algorithms to drive them smoothly and predictably. These algorithms are built into BMW CPUs and are not available to the public. To buy an aftermarket controller for the valve would cost over $1200. It was decided that the better option would be to find and purchase a large valve with these features already built into it. At this point a number of valve companies were contacted and concern their products, cost, and lead times.

The search for an appropriate valve was narrowed down to two main companies. Both Flow Tech and Woodward Valves are high quality with built in controls, taking a 0-5V signal, and offered high reliability. Flow Tech had separate valves and actuators, allowing us to buy 2 large

valves for the main engine and one smaller valve for the CFR for testing. This was a very appealing option, however it was determined that the Flow Tech valves were not designed for an intake and thus can close too completely to comply with regulations. The Woodward valves were designed for throttling engines and thus have all the necessary safety features. They are also less expensive than the Flow Tech valves. Calculations were performed to determine the air flow rate into the engine at maximum speed and was correlated to matching a 60mm butterfly valve. An order was placed with Woodward, but due to delays we did not receive the valves nor were we charged during the month of February.

Time was spent researching and understanding oxygen and lambda sensing devices to be used to control the engines. Typical narrow band sensors were originally considered as they are highly standardized and provide an indication of whether the engine is running rich or lean. Such devices are made of a thimble shaped device constructed of a zirconia ceramic tube with porous platinum electrodes attached on both the inner and out faces. The inside of the device is then left open to ambient air while the outside is exposed to the exhaust. The partial pressures of oxygen between the air and the exhaust is then compared using the charged particle transport defined by Nernst Transport. When there is oxygen in the exhaust and the stream is lean few electrons flow across the device, resulting in a low voltage. Conversely when the stream is rich oxygen wants to flow across the device resulting in a high voltage being measured. Unfortunately such devices have very rapid response curves and quickly saturate, so the magnitude of how rich/lean the exhaust cannot be determined. Also, these devices are quite sensitive to both pressure and temperature, varying linearly with pressure differential and exponentially with temperature, making them somewhat unreliable.

A superior device for measuring lambda is the Universal Exhaust Gas Oxygen Sensor (UEG.O sensor). These devices, more commonly known as wideband lambda sensors, use an ion pump to control the oxygen content of a small chamber exposed to the exhaust only through an orifice. What they measure is the diffusion rate of the oxygen into the depleted chamber through the orifice and thus can determine precisely the oxygen content over a wide range of lambdas. In order for the process to work it is necessary to have an external controller which provides current to the ion pump to keep the concentration gradient constant with time as well as a more sophisticated sensor device. The advantage of these devices is that they provide a nearly linear output over a wide range of lambdas, have no pressure dependence, and less than a linear temperature dependence.

For testing and characterization several UEGO sensor units were purchased from Innovate Motorsports, including LC-1 controllers and Bosch LS 4.2 wideband lambda sensors. These devices are some of the most affordable and easily calibrated devices on the market.

11.3 Software and Controls

National Instruments and their software Labview were chosen as the communication equipment between the engine and the computer. This option was chosen because NI is widely available and used and Labview is already used on the Woodland site and at the Berkeley combustion labs. Significant amounts of time were spent learning the software, including the different programming options and the hardware they require. It was determined the best option was to use a Compaq RIO DAQ board for several reasons. One is that it has interchangeable cards, allowing it to be custom tailored to fit the needs of the experiment, and can be expanded on if additional inputs or outputs are required. Another is that it has the

ability to run real-time software onboard, meaning the computer only tells it when to start and stop but does not actually have to take in the signals, process them, and then output them again. This has the distinct advantage that the real-time system has no operating system, thus there is no possibility of a crash or lag due to an external problem. This is a significant advantage when controlling an engine as even a small lag in the control signal could cause it to stall or drastically change its run condition causing damage to the engine, intake, exhaust system, or more.

Based on the literature review it was determined that catalysts perform best at reducing NOx when the air fuel ration is oscillated around stoichiometric with approximately a 1 Hz frequency. To improve the robustness of the cleanup system the engine controls will be designed such as to allow variation of both the frequency and the magnitude of the oscillations. A Simulink model was created to simulate a possible controller of the engine including valve flow characteristics, simple combustion chemistry, and feedback control. The models response to a ramp and step input are shown in Figs. 4 and 5. It was found that the most robust system was a simple PI controller tuned for the specific engine. Look up tables and advanced feedback controllers were determined to add too many instabilities for a system with unknown fuel energy density and are not necessary as transient situations are minimal.

Figure 51: Response of the controller modeled in Simulink to a ramp input – the controller showed a good ability to adapt to such a change.

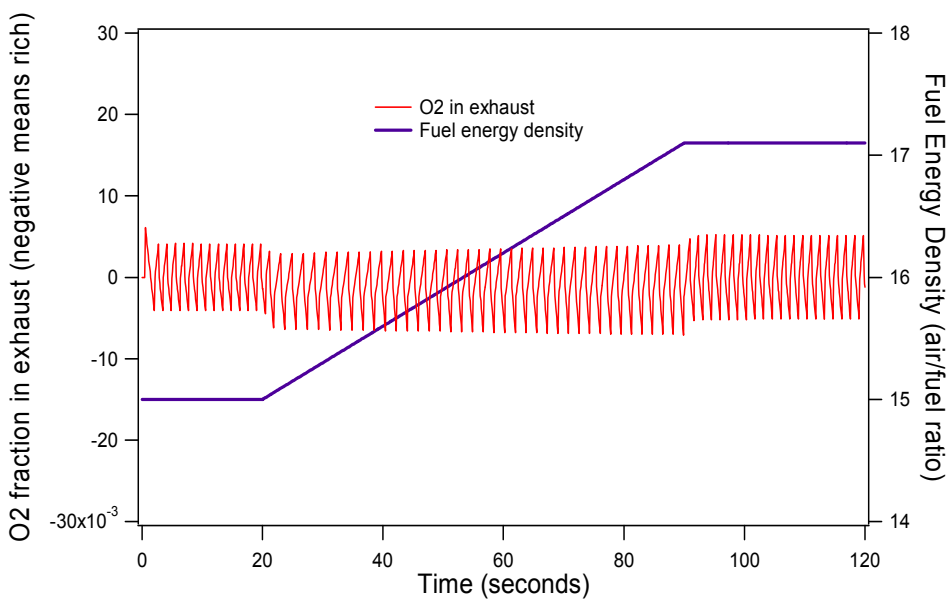

Figure 52: Response of the controller modeled in Simulink to a step change – without lookup tables or fuel data the system takes time to respond to a large, rapid change.

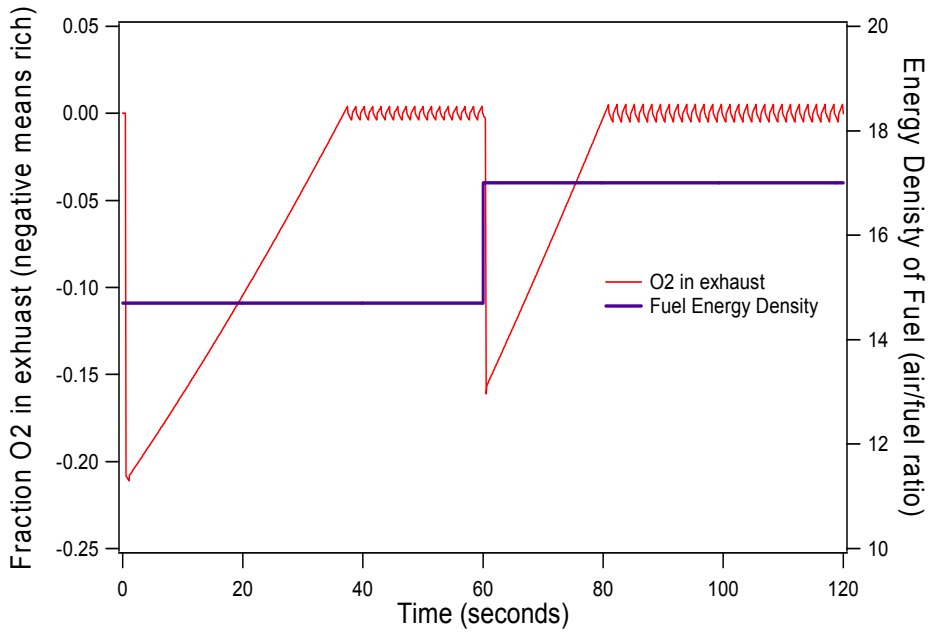

Since the engine was operated on Labview based equipment, a basic software control was written and tested in Labview based on using the input of a wideband lambda sensor and an output to a 0-5V throttling valve. Several different designs were written and tested to compare efficiency and accuracy. The final controller design is shown in Fig. 6. Results from the model were obtained for a variety of different input conditions, with some examples shown in Fig. 7.

Figure 53: The final feedback-controller design implemented into labview.

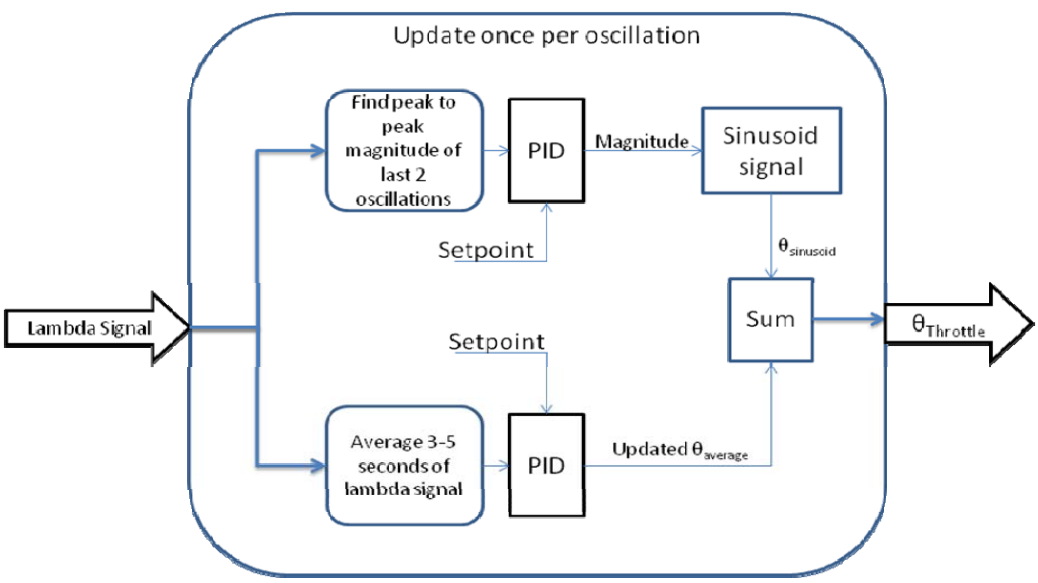

Figure 7: The labview models response to some sample scenarios.

Figure 7: The labview models response to some sample scenarios.

Figure 54: The labview models response to some sample scenarios.

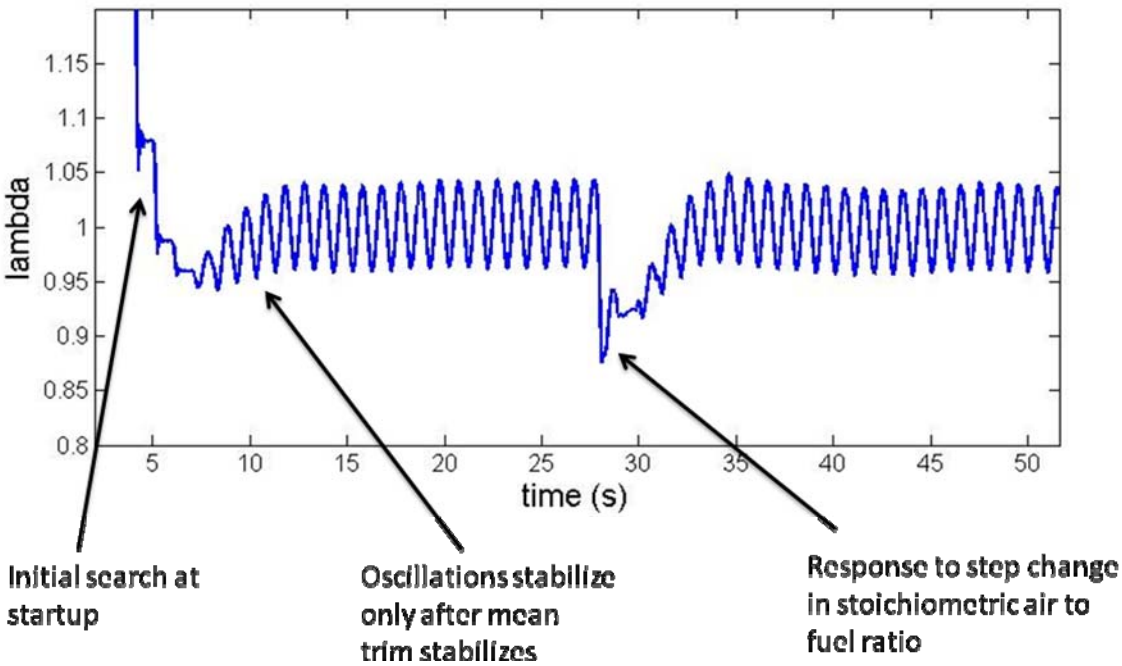

Chapter 12:
Task 2.2.4 Fabricate Exhaust Clean-up System for Engine

12.1 Engine Exhaust Assembly

Figure 55: Engine intake and exhaust design

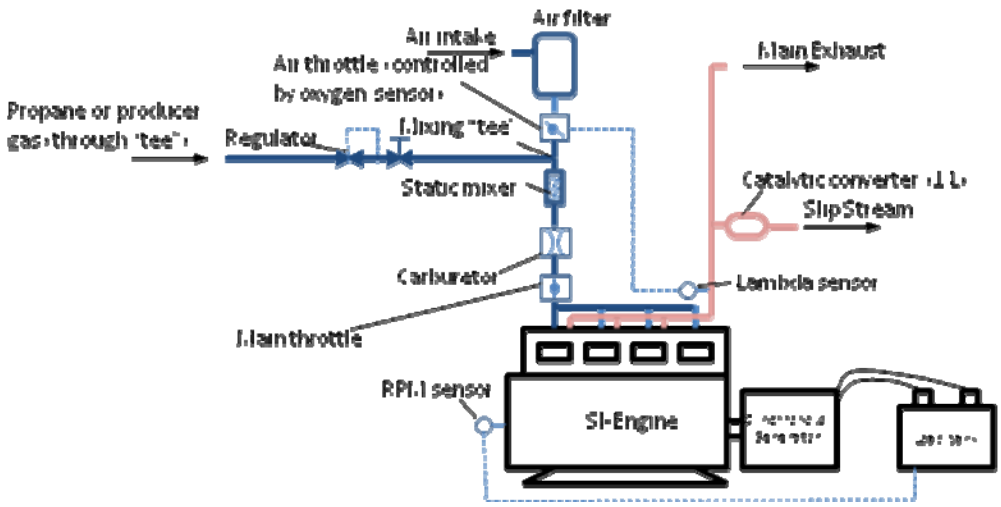

The engine intake and exhaust schematic is shown in Fig. 8. Critical to the success of the system is the lambda sensors located in the exhaust, which communicate with the intake air throttles through the Labview cRIO controller. The 1 liter catalyst is mounted in a slip stream off of the main exhaust, with a 'flapper' mounted on the end of the exhaust, which allows the operator to control the flow rate which is forced through the catalyst. Figure 9 shows the engine prior to the installation of the catalyst, and Fig. 10 shows the exhaust with the catalyst in place. In figure 10, two catalysts are mounted in series in a slip stream which runs parallel to the main exhaust line. The white insulation which is clearly visible in the picture is wrapped around the elbow, first catalyst, mixing tube, and second catalyst, to maintain temperatures. Figure 11 provides a better angle from which to observe the 'flapper plate' which was the restriction which could be closed various amounts to force exhaust gas through the catalysts.

Figure 56: The engine before the installation of the catalyst and flapper plate.

Figure 57: The engine exhaust with catalyst installed.

Figure 58: The flapper plate can be seen in this picture in a mostly-open state.

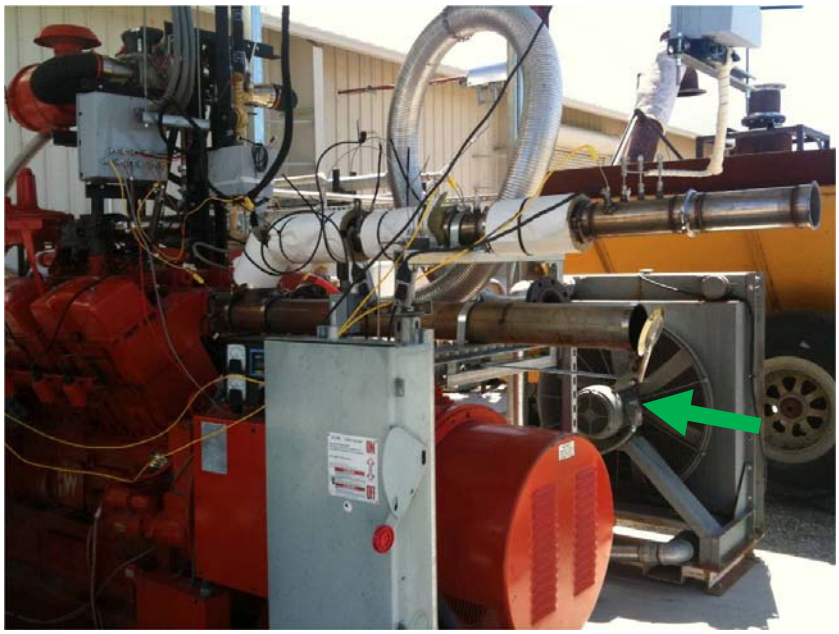

12.2 Installation of Sensors

Two wideband lambda sensors were fully wired and powered. The accompanying software was installed and tested. It was noted that the sensors can only be programmed for specific gases and cannot function purely as an oxygen/excess fuel sensor. For our system this means we will not be able to accurately read the true lambda since we do not know the exact makeup of our fuel, but it should be able to correctly indicate stoichiometric as well as provide an accurate indication of how rich or lean the stream it. Innovate was contacted to better understand these limitations, but customer service was terrible and despite our efforts their companies engineers never contacted us. It was determined in the future if the sensors do not work as well as hoped we will switched companies.

A test assembly for the wideband lambda signals was designed and assembled. It consisted of a vessel which the lambda sensor could be mounted into with ports for adding gases of known oxygen concentration. The objective was to determine how accurately the sensors could measure mixtures in a stable environment. It was concluded that over the range from ambient air to stoichiometric the sensors were accurate to within 0.02 lambda. This is very good for most of our needs, but could be a problem if the stoichiometric point is off as far as 0.02 in either direction as it is critical to be able to pinpoint the correct value for proper functioning of the exhaust system.

The experimental setup for the lambda sensors and catalysts was completed and tests were performed. Noise turned out to be major issue, as lambda fluctuations as large as 0.05 were observed regularly. This magnitude of noise would cause serious problems for the controller, which needs to keep the average lambda within 0.02 of stoichiometric for the catalysts to work effectively. A wide variety of solutions were attempted, including dampening the vibrations of the exhaust, averaging the signal over varying periods of time, and filtering the signal with

different cutoff points. It was determined that the only acceptable solution was to use filtering. An issue becomes apparent that filtering reduces the sensors response time, which is supposed to be approximately 0.1 seconds. With the filtering the system only responds on the order of a second or longer, making it impossible to sense our desired oscillations in the air fuel ratio. It was determined that for initial testing it would be acceptable to not include the oscillating component of the control, and that oscillations can be manually controlled for testing the exhaust cleanup system, but for the fully automated system it will be necessary to either find a better way to isolate and remove the noise or to find a higher quality sensor controller which will not have these negative features.

These tests also reflected the first true application of the cRIO board for real time data acquisition. Many modifications and corrections were made along the way to streamline the collection, analysis, and recording of the data. This will be of great benefit for starting the testing on the actual test engine as it will provide confidence that runs will be efficiently displayed and documented by the software.

The valves were wired and the operation of them was tested. Performance of one of the valves was not satisfactory and time was spent troubleshooting. It was determined that the power supplies available were not large enough to power the valves, so larger units capable of producing much larger amounts of power were purchased and wired. This fixed the issue.

12.3 Initial Exhaust System Test

Initial testing of the catalysts was performed using gasoline and methane. The catalysts were found to work much more effectively on gasoline than methane, likely due to the tightly bound structure of the methane. It was determined that more heat might make the catalysts far more effective at converting methane and its emissions as it would promote the breakdown of the CH4 molecules. Additional heat required special insulation as well as modifications of the exhaust system which were started during the period. Additional running was performed at various times to break in the catalysts, which perform well above the normal operating efficiency for the first ~20 hours of operation.

Testing of the catalysts continued using the un-insulated exhaust system. It is believed that when a fuel rich mixture passes through the catalysts ammonia is formed. If that stream then has an oxidizer added to it and is passed through a second catalyst the ammonia breaks down and the fuel bound nitrogen converts largely to NOx, causing the initial cleanup to be almost cancelled out. This phenomenon was tested numerous times with numerous fuels all with the same result. It is desired to repeat the tests using hydrogen as the fuel to see if similar issues still exist. To better understand the results other catalysts will be chosen and purchased to determine how differing precious metal loading effects this production of ammonia. If this phenomenon can be overcome using hydrogen or possibly different catalyst it could make the cleanup of the gasifier engine far more stable and predictable than any other technique currently being used today so a large amount of energy has been focused on this area.

The exhaust system was modified to allow higher heats to be maintained without damaging the system and insulation was installed. Leak testing was performed. It was necessary to machine additional components to prevent leaks while keeping the exhaust in line with the engine.

Chapter 13:
Task 2.2.5 Exhaust Gas Clean-up System Performance Tests

13.1 Propane Emissions

For initial testing propane was metered into the intake at low pressure, simulating the low pressure producer gas. The electronic throttle valves were used to control the stoichiometry based on the wide band lamba sensors located in the exhaust. For initial testing a wide range of lambda values were run, allowing us to produce a plot (Fig. 12) showing how CO and NOx concentrations varied as the oxygen concentration varied. As expected the catalyst performed well at reforming NOx at low oxygen levels, but there is a sharp cutoff point where additional oxygen results in rapid increases in NOx quantities. Note that the NOx detector used maxes out at 1000ppm, which is why the NOx data flat lines at this value as the oxygen concentration continues to increase. CO displays the inverse trend, but the cutoff point is much less defined and the rate of increase is not as severe. An ideal operating point which satisfies both NOx and CO emissions requirements does exist between O2 concentrations of -0.3 and -0.2 with NOx readings consistently below 20ppm and CO readings around 300ppm or lower.

Figure 59: CO and NOx levels after the three way catalyst vs. the oxygen concentration.

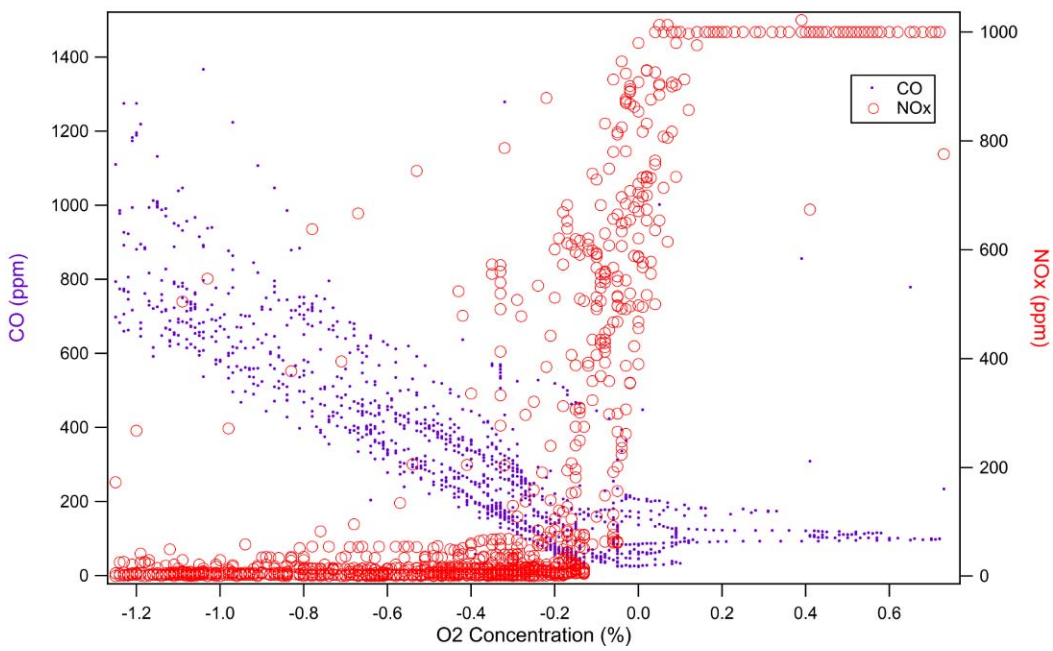

13.2 Flow Rate Effect

Exhaust was forced through our slipstream catalyst by means of a restrictive 'flapper' plate which could be positioned in front of the main exhaust pipe. The relative blockage was evaluated based on the flappers position, which was scaled based on 0 being fully opened and

approximately 22 being fully blocked. It was found that any positions below 14 resulted in almost no detectable flow passing through the catalyst, and thus the majority of testing was performed at positions 16 and higher. To gain a better understanding of the effect of the flapper position a sweep test performed for which the lambda was kept constant using our automatic feedback control and the flapper position was slowly changed over time. The result of one of these tests is shown in Fig. 13. With the flapper operating in positions 17 and 18 the results seem relatively constant, but position 19 results in a significant increase in CO emissions. NOx emissions did not vary significantly for any of the positions, which could indicate a few conclusions: 1) we were too rich relative to stoichiometric for this testing, or 2) the catalyst is much more effective at NOx conversion than CO conversion. Results indicate that the optimum operating point for our testing is approximately 18, since it represents the highest flow rate which was still able to maintain very good conversion efficiencies for CO. Repeating this test at varying lambda set points and with a more responsive HORIBA system will provide more insights and help confirm ideal operating points.

Figure 60: Emission levels exiting the three way catalyst for several different flow rates, indicated by the 'flapper position. It can be seen that the catalyst has an ideal operating flow rate.

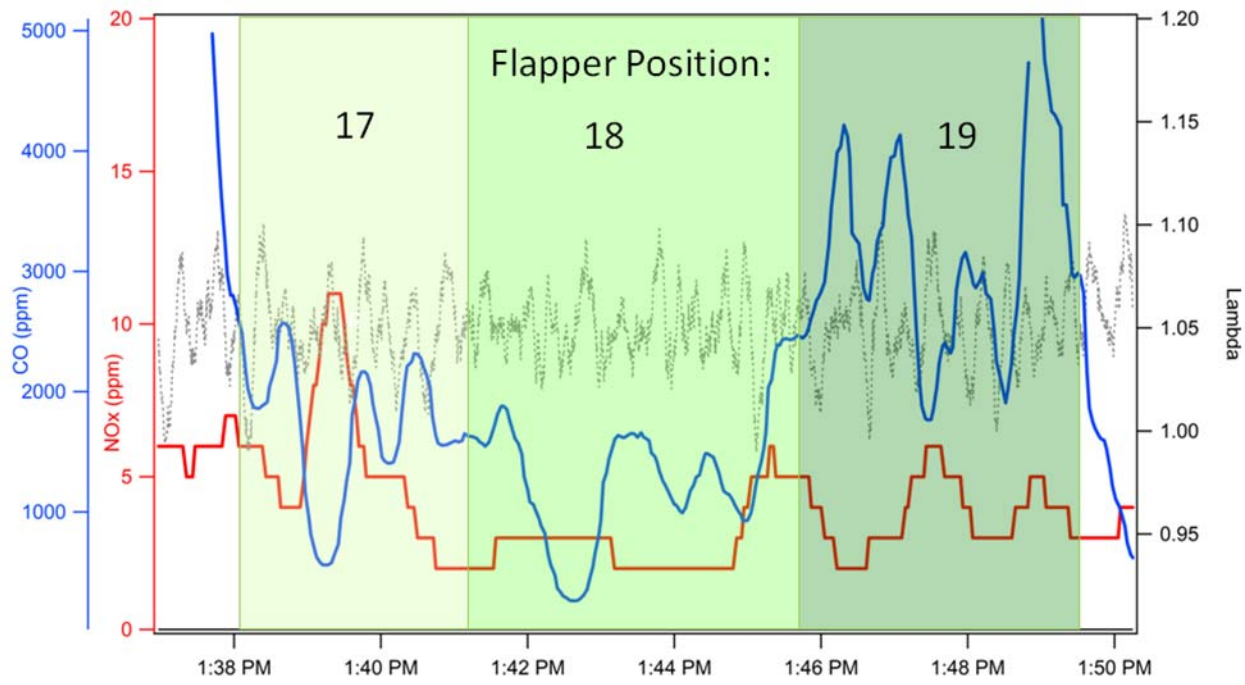

Time delay and possible time averaging were major concerns for our testing. The HORIBA gas analyzer was located inside a building approximately 50 yards from the test engine, and as a result it required nearly one minute for changes in engine operating conditions to reach at stabilize at the HORIBA.

13.3 Producer Gas Results

Rich/lean dual catalyst

In this test two catalysts were mounted in the exhaust in series with ports for air injection in

between. The system was designed to allow one catalyst to run rich, removing NOx, and the second to run lean, removing CO and hydrocarbons. Since each catalyst needs to be rich or lean and not precisely stoichiometric, this design should be highly robust with very little emissions slip. In order to achieve such a system some efficiency must be sacrificed. Extra fuel must be present in the exhaust to convert NOx in the first catalyst, while air must be compressed for injection between the two catalysts.

For our tests the engine was run rich and air was injected between the two catalysts. The engine was run at a variety of set points, ranging from slightly rich, to very rich. All cases showed excellent NOx conversion through the first catalyst, but NOx was present after the second catalyst. It was determined the first catalyst, under rich conditions, was producing ammonia. Unfortunately when ammonia oxidizes on a three way catalyst the most favorable reaction is the formation of NOx. Thus, a significant amount of NOx exits the system due to the formation of ammonia. Our electronic NOx sensors also detect ammonia, and as shown in Fig. 14 it was possible to observe ammonia in the exhaust prior to the first catalyst and NOx in the exhaust after the second catalyst.

Figure 61: Ammonia is produced in the first catalyst (shown in purple), and is subsequently converted back to NOx in the lean catalyst (shown in red) at a rate of over 90%

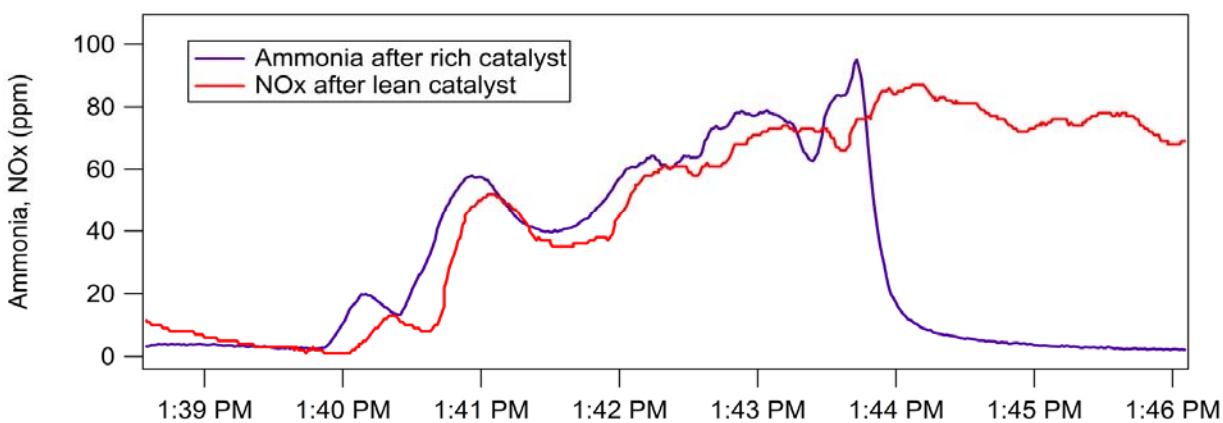

Ammonia is oxidized in three main ways:

$$2\ NH_3 + 3/2\ O_2 \rightarrow N_2 + 3\ H_2O + 151\ \text{kcal} \quad (1)$$
$$2\ NH_3 + 2\ O_2 \rightarrow N_2O + 3\ H_2O + 132\ \text{kcal} \quad (2)$$
$$2\ NH_3 + 5/2\ O_2 \rightarrow 2\ NO + 3\ H_2O + 108\ \text{kcal} \quad (3)$$

Under normal TWC conditions reaction 3 is favored over 90 percent. Due to this issue a two catalyst system is not feasible for robust emissions cleanup. However, certain catalytic wash coats have been found to favor reaction 1 as much as 95 percent. With such a catalyst in place the system could be feasible, but would require 3 catalyst in series to first convert the NOx, then to react any ammonia via reaction 1 above, and finally to oxidize CO and hydrocarbons. A diagram of a possible system is shown in Fig. 15. More research is required to more fully determine the capabilities of such a system.

Figure 62: A system capable of running the rich/lean system would require 3 catalyst: a TWC running rich followed by air injection and then an ammonia selective catalyst and a CO and HC oxidation catalyst

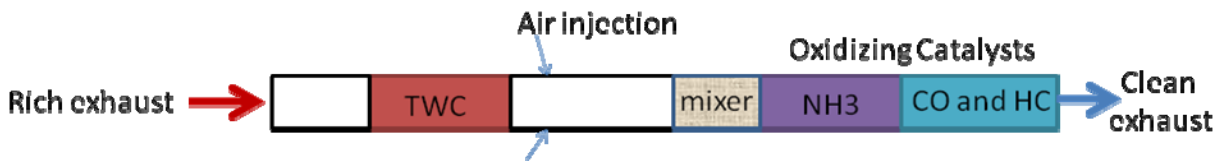

High H2/CO ratio producer gas through a single catalyst

Encouraging results have been produced when running on producer gas with a high H2/CO ration, as shown in Figs. 16 and 17. Running at stoichiometric to take advantage of the TWC simultaneous reduction of both CO and NOx have been achieved for prolonged periods with no measurable ammonia production.

For these tests the two catalyst system was left in place, but no air was injected. This allowed for the control system to measure and react to emissions after the first catalyst, with the second catalyst acting as a buffer to prevent emissions slips while the controller corrects the run point. The figure below gives an overview of the emissions. The lambda sensor (shown in blue, corresponding with the blue axis on the far left side) is close to 1. This is in contrast to previous runs using low H2/CO ratios for which the sensor reported 1.07 when the TWC was in its optimal operating range. NOx after the first and second catalyst are shown in red and purple respectively and corresponding to the left axis in red. The advantage of having two catalysts is clear as there are frequent NOx slips through the first, but almost no NOx slips out the tailpipe. This is the result of the catalyst's ability to store molecules on its surface – when the first catalyst becomes saturated the second can absorb the excess for a short period. During this time the engine run point can be adjusted to correct the saturation. The same effect can be noted in the oxygen signals, shown in black and green dashes.

Figure 63: An overview of the system operating with two catalysts in series with no air injection.

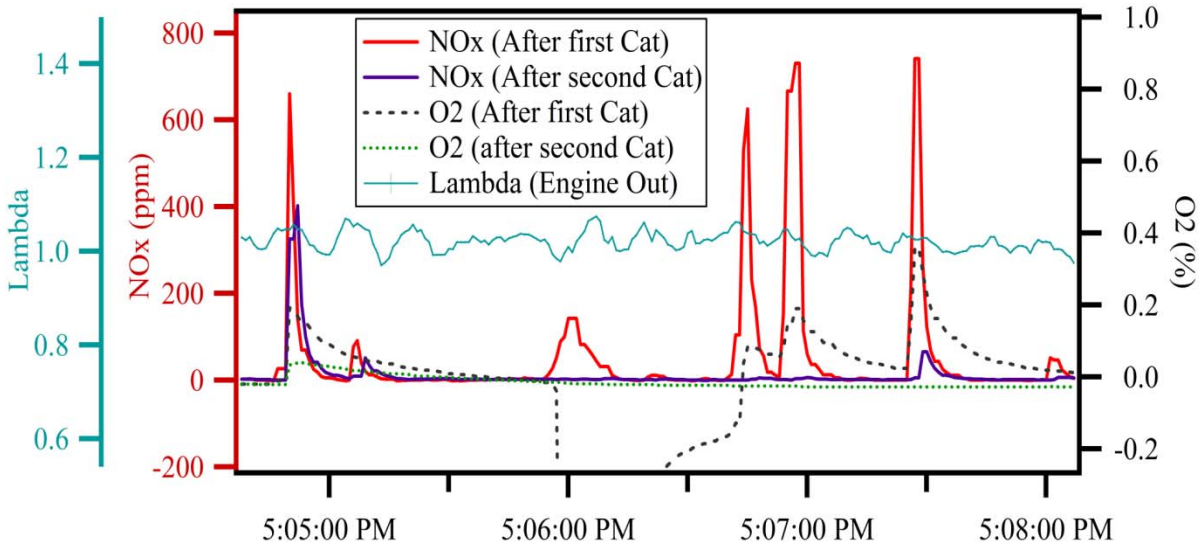

The frequent but irregular 'bursts' of NOx through the first catalyst are not fully understood as they do not seem to have any direct correlation to the lambda sensor readings. This phenomenon has been noted in previous catalyst work at UC Berkeley, and while it has not be completely explained is has been found that with advanced dithering strategies the frequency and magnitude of the bursts can be significantly reduced.

Good exhaust clean-up while running on producer gas was achieved, as shown in the plot below. Aside from an occasional 'slip' the NOx and CO levels are very nearly zero for the entire run. The average values of both NOx and CO are below 8ppm for this entire 14 minute test, which is very encouraging. The system design is effective and can be used to clean the exhaust of internal combustion engines running on producer gas.

Figure 64: NO_X and CO exhaust emission cleanup performance.

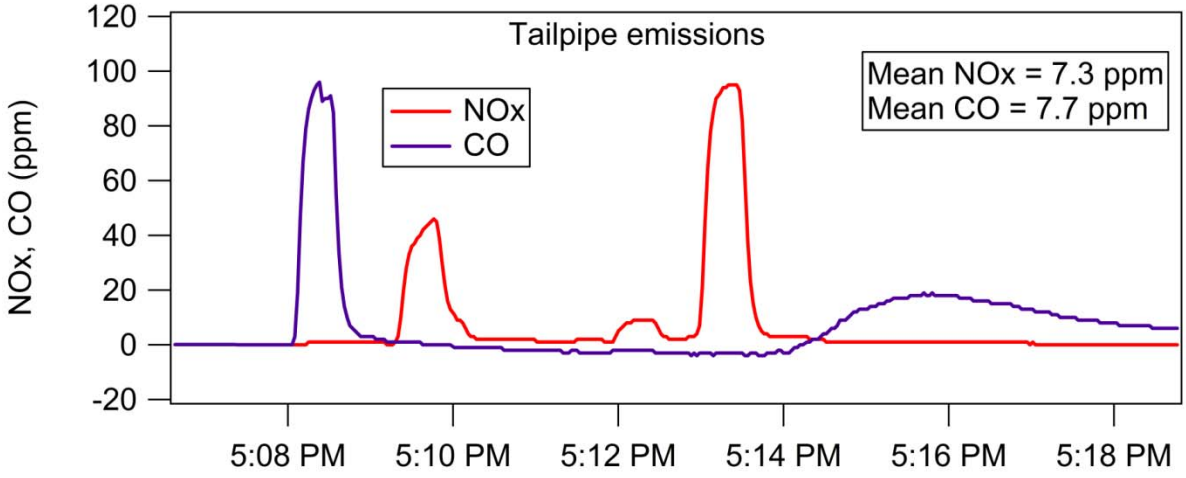

Chapter 14:
Task 2.3 Power Generation from Gasification of Wood Waste.

14.1 Task 2.3.1 Selection/Acquisition of 100 kW Generator Set.

To convert biomass to a fuel gas, a thermochemical conversion process is used in which the carbon from a biomass source (forest wood waste/residue) is combined with water at high temperature (steam) in a gasification reactor to generate producer gas which is composed primarily of carbon monoxide (CO), hydrogen (H_2), carbon dioxide (CO_2), methane (CH_4), mixed with some water vapor (H_2O) and hydrocarbons with molecular weight higher than that of CH_4. For electricity, a stationary SI-engine is planned to be installed and operated on the unreformed or reformed gas from the plant. The unreformed gas contains larger amounts of methane, while in the reformed gas (syngas) most methane is converted to hydrogen and carbon monoxide. A table of the expected gas producer gas composition is shown in Table 1 [1].

Table 19: Producer gas composition from gasification of wood waste.

Gasifier outlet gas composition	mol% (wet)	mol% (dry)
H_2	15.0	25.1
CO_2	7.4	12.4
CO	25.1	41.9
H_2O	40.2	–
CH_4	9.0	15.1
C_2H_2	0.3	0.4
C_2H_4	2.5	4.1
C_2H_6	0.1	0.2
C_6H_6	0.1	0.1
tar ($C_{10}H_8$)	0.1	0.2
NH_3	0.2	0.3
H_2S	0.04	0.07
H_2:CO molar ratio	0.60	

A SI-engine that is built to operate on natural gas can under certain circumstances be powered by producer gas. One criterion is the compression ratio and the resulting minimum octane number. Since the octane number of natural gas (methane) is quite high (~130), the octane number of producer gas will be lower. Therefore, an engine with a lower compression ratio is desired than would be possible for natural gas.

14.2 Engine Selection

The engine in that was selected was a natural gas engine made by Waukesha (Fig. 1). The details and specifications are shown in Table 2.

Table 20: Engine specifications for Waukesha H-2475G

Engine	
Model	H-2475G
Spec	W33298
Serial No.	52647
RPM	1200
Compression Ratio	9.41
Bore	7.5"
Displacement	40.5 L
Type	V8
Generator	
Part No.	P307493
Serial No.	85838
Volts	277/480
Phase	3
Hz	60
KW	200
Amperes	240

Figure 65: Waukesha H-2475G engine at the Woodland Biomass Research Center

14.3 Engine Setup

The engine was delivered to the Woodland Biomass Research Center in April 2009. In September 2009, the engine was test-run on propane (Fig. 2). In October 2009, a concrete pad was designed and poured (Figs. 3 and 4). The following photographs show some of the timeline.

Figure 66: Test run of engine on propane in September 2009

Figure 67: Concrete pad reinforcement with rebar before pouring, October 2009.

Figure 68: Concrete pad with engine, October 2009

Chapter 15:
Task 2.3.2 Installation of a 100 kW Generator Set on Research Reactor

15.1 Preparations for Engine Installation

After the engine-generator-set was purchased and delivered, the team at the WBRC began preparations for the installation. They choose a location outside the main building near the location where the producer gas is routed to the flare. Figure 5 shows a schematic of the location relative to the rest of the pilot plant. At this location, the staff prepared and poured a concrete pad capable of supporting the engine-generator-set. This is shown in Fig. 6. In order to support later installation of measuring and control equipment, the team created an additional area of concrete around the engine pad and subsequently constructed a roof above the engine area. These steps are illustrated in Figs. 7 and 8.

Figure 69: Schematic Illustration of the Pilot Plant with engine location (shown as orange box). Gas sampling lines (shown in green) transport gas samples from the engine exhaust and other locations to the measuring instruments (shown as blue boxes).

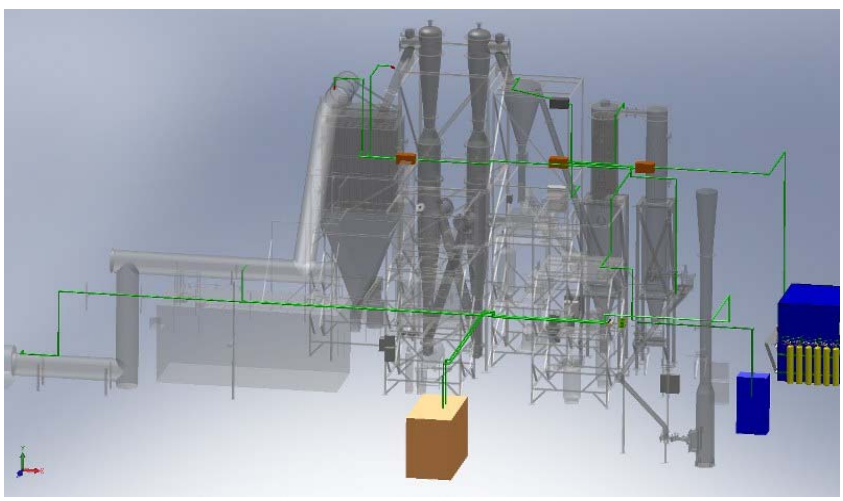

Figure 70: Concrete pad reinforced with steel is used to support the engine generator set.

Figure 71: Preparation for Concrete Area around Engine Pad

Figure 72: Construction of Roof above Engine-Generator-Set

Researchers from the University of California San Diego and Berkeley designed a procedure for operating the SI-engine. They set out with the goal to take all the fuel as it is produced from the gasification plant even as the quantity of the gas varies over time. The algorithm involves three control loops (depicted in Fig. 9). The first control loop monitors a measurement variable that indicates the gas flow from the plant, such as a pressure of an intermediate vessel. The manipulated variable is the load, and as more gas is supplied from the plant, the load is increased. The second control loop measures the lambda value at the exhaust of the engine. For a stoichiometric operation using a 3-way catalyst, the setpoint for lambda is 1.0. The manipulated variable is the position of the air-throttle to control the necessary amount of air for a given fuel. The third control loop is provided by the engine, as it is equipped with an electronic governor, and its throttle valve is controlled to achieve a constant engine speed of 1200 rpm.

Figure 73: Schematic Illustration of Engine Control

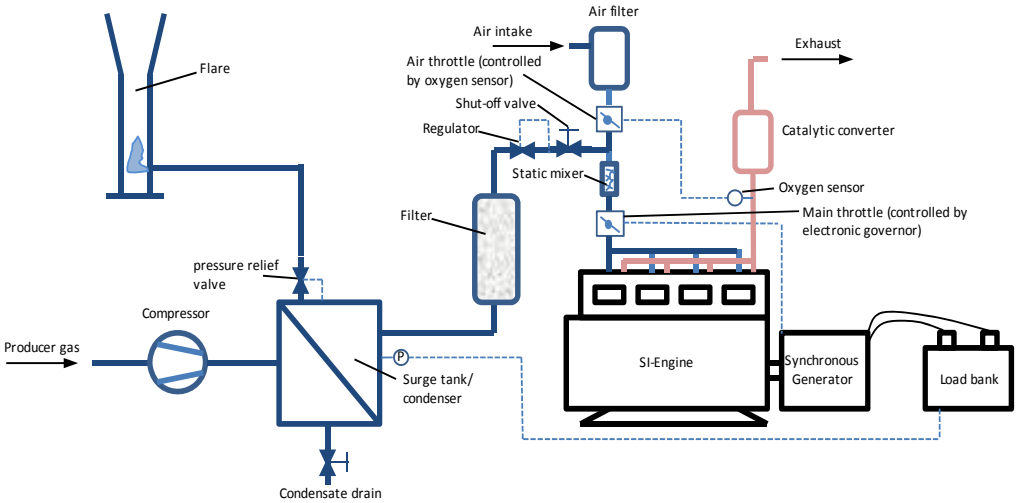

The schematic engine setup in Fig. 9 shows a pressure relief valve, which serves as a safety mechanism. If the engine for any unexpected reason is not able to use all the fuel generated at the plant, then the pressure-relief valve will open and vent the excess gas to a flare. The pressure-relief valve is set to a pressure slightly above atmospheric by its own weight without any additional weights applied to the lever arm. The research team acquired a pressure-relief valve and installed it as shown in Fig. 10.

Figure 74: Pressure-relief valve vents excess gas to a safety flare if the pressure rises above atmospheric

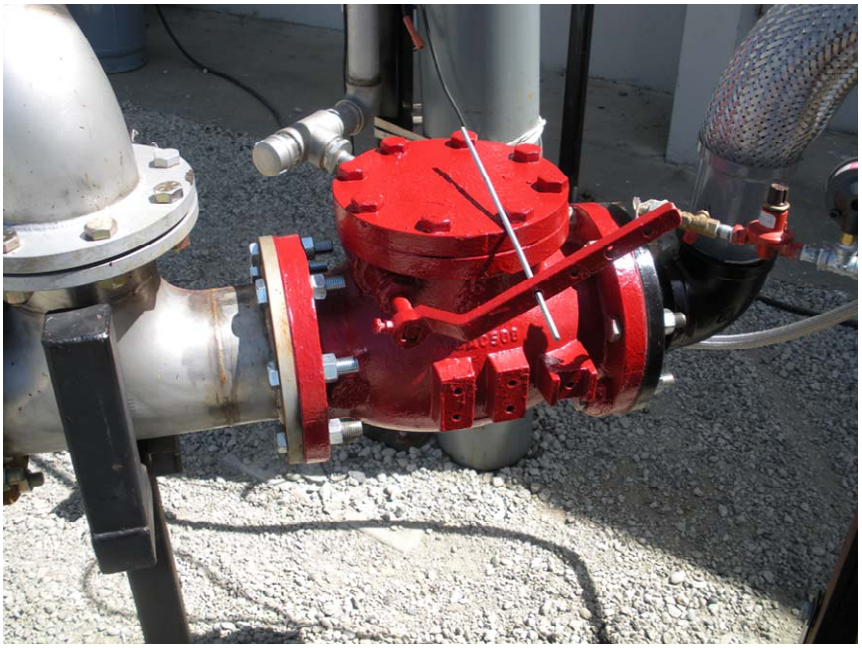

15.1.1 Final Engine Installation

The staff at WBRC finalized the installation of the engine-generator-set by bolting down the engine to the concrete pad and installing all piping and auxiliary units. They purchased a radiator/fan assembly for cooling the engine coolant. The manufacturing team of West Biofuels constructed two filter housings and equipped them with fabric filters, capable of cleaning the gas of fine particles. These units are shown in Fig. 11. For electrical and electronic installations, the team at the site mounted several electrical enclosures next to the engine (Fig. 12). These enclosures will used for computer control equipment, lamda-sensor controllers, power meter, and fuses. Figure 12 also shows the engine in its final installed location

Figure 75: Fuel filters in the background in the middle of the photograph. A radiator/fan assembly is installed for cooling the engine coolant (shown on the right).

Figure 76: Engine-generator-set installed on concrete pad with electrical enclosures protecting various electrical and electronic components.

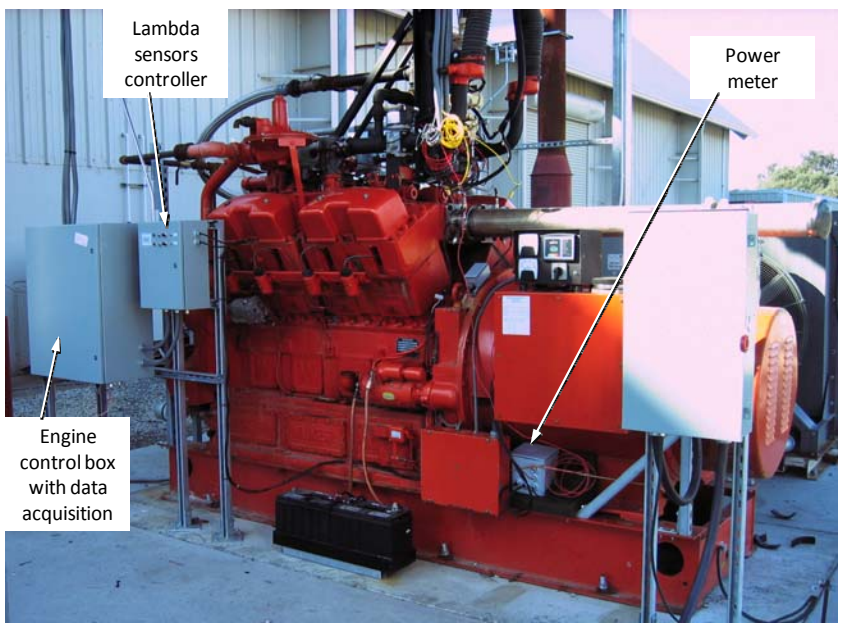

15.2 Engine Testing with Propane

The mechanical staff at WBRC prepared the engine for operation by bringing all lubricant and cooling fluids to the proper level and by selecting an ignition timing of 27 degrees before-top-dead-center (BTDC). They also installed propane pressure regulators for both, the carburetor fuel inlet, and for the manifold fuel inlet. First, they tested the engine in its original carburetor configuration. Here, the carburetor automatically creates a fuel-rich fuel/air mixture, which

makes it easy for the engine to start. The team started and stopped the engine several times in this configuration and verified that all systems were working as planned. Then, in the next step, the team started the engine by metering propane through a manifold toward the mixing tee, where it mixed with air. The research group controlled the amount of air using the electronic throttle valves. During startup (cranking of the started motors with batteries), the researchers set the throttle valves to about 60 percent open, and with this setting the engine started at a slightly fuel-rich condition. As soon as the lambda-sensors in the engine exhaust registered a stable signal, the automatic air-throttle control took over and the engine was running at a stoichiometry of around lambda=1.0.

To monitor the power output of the engine, the staff research team purchased a power meter from Eaton Corp. They installed the power meter by tying into the current transducers installed in the engine control enclosure. They tested the engine and power meter at various loads and found satisfactory results. In Figure 13, the output screen of the software for a 107 KW test is shown.

Figure 77: Power Output during Testing on Propane output from Eaton power meter showing 3-phase power of 107 kW (271 V and 132 A).

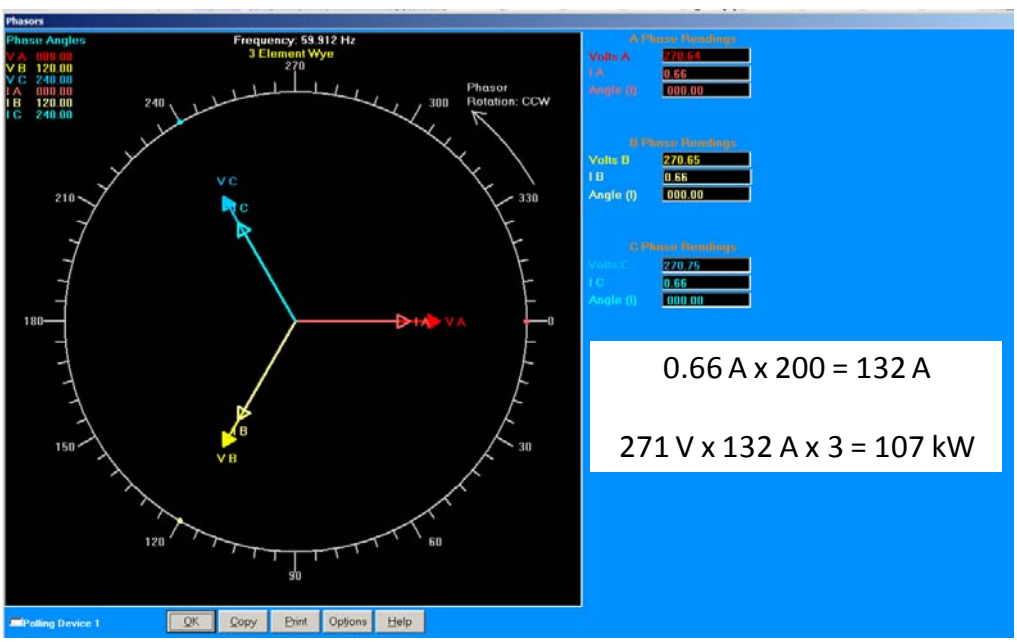

Chapter 16:
Task 2.3.3 Engine Parameter/Emissions Instrumentation

16.1 Control Equipment for Engine Operation

The conceptual design of the emission control system for the operation of the Waukesha engine-generator at the Woodland Biomass Research Center is illustrated in the schematic given in Fig. 14. The intake manifold, air intake throttle valve, and lambda sensor used to control the air-fuel ratio of the entire inlet stream, and this fuel/air mixture is then divided between all cylinders. Previously, the team at WBRC had pursued the concept of installing an air-throttle for each of the two engine banks (4 cylinders), but this configuration proved unstable with fuel not reaching both sides of the engine evenly. The main control valve for the air inlet is an electronic butterfly valve, and depicted in Fig. 14 with the label "V-5". Details of the valve are shown in Fig. 15.

Figure 78: Schematic of SI-engine with Control System

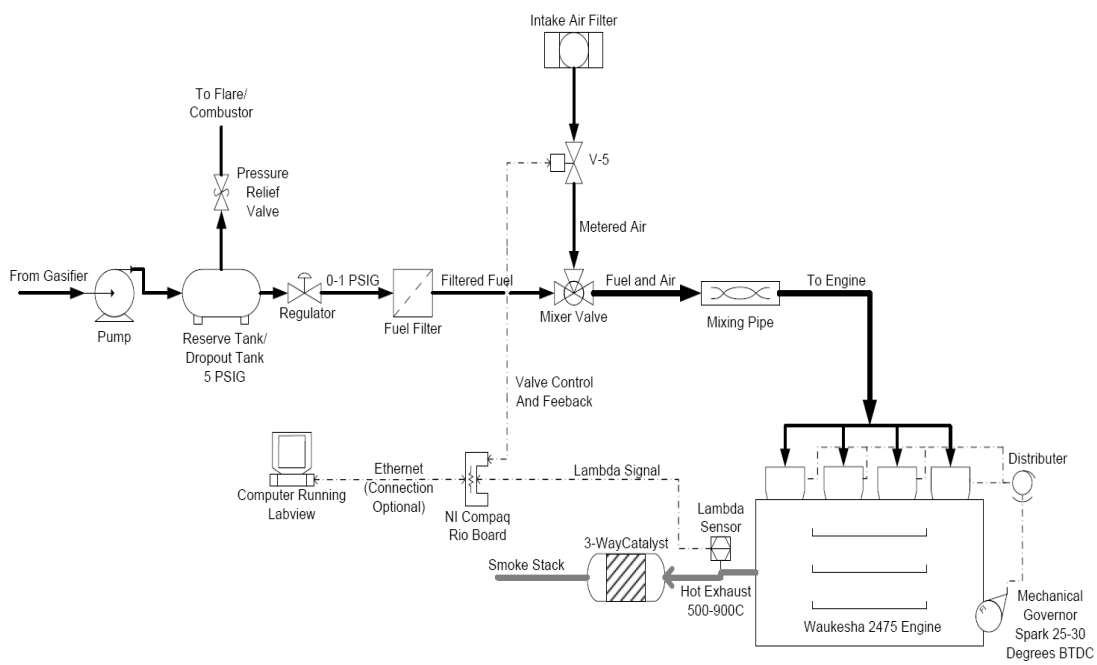

Figure 79: Woodard Model F-Series with integrated actuator

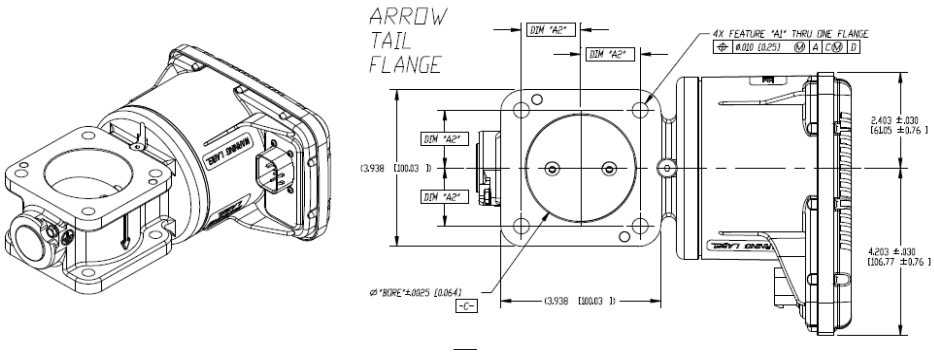

Work on the emission control system during this period focused on developing the Labview program for signal acquisition using the National Instruments Compaq RIO board. The research team had initially communications problems with the Compaq RIO data acquisition, and National Instruments Inc. replaced the software with a new driver for the equipment. With the corrected software, the Compaq RIO board provided both input signals and output voltages necessary to operate the engine emission control system.

The air/fuel-ratio control for engine operation and emission control is based on monitoring the oxygen content in the engine exhaust with a lambda sensor (air/fuel ratio). The researchers selected as lambda sensor a Bosch Universal Exhaust Gas Oxygen (UEGO) model LSU4.2 (shown in Fig. 16) with a Motorsports model LC-1 controller which they interfaced to the National Instruments Compaq Rio data acquisition board.

Figure 80: Bosch Universal Exhaust Gas Oxygen (UEGO) Sensor Unit LSU4.2

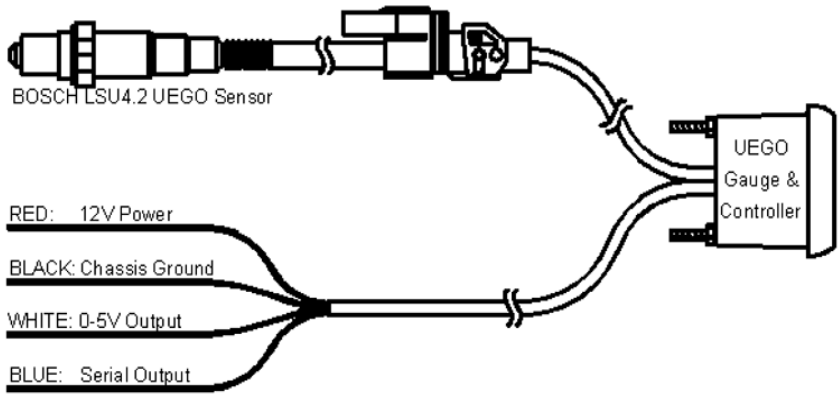

In total, the research team purchased four Bosch UEGO sensors. They installed and tested the accompanying software. They noted that the sensors can only be programmed for specific gases and cannot function purely as an oxygen/excess fuel sensor. For the gas produced from the gasification of biomass, this means that there will be some error in reading the true lambda value since the exact makeup of the gas produced from the biomass can vary, but it should be able to correctly indicate a stoichiometric condition as well as provide proportional indication of how rich or lean the air-fuel ratio is at the engine inlet.

In order to test the wideband lambda signals, the research team designed a test assembly. It consisted of a vessel in which the lambda sensor could be mounted with ports for adding gases of known oxygen concentration. The objective was to determine how accurately the sensors could measure mixtures in a stable environment. The results of the oxygen measurements with four Bosch UEGO model LSU4.2 are summarized in Table 3.

Table 21: Oxygen calibration of four Bosch UEGO sensors model LSU4.2.

Lambda Sensor	1	2	3	4
Air (%O2)	20.7	20.6	20.7	20.7
Nitrogen (lambda)	0.99	0.98	0.98	0.99

The researchers concluded that over the range from ambient air to stoichiometric, the sensors were accurate to within 0.02 lambda. A problem can arise if the stoichiometric point is off as far as 0.02 in either direction since it is critical to be able to pinpoint the correct value for proper functioning of the exhaust system. Further testing will be conducted to determine if this will be a problem and also how various fuels affect these readings. The next step was to test the sensors in an actual exhaust environment.

At the WBRC, the mechanics team mounted and wired the Woodard valves and tested them. They found that the performance of one of the valves was not satisfactory. They determined that the power supplies available were not large enough to power the valves, so larger units capable of producing much larger amounts of power were purchased and interfaced to the valves.

The team also modified the Waukesha engine exhaust system by adding custom flanges and straight exhaust tubes (without catalyst). These are shown in Fig. 17. The researchers then installed the exhaust gas oxygen sensors and flexible stainless steel gas-samplings lines for measuring exhaust emissions.

Figure 81: Waukesha engine exhaust system with custom flanges and straight exhaust tubes with installation of exhaust gas oxygen sensors (shown with black cable).

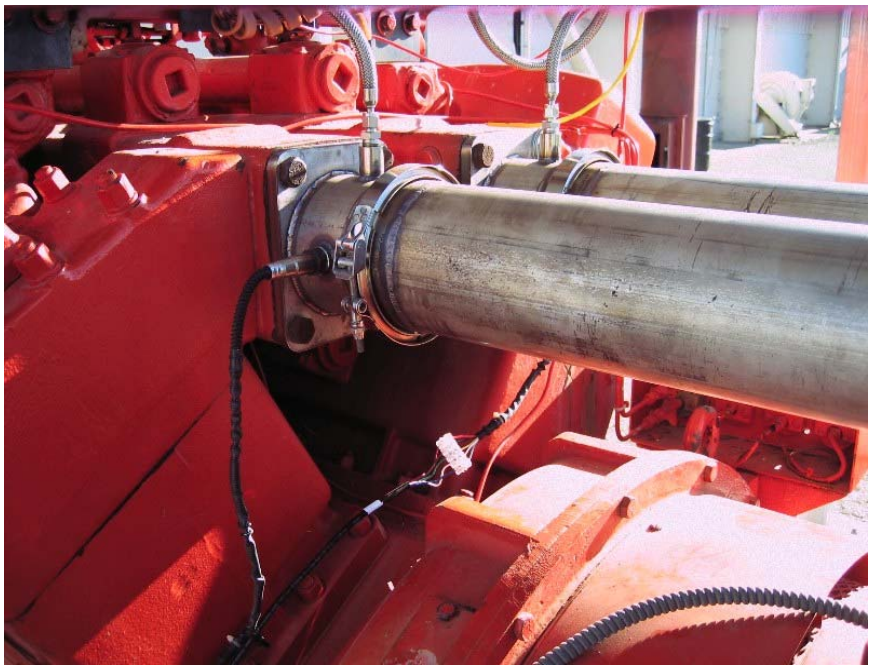

Originally, the research team ordered two Woodard Model F-Series throttle valves for controlling the air/fuel ratio on each of the banks on the 100 kW Waukesha-Engine. The valves were tested at UC Berkeley before installation. It was determined that one of the valves was defective and needed to be repair/replacement. A substitute valve was located with a slightly larger (68 mm as opposed to 60 mm) and uses a 0-200 mA signal (as opposed to 0-5 V) which can be used as a temporary substitute to maintain progress on the engine control while the second valve is replaced. The Labview software for engine control was modified to support the new valve.

16.2 Additional Instrumentation on Engine

The Waukesha Engine has two throttles before the intake manifold. The first throttle is manually adjustable and is usually used to restrict the amount of flow during startup and warmup. It can also be used to restrict the flow rate when running on small loads. The second throttle is controlled by an electronic governor and adjusts automatically to keep engine speed at 1200 rpm. It is possible that the continuous movement of this governor-throttle interferes with the other control strategy. In this case, the research team contemplated to operate the engine at a speed slightly below 1200 rpm, which would ensure that the governor throttle would be open at all times. To monitor the governor-throttle position, the researchers installed a throttle-position sensor (see Fig. 18). This enabled the recording and viewing of status through the Labview software. The team conducted a test in which the air-throttles were slowly closed and the governor-throttle position recorded. While the air-throttles were closed, the governor-throttle opened until it was all the way open and the engine speed started dropping. The recording of the governor-throttle position is shown in Fig. 19.

Figure 82: Waukesha engine-intake manifold with governor throttle and throttle-position sensor; the throttle above the governor throttle is a manual throttle used for low loads

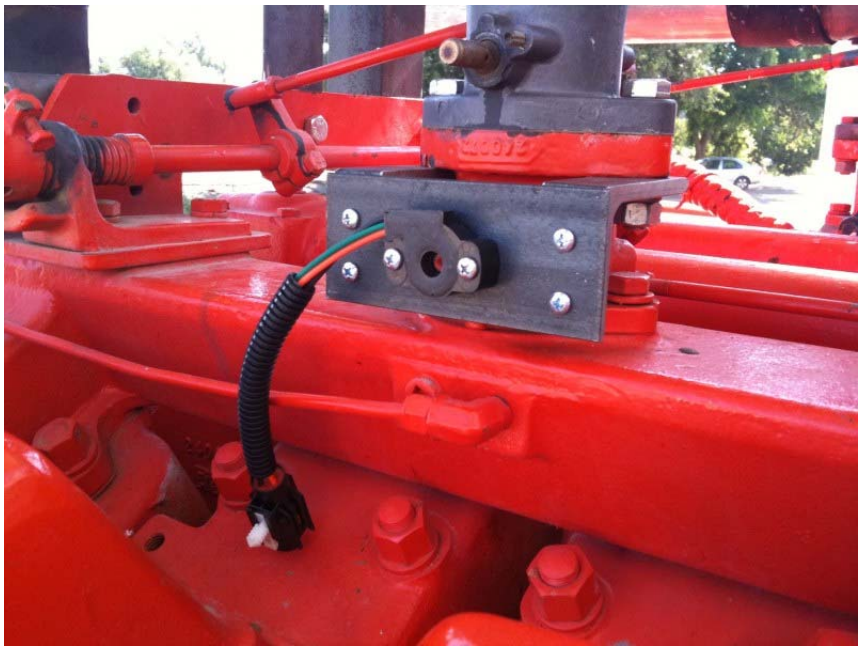

Figure 83: Plot of engine governor position measurement with LabView during simultaneous operation of Woodard air intake control valves; when air-valves close sufficiently, the governor throttle is fully open.

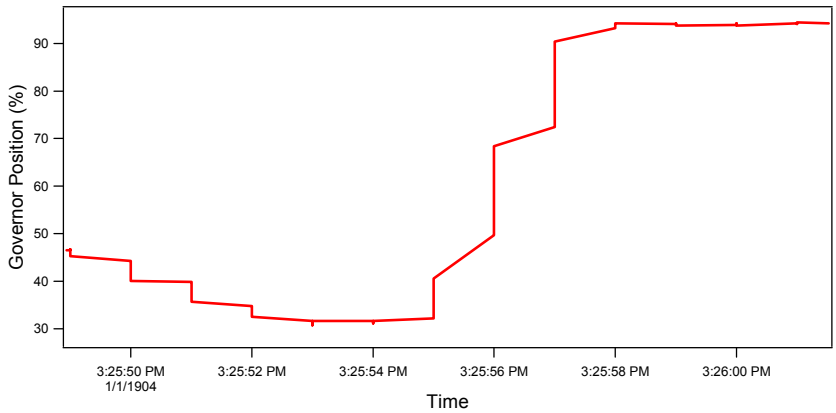

The staff research team at WBRC also installed pressure and temperature measurement at the Waukesha engine. For example, they installed pressure transducers in the intake before the two engine throttles. This will give an indication of how much pressure loss is generated by the air-throttles and helps determining if both engine banks behave similarly. The team installed thermocouples at various location, but most importantly is the measurement of the exhaust temperature before and after the catalyst. The performance of the catalyst is depending on the temperature, and generally higher temperatures are preferable. With producer gas and at low loads, it is more difficult to maintain high exhaust temperatures, mainly because the exhaust flow rate is lower, and therefore relatively more heat is lost until the catalyst is reached. With high amounts of H_2 and CO in the fuel, lower exhaust volume is produced, since both of these

fuels only generate 1 mol of product for 1.5 moles of reactants (1 mol of fuel plus 0.5 moles of O_2).

The research team obtained and installed a Monarch Instruments RPM meter on the SI-engine. It can be programmed to output a 0-5V signal for a specified RPM range. The team programmed the RPM meter for a linear output between 0 and 1300 RPM. They enhanced the control program for adjusting the load bank in real time by setting the power output from the engine/generator automatically based on the RPM. This insures that the governor throttle, which operates in parallel with the custom control system, is maintained wide open by keeping the engine RPM below the governor's pre-programmed RPM setpoint.

16.3 Variable Loadbank

For testing of the engine under variable fuel flow, the research staff assembled a variable loadbank. With this unit, the control software can select a load that matches the fuel flow and can therefore maintain constant engine speed without the need of the governor. The loadbank included resistors of various sized, and a matrix was generated by the computer for selecting the proper resistors for a given load. With this method, the loadbank had a range of 0-140 kW with increments of 2.8 kW, in its final configuration. Figure 20 shows photographs of the loadbank.

Figure 84: Variable loadbank for testing of the engine control system; the left photograph shows the backside of the loadbank with the cooling fans. The right photograph shows the control end with breaker panel and optional manual control switches

16.4 Exhaust Emissions Sampling

The gas sampling system was installed from the engine exhaust to the Horiba exhaust gas analyzer. At the engine exhaust (see Fig. 21), sample lines and filters needed to be isolated from engine vibration. Sampling was successfully tested with a cold trap before the Horiba that was able to remove excess moisture.

The research team installed a 1L three-way catalyst on a slip stream on one of the engine banks. To choose an appropriate flow rate, they mounted a cap at the end of the main exhaust tube that creates enough back-pressure so that a portion of the engine exhaust flows through the catalyst. They then installed two sampling lines, one before and one after the catalyst, shown in Fig. 21.

Researchers at WBRC have designed an elaborate network of gas sampling lines for the gasfication reactor (Fig. 22). They also connected the two sampling lines from the engine exhaust to this network, which enables all gas analysis instruments to analyze the exhaust gas composition. One instrument is a Horiba Gas Analyzer, which is capable of measuring NOx, CO, CO_2, and O_2. The instrument together with enclosure is shown in Fig. 23.

Figure 85: Catalytic Converter and Gas Sampling Probes The left photograph shows the adjustable exhaust cap on the end of the main exhaust tubes to create necessary back pressure. The right photograph shows the catalyst and two gas sampling lines.

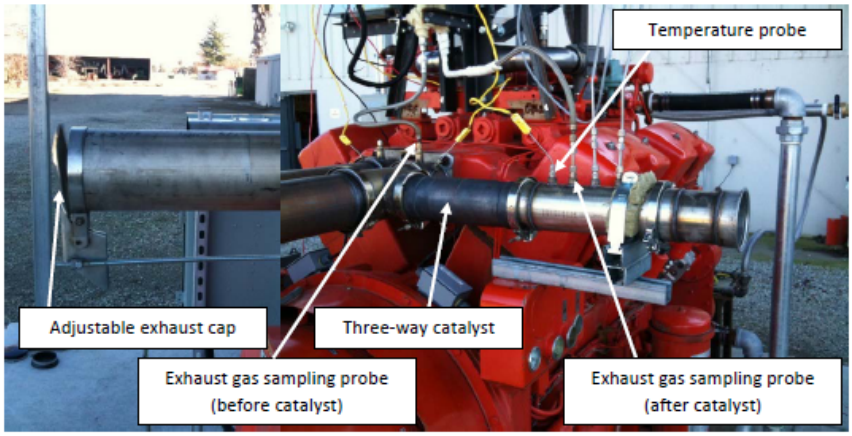

Figure 86: Sample Lines Piping and Instrumentation

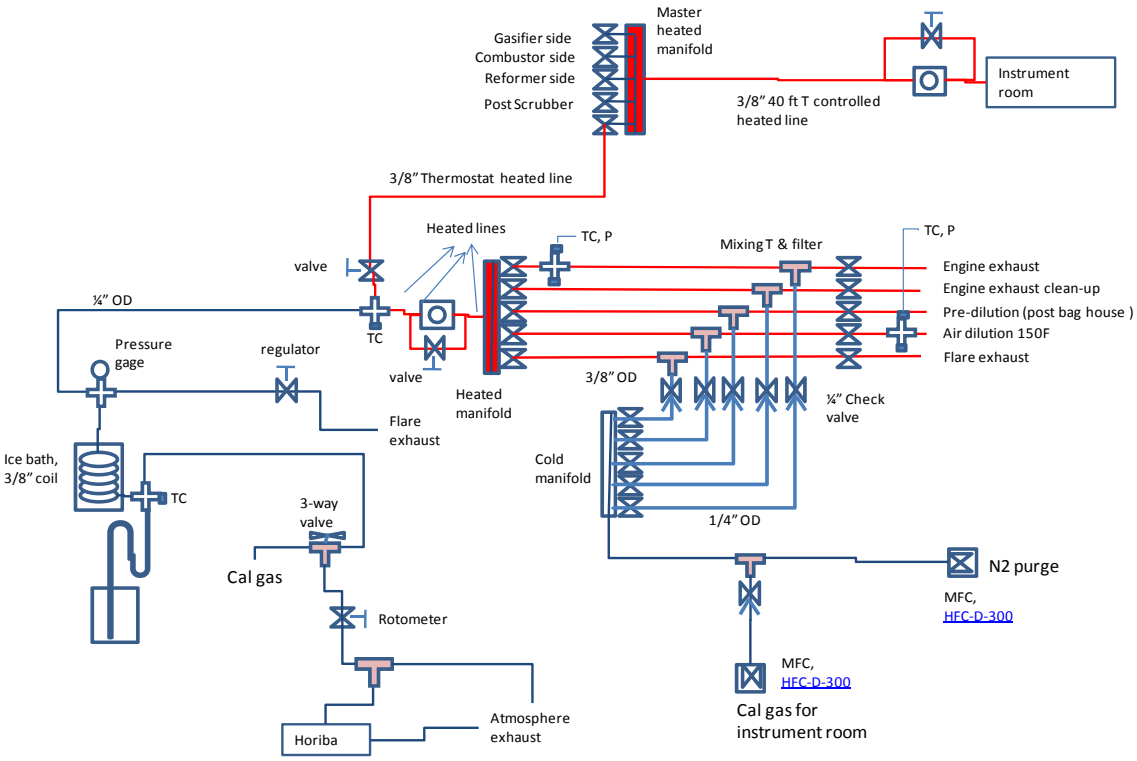

Figure 87: Horiba Gas Analyzer: gas analyzer during operation on left. The right photograph shows the gas analyzer in its enclosure, the water trap, and the heated gas sampling lines.

16.5 Testing of Engine Control and Instrumentation

16.5.1 Two Independent Air Throttle Valves

Initially, the team at WBRC installed one air valve on each 4-cylinder engine bank. The team was interested in the general performance of the control software and the electronic throttle valves. They performed an initial test using propane as fuel and a load bank with a 20 kW fixed load. Since the amount of fuel did not exactly match the power of the load bank, one engine bank ended up running fuel rich, while the researchers were able to test the other engine bank. The bank on the west side of the engine was able to be well controlled with an air fuel ratio to match the required value of lambda = 1.0. In this initial test, it was however not possible to test the automatic control on both banks simultaneously without having a variable load bank. The successful control of the stoichiometry (lambda) control for the west bank of 4 cylinders is shown in the Fig. 24.

Figure 88: Single Engine Bank control of air fuel ratio (Lambda) of the two 4-cylinder banks of the Waukesha engine with and without automatic control with LabView Software

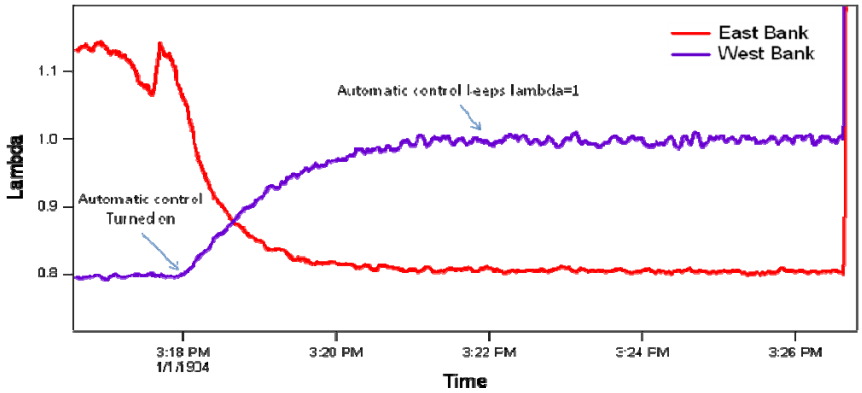

As described, with two independent air-valves but one fuel supply, the research team encountered control problems in balancing the two 4-cyclinder banks of the engine. The fuel flow was too sensitive to small changes in the throttle valve positions. The team contemplated that increasing the volume of propane by diluting it (making the energy density more similar to producer gas) could reduce the sensitivity. They considered the following possible dilution methods: nitrogen, EGR, exhaust from gasifier, or to replace propane with methane. They regarded, however, most of these options as too problematic, with nitrogen from a liquid nitrogen tank chosen as the best option. They estimated that using a 250-liter liquid nitrogen dewar to dilute the propane to approximate producer gas concentration would provide 20 minutes of running.

As a final solution the team concluded that by closing a manual throttle upstream of the engine governor but downstream of the air throttles would produce a similar effect as diluting the fuel for a narrow range of operation. Closing the manual throttle valve allowed automatic control to operate more stably, but balancing the two banks was still too sensitive for satisfactory operation.

16.5.2 One Air Throttle Valve for both Engine Banks

After these tests, the research team concluded that for the engine control system to operate with unknown producer gas, the intake manifold system needs to be redesigned. They decided that the air throttle valves should be operated in parallel upstream of the mixing tee so that the instability introduced by separate engine bank air/fuel-ratio control was eliminated. With this method, the air valves essentially act as one larger valve. The entire air is mixed with the entire fuel and the mixture is then split between the two banks. This allows the air throttle valves to adjust the stoichiometry of the fuel air mixture and it greatly improves the fine control of the system and reduces the need for an additional PID control system for balancing the two engine banks. The system layout is shown in Fig. 25.

Figure 89: New engine inlet configuration with combined intake manifold for both engine banks

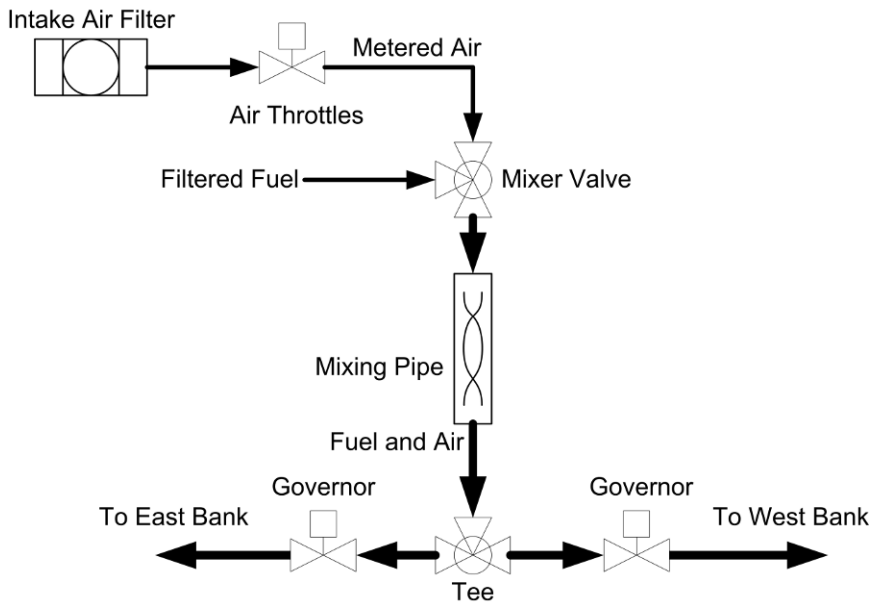

In the new design, the researchers found that the air -throttle valves work together rather than compete, making the engine much more stable. This also allows for the governor to operate without greatly impacting the stoichiometry of the engine. The ability to operate the air-throttle valves in unison with the governors is a great asset as it reduces the complexity of the problem system and ensures that the power produced will always be of a high enough quality to drive electrical equipment. The team at WBRC will use this configuration in subsequent tests on emissions reduction and power production from producer gas.

Chapter 17:
Task 2.3.4 Exhaust Cleanup System

17.1 Installation of Catalyst on Slip-stream

Catalytic converters are expensive and at risk of failure if overheated. For the Waukesha SI-engine, the appropriate catalyst size would have to be custom ordered. The research team decided to perform all measurements on a catalyst that was readily available, a 1 liter three-way catalyst mounted in a 4 in. diameter tube. They acquired several catalysts and mounted two of them in series on an exhaust slip-stream. This system allows to evaluate the performance and to determine the size of the catalyst for the full-scale system. The slip-stream arrangement is shown in Fig. 26. For the evaluation of the emissions, the research team installed three sampling ports on this section of the exhaust: One before the first catalyst, one between the two catalysts, and one after the second catalyst. These sampling ports are connected to the heated sample-line system and lead to the Horiba gas-analyzer. The researchers could then sample alternately from the three locations, but the most widely used ports were the one before the first catalyst (to determine engine-out emissions) and the one after the second catalyst (to determine the cleaned gas). To maintain higher catalyst temperatures, the team insulated parts of the catalysts and exhaust piping with mineral wool. A photo of the catalysts is shown in Fig. 27.

Figure 90: Drawing showing the catalyst system: two catalysts (in purple) are mounted in series on a slip stream off one of the engine banks.

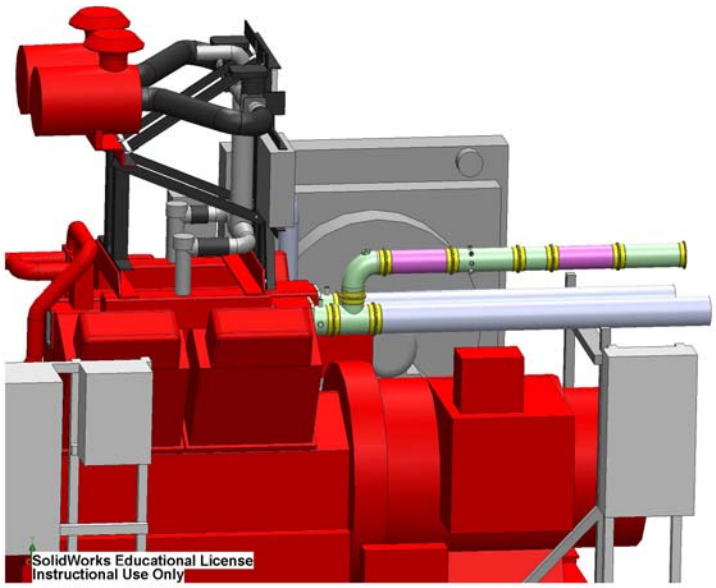

Figure 91: Exhaust of engine showing tube with two insulated (in white) catalysts. The adjustable flapper valve at the end of the exhaust is used to force the exhaust through the catalyst.

The Horiba gas-analyzer recorded the emissions with about a 20-second delay due to the length of the sampling lines. To get a real-time measurement of NOx, the research team acquired two Siemens NOx sensors and mounted them into the exhaust system, one after the first and one after the second catalyst. These sensors showed the real-time value of NOx and oxygen (near zero) and were used to decide on an optimized control algorithm.

17.2 Catalyst Testing on Propane

The research team first conducted tests on propane, because the fuel is readily available, and it allowed steadier and longer test intervals. The team added propane into the fuel inlet where normally the producer gas arrives from the gasification plant, and not through the carburetor. This allowed fine control of the stoichiometry using the valves for metering the air into the system. Propane has a much higher energy density per volume than producer gas. This is mostly because it has a higher molecular weight but also because it is not diluted with any inert gases such as carbon dioxide or nitrogen. Therefore, much smaller flow rates of propane are required, and even the overall rate of intake charge is smaller. To simulate a behavior more similar to producer gas, the manual throttle valves were slightly closed. This allowed the governor throttle to be wider open, more closely to the case of running producer gas.

For initial testing, the researchers investigated a wide range of lambda values and used the results to produce a plot showing how CO and NOx concentrations varied with oxygen concentration. Negative values of oxygen indicate extrapolation into the fuel-rich region. Results are shown in Fig. 28. As expected, the catalyst performed well at reforming NOx at low oxygen levels, but there is a sharp cutoff point where additional oxygen results in rapid increases in NOx quantities. Note, that the NOx detector used has a maximum of 1000 ppm, which is shown as the oxygen concentration continues to increase. CO displays the inverse

trend, but the cutoff point is much less defined and the rate of increase is not as severe. An ideal operating point which satisfies both NOx and CO emissions requirements does appear to exist between O2 concentrations of -0.3 percent and -0.2 percent with NOx readings consistently below 20 ppm and CO readings around 300 ppm or lower.

Figure 92: Emissions using Propane: CO and NOx concentration as a function of O2 concentration in the exhaust from a 120 kW engine generator operating on propane.

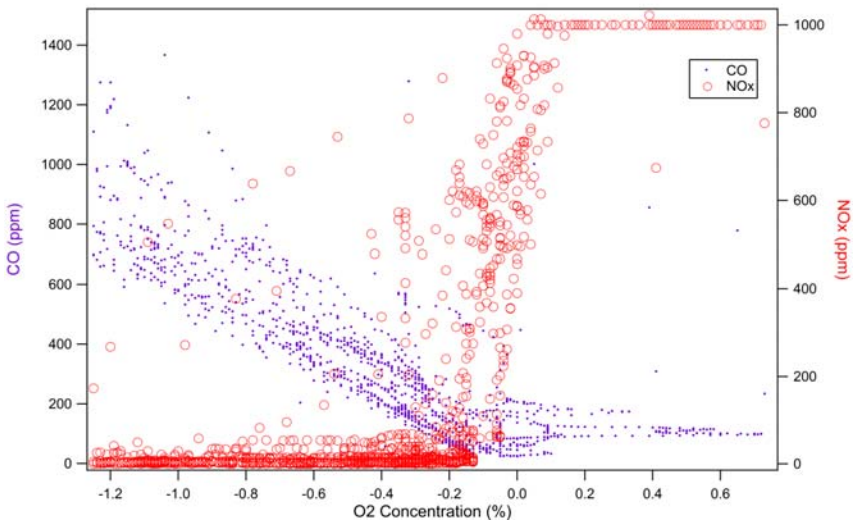

To get a better understanding of the flow rate through the catalyst and its effect on conversion, three different settings of the restrictive 'flapper' plate at the main exhaust pipe were evaluated. The flapper position was scaled based on 0 being fully opened and approximately 22 being fully blocked. The results are shown in Fig. 29. With the flapper operating in positions 17 and 18 the results seem relatively constant, but position 19 results in a significant increase in CO emissions. NOx emissions did not vary significantly for any of the positions, which could indicate a few conclusions: 1) The engine was operated too rich relative to stoichiometric for this testing, or 2) the catalyst is much more effective at NOx conversion than CO conversion. Results indicate that the optimum operating point for our testing is approximately 18, since it represents the highest flow rate which was still able to maintain very good conversion efficiencies for CO.

Figure 93: CO and NOx concentrations and exhaust temperatures over time with three different flow rates through the catalyst were evaluated by restricting the flapper position on the main exhaust pipe.

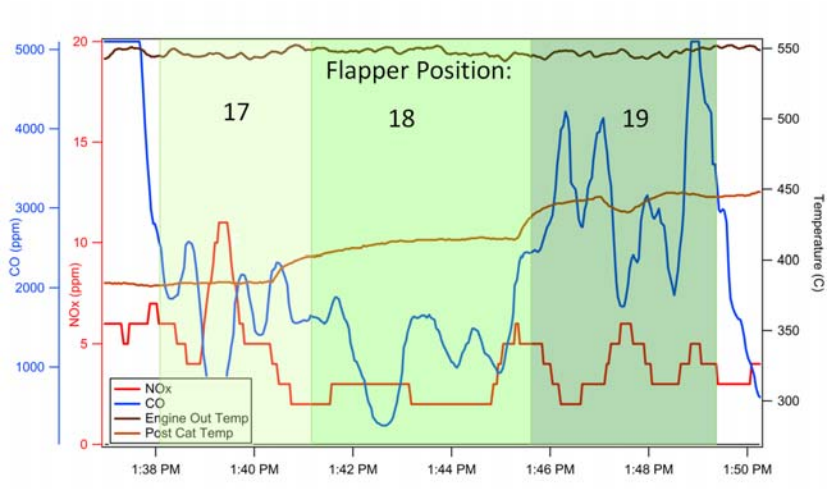

17.3 Catalyst Testing on Producer Gas

During a gasifier test at the WBRC, the research team operated the engine on producer gas and tested the performance of the three-way catalyst. They measured emissions before and after a single catalyst. The emission from a 20 minute operation of the engine on producer gas from the on 1/26/2011 is shown in Fig. 30. Initial testing of the emissions system has shown good conversion of NOx but a very large amount of scatter is present. This is a result of many factors, including variation in engine control strategy and uncertainty in the reading of the HORIBA emission sensor. The most significant result is that even when enough oxygen was present to consistently reduce NOx conversion the CO levels rarely dropped below 500 ppm and typically are above 1000 ppm. This result is believed to be caused by the already high concentration of CO in the fuel and the fact that CO is fairly unreactive near cold wall regions. The research team concluded at this point that secondary treatment (such as a second catalyst) might be necessary to obtain good conversion of both NOx and CO.

The researchers also performed a gas analysis of the emissions (after the catalyst) using a gas-chromatograph. Table 4 shows the mole fraction of major species. Carbon monoxide is confirmed at about 500 ppm, and methane is measured at 64 ppm. Other hydrocarbons were below the significance limit.

Figure 94: Emissions using Producer Gas as Fuel NOx and CO concentration as a function of O2 concentration in the exhaust from a 120 kW engine generator operating on producer gas from the gasification of wood

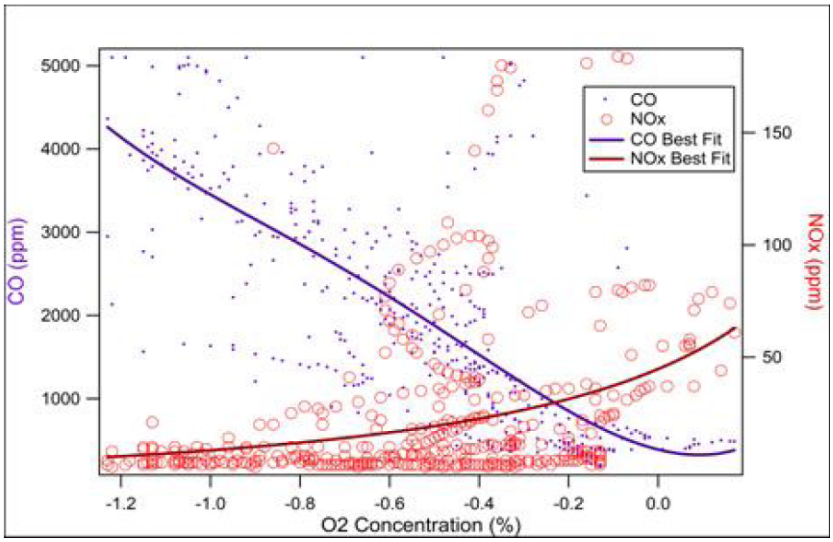

Table 22: Exhaust emissions (after catalyst) from a 120 kW engine generator operating on producer gas from the gasification of wood;

Compound	Amount	
Hydrogen	0.15	vol%
Oxygen	0.01	vol%
Nitrogen	70.26	vol%
Methane	63.99	ppmv
Carbon Monoxide	564.92	ppmv
Carbon Dioxide	16.04	vol%
Water	13.47	vol%

Chapter 18:
Task 2.3.5 Engine/Power Performance Monitoring

18.1 Initial Testing on Propane

Researchers at WBRC configured a Waukesha engine-generator such that it can convert all producer gas that is produced from the gasifier to electricity. They choose a setup in which the amount of air is controlled by electronic throttle valves to match a given amount of fuel from the plant. They also installed a valving system so that the engine can be started and operated on propane, which is available from storage tanks at the site. Figure 31 shows the schematic of the SI-engine configuration. In the original configuration, propane flows through the carburetor, and while easy to start and operate, the engine does not maintain a precise fuel/air ratio. In the new configuration, fuel is added and mixed with a controlled air flow before the carburetor. The research team demonstrated the project by adding propane in the new inlet as a test for the producer gas that was later be generated by the gasifier. The tuned PID feedback system was successfully tested on propane before running on producer gas.

Figure 95: Schematic of SI-engine configuration during testing with two possible fuel inlets: the lower inlet is the original configuration with propane flowing through the carburetor. The upper inlet is for producer gas or propane and they mix with an accurately controlled air stream.

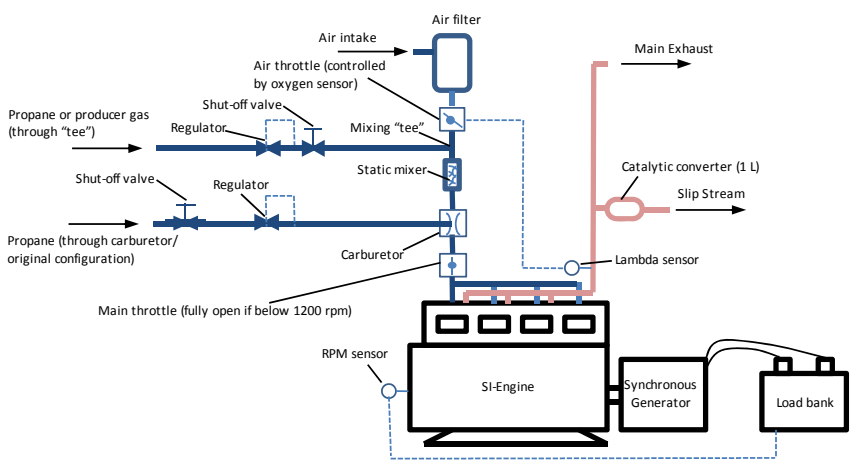

The research team continued the work on the dithering concept, and they found good improvements when running the engine on propane. Figure 32 shows the valve position vs. time during a run where dithering was applied. With minimal optimization, dithering the air supply while running on propane has delivered superior results to steady state operation. Figure 33 shows the emissions results of over an hour of dithering the engine. With additional adjustments, further reduction of both NOx and CO should be attainable. Dithering has had limited success when applied to producer gas, but it is expected its effectiveness will increase as the engine controls are refined.

Figure 96: Air valve positions versus time; both valves meter into the same mixing chamber, so it is only necessary to oscillate one valve.

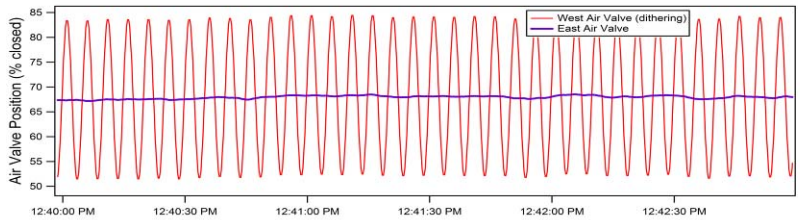

Figure 97: NOx and CO Emissions during testing on propane with dithering

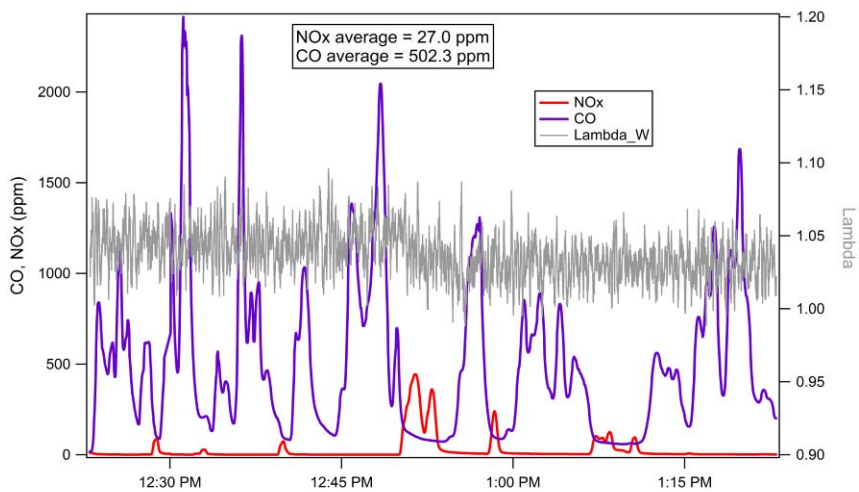

18.2 Producer Gas Production

The producer gas is generated in a dual fluidized-bed gasifier at WBRC. Researchers at this center are working on this pilot plant to learn how to operate it, how to improve it, and how to scale up to a commercial size in the future. Depending on the configuration and operating conditions, the producer gas will have a different composition. This is very relevant, since different components strongly affect combustion and pollutant formation in an internal combustion engine.

During the initial gasification tests, the team at WBRC utilized as fluidization gases recycle gas at the top of the gasifier and the exhaust from a propane/air burner at the bottom of the gasifier. As feedstock they used wood pellets with low moisture content. During the operation, the research staff measures the composition of the producer gas and other operational parameters. Figure 34 shows the typical gas composition in this configuration during three different tests. The temperature of the reactor during these tests was in the range of 675 C – 825 C. The main combustible component is CO with a mole fraction of around 20 percent. Nitrogen is an inert entrained together with air and had a mole fraction of around 34-41 percent in the producer gas.

Figure 98: Producer gas composition measured by gas chromatograph. The gas for fluidization was recycle gas at the top of the gasifier and the exhaust of a propane/air burner at the bottom of the gasifier.

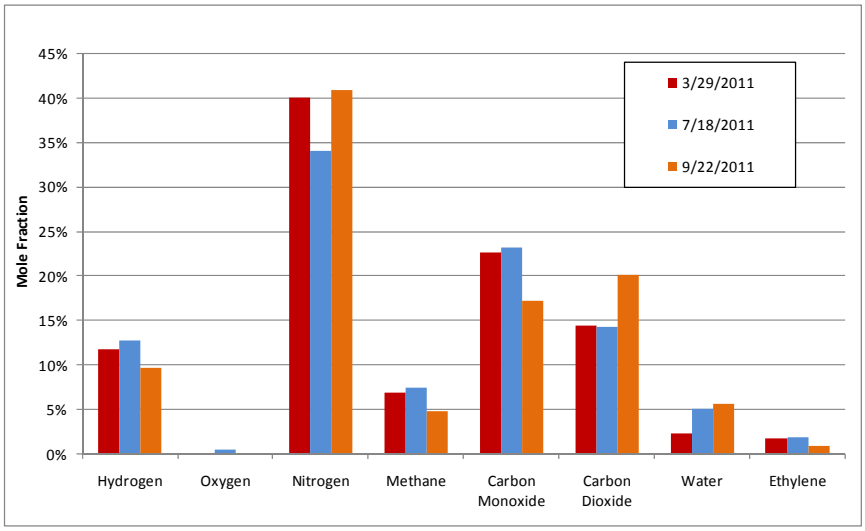

In subsequent tests, the team at WBRC operated the gasifier with steam into the bottom. This reduced the nitrogen content in the producer gas and gave it higher energy content. Figure 35 shows the major components in the producer gas from three different gasification tests. Besides lower nitrogen content, the H_2/CO ratio is generally higher when steam is used for gasification. The reason is the water-gas shift reaction $CO + H_2O \rightarrow CO_2 + H_2$ that shifts the equilibrium to the right side of the reaction when more H_2O is used. Consequently H_2, and also CO_2 increase.

Figure 99: Producer gas composition with steam operation measured by gas chromatograph. The gas for fluidization was recycle gas at the top of the gasifier and steam at the bottom of the gasifier.

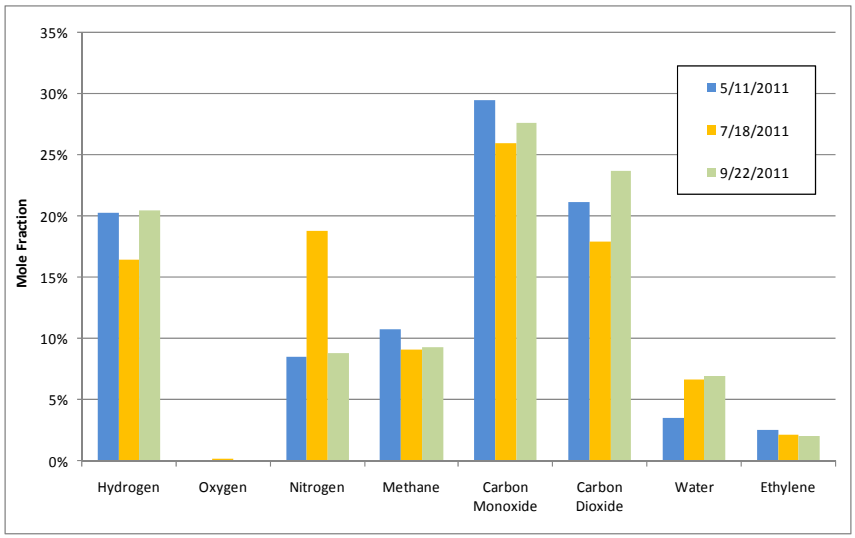

18.3 Engine Performance on Producer Gas

18.3.1 First test on producer gas

The research team operated the engine on full producer gas on December 1, 2010, the first integrated operation of the West Biofules Gasifier with power production. The engine/generator was operated for approximately 15 minutes in fully automatic mode with very stable operation. In Table 5 and in Figs. 36 and 37, the engine/generator operating parameters are presented. It should be noted that the system operated with only small standard deviations for all parameters indicating the stability of the system while running on an unknown, non-constant producer gas.

Table 23: First engine operation on producer gas gas on December 1, 2010; the temperatures are measured in the exhaust of the two engine banks.

	Average	Standard Deviation
Power	104.6 kW	0.99 kW
Freq	59.6 Hz	0.49 Hz
Lambda	1.0004	0.011
RPM	1194.2	11.11
Temp W	563.8 C	4.39 C
Temp E	569.4 C	7.75 C

Figure 100: Air throttle valve position versus time with engine generator operation on producer gas

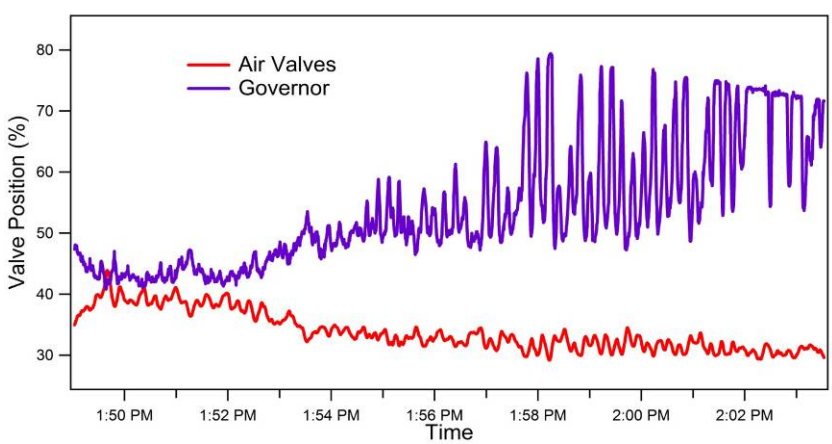

The goal of the test was to demonstrate stable power output even though the energy density of the gas was changing. The closing of the air valves (decreasing air flow) and the opening of the governor in Figure 36 show that the energy density/flow rate of the gas was decreasing over time. Smaller perturbations are primarily caused by the changing fuel supply and a non-ideally

tuned governor response, and partially due to the natural fluctuations expected in a time delayed PID feedback system.

Figure 101: Probability distribution of the relative fuel/air ratio (lambda) during engine/generator operation

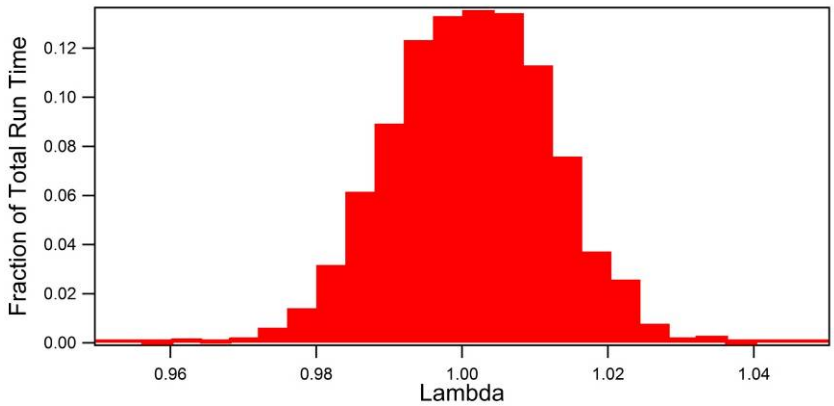

The fuel air ratio (lambda) shown in Figure 37 was between 0.99 and 1.01 for the majority of the test run, and did not significantly deviate more than +/-0.02. Combined with Figure 36, which indicated that the gas was not constant, the research team effectively demonstrates that the customed designed engine control system is capable of operating on and adapting to producer gas.

The engine researchers subsequently improved the control and measurement of the engine and its exhaust and obtained improved emission results. Figure 38 below shows the post catalyst CO vs. NOx curves for two different runs. The red x-shaped symbols represent an early run case, while the purple plus symbols show results from the latest series of testing. The later run clearly has less scatter and follows closer to the ideal curve, which demonstrates improvements made to control stability. Results have indicated that it will be possible to reach emission goals with further refining of the system.

Figure 102: Post-catalyst NOx vs. CO emissions from producer gas runs with improved results with purple plus-shaped symbols.

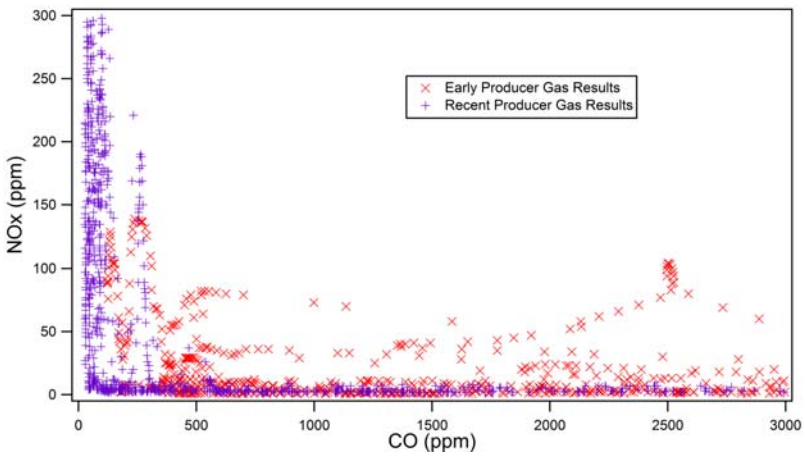

For the catalyst work, the researchers mainly focused on the results at a stoichiometric run condition. Figure 39 shows the amount of NOx and CO that slip through the catalyst relative to the O_2 percent. Although some scattering is still present, it is clear that an ideal operating window exists just below the 0.0 percent point.

The research team noted that the lambda sensors were quite sensitive to drifting and biasing due to the large amounts of CO and H_2 in the exhaust stream when running on producer gas. Additional sensors, such as O_2 and NOx sensors, have been shown to be more reliable indicators of the run condition and will likely be incorporated in to the control strategy. The team considered as a future option to install a second lambda sensor downstream of the catalyst. The catalyst should allow the majority of the CO and H_2 to react, allowing the second lambda sensor (after the catalyst) to get an accurate measure of the stoichiometry. The bias of the first sensor can then be determined and its setpoints and the control constants can be adjusted accordingly.

Figure 103: Post-catalyst CO and NOx vs. O2 in exhaust with ideal operating point at just rich of stoichiometric.

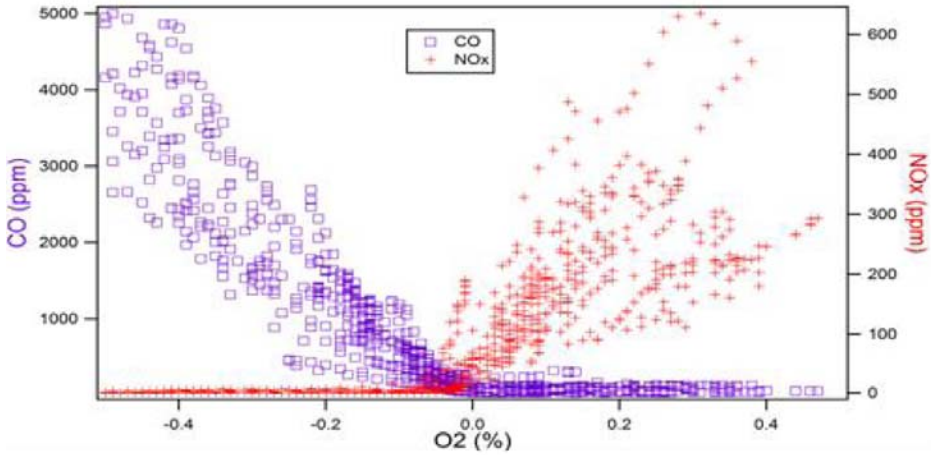

18.3.2 Rich/lean dual catalyst

It has been demonstrated that NOx conversion is very good when the engine runs rich, and CO conversion is good when the engine runs lean (see Figure 39). To utilize this effect, a system is being constructed which consists of two catalysts in series. In this system, the engine can be run slightly rich, which will results in full NOx conversion in the first catalyst. After the first catalyst a small amount of air can be injected into the exhaust. This extra air will provide additional oxygen, making the exhaust 'lean', and allowing full conversion of CO and hydrocarbons in the second catalyst. The system was being installed on the Woodland Engine and tested (see Figure 40). The major concern for such a system is ammonia being formed in the first catalyst, as the fuel bound nitrogen in the ammonia will react with excess air in the second catalyst becoming NOx again. Ammonia formation is known to occur when running rich through a catalyst with larger hydrocarbons, but producer gas contains almost no larger hydrocarbons, and this could suppress the ammonia formation to an acceptable level.

Relative to a single three-way catalyst, the dual catalyst method could produce more reliable and complete emission conversion. It is seen as a competing technology which has many potential pitfalls but could have a very rewarding payoff.

Figure 104: CAD model of the dual catalyst design for rich/lean operation with air injection in between the two catalysts.

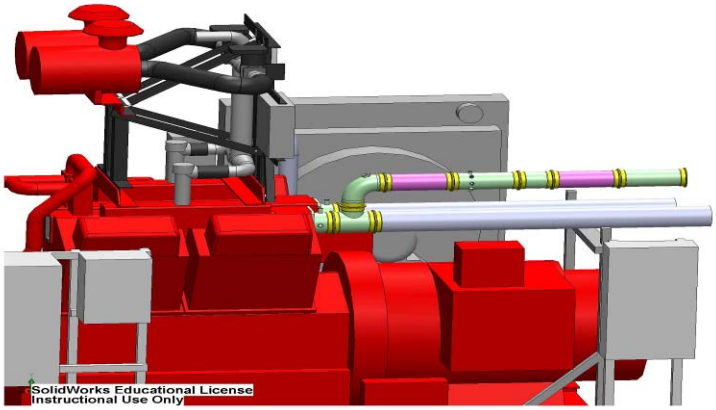

In this test, the engine research team mounted two catalysts in series with ports for air injection in between. The system is designed to allow one catalyst to run rich, removing NOx, and the second to run lean, removing CO and hydrocarbons. Because each catalyst needs to be only rich or lean (and not precisely stoichiometric), the design should be highly robust with very little emissions slip. In order to achieve such a system some efficiency must be sacrificed. Extra fuel must be present in the exhaust to convert NOx in the first catalyst, while air must be compressed for injection between the two catalysts.

The researchers operated the engine at a variety of set points, ranging from slightly rich to very rich. All cases showed excellent NOx conversion through the first catalyst, but NOx was present after the second catalyst. The team determined that the first catalyst, under rich conditions, was producing ammonias shown in Fig. 41. When ammonia oxidizes on a three-way catalyst (in the current design the second catalyst) the most favorable reaction is the formation of NOx. Thus, a significant amount of NOx exits the system due to the formation of ammonia.

Figure 105: Ammonia production in Rich/Lean Catalyst System. Ammonia is produced in the firscatalyst (shown in purple) and is subsequently converted back to NOx in the lean catalyst (shown in red) at a rate of over 90%

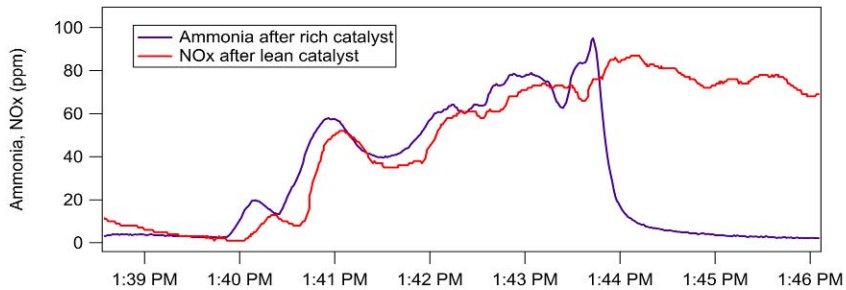

Ammonia is oxidized in three main ways:

$$2\ NH_3 + 3/2\ O_2 \rightarrow N_2 + 3\ H_2O \quad \Delta H=+151\ kcal \quad (1)$$

$$2\ NH_3 + 2\ O_2 \rightarrow N_2O + 3\ H_2O \quad \Delta H=+132\ kcal \quad (2)$$

$$2\ NH_3 + 5/2\ O_2 \rightarrow 2\ NO + 3\ H_2O \quad \Delta H=+108\ kcal \quad (3)$$

Under normal TWC conditions reaction 3 is favored over 90 percent. Due to this issue, the researchers found that a system consisting of two three-way catalysts is not feasible for rigorous emissions cleanup. However, certain catalytic wash coats exist to favor reaction 1 as much as 95 percent. With such a catalyst in place, the system could be feasible, but would require three catalysts in series. The first converts NOx, the second removes any ammonia via reaction 1 (see above), and finally the thirds oxidizes CO and hydrocarbons. The research team concluded that more research would be required to fully determine the capabilities of such a system.

18.3.3 High H_2/CO ratio producer gas with three-way catalyst

Encouraging results have been produced when running on producer gas with a high H_2/CO ratio. Running at stoichiometric to take advantage of the TWC simultaneous reduction of both CO and NOx have been achieved for prolonged periods with no measurable ammonia production.

For these tests, the research team left the two-catalyst system in place, but did not inject any air between the catalysts as shown in Fig. 42. This allowed for the control system to measure and react to emissions after the first catalyst, with the second catalyst acting as a buffer to prevent emissions slips while the controller corrects the run point.

Figure 106: Design of rich/lean 3-Catalyst capable of running the rich/lean system would require 3 catalysts: a TWC running rich followed by air injection and then an ammonia selective catalyst and a CO and HC oxidation catalyst

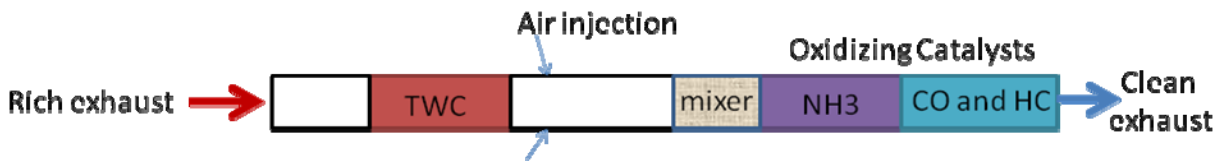

Figure 43 gives an overview of the system. The lambda sensor (shown in light blue, corresponding with the blue axis on the far left side) is close to 1. This is in contrast to previous runs using low H_2/CO ratios for which the sensor reported 1.07 when the TWC was in its optimal operating range. NOx emissions after the first and second catalyst are shown in red and purple respectively and corresponding to the left axis in red. The advantage of having two catalysts is clear as there are frequent NOx slips through the first, but almost no NOx slips out the tailpipe. This is the result of the catalyst's ability to store molecules on its surface – when the first catalyst becomes saturated, the second catalyst can absorb the excess for a short period. During this time, the engine run point can be adjusted to correct the saturation. The same effect can be noted in the oxygen signals, shown in black and green dashes.

Figure 107: Dual stoichiometric catalyst design with two catalysts in series with no air injection; while some NOx passes beyond the first catalyst, almost no NOx is observed after the second catalyst; Negative O2 values result from extrapolation of the lambda signal from the lean side.

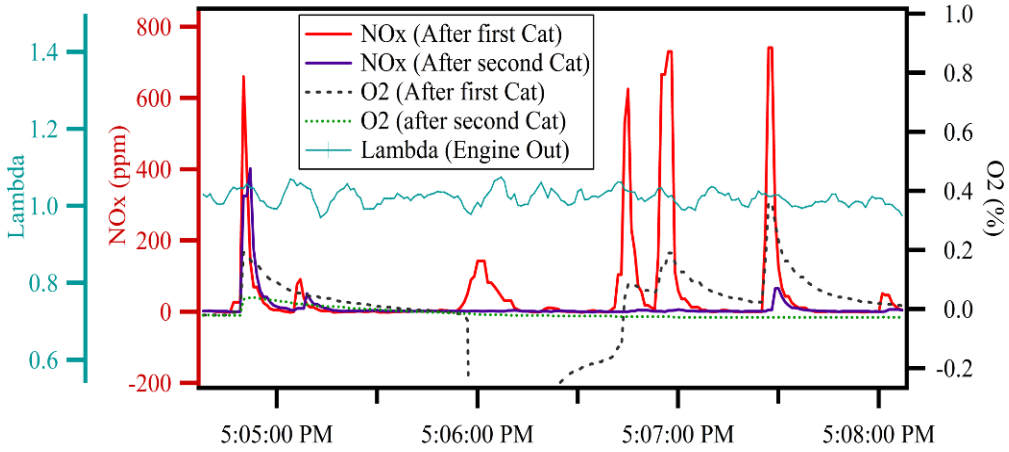

The frequent but irregular 'bursts' of NOx through the first catalyst are not fully understood as they do not seem to have any direct correlation to the lambda sensor readings. This phenomenon has been noted in previous catalyst work at UC Berkeley, and while it has not be completely explained, is has been found that with advanced dithering strategies the frequency and magnitude of the bursts can be significantly reduced. Such control is harder to implement in an engine of this type, but continued research is recommended.

The research team also attempted dithering, but the results are unclear. They found that implementing dithering is beneficial, but the fluctuations in the producer gas' makeup and supply lead to a natural dithering of the exhaust, and therefore any applied dithering is hard to decouple. Figure 44 shows very encouraging results that have been obtained over extended

periods of time, and with further refinement of the system reduction of NOx should be even more complete.

Figure 108: Optimized emissions control with an average of less than 8 ppm NOx and CO.

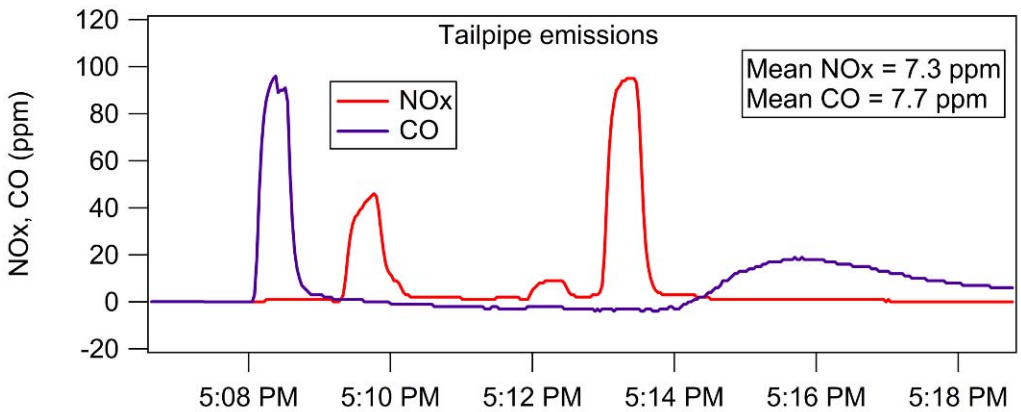

18.3.4 Performance summary for gasifier and engine

Table 6 shows a summary of the gasifier performance during the above listed engine test. The biomass rate was lower than the maximum plant capacity to obtain a higher-quality gas. A biomass rate (wood pellets) of 3 tons(wet)/day produced 68 scfm of producer gas. The lower heating value (LHV) of the gas is 52 percent of the lower heating value in the biomass. If all volatiles would be converted to producer gas and the fixed carbon was not actively used to generate extra gas, then 69 percent of the biomass energy could be converted to producer gas. The present results are lower for two reasons. First, some of the gas was oxidized with oxygen above the fluidized bed to increase the temperature and reduce the tar content. Therefore, some of the gas was converted into CO_2 and H_2O and the energy content was lowered. Without this step, 58 percent of the biomass would have been converted to producer gas. Second, some gas (O_2 and air) entered into the gasifier from the combustor through the downcomer connected to the regeneration section of the gasifier. At the same time, not all of the volatile fraction of the biomass might have been converted and some was moved over to the combustor. This explains the remaining difference between the 58 percent and 69 percent conversion. Since the gasification process in general only converts the volatile fraction of the carbon in the biomass the maximum conversion for the wood biomass could only be 69 percent conversion. However, the 31 percent of the energy is not lost. The energy in the fixed carbon is used in the combustion regenerator to produce the necessary heat for the endothermic gasification process and can be recovered as waste heat and has been demonstrated in an integrated co-gen gasification systems to contribute to an overall energy utilization of 80 percent.

Table 24: Gasifier biomass input and producer gas production.

Biomass rate	3	t/day
Biomass rate per minute	2.09	kg/min
LHV Biomass	614	kW
Producer gas rate (to flare and engine)	68	scfm
Producer gas rate (mass)	1.88	kg/min
LHV Producer gas	322	kW
Mass conversion	0.90	kg gas/kg biomass
Energy conversion	0.52	LHV gas/LHV biomass
Loss through partial oxidation	35	kW
LHV Producer gas (before POx)	357	kW
Energy conversion	0.58	LHV gas before POx/LHV biomass
Loss through mass transfer in downcomer	66	kW
LHV Producer gas (before POx and any transfer losses)	423	kW
theoretical energy conversion	0.69	LHV volatiles/LHV biomass

The engine was able to take about 80 percent of the producer gas with the remaining 20 percent burned in the flare. The reasons for not taking all the gas for the electricity generation were velocity fluctuations that could not all be buffered out by the engine control. The 54 scfm of producer gas was stoichiometrically burned in the engine and generated about 180 scfm of exhaust gas (Table 7). With less than 8 ppm(vol) of NOx and CO, this would correspond to 0.16 lb/MWhr and 0.15 lb/MWhr of NOx and CO output. Since the engine was only generating 42 kW at this point, throttling and mechanical losses were comparatively high, and the thermal efficiency was only 16 percent. Using a smaller engine or running the existing engine at higher power would most likely move the efficiency into the 25-30 percent range. This would lower the brake-specific emissions accordingly.

Table 25: Summary of engine performance and emissions.

Producer gas flow to engine	54	scfm
Exhaust flow	180	scfm
Power generated	42	kWe
Engine efficiency	16	%
NO	8	ppmv
CO	8	ppmv
NO emissions	0.16	lb/MWhr
CO emissions	0.15	lb/MWhr

Chapter 19:
Task 2.4 Combustion Properties and Chemical Mechanism for Producer Gas

19.1 Task 2.4.1 Autoignition/Extinction Properties of Producer Gas

In view of uncertainties in the supply of oil and natural gas and environmental concerns, there has been growing interest in exploring alternate sources of energy. The fuels such as coke oven gas, biogas obtained by wood pyrolysis, reformate gas, synthetic gas from biomass gasification, blast furnace gases etc., which were either flared or not considered worthy for the existing combustion systems, are now considered to be environmentally friendly, and economically viable and profitable [1]. The gasification process can be accomplished with a variety of gasifier designs. The producer gas from these gasification systems are almost universally used to produce electricity from a conventional furnace steam cycle system or an engine generator system. Although, the specific composition of the producer gas depends upon the fuel sources and processing techniques, a typical mix mainly contains methane, hydrogen, carbon monoxide, carbon dioxide, nitrogen, and trace amounts of ethane and propane. The application of these fuels in the existing energy infrastructure requires modifications in the current combustion systems to burn the fuel efficiently with low emissions and mitigate the risks of accidental fires and explosions. Depending on the sources, there is a substantial variability in the fuel composition, and heating values [2]. This poses a challenge to combustion scientists and engineers in designing the combustion systems which runs efficiently on a wide range of operating conditions. In order to understand the impact of the variability in fuel compositions on the combustion performance and emissions, understanding of the changes in combustion properties of methane in presence of hydrogen, carbon monoxide, carbon dioxide, nitrogen etc. is required.

Here, an experimental and numerical study is carried out to characterize nonpremixed combustion of mixtures of producer gas and methane. The producer gas used in this work is made up of 42 percent CO, 25 percent H_2, 12 percent CO_2, 17 percent CH_4, and 4 percent C_2H_4 by volume at standard temperature (273 K) and pressure (1.013 bar).

19.2 Experimental

The experiments were performed at a pressure of 1 atm. Figure 1 shows a schematic illustration of the counterflow configuration employed in the experimental and numerical studies.

Figure 109: Schematic of the counterflow configuration employed in the experimental and numerical studies.

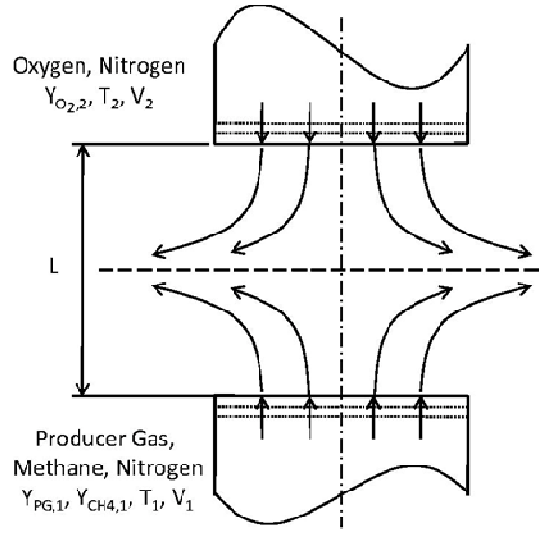

The counterflow burner is made up of two ducts. From one duct, called the fuel-duct, a fuel stream made up of fuel mixed with nitrogen is injected into a mixing layer, and from the other duct, called the oxidizer-duct, an oxidizer stream made up of air mixed with nitrogen is injected into the mixing layer. A stagnation plane is formed in the mixing layer established between these counterflowing streams. Fine wire screens are placed at the exits of the fuel-duct and the oxidizer-duct. This makes the tangential component of the flow velocity to be negligibly small at the exit of the duct (plug-flow boundary conditions). The distance between the exits of the two opposing ducts is L. The exit of the fuel-duct is called the fuel boundary, and the exit of the oxidizer-duct the oxidizer boundary. The mass fraction of fuel, the temperature, and the component of the flow velocity normal to the stagnation plane at the fuel boundary are represented by $Y_{F,1}$, T_1, and V_1, respectively. The mass fraction of oxygen, the temperature, and the component of the flow velocity normal to the stagnation plane at the oxidizer boundary are represented by $Y_{O_2,2}$, T_2, and V_2, respectively. The mass fraction of the fuel at the fuel boundary $Y_{F,1} = Y_{CH_4,1} + Y_{PG,1}$, where $Y_{CH_4,1}$ and $Y_{PG,1}$ are the mass fractions of methane and producer gas respectively. Experimental studies are conducted with the momenta of the counterflowing streams $\rho_i V_i^2$, i=1,2 kept equal to each other. Here, ρ_1 and ρ_2 represent the density of the mixture at the fuel boundary and at the oxidizer boundary, respectively. The velocities of the reactants at the boundaries are presumed to be equal to the ratio of their volumetric flow rates to the cross-section area of the ducts. All gaseous flow rates are measured by computer-regulated mass-flow controllers. The calibrated accuracy of these mass-flow controllers is ±1 percent.

The value of the strain rate, defined as the normal gradient of the normal component of the flow velocity, changes from the fuel boundary to the oxidizer boundary [3]. The characteristic strain rate on the oxidizer side of the stagnation plane a_2 is given by [3]

$$a_2 = \frac{2|V_2|}{L}\left(1 + \frac{|V_1|\sqrt{\rho_1}}{|V_2|\sqrt{\rho_2}}\right). \tag{1}$$

Equation 1 is an exact solution of the describing equations obtained in the asymptotic limit where the Reynolds numbers of the laminar flow at the boundaries are presumed to be large [3]. Critical conditions of extinction are presumed to be given by the strain rate, $a_{2,e}$, and the mass fraction of fuel at the fuel boundary. Critical conditions of autoignition are presumed to be given by the strain rate, $a_{2,I}$, the temperature of the oxidizer stream, $T_{2,I}$, and the mass fraction of fuel at the fuel boundary.

19.2.1 Critical conditions of extinction

The structure of the reactive flow field depends on the five independent boundary values $Y_{CH_4,1}$, $Y_{PG,1}$, $Y_{O_2,2}$, T_1 and T_2. The experiments were conducted with $T_1 = T_2 = 298$ K. This reduces the number of independent variables to three. Two sets of experiments were performed. These sets differ in the procedure employed in the selection of the independent variables $Y_{CH_4,1}$, $Y_{PG,1}$, and $Y_{O_2,2}$. In the first set of experiments the oxidizer stream was air with $Y_{O_2,2} = 0.233$. The relative proportions of methane and producer gas was fixed, and critical conditions of extinction were measured as a function of $Y_{F,1}$. The extinction experiments were conducted by establishing a flame at a strain rate $a_2 < a_{2,e}$. The strain rate was then increased by increasing V_1 and V_2 simultaneously until extinction was observed. The strain rate at extinction, $a_{2,e}$, was recorded as a function of the mass fraction of fuel $Y_{F,1}$.The experimental results are shown later.

In the second set of experiments, the temperature for complete combustion, T_{st}, and the stoichiometric mixture fraction ξ_{st} was fixed. This reduced the number of independent variables by two leaving only one independent variable. The critical conditions of extinction were measured for various values of $Y_{F,1}$. The stoichiometric mixture fraction, ξ_{st}, is calculated from the equation

$$\xi_{st} = [1 + (\nu\ Y_{F,1}) / Y_{O_2,2}]^{-1} \tag{2}$$

Here, ν is the stoichiometric mass ratio of oxygen to fuel (sum of mass of methane and producer gas). The stoichiometric mass of oxygen depends on the relative amounts of methane and producer gas. The temperature for complete combustion, T_{st} is calculated assuming that the products of reaction are H_2O and CO_2. This set of experiments elucidates the chemical influence of producer gas on flame extinction.

19.2.2 Critical conditions of autoignition

Critical conditions of autoignition were measured with the fuel stream made up of producer gas only, thus $Y_{CH4,1} = 0$. The temperature of the fuel stream, $T_1 = 298$ K. The oxidizer stream was air with $Y_{O_2,2} = 0.233$. Two sets of experiments were carried out to establish the critical conditions of autoignition. In one set of experiments the mass fraction of producer gas in the fuel stream, $Y_{PG,1}$ was maintained at a constant value. At chosen values of strain rate the flow field was established. The temperature of air was increased until autoignition takes place. The temperature of the air stream, $T_{2,I}$ was recorded using a thermocouple as a function of the strain rate, $a_{2,I}$. The temperature recorded by the thermocouple was corrected to account for radioactive losses from the bead. The accuracy of the measurement of the temperature of air at autoignition is expected to be ±30 K, the strain rate ±10 percent, and fuel mass fraction ±3 percent of recorded value. The experimental repeatability in the measurement of the temperature of air at autoignition is ±5 K. The second set of experiments is carried out with $a_2 = 250\ s^{-1}$. Here the

temperature of the oxidizer stream, $T_{2,1}$, is recorded as a function of $Y_{PG,1}$. The results are shown later.

19.3 Numerical procedure

Numerical calculations are performed using a computer program called FlameMaster developed at RWTH-Aachen [4]. The conservation equations of mass, momentum, and energy and the species balance equations used in the formulation of the numerical problem are summarized elsewhere [4, 5]. The species balance equations include thermal diffusion and the energy conservation equation includes radioactive heat losses from carbon dioxide and water vapor [4]. Buoyancy is neglected. At the boundaries of the mixing layer the mass fluxes of the reactants and their exit velocities are specified, according to the values used in the experiments. Plug-flow boundary conditions are used. A chemical-kinetic mechanism called the San Diego mechanism [6] is used to describe the oxidation of the fuel. This mechanism is comprised of 233 reversible reactions among 46 species.

19.4 Results

19.4.1 Critical conditions of extinction

Figure 2 shows the strain rate at extinction, $a_{2,e}$ as a function of the mass fraction of fuel, $Y_{F,1}$ in the fuel stream. The symbols represent experimental data and the lines are best fits to the data. The figure shows data for with the fuel stream made up of methane with $Y_{PG,1} = 0$, of a mixture of methane and producer gas with the mole fraction of producer gas in the mixture maintained at a constant value of 25 percent, and for producer gas with $Y_{CH_4,1} = 0$. The symbols in Figure 2 indicate the boundary separating the flammable region for $a_2 < a_{2,e}$ from the nonflammable region for $a_2 > a_{2,e}$. Figure 2 shows that flames burning methane are easier to extinguish than flames burning to producer gas. At low values of $Y_{F,1}$ the strain rate at extinction for the mixture of these fuels is nearly the same those for produced gas, while at higher values of $Y_{F,1}$ the strain rate at extinction for the mixture is lower than that for producer gas but higher than that for methane.

Figure 110: The strain rate at extinction, $a_{2,e}$ as a function of the mass fraction of fuel, $Y_{F,1}$ in the fuel stream. The symbols represent experimental data and the lines are best fits to the data.

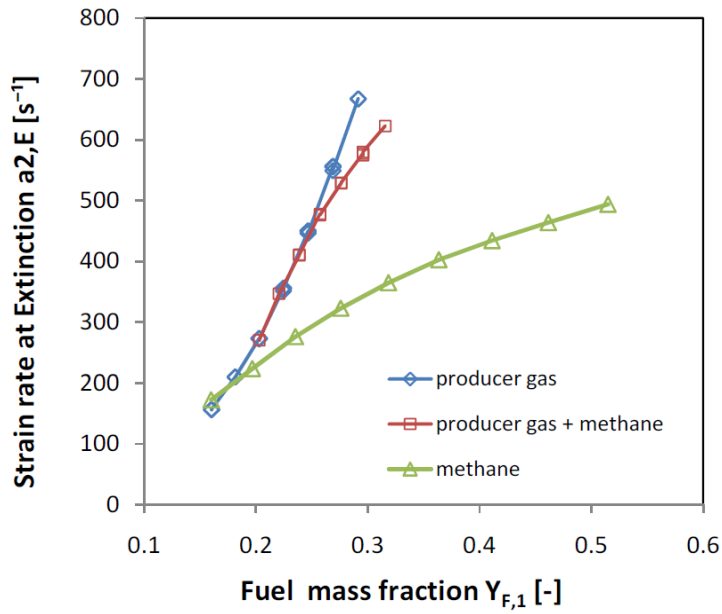

Figure 3 shows the strain rate at extinction, $a_{2,e}$ as a function of the mass fraction of producer gas, $Y_{PG,1}$ in the fuel stream, with $Y_{CH_4,1} = 0$. The symbols represent experimental data and the lines are results of numerical calculation using the San Diego Mechanism [6].

Figure 111: The strain rate at extinction, $a_{2,e}$ as a function of the mass fraction of producer gas, $Y_{PG,1}$ in the fuel stream, with $Y_{CH4,1} = 0$.

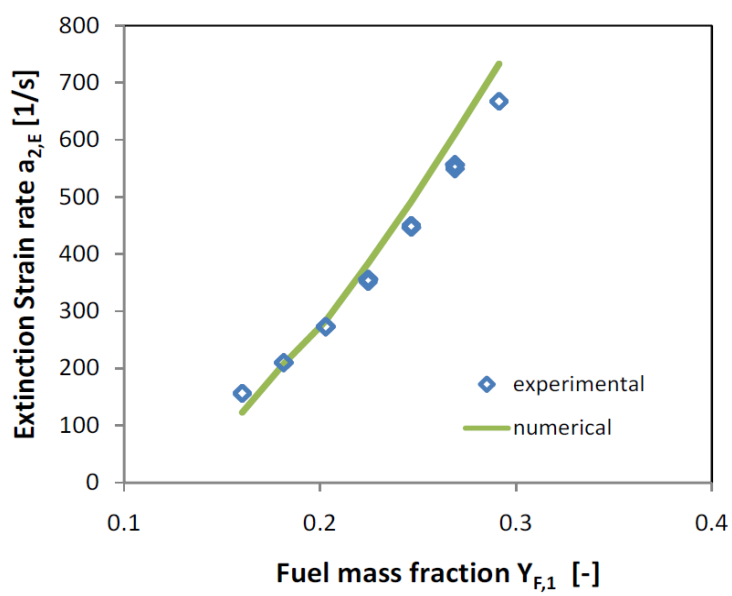

The experimental data in Fig. 3 are the same as those in Fig. 2. The calculated values of the critical conditions of extinction agree well with experimental data. Figure 4 shows the strain rate at extinction, $a_{2,e}$ as a function of the mass fraction of fuel in the mixture with the mole fraction of producer gas in the mixture maintained at a constant value of 25 percent. The symbols

represent experimental data and the lines are results of numerical calculation using the San Diego Mechanism [6]. The experimental data in Fig. 4 are the same as those in Fig. 2. The differences between calculated values of the critical conditions of extinction and experimental data increase with increasing values of $Y_{F,1}$. This is attributed to inaccurate prediction of critical condition of extinction of flames burning methane.

Figure 112: The strain rate at extinction, $a_{2,e}$ as a function of the mass fraction of fuel in the fuel stream, $Y_{F,1}$ with the mole fraction of producer gas maintained at a constant value of 25%.

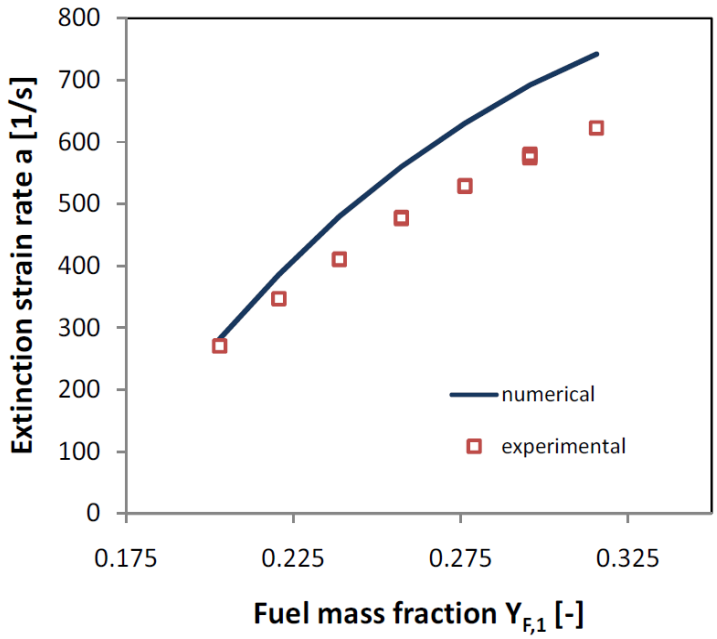

Figure 5 shows the strain rate at extinction, $a_{2,e}$ as a function of the mass fraction of producer gas in the fuel stream, $Y_{PG,1}$. The experimental data was obtained at constant values of ξ_{st} =0.4, and T_{st} = 1800 K. The symbols represent experimental data and the line is a best fit to the data. Figure 5 shows that the value of $a_{2,e}$ increases with increasing $Y_{PG,1}$.

19.4.2 Critical conditions of autoignition

Figure 6 shows the temperature of air at autoignition, $T_{2,I}$, as a function of the strain rate, $a_{2,I}$ for producer gas, with $Y_{CH_4,1} = 0$. The symbols represent experimental data and the lines are best fits to the data. The experimental data is taken at fixed values of the mass fraction of producer gas, $Y_{PG,1}$ equal to 0.078, 0.163, and 0.247. These lines are boundaries separating a region $T_2 < T_{2,I}$ where autoignition can take place from a region where autoignition is not possible. Figure 7 shows the temperature of air at autoignition, $T_{2,I}$, as a function of the mass fraction of producer gas in the fuel stream, $Y_{PG,1}$, at a fixed value of the strain rate. a_2 = 250 s^{-1}. The symbols represent experimental data and the line is a best fit to the data. Figure 7 shows that the value of $T_{2,I}$ decreases with increasing $Y_{PG,1}$.

Figure 113: The strain rate at extinction, $a_{2,e}$ as a function of the mass fraction of producer gas in the fuel stream, $Y_{PG,1}$. The experimental data was obtained at constant values of ξ_{st} =0.4, and T_{st} = 1800 K.

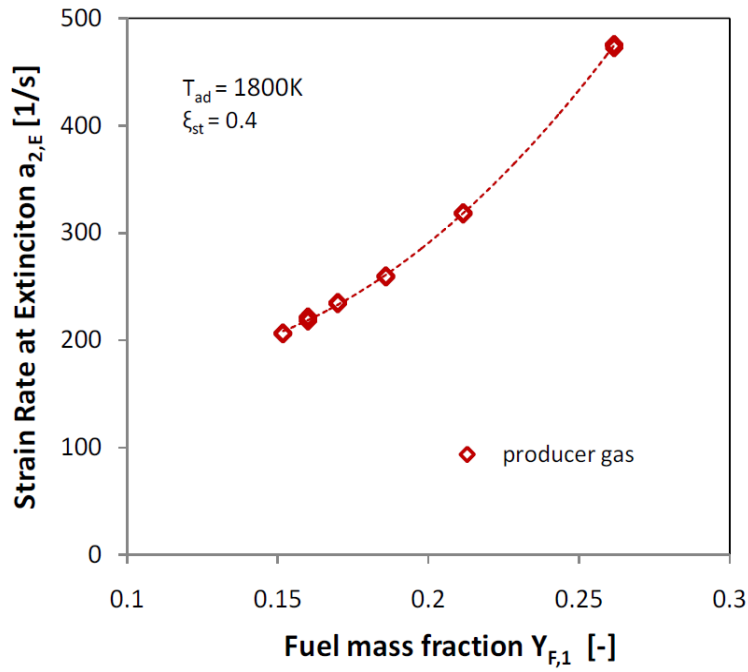

Figure 114: The temperature of air at autoignition, $T_{2,I}$, as a function of the strain rate, $a_{2,I}$ for producer gas.

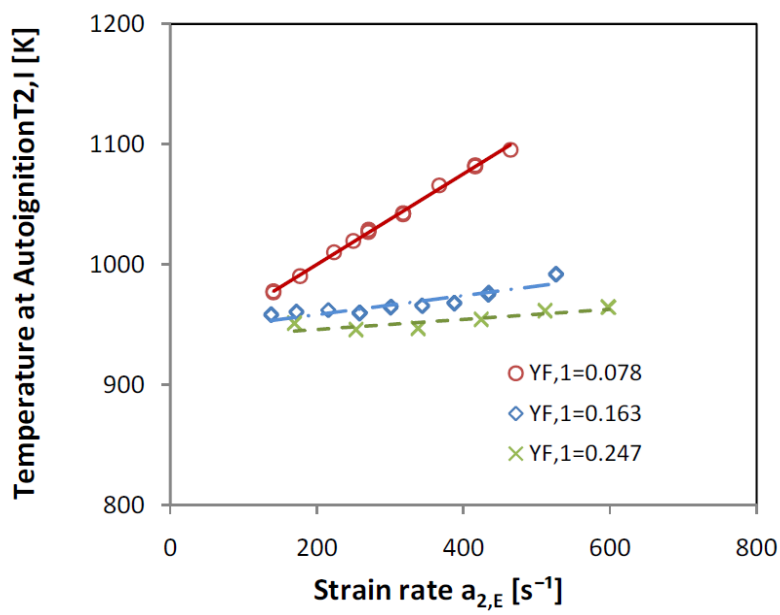

Figure 115: The temperature of air at autoignition, $T_{2,I}$, as a function of the mass fraction of producer gas in the fuel stream, $Y_{PG,1}$, at a fixed value of the strain rate. a_2 = 250 s^{-1}.The symbols represent experimental data and the line is a best fit to the data.

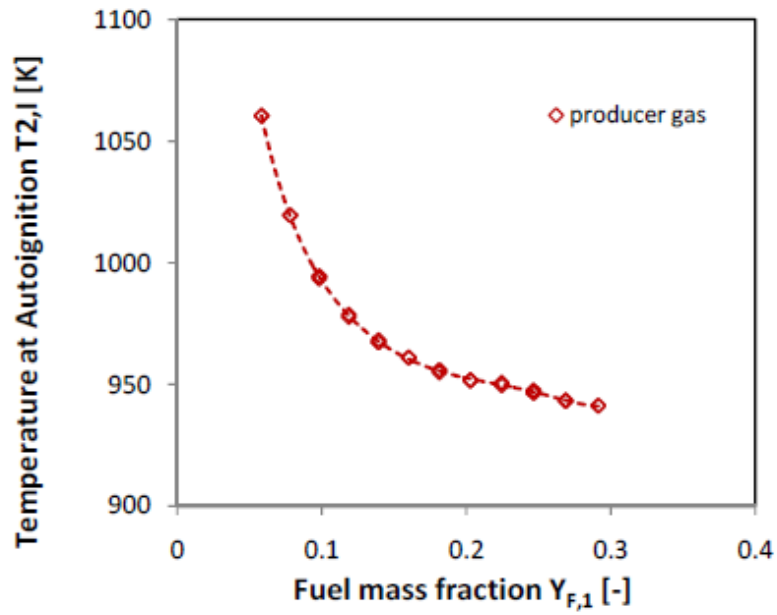

19.5 Conclusions

The experimental data show that producer gas is more reactive than methane. The chemical kinetic mechanism accurately predicts the critical conditions of extinction and autoignition of producer gas.

Chapter 20:
Task 2.4.2 Chemical Mechanisms for Producer Gas

To convert biomass to a fuel gas a thermochemical conversion process is used in which the carbon from a biomass source (forest wood waste/residue) is combined with water at high temperature (steam) in a gasification reactor to generate producer gas which is composed primarily of carbon monoxide (CO), hydrogen (H_2), carbon dioxide (CO_2), methane (CH_4), mixed with some water vapor (H_2O) and hydrocarbons with molecular weight higher than that of CH_4. In order to investigate the impact of various fuel components on the combustion performance and emissions, a detailed chemical-kinetic mechanism is used in numerical computations.

Methane is the simplest hydrocarbon fuel with relatively large heat release and lower greenhouse gases. The combustion properties of methane as a fuel has been extensively studied by various research groups for example autoignition delay times [7, **8**], laminar burning velocities [9], flame structures [10], ignition and extinction of nonpremixed and partially premixed flames [11]. The enrichment of methane fuel with hydrogen results in extension of lean flammability limits [12] which in turn improve operation of low emission combustion systems used in gas turbines and internal combustion engines. The studies on fundamental and practical aspect of methane air mixtures enriched with hydrogen are still on-going. The experimental and numerical results on laminar and turbulent burning velocities of methane air mixtures with hydrogen addition were reported in previous studies [13–16]. Recently, an experimental and numerical study on autoignition and laminar burning velocities on practical bio-fuels has been published [17]. The effect of carbon monoxide addition on methane flames was discussed in [14].

20.1 Numerical Computations

Calculations of autoignition, premixed and nonpremixed flames can be performed using the San Diego Mechanism. It was developed for the combustion of hydrogen [18], carbon monoxide [18], methane [10, 19], ethane [20], ethene [21], ethyne [22, 23], propane [24], propene [24], propyne [24], allene [24], and methanol [25, 26]. Recently, it was enhanced to include the combustion of ethanol [27, 28], and was validated against the newer experimental data for the fuels listed above, and the modifications were discussed and reported in [28]. The San Diego Mechanism along with the thermodynamic and transport data can be downloaded from the web [6]. For calculations in this paper, reactions related with ethanol and propane were removed since they had insignificant effect on the results.

The computation of burning velocities are obtained with Chemkin PREMIX [29] including multicomponent diffusion and Soret effects and radiant energy loss from CO_2 and H_2O bands. The mesh independence of the solutions was established. The adaptive meshing feature was used such that the mesh used for mixtures with high concentrations of methane or carbon monoxide was approximately 600 grid points while that for mixtures with high concentrations of hydrogen was approximately 1000 grid points. The results are shown in Task 2.4.3.

20.2 Results and Discussion

The San Diego Mechanism contains the major species for modeling producer gas. It has been used for premixed and nonpremixed flames. Figures 3 and 4 from Task 2.4.1 have shown calculations of extinction condition of producer gas flames and those of methane/producer-gas mixtures. Figures 8 and 9 show the comparison of autoignition experiments (from Figs. 6 and 7) with the numerical computations. Except for very low fuel concentrations, the mechanism predicts the ignition temperatures well.

Figure 116: The temperature of air at autoignition, $T_{2,I}$, as a function of the strain rate, $a_{2,I}$ for producer gas and a comparison with numerical computations employing the San Diego Mechanism.

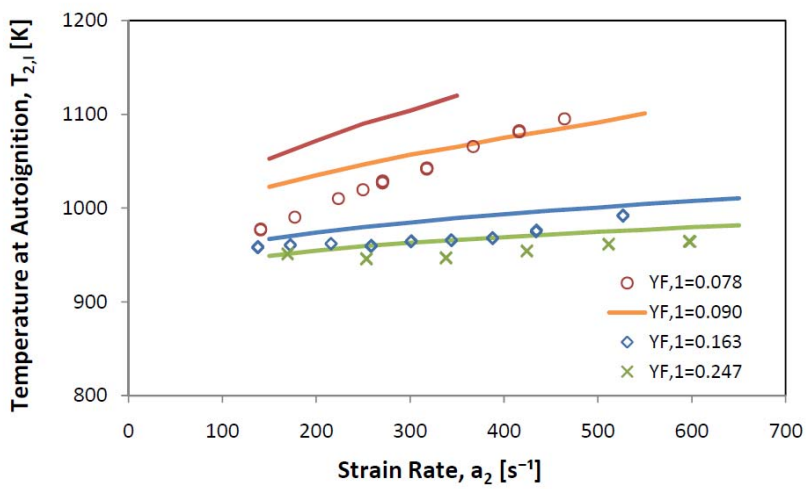

Figure 117: The temperature of air at autoignition, $T_{2,I}$, as a function of the mass fraction of producer gas in the fuel stream, $Y_{PG,1}$, at a fixed value of the strain rate. a_2 = 250 s^{-1}.The symbols represent experimental data and the line is a best fit to the data.

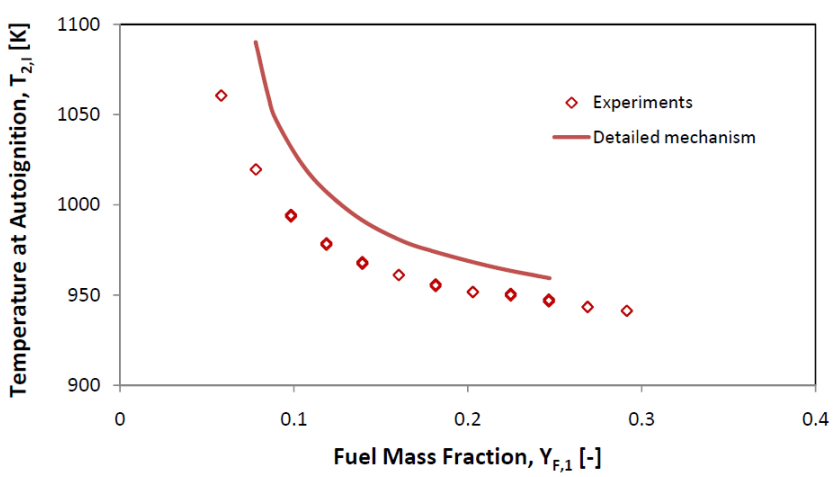

Chapter 21:
Task 2.4.3 Computational Prediction of Laminar Burning Velocity

Although, the specific composition of producer gas depends upon the fuel sources and processing techniques, a typical mix mainly contains methane, hydrogen, carbon monoxide, carbon dioxide, nitrogen, and trace amounts of ethane and propane. In order to understand the impact of the variability in fuel compositions on the combustion performance and emissions, understanding of the changes in combustion properties of methane in presence of hydrogen, carbon monoxide, carbon dioxide, nitrogen etc. is required. Recently, an experimental and numerical study on autoignition and laminar burning velocities on practical bio-fuels has been published [17]. The effect of carbon monoxide addition on methane flames was discussed in [14].

The work addressed in Task 2.4.3 is concerned with combustion properties of producer gas with varying composition used as fundamental baseline data in simulation codes for performance and emission predictions. In particular the objective of this task is to establish the burning velocities for premixed combustion of producer gas from laboratory measurements, and to predict laminar burning velocities using kinetic models described in Task 2.4.2 for predicting.

In the present work the influence of hydrogen and carbon monoxide on the structure and laminar burning velocities of laminar premixed methane flames was numerically investigated. A premixed mixture of methane, hydrogen, carbon monoxide, oxygen and nitrogen is considered. In one set of calculations the mass fraction of carbon monoxide is set equal to zero and the influence of hydrogen is investigated and in the other set of calculations the mass fraction of hydrogen is set equal to zero and the influence of carbon monoxide is considered. In both set of calculations the equivalence ratio is set equal to unity and the mass fraction of the reactants in the mixture are so chosen that the adiabatic temperature is constant. The burning velocities are calculated for various values of the mass fraction of hydrogen and carbon monoxide. The calculations are repeated for different values of the adiabatic temperature. The objective here is to elucidate chemistry effects of hydrogen and carbon monoxide addition on the methane flames.

21.1 Numerical Computations

The paper presents the results of laminar burning velocities and the structure of methane flames enriched with hydrogen and carbon monoxide. The calculations were performed using the San Diego Mechanism. The San Diego Mechanism, along with the thermodynamic and transport data, can be downloaded from the web [6].

21.2 Results and Discussion

Reactive mixtures made up of methane (CH_4), oxygen (O_2), hydrogen (H_2), carbon monoxide (CO), and nitrogen (N_2) are considered. The initial mass fraction of these species in the reactive mixture is $Y_{F,u}$, $Y_{O2,u}$, $Y_{H2,u}$, $Y_{CO,u}$, and $Y_{N2,u}$ respectively. The initial temperature of the reactive mixture is T_u. Here subscript u represents the initial conditions. The reactive system is thus characterized by five independent variables. In the calculations the initial temperature is set equal to 300 K. The values of the mass fraction of the reactants are so chosen that the

equivalence ratio is unity. These selections reduce the number of independent variables to three. Two sets of calculations are performed. In one set of calculations the value of $Y_{CO,u}$ = 0. The concentrations of other independent variable are so chosen that the adiabatic temperature for complete combustion T_c is constant. The value of T_c is that obtained for complete combustion of the reactants to form the products water vapor (H_2O) and carbon dioxide (CO_2). The reactive system now has only one independent variable. The burning velocity and flame structures are calculated for various values of $\alpha = Y_{H2,u}/Y_{F,u}$. The second set are calculations are performed with $Y_{H2,u} = 0$ and various values of $\beta = Y_{CO,u}/Y_{F,u}$.

21.2.1 Influence of Hydrogen

Figure 10 shows the burning velocity s_L as a function of the mass fraction of hydrogen for various values of T_c. The value of s_L increases with increasing $Y_{H2,u}$. Figure 11 shows the flame structure for $Y_{CO,u} = Y_{H2,u} = 0$. Figure 12 shows the rate of production of various species. It shows that fuel-consumption, H_2-consumption and CO-consumption take place in three distinct layers. In the region where fuel is consumed H_2 and CO are formed. These species are then consumed in separate layers. Figures 13 and 14 show the flame structure and rates of production of various species for α = 0.625. Figures 13 and 14 show similar results for α = 6.25. Comparison of Fig. 12 with Fig. 16 shows that for α = 6.25, consumption of CH_4 and H_2 take place in the same layer.

Figure 118: The burning velocity s_L as a function of the mass fraction of hydrogen for various values of T_c. The calculation were performed at $Y_{CO,u}$ = 0, and equivalence ratio, φ = 1.0.

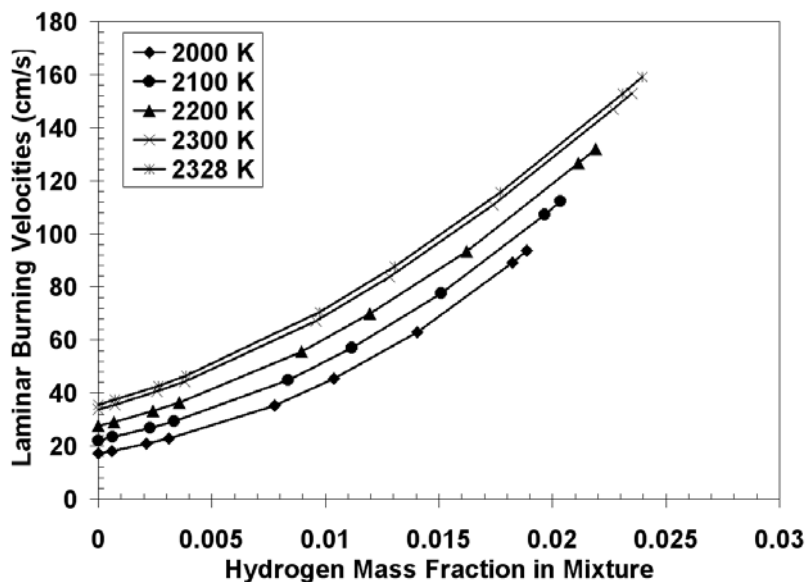

Figure 119: Structure of methane flame CH_4, O_2, CO, H_2, H, CO_2, H_2O, and temperature T, as a function of distance. The calculation were performed at T_c = 2300 K, $Y_{CO,u} = Y_{H2,u} = 0$, and equivalence ratio, φ = 1.0.

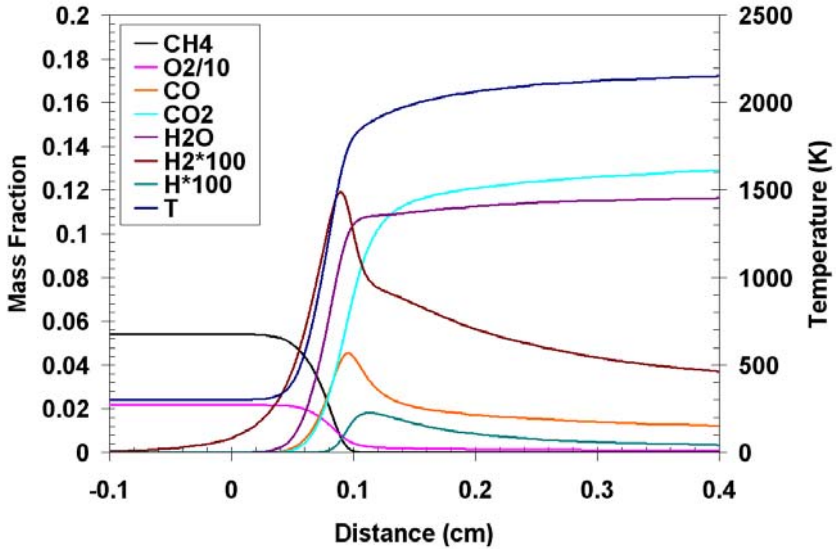

Figure 120: Net reaction rates production of CH_4, O_2, CO, H_2, H, CO_2, H_2O, and temperature T as a function of distance. The calculation were performed at T_c = 2300 K, $Y_{CO,u} = Y_{H2,u} = 0$, and equivalence ratio, φ = 1.0.

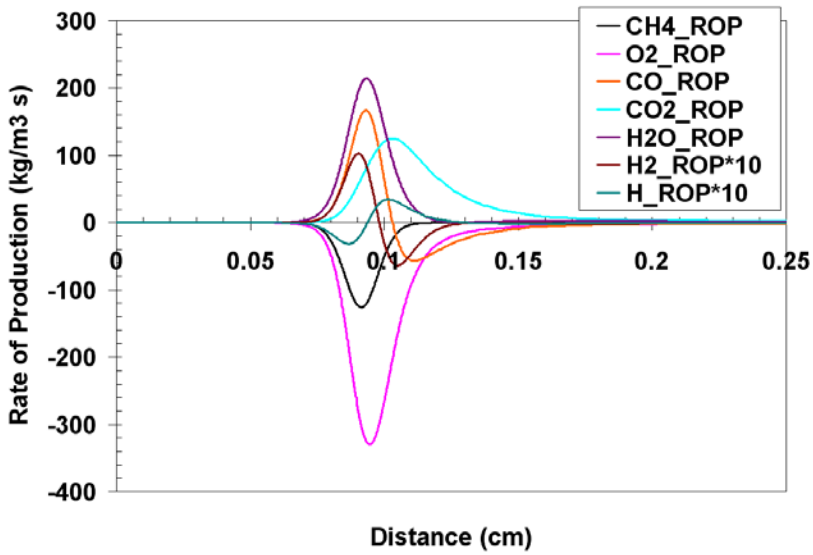

Figure 121: Structure of methane flame with hydrogen addition for CH_4, O_2, CO, H_2, H, CO_2, H_2O, and temperature, T, as a function of distance. The calculation were performed at T_c = 2300 K, $Y_{CO,u}$ = 0, α = 0.625 and equivalence ratio, φ = 1.0.

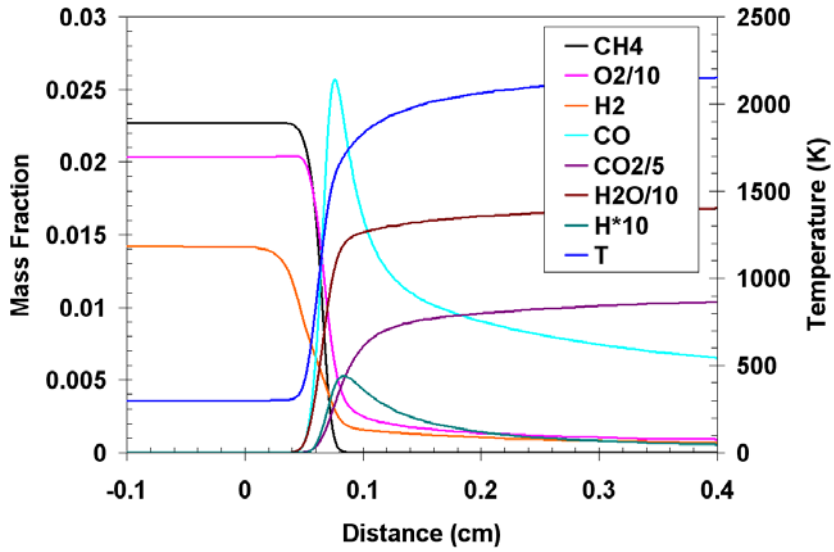

Figure 122: Net reaction rates for production of CH_4, O_2, CO, H_2, H, CO_2, H_2O, and temperature, T, as a function of distance. The calculations were performed at T_c = 2300 K, $Y_{CO,u}$ = 0, α = 0.625 and equivalence ratio, φ = 1.0.

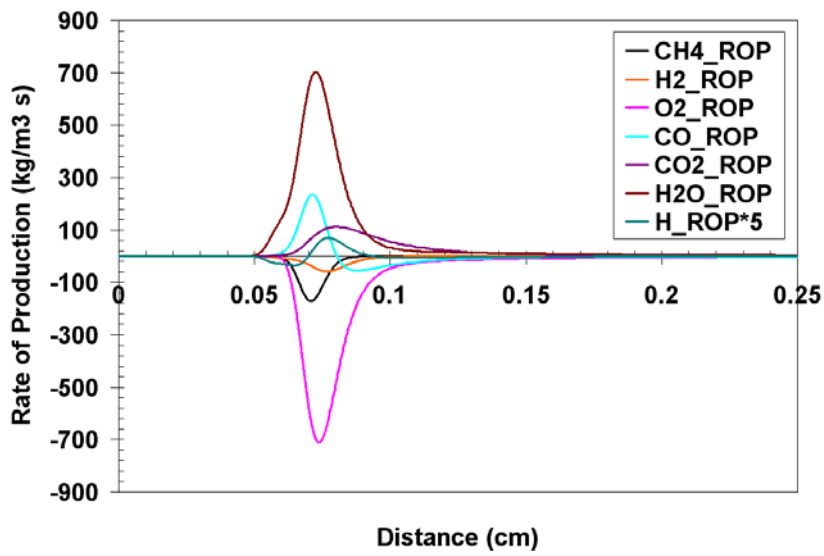

Figure 123: Structure of methane flame with hydrogen addition for CH_4, O_2, CO, H_2, H, CO_2, H_2O, and temperature T as a function of distance. The calculation were performed at T_c = 2300 K, $Y_{CO,u}$ = 0, α = 6.25 and equivalence ratio, φ = 1.0.

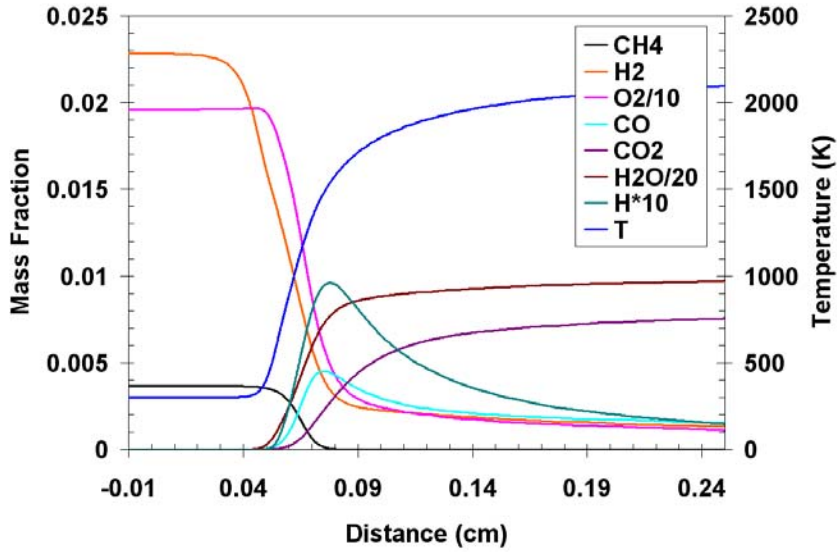

Figure 124: Profiles of net rates of production of CH_4, O_2, CO, H_2, H, CO_2, H_2O, and temperature T as a function of distance. The calculation were performed at T_c = 2300K, $Y_{CO,u}$ = 0, α = 6.25 and equivalence ratio, φ = 1.0.

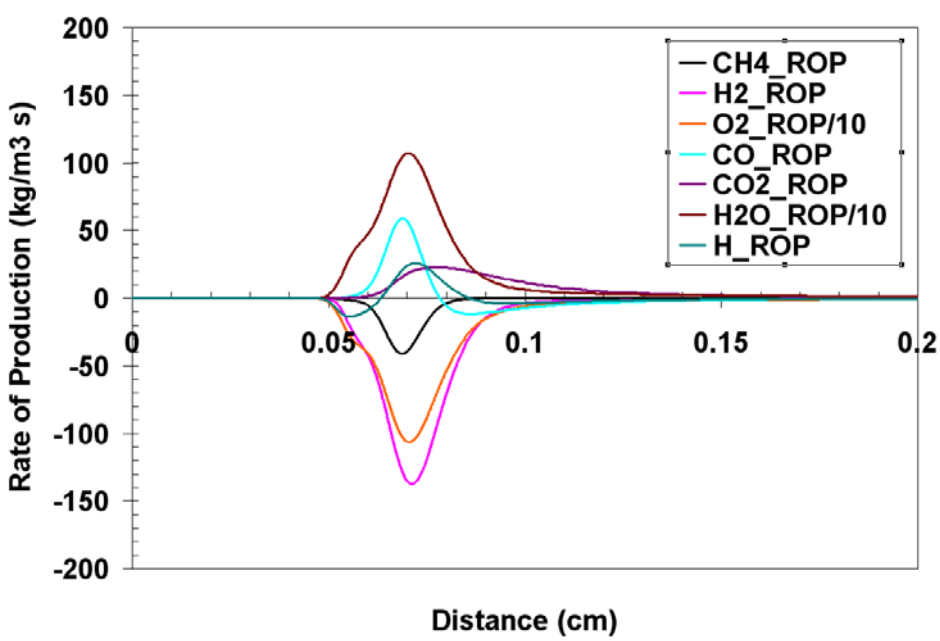

21.2.2 Influence of Carbon Monoxide

Figure 17 shows the burning velocity s_L as a function of the mass fraction of carbon monoxide for various values of T_c. The value of s_L first increases with increasing $Y_{CO,u}$ and then decreases. Figures 18 and 19 show the flame structure and rates of production of various species for β = 0.625. Figures 20 and 21 show similar results for β = 6.25.

Figure 125: The burning velocity s_L as a function of the mass fraction of carbon monoxide for various values of T_c. The calculation were performed at $Y_{H2,u}$ = 0, and equivalence ratio, φ = 1.0.

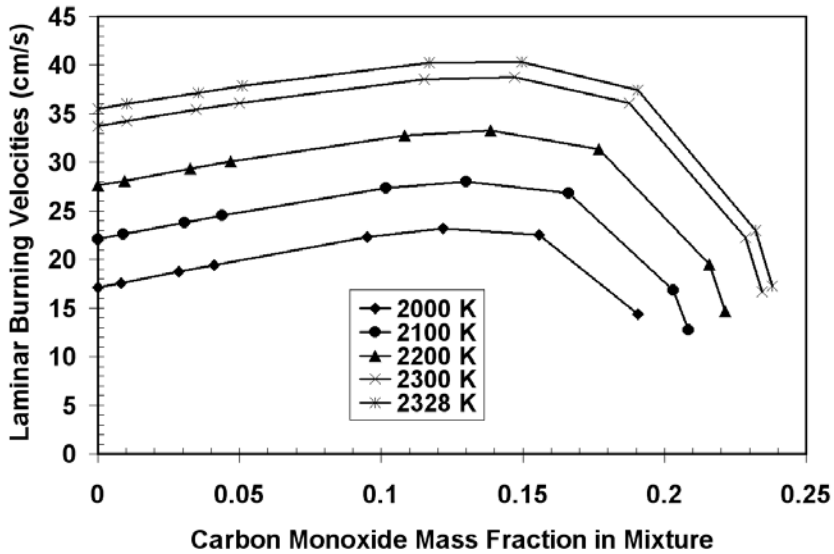

Figure 126: Structure of methane flame with CO addition profiles of CH_4, O_2, CO, H_2, H, CO_2, H_2O, and temperature T as a function of distance. The calculation were performed at Tc = 2300K, $Y_{H2,u}$ = 0, β = 8.25 and equivalence ratio, φ = 1.0.

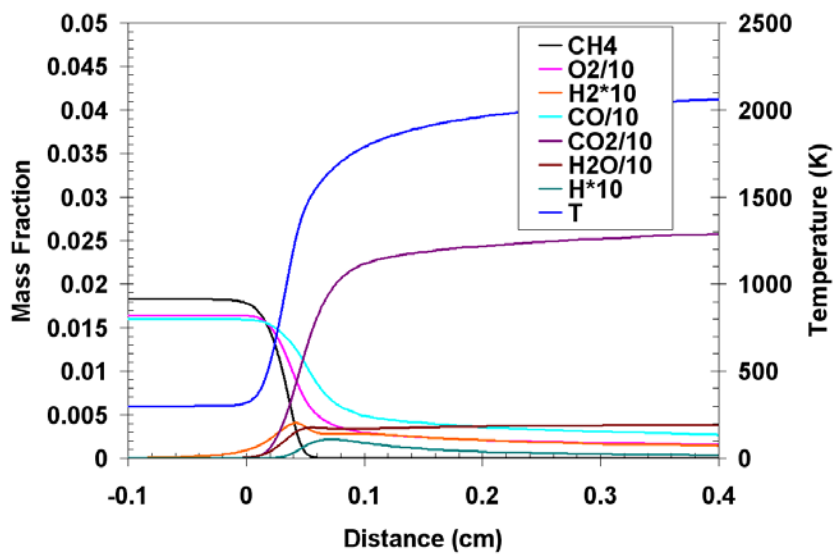

Figure 127: Reaction rate profiles of net rates of production of CH_4, O_2, CO, H_2, H, CO_2, H_2O, and temperature T as a function of distance. The calculation were performed at Tc = 2300K, $Y_{H2,u}$ = 0, β = 8.25 and equivalence ratio, φ = 1.0.

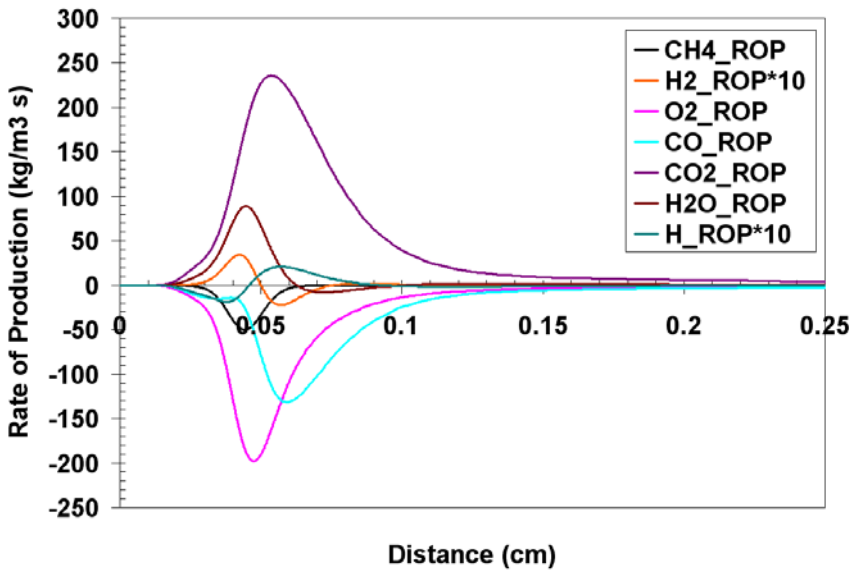

Figure 128: Structure of methane flame with CO addition profiles of CH_4, O_2, CO, H_2, H, CO_2, H_2O, and temperature T as a function of distance. The calculation were performed at Tc = 2300K, $Y_{H2,u}$ = 0, β = 82.5 and equivalence ratio, φ = 1.0.

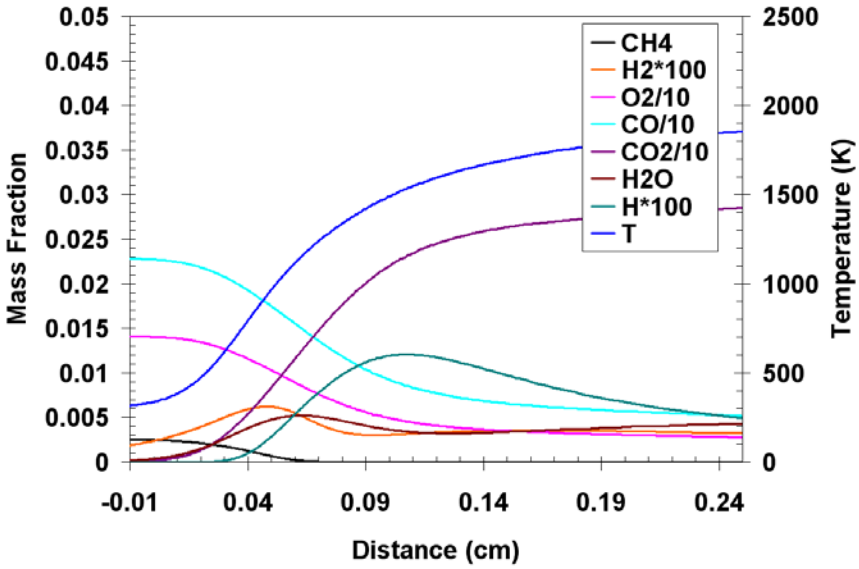

Figure 129: Reaction rate profiles of CH_4, O_2, CO, H_2, H, CO_2, H_2O, and temperature T as a function of distance. The calculation were performed at T_c = 2300K, $Y_{H2,u}$ = 0, β = 8.25 and equivalence ratio, φ = 1.0.

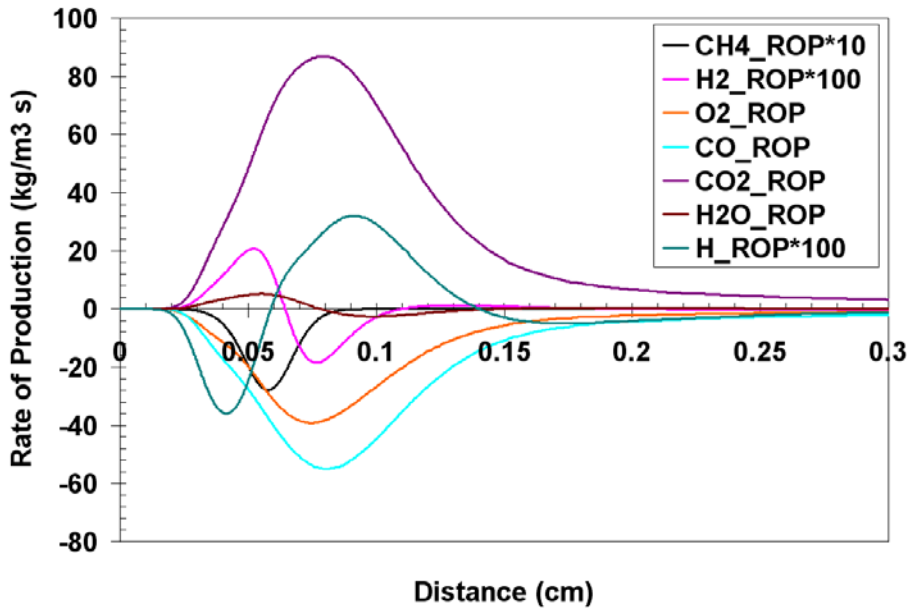

Chapter 22:
Task 2.4.4 Reduced Chemical Kinetic Mechanism for Producer Gas

Chemical-kinetic mechanism can be used to describe the combustion of a variety of fuels. Most of them, such as the San Diego Mechanism, contain the major compounds found in producer gas, such as H_2 (hydrogen), CO (carbon monoxide), CH_4 (methane), C_2H_4 (ethylene), and CO_2. In our previous work the research team reported on measurements of critical conditions of extinction and auto-ignition of producer gas. They also reported on the performance of the detailed chemical kinetic mechanism to describe combustion properties of producer gas. The mechanism was successful in predicting critical conditions of extinction and autoignition as found in the experiments. Subsequently, the research team developed a reduced chemical kinetic mechanism which contains a smaller number of intermediated species and a smaller number of reactions. This chemical kinetic mechanism can then be used in Computational Fluid Dynamic (CFD) codes. These CFD codes are used to model combustion and pollutant formation in practical systems, where computation times would otherwise be very long.

In the following, a systematic procedure will be employed to deduce reduced chemical kinetic mechanism from the detailed mechanism. Steady-state approximations will be used for many of the intermediate species. The reduced mechanism will be tested by comparing their predictions with those using the detailed mechanism.

The producer gas used in this work is made up of 42 percent CO, 25 percent H_2, 12 percent CO_2, 17 percent CH_4, and 4 percent C_2H_4 by volume at standard temperature (273 K) and pressure (1.013 bar).

22.1 Skeletal Chemical Kinetic Mechanism

The detailed mechanism for the combustion of producer gas was reduced to a skeletal mechanism by performing a chemical path analysis and sensitivity analysis. Typical combustion conditions were considered for the applicability of skeletal mechanism. This procedure reduced the number of species from 43 to 15 and the number of reactions from 470 to 18. The skeletal mechanism is shown below in the following Table 1.

Table 26: Skeletal chemical kinetic mechanism derived from the San Diego Mechanism for the combustion of producer gas (Version sd20111122skel14r)

Number	Reaction			A	n	E
1f	$H + O_2$	$\rightarrow$	$OH + O$	3.520E+16	-0.70	71.4
1b	$O + OH$	$\rightarrow$	$O_2 + H$	7.036E+13	-0.26	0.6
3f	$H_2 + OH$	$\rightarrow$	$H_2O + H$	1.170E+09	1.30	15.2
3b	$H + H_2O$	$\rightarrow$	$OH + H_2$	1.287E+10	1.20	78.3
4	$H_2O + O$	$\rightarrow$	$2\,OH$	7.600E+00	3.84	53.5
6	$H + OH + M''$	$\rightarrow$	$H_2O + M''$	4.000E+22	-2.00	0
10	$H + O_2 + M5$	$\rightarrow$	$HO_2 + M5$ k_0	5.750E+19	-1.40	0
			k_∞	4.650E+12	0.44	0
14	$HO_2 + O$	$\rightarrow$	$OH + O_2$	2.000E+13	0.00	0
22f	$CO + OH$	$\rightarrow$	$CO_2 + H$	4.400E+06	1.50	-3.1
22b	$H + CO_2$	$\rightarrow$	$OH + CO$	2.409E+13	0.22	105
25	$HCO + M7$	$\rightarrow$	$CO + H + M7$	1.860E+17	-1.00	71.1
35	$CH_2O + OH$	$\rightarrow$	$HCO + H_2O$	3.900E+10	0.89	1.7
38	$CH_4 + H$	$\rightarrow$	$H_2 + CH_3$	1.300E+04	3.00	33.6
43	$CH_3 + H$	$\rightarrow$	$T\text{-}CH_2 + H_2$	1.800E+14	0.00	63.2
46	$CH_3 + O$	$\rightarrow$	$CH_2O + H$	8.430E+13	0.00	0
53	$H + CH_3 + M9$	$\rightarrow$	$CH_4 + M9$ k_0	2.470E+33	-4.76	10.2
			k_∞	1.270E+16	-0.63	1.6
65	$T\text{-}CH_2 + O_2$	$\rightarrow$	$CO + OH + H$	6.580E+12	0.00	6.24
90	$C_2H_4 + O$	$\rightarrow$	$CH_3 + HCO$	2.250E+06	2.08	0

The skeletal mechanism was tested on producer gas, methane, and mixtures of producer gas and methane. The strain rate is a measure proportional to the opposing velocities of the fuel and air streams. The figures in the following show at which strain rate flames extinguish for a given fuel mass fraction in the fuel stream. The producer gas used in this work is made up of 42 percent CO, 25 percent H_2, 12 percent CO_2, 17 percent CH_4, and 4 percent C_2H_4 by volume. Figure 22 shows the comparison of the detailed and skeletal mechanisms with experiments on producer gas. As the amount of producer gas increases, the flame becomes stronger and more difficult to extinguish. Both mechanisms agree well with the experiments.

Figure 130: Extinction of producer gas / air flames; the producer gas stream is diluted with nitrogen. The symbols show experimental data, the lines show the results of numerical computations.

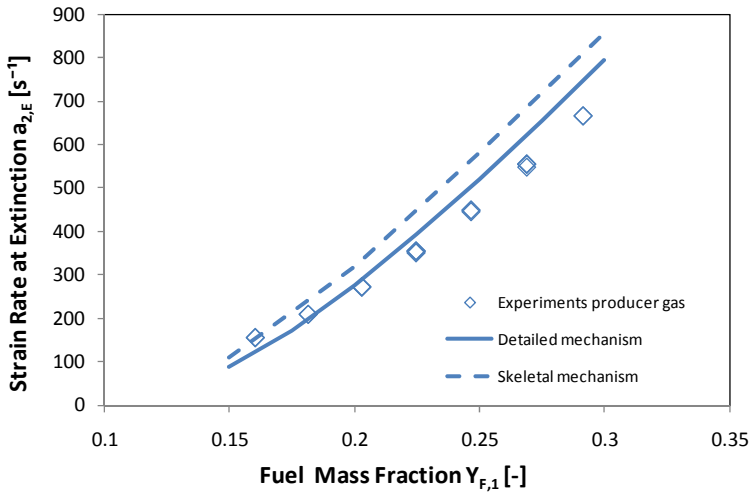

Figure 23 shows the extinction characteristics of methane flames. As the fuel mass fraction of methane is increased, the flame becomes stronger. Numerical simulations show that both, the detailed and skeletal mechanism capture this trend, but show somewhat higher extinction strain rates.

Figure 131: Extinction of methane / air flames; the methane stream is diluted with nitrogen; the symbols show experimental data, the lines show the results of numerical computations.

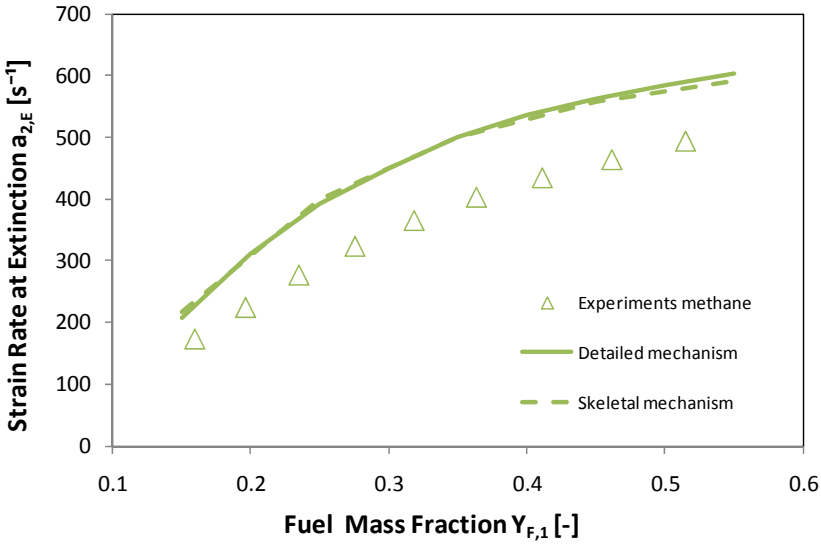

Figure 24 shows the extinction results of flames that are mixtures of producer gas and methane. Here, producer gas is always 25vol% in the fuel stream, but methane is added and increases the overall fuel mass fraction. The balance is nitrogen. The oxidizer is air. The detailed mechanism shows slightly higher strain rates, and the skeletal mechanism in turn slightly above that.

Figure 132: Extinction measurements of flames of mixtures of producer gas and methane; the fuel stream contains 20vol% producer gas and varying amounts of methane and the balance is nitrogen.

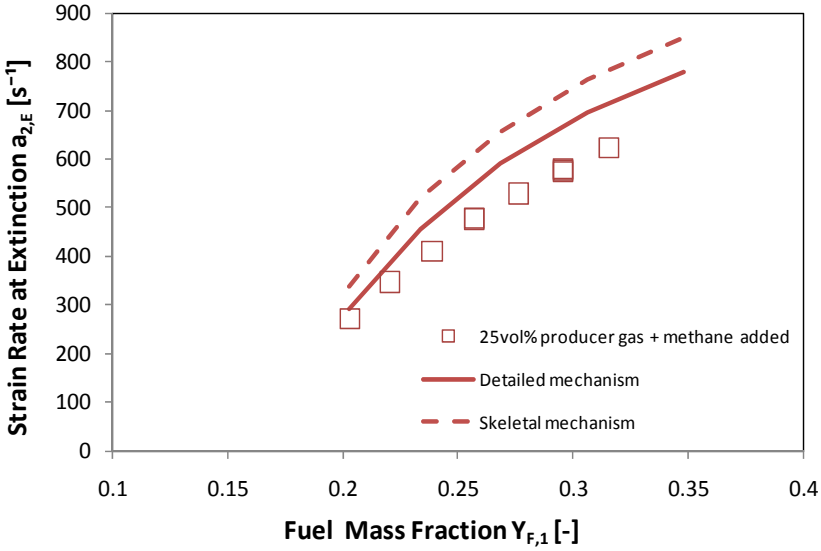

To isolate the chemical influences of producer gas on flame extinction, an experimental dataset from laboratory measurements of extinction was then modeled. In this experiment, the fuel is a mixture of methane and producer gas with variable proportions. The temperature for complete combustion, T_{st} was held at 1800 K. The stoichiometric mixture fraction ξ_{st} was fixed at 0.4. ξ_{st} is calculated from $\xi_{st} = (1+(\nu Y_{F,1})/Y_{O2,2})^{-1}$. Here ν is the stoichiometric mass ratio of oxygen to fuel (sum of mass of methane and producer gas). In short, the portion of producer gas is varied, by keeping other criteria such as flame temperature and flame location constant.

Figure 25 shows the comparison of experimental data, the detailed mechanism, and the skeletal mechanism. The skeletal mechanism agrees reasonably well with the experimental data.

Figure 133: Extinction characteristic of mixtures of producer gas and methane; the symbols show experimental data, the lines show the results of numerical computations.

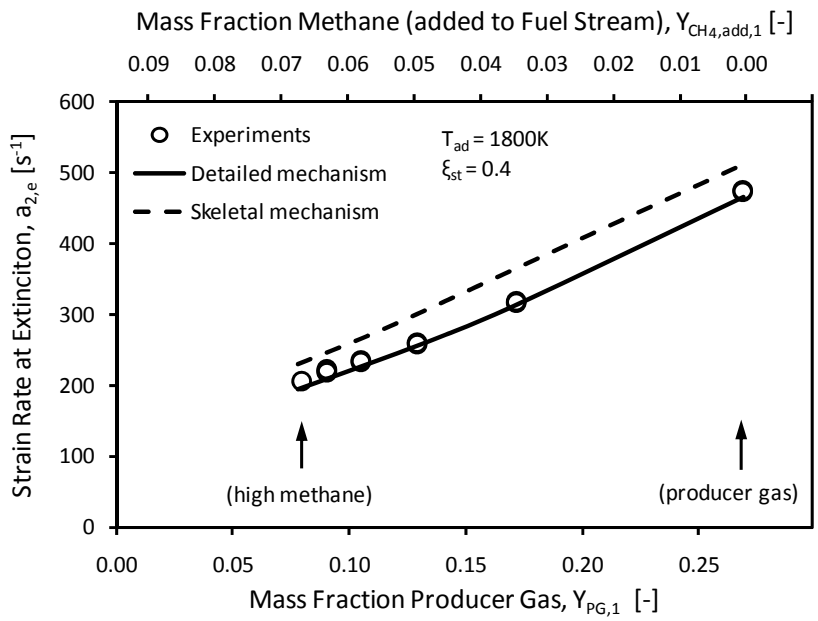

22.2 Reduced Chemical Kinetic Mechanism

A further reduction of the skeletal mechanism to a reduced mechanism is desirable. For this, species have to be set into steady state, and algebraic equations can be formulated for the species balance equations of those steady state species. These algebraic equations can also be modified for partial equilibrium assumptions or branching ratios.

The skeletal mechanism (shown in Table 1) contains 15 reactive species and 18 irreversible reactions. In order to develop a reduced mechanism, certain highly reactive species were set into steady-state. Since these species are rapidly consumed, balance equations for these species (differential equations) can be transformed into algebraic equations which reduce the time for the numerical solver dramatically. The goal of the final reduced mechanism is that it can be applied in more complicated geometries, where computation time is a major factor.

The reduced mechanism contains seven steady-state species: OH, O, HO_2, CH_3, CH_2O, HCO, and T-CH_2. With a total of 15 species, 7 steady-state species, and 3 elements (C, H, O), this system can be transformed into a set of 5 global reactions, where the rates are combinations of elementary rates. This will be the next step of the study. The results of the global mechanism are identical with those of the reduced mechanism, except the formulation differs for a simpler description which is better suited for inclusion in computational simulations of engine combustion.

The development of the reduced mechanism was completed by the research team. To summarize again, the overall procedure to arrive at the reduced mechanism included the following steps (as outlined by Prof. N. Peters):

1. Identify the starting mechanism (skeletal mechanism) from an appropriate full mechanism. Identify the principal path of oxidation.

2. Identify those species for which steady-state approximations can be introduced. Overall or global steps are then identified.

To simplify computations of steady-state concentrations of species from algebraic relations introduce appropriate "truncations". The number of global steps can be calculated by G = N - L - S, where N is the number of species in the skeletal mechanism, L is the number of chemical elements, and S is the number of steady-state approximations. Generally, G is an upper bound. The number of steps in the reduced mechanism could be less than G. For the current reduced mechanism, the number of global steps G = 15 − 7 −3 = 5. Species that are set in steady state are: OH, O, HO_2, CH_3, CH_2O, HCO, CH_2.

3. Applying steady state approximations to the skeletal mechanism leads to a reduced mechanism with the following global rates:

$$
\begin{array}{rcll}
CH_4 + 2H + H_2O & \rightarrow & CO + 4H_2, & \mathrm{I} \\
C_2H_4 + 2H + 2H_2O & \rightarrow & 2CO + 5H_2, & \mathrm{II} \\
CO + H_2O & \rightarrow & CO_2 + H_2, & \mathrm{III} \\
H + H + M & \rightarrow & H_2 + M, & \mathrm{IV} \\
O_2 + 3\,H_2 & \rightarrow & 2\,H + 2\,H_2O. & \mathrm{V}
\end{array}
$$

4. The rates of these global rates are derived among others from the following elementary reactions:

$$
\begin{array}{rcll}
CH_4 + H & \rightarrow & CH_3 + H_2, & 38 \\
C_2H_4 + O & \rightarrow & CH_3 + HCO, & 90 \\
CO + OH & \rightarrow & CO_2 + H, & 22 \\
H + O_2 + M & \rightarrow & HO_2 + M, & 10 \\
H + O_2 & \rightarrow & OH + H. & 1
\end{array}
$$

5. The rates for the global reactions are calculated from the elementary rates using the following equations:

$$
\begin{array}{rcl}
\omega_{\mathrm{I}} & = & w_{38} - w_{53}, \\
\omega_{\mathrm{II}} & = & w_{90}, \\
\omega_{\mathrm{III}} & = & w_{22}, \\
\omega_{\mathrm{IV}} & = & w_{6} + w_{10} + w_{53}, \\
\omega_{\mathrm{V}} & = & w_{1} + w_{43}.
\end{array}
$$

The following figures show a comparison of the three different mechanisms with experimental data. Figures 26 - 29 shows the same data as in the previous figures, but the reduced mechanism is included. The reduced mechanism shows good agreement with the detailed mechanism in most cases. Only for the methane case (Fig. 27), the reduced mechanism shows a different trend and higher extinction strain rates at high fuel mass fractions.

Figure 134: Extinction measurements of producer gas / air flames; the producer gas stream is diluted with nitrogen.

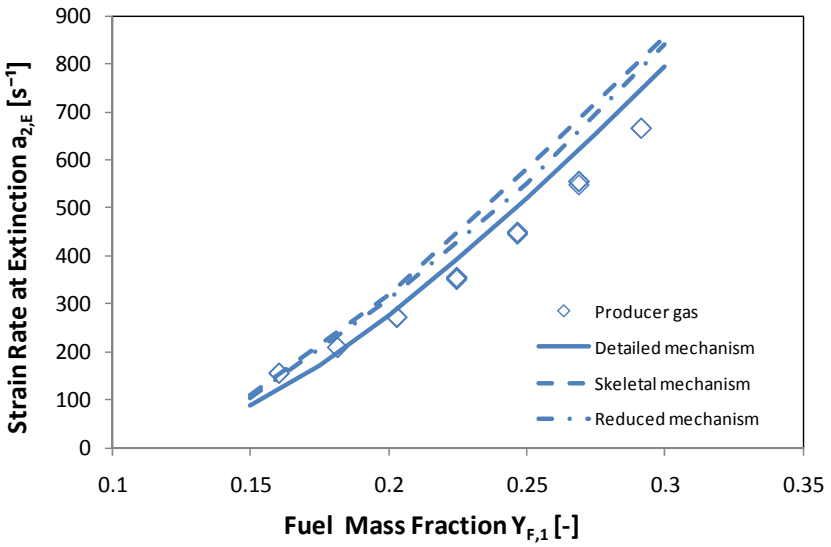

Figure 135: Extinction measurements of methane / air flames; the methane stream is diluted with nitrogen.

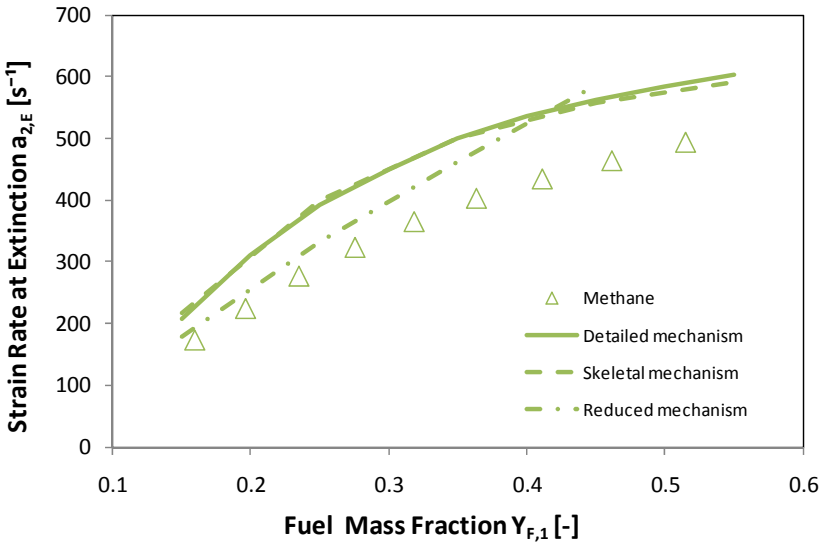

Figure 136: Extinction measurements of flames of mixtures of producer gas and methane; the fuel stream contains 20vol% producer gas and varying amounts of methane with the balance nitrogen.

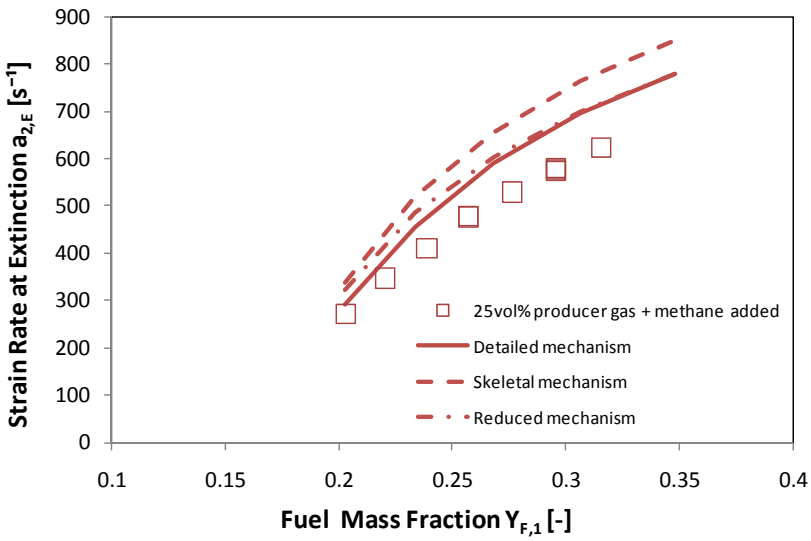

Figure 137: Extinction characteristic of mixtures of producer gas and methane; the symbols show experimental data, the lines show the results of numerical computations.

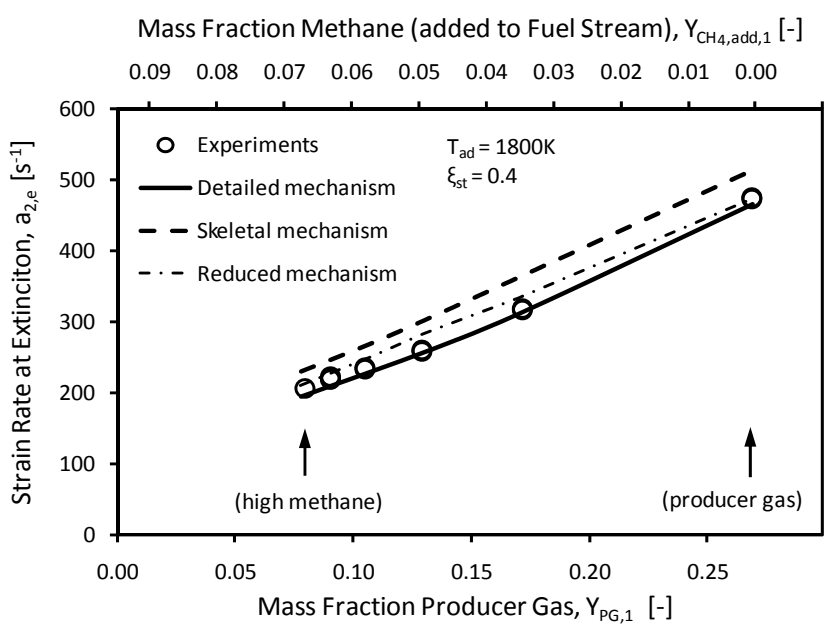

22.3 Further Improvements

Some work was performed to improve the chemical mechanism, since the detailed mechanism shows some over prediction of extinction strain rates for methane flames. It was identified that the reaction CH_4 (+ M) → CH_3 + H (+ M) plays an important role in methane flames while an only minor role in producer gas flames. This reaction has also been suspected for a while to have greater uncertainty. It will be further evaluated if this reaction rate should be increased and if there is other evidence in the literature.

This task was essentially completed during the last reporting period. A few calculations have been performed using the San Diego Mechanism using various rates for CH_4 (+ M) → CH_3 + H (+ M), which is a pressure dependent reaction. This reaction is suspected to have some uncertainty and be the source of inaccuracies for fuel mixtures with high CH_4 content. For a test, the frequency factor of this reaction was increased by 50 percent, and the results show an improved agreement with the experiments (see Figs. 30-32). The next step will be to investigate various reports on this reaction in the literature, in order to see which other researchers propose a higher rate for this reaction.

Figure 138: Extinction experiments using methane as fuel. The lines show comparisons to numerical computations using the San Diego Mechanism and one in which the rate of CH_4+M→ CH_3+H+M was increased by a factor 1.5.

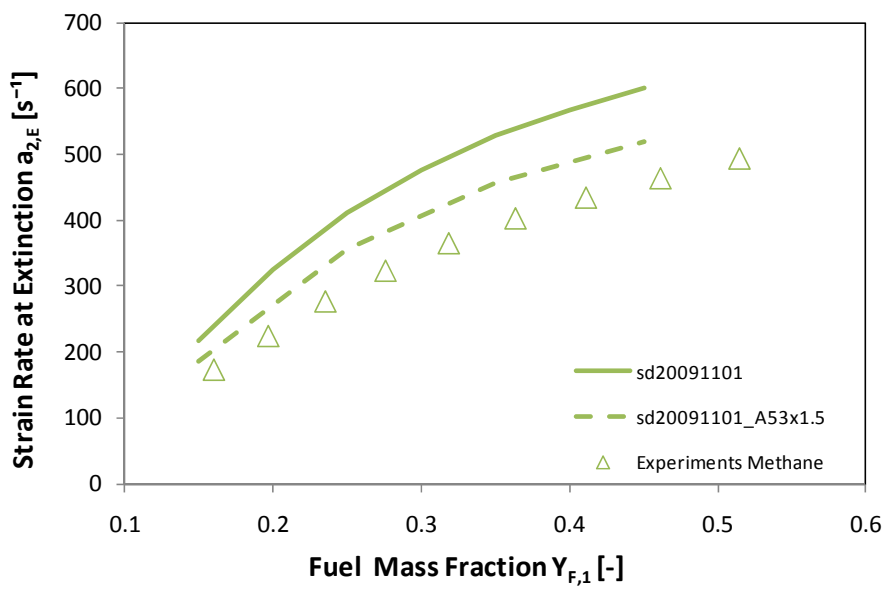

Figure 139: Extinction experiments using a mixture of producer gas (25vol%) and methane as fuel; the lines show comparisons to numerical computations using the San Diego Mechanism and one in which the rate of CH_4+M→CH_3+H+M was increased by a factor 1.5.

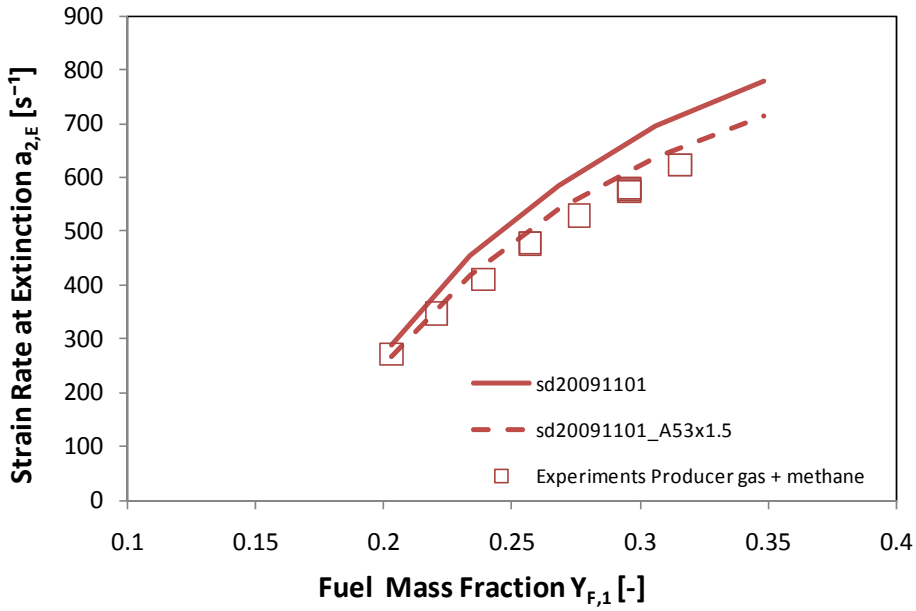

Figure 140: Extinction experiments using producer gas as fuel. The lines show comparisons to numerical computations using the San Diego Mechanism and one in which the rate of CH_4+M→ CH_3+H+M was increased by a factor 1.5.

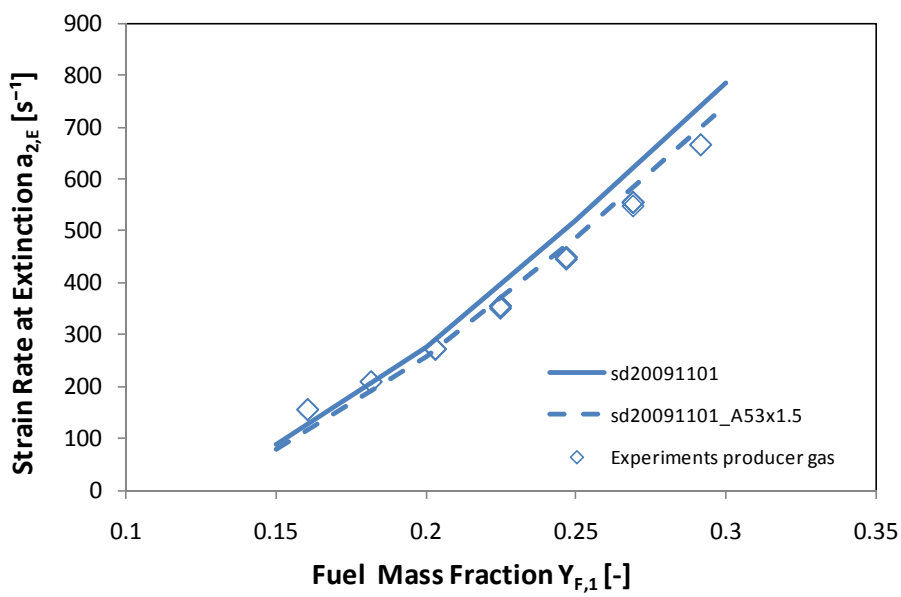

Chapter 23:
Task 2.5 Technology Transfer Activities

The research sponsored by the California Energy Commission grant CEC-PIER-2007-002 on Power Generation Using Advanced Thermochemical Gasification of Biomass has resulted in the development and evaluation of technologies for the production of renewable energy from the biomass resources in California To communicate the development of these technologies, faculty, staff, and students at the University of California San Diego, Davis, and Berkeley have provided to industry, government, educational institutions, and the professional engineering community information on the performance of the biomass energy system that was development with the aid of PIER sponsorship and in collaboration with other sponsors including the UC Discovery Pilot Program and an industrial sponsor, West Biofuels, LLC. This information was communicated through presentations to these entities and through written publication. In addition, through the University of California educational function both undergraduate and graduate students were exposed to critical issues associated with biomass energy production through associated research projects

23.1 Industrial and Government Presentations

Transfer of information with respect to the technology developed from PIER sponsored Power Generation Using Advanced Thermochemical Gasification of Biomass to industrial and government institution was accomplished through site visit presentations at the Woodland Biomass Research Center in Woodland Ca., the Department of Biological and Agricultural Engineering at University of California Davis, the Department of Mechanical and Aerospace Engineering at the University of California San Diego, and invited presentations at Industrial and Government Institution. Funding for travel outside California was provided by complementary funds and not PIER resources. A summary of the presentation are presented in Table 1.

Table 27: Industrial and Government Presentations

Date	Institution	Principal	Location
5/21/2008	Mitsui Engineering	Mr. Ken Miyachi Chief Research Engineer	UC Davis Davis, California
10/8/2008	Yolo County	Mr. Max Rexroad, Supervisor	Yolo Couty Office Woodland, CA
10/14/2008	California Integrated Waste Management	Gary Petersen, Commissioner	Woodland Biomass Research Center
3/4/2009	HydroChem – a Division of Linde	Raju Natarajan, President	Atlanta, Georgia
4/17/2009	DOE - INL	Dr. Donna Post Guillen Idaho National Laboratory	Idaho Falls, ID
5/15/2009	DOE - NREL	Dr. Richard Bain, National Renewable Energy Lab.	Golden, Colorado
8/22/2009	Sacramento County	Paul Philleo, Director Depart. of Waste Management	UC Davis Davis, California
11/22/2009	INSER Turin, Itlay	Dr. Gian Claudio Fausonne Marketing Director	Woodland Biomass Research Center
3/3/2010	ENI	Director of Research	UC San Diego

		National Energy of Italy	La Jolla, CA
4/26/2010	DOE– Los Alamos National Laboratory	Dr. Jose Olivares, Director National Alliance for Advanced Biofuels and Bioproducts	UC San Diego La Jolla, CA
5/28/2010	Northern Nevada Development Assoc.	Judy Bishop, Executive Director	Minden, Nevada
10/4/2010	Nevada County	Brett Storey, Senior Analysis Biomass Energy Resources	Woodland Biomass Research Center
10/15/2010	Gallo Winery	Roger Avery, Project Manager Utilities/Energy Conservation	Woodland Biomass Research Center
10/22/2010	Sempra Corp.	Mr. Ron Kent, Technology Development Manager	Woodland Biomass Research Center
2/8/2011	Linde Corp	Robert D Orazio, Chemical Segment Manager North America	UC San Diego
8/18/2011	Gussing Renewable Energy	Michael Dichand, President	Woodland Biomass Research Center
10/19/2011	Solar Turbines	Dr. Andy Luts, Manager Combustion Engineering	San Diego, CA
4/10/2011	Boswell Farms	Tom Miller, Plant Manager	Woodland Biomass Research Center

23.1.1 Presentations at Academic Institutions

As part of the technology development in the PIER sponsored Power Generation Using Advanced Thermochemical Gasification of Biomass project presentations/seminars were made at academic meetings and at Universities performing similar research and development in the areas of biomass gasification and power production. A summary of the meetings and Universities at which the PIER sponsored research was presented in shown in Table 2.

Table 28: Invited Presentations/Seminars at Academic Institutions

Date	Institution	Principal Contact	Location
7/1/2008	University of Bath	Peter Thomas, Director, UC-UK Science Bridge Program	Bath, England
7/14/2008	Vienna Technical University	Professor Ernst Pucher Depart of Mech Engineering	Vienna, Austria
9/11/2008	Brigham Young University	Prof. Tom Fletcher Department of Chemical Engineering	Prove, Utah
5/15/2009	Colorado School of Mines	Prof. Robert Kee, Department of Chemical Engineering	Golden, Colorado
6/4-5/2009	Scripts Institute of Oceanography	Peter Thomas, Director, Global Connect, Univ. of Calif. San Diego	La Jolla, CA
12/15/2009	University of Newcastle	Prof. Behdad Moghtaderi Depart. of Chemical Engineering	Callaghan, NSW
5/11-12/2010	Uni. of California Davis	Dr, Sharon Shoemaker, Director UC – Canada Innovation Partnership	Davis, California
6/8/2010	University of Bath	Prof. Stan Kolaczkowski Depart. of Chem. Engineering	Bath, England
6/16/2010	Politecnico Milan	Prof Elieso Ranzi Depart. of Chemical Engineering	Milan, Italy
8/29/2011	Vienna Technical University	Prof. Herman Hofbauer Department of Chemical Engineering	Vienna, Austria

23.1.2 Annual Program Review

The PIER sponsored Power Generation Using Advanced Thermochemical Gasification of Biomass project is complementary to the broader study of Biomass Gasification for the production of Power and Liquid Fuels funded by the University of California Discovery Program in partnership with West Biofuels, LLC. A summary of the entire program including the PIER funded project was presented annually at a program review. The agendas for these annual program review meetings in 2008, 2009, 2010, and 2011 are presented in Tables 3, 4, 5, and 7. A Separate CEC program review meeting was held in 2011 with the agenda in Table 6.

Table 29: UC Discovery/West Biofuels/CEC Technology Review Meeting – UC San Diego, UC Davis, and UC Berkeley, Sept 18-19, 2008.

Thursday, September 18th, 2008 – UC Berkeley

11:00 – 11:30	Welcome and Introduction	Robert Cattolica (UCSD)
11:30 – 12:30	Lunch break (Food Court next to Etcheverry Hall)	
12:30 – 1:00	First View of Joint Program Berkeley with Humbolt State where Wood Gasifier, purchased from India, is used to generate fuel for 20kW piston driven genset.	Anand Gopal and Ranjit (UCB)
1:00 – 1:30	Status of Methanol Reformer to fuel the Single Cylinder "CFR" Research Engine	Bryan Boyce and Andrew Van Blarigan (UCB)
1:30 – 2:00	Status of the Combustion of Mixed Alcohols in the CFR research Engine	Wolfgang Hable (UCB)
2:00 – 2:30	Numerical Modeling of Combustion in Piston Engines.	J Y Chen (UCB)
2:30 – 3:00	Break	
3:00 - 3:30	Combustion Characteristics of Gasoline and Surrogates	Kal Seshadri (UCSD)
3:30 – 4:00	Combustion Characteristics of Gasoline and Alcohols	Juergen Weissenbek (UCSD)
4:00 – 4:30	NOx Formation in Syngas/Oxygen Blends	Reinhard Seiser (UCSD)
5:00 – 6:30	Dinner at UC Faculty Club	
7:00 – 8:00	Drive from UC Berkeley to UC Davis	

Friday, September 19th, 2008 – UC Davis, Kemper Hall, Room 1003

10:00 – 10:15	Introduction	Robert Cattolica (UCSD)
10:15 – 10:30	Description of West Biofuels Gasifier	Matt Summers (West Biofuels)
10:30 – 11:00	Characterization of Bed Materials for Gasification	Chethan Acharya (UCSD)
11:00 – 1130	CFD Modeling of Fluidized Beds	Anjani Didwania (UCSD)
11:30 – 12:30	Lunch	
12:45 – 1:00	Overview of Recent Developments in Biomass Gasification	Bryan Jenkins (UCD)
1:00 – 1:30	Energy/Mass Balance Model of West Biofuels Gasifier	Chang-Hsien Liao (UCD)
1:30 – 2:00	Aspen Modeling of Biomass Reforming	Richard Herz (UCSD)
2:00 – 2:15	Break	
2:15 – 2:45	Economics of Biomass Power Generation	Robert Cattolica (UCSD)
3:15 - 5:00	Visit Pilot Plant Woodlands	

Table 30: UC Discovery/West Biofuels/CEC Technology Review Meeting, UC San Diego – UC Berkeley – UC Davis October 22nd-23rd, 2009

Thursday, October 22th, 2009 – UC Davis, Bainer Hall, Room 2045

1:00 – 1:15	Welcome and Introduction	Robert Cattolica (UCSD)
1:15 – 2:00	Chemical-kinetic Studies on Alcohol Fuels	Kal Seshadri (UCSD)
2:00 – 2:15	Gas-chromatographic Measurements of Alcohol Combustion	Reinhard Seiser (UCSD)
2:15 – 2:45	Green House Gas Impact of Biomass to Mixed Alcohol	Jamie Rhodes (UCSD)
2:45 - 3:00	Break	
3:00 – 3:45	Fuel Studies in Single Cylinder "CFR" Research Engine	Robert Dibble (UCB)
3:45 – 4:30	Numerical Modeling of Combustion in Piston Engines	J Y Chen (UCB)
4:30 – 5:00	Future Work Discussion	UCB/UCSD

Friday, October 23th, 2009 – UC Davis, Bainer Hall, Room 2045

9:00 – 9:15	Introduction	Robert Cattolica (UCSD)/Rizaldo Aldas (CEC)
9:15 – 9:45	Chemical-kinetic Studies on Producer Gas Combustion	Kal Seshadri (UCSD)
9:45 – 10:15	Status of Woodland Electricity Generation and Measurements	Reinhard Seiser (UCSD)
10:15 – 11;00	Engine Configuration for Producer Gas and Exhaust Gas Cleanup	Robert Dibble (UCB)
11:00 – 11:15	Break	
11:15 – 12:00	Biomass Characterization and Producer Gas Cleanup	Bryan Jenkins (UCD)
12:00 – 12:15	General/Administrative Discussions and Next Steps (CEC Component)	CEC/UCSD/UCB/UCD
12:15 – 1:00	Lunch	
1:00 – 1:40	CFD Modeling of Dual Fluidized-bed Gasifier	Anjani Didwania (UCSD)
1:40 – 2:20	Reforming of Producer Gas in Laboratory Scale	Chethan Acharia (UCSD)
2:20 – 2:30	Break	
2:30 – 3:00	Measurement of Producer Gas Composition with FTIR and Laser Absorption	Andrew Effenberger (UCSD)
3:00 – 3:30	Modeling of Biomass Gasification to Power and Liquid Fuel	Rich Herz (UCSD)
4:00 - 5:00	Tour Pilot Plant Woodland	
5:30 – 7:00	Dinner Woodland	

Table 31: UC Discovery/West Biofuels Program Review Meeting UC San Diego - UC Berkeley - UC Davis, October 28th-29th, 2010.

Thursday, October 28th, 2010 – UC Davis, Kemper Hall, Room 1003

9:15 – 9:30	Welcome and Introduction	Robert Cattolica (UCSD)
9:30 – 10:15	Laboratory Studies of Fluidization with Bed Materials	Kevin Mandich (UCSD)
10:15 – 11:00	CFD Modeling of Dual Fluidized-bed Gasifier	Anjani Didwania (UCSD)

11:00 – 11:30	Biomass Gasifier System Status	Cheng-hsien Liao (UCD)
11:30 - 12:00	Gasifier Operational Performance	Reinhard Seiser (UCSD)
12:00 – 12:45	Lunch in Room 1003	
12:45 – 1:30	Gasiifer System Modeling and Analysis	Richard Herz (UCSD)
1:30 – 2:30	Catalytic Gas/Tar Reforming	Chethan Acharya (UCdD)
2:30 – 3:00	Chemical Kinetics of the Combustion of Alcohol Fuels	Kal Seshadri (UCD)
3:30 – 4:00	Alcohol Fuel Engine Studies	Robert Dibble/JY Chen (UCB)
4:00 – 4:30	Transit to Woodland Biomass Research Center	
4:30 – 5:30	Tour Biomass Gasification Facility and Power Production	

Friday, October 29th, 2010 – UC Davis, Kemper Hall, Room 1003

9:15 – 9:30	Introduction	Robert Cattolica (UCSD)/ Rizaldo Aldas (CEC)
9:30 – 10:00	Chemical-kinetic Studies on Producer Gas Combustion	Kal Seshadri (UCSD)
10:00 – 10:30	Status of Engine-Generator System for Power Production	Reinhard Seiser (UCSD)
10:30 – 11:00	Status of Engine Control and Exhaust Gas Cleanup	Andrew Van Blarigan (UCB)
11:00 – 11:15	Break	
11:15 – 12:00	Biomass Characterization and Producer Gas Cleanup	Bryan Jenkins (UCD)
12:00 – 12:15	General/Administrative Discussions and Next Steps (CEC Component)	CEC/UCSD/UCB/UCD
12:15 – 1:00	Lunch in Room 1003	
1:00 – 1:30	Transit to Woodland Biomass Research Center	
1:30– 2:30	Tour Biomass Gasification Facility and Power Production	

June 7, 2011 – California Energy Commission, Hearing Room B, 1516 9th Street, Sacramento, CA

Table 32: UC/CEC Program Review Meeting Tuesday, June 7, 2011

10:00 – 10:15	Introduction	Robert Cattolica (UCSD)/Rizaldo Aldas (CEC)
10:15 – 11:00	Status of Gasifier Operations /Engine-Generator Woodland Biomass Research Center	Reinhard Seiser (UCSD)
11:00 – 11:30	Status of Engine Control and Exhaust Gas Cleanup	Andrew Van Blarigan (UCB)
11:30 – 12:00	Biomass Characterization and Producer Gas Cleanup	Zach Mccaffrey (UCD)
12;00 – 1:00	Lunch	
1:00 – 1:30	Chemical-Kinetic Studies on Producer Gas Combustion	Kal Seshadri (UCSD)
1:30 – 1:50	System Modeling of Gasifer/Engine-Generator Operations	Chethan Acharya/David Backhouse (UCSD)
1:50 – 2:10	General/Administrative Discussions	CEC/UCSD/UCB/UCD
2:10 – 3:00	Transit to Woodland Biomass Research Center	
3:00– 4:00	Tour Biomass Gasification Facility and Power Production	

Table 33: UC Discovery/WestBiofuels/CEC Program Review Meeting UC San Diego – UC Berkeley – UC Davis, October 12, 2011

Wednesday, October 12, 2011, UC Davis, Ghausi Hall, Room 3102-B

10:00 – 10:20	Introduction/Overview of Program Plan	Robert Cattolica (UCSD)
10:20 – 10:50	Gasifier Operational History/Performance	Reinhard Seiser (UCSD)
10:50 – 11:10	Gasifier Modeling –Aspen Plus	Chang-hsien Liao (West Biofuels)
11:10 – 11:30	Tar Sampling from Gasifier/UCD Gasifier Status	Zach McCaffrey/R. Williams (UCD)
11:30 - 11:50	New Rapid Tar Sampling Method	Patrick Fitzgerald (UCD)
11:50 – 12:10	Bed Material Characterization with SEM	Tei Newman-Lehman (UCSD)
12:15 – 1:00	Lunch in Room 3102-B	
1:00 – 1:20	Fluidization Experiments and Modeling	Kevin Mandich (UCSD)
1:20 – 1:40	Chemical Kinetics Syngas/Flash Pyrolysis Biomass	Kal Seshadri (UCSD)
1:40 – 2:10	Engine Emission Control using Producer Gas	Andrew Van Blarigan/Dibble (UCB)
2:10 – 2:30	Engine Modeling using Producer Gas	JY Chen (UCB)
2:30 – 3:15	Discussion of Future Objectives for Investigators	All
3:15 – 3:45	Transit from UC Davis to Woodland Biomass Center	
3:45 – 4:45	Tour Biomass Gasification Facility	
4:45 – 5:15	Transit to Steve's Pizza in Woodland	
5:15 – 6:45	Dinner	
6:45 – 7:00	Transit to Sacramento Airport	

23.1.3 Presentations at Professional Engineering Meetings

The performance of the biomass gasification energy system that was development with PIER and complementary funding from the University of California and West Biofuels was presented to the professional engineering community (13 presentations) at both national and international meetings. These presentations are summarized below. Support for travel for these meetings was provided by complementary funds and not by PIER funding.

23.2 Undergraduate and Graduate Research Projects

Through the University of California educational function both undergraduate and graduate students were exposed to critical issues associated with biomass energy production through associated research projects. Over 23 undergraduate students, 10MS graduate students, and 3 Ph.D. students performed research in support of the research and development sponsored by the California Energy Commission grant CEC-PIER-2007-002 for Power Generation Using Advanced Thermochemical Gasification of Biomass. Funding support for the undergraduate and graduate training and research was provided by complementary research funds, except for the doctoral student at UC Berkeley.

Table 34: Undergraduate Student Training and Research

2008-2009	Degree	Year	Quarter	Class	Research/Design Topic
Amy Stapp	BS Chem Eng	2009	Summer 2008 through Summer 2009	Chem Eng Research Project	Biomass Gasifier System Model and Exergy Analysis
Hsu-Wen Hsiao	BS Chem Eng	2009	Fall 2008	Chem Eng Research Project	Exergy Systems Analysis of Biomass Gasification Power Production
2009-2010					
Kevin Mandich	BS ME	2009	Winter 2009	MAE 156B: Senior ME Design Project	Design of char extraction sampling probe for Gasifier (2nd Iteration)
Matthew Drasner	BS ME	2009			
Jeremy McKeehen	BS ME	2009			
Paul Scannell	BS ME	2009			
Matthew Drasner	BS ME	2009	Spring 2009	MAE 171B: Senior ME Res.Project	Fluid separation of char from bed material
Barry Ju	BS ME	2009			
Eric Obana	BS ME	2009			
Owen Richey	BS ME	2009			
Kevin Mandich	BS ME	2009	Spring 2009	MAE 171B: Senior ME Res. Project	Fluidization properties of bed materials; non-invasive measurements of pressure and granular temperature
Jeremy McKeehen	BS ME	2009			
Su-min Lee	BS ME	2009			
Minh-vu Pham					
Jay Cox	BS ME	2009	Spring 2009	MAE 171B: Senior ME Res. Project	Creation of sampling chamber for char sampler; Testing of char sampler designs
Joshua Marcley	-	-			
Jonathan Novak	BS ME	2009			
Paul Scannell	BS ME	2009			
Maria Farrier	BS Chem Eng	2010	Spring 2009 Fall 2009	Chem Eng Research Project	Exergy Systems Analysis of Biomass Gasification Power Production
2010-2011					
Taylor Maxwell	BS ME	2010	Spring 2010	MAE 156B: Senior ME Design Project	Design of char extraction sampling probe for Gasifier (3rd Iteration)
Mark Melikian	BS ME	2010			
David Rosenow	BS ME	2010			
Frank Zabatta	BS ME	2009			

Table 35: Graduate Student Training and Research

2008-2009				
Wolfgang Hable	MSME 10/09	Vienna Technical University	4/08 to 5/09	Combustion Performance of Mixed Alcohol in a CFR Engine.
Jason Kranz LCDR, USN	MSME 12/08	UC San Diego	4/09 to 8/09	Biomass Economic Feasibility
Jim Giolitto	MBA 12/08	UC San Diego	4/09 to 8/09	Biomass Economic Feasibility
Kathy Lin	MBA 6/09	UC San Diego	4/09 to 8/09	Biomass Economic Feasibility
Robert Peele	MBA 6/09	UC San Diego	4/09 to 8/09	Biomass Economic Feasibility
Rex Motes	MBA 12/09	UC San Diego	4/09 to 8/09	Biomass Economic Feasibility
Jeffrey Skacel	MSME 6/10	UC San Diego	1/08 to 6/09	Mass Flow Methods for Fluidized Bed Gasifier
2009-2010				
Kevin Mandich	MSME 3/10	UC San Diego	7/09 to 6/10	An Experimental Study of a Vertical Fluidization Tube.
2010-2011				
Matthew Sprague	MSChem 6/10	University of Bath	1/09 to 6/09	Chem. Engineering Model of a Biomass Gasifier
David Blackhouse	MSChem tbd	University of Bath	2/11 to 7/11	Chem. Engineering Model of Integrated Gasifier System.
2008 –2011 Doctoral Students				
Andrew Van Blarigan	Ph.D. Tbd	Univ. of Calif. Berkeley	9/08 to 3/12	Advanced Emission Controls for Biomass Power Production
Kevin Mandich	Ph.D. tbd	Univ. of Calif. San Diego	9/10 to 3/12	Stability Analysis of Fluidized Bed
Zach McCafferty	Ph.D	Univ. of Calif. Davis	9/10 to 3/12`	Gas Cleaning for Biomass Gasification

Chapter 24:
Task 2.6 Production Readiness Plan.

This research and demonstration project at the Woodland Biomass Research Center (WBRC) has demonstrated that synthetic gas produced from biomass gasification can be used in conventional spark-ignited engines by implementing gas cleanup technology and a successful engine control strategy for ultra-low emissions. In order to bring this technology to the marketplace, the entire package of a biomass gasifier, gas conditioning, and low-emissions engine generator will be commercialized together as a biomass combined heat and power (BCHP) system.

West Biofuels, the commercial partner of UC San Diego on this project, has been working on implementing BCHP technology in California and North America. In order to become established in the marketplace and attract conventional investment and project financing, West Biofuels has teamed with companies with commercially proven technologies for each step of the process. This report outlines the processes, key facilities and partners, targeted production costs and investment requirements, and implementation plan for the commercial production of BCHP systems in California.

24.1 Production Processes

The West Biofuels process for the conversion of biomass to energy in the form of heat and power in this project is based on a four step process: (1) Feedstock handling, (2) Reforming in a Dual Fluidized Bed (DFB) Gasifier, (3) Gas Conditioning, and (4) Energy Generation. These steps are illustrated in Fig. 1.

Figure 141*:* Steps in the Biomass Combined Heat and Power system using a DFB Gasifier

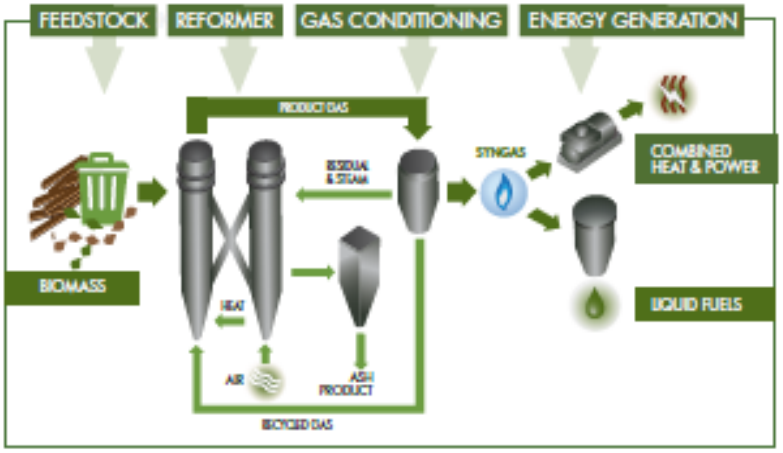

On feedstock handling, West Biofuels has been working with Western Agricultural Processors Association to identify waste agricultural biomass that is available for using in a BCHP facility. Agricultural processers have various feedstock available including shells and hulls, ginning waste, pits, straw, stalks, prunings, orchard removals, etc. These processors also have a need for power, steam and hot water for processing and preservation of agricultural products. West

Biofuels believes that these facilities are the first potential applications for the BCHP technology. On reforming and gas conditioning, West Biofuels has teamed with Gussing Renewable Energy to bring their gasification technology to the California and North American marketplace. On heat and power generation, West Biofuels has demonstrated low emissions power generation and will team with a global engine manufacturer and an emissions control supplier to bring this to the marketplace as part of the BCHP system.

The production of syngas (primarily H_2, CH_4, CO, and CO_2) using indirect heating of the biomass in a dual fluidized bed (DFB) gasification process is illustrated in two configurations in Fig. 2. Biomass is fed to a high temperature (850 C) reactor containing sand-like material that is fluidized with steam to convert the volatile carbon (~70 percent) in the biomass into gas. The gasifier bed material is transported along with the fixed carbon (~30 percent) from the biomass to a second reactor where combustion raises the temperature of the bed material (950 C) and recycles it back to the gasifier. This process produces a high quality gas with minimal nitrogen that is suitable for power production or for the synthesis of liquid fuels.

In Austria, Gussing Renewable Energy in collaboration with Vienna Technical University has developed and operated a DFB design (shown in Fig. 2a) at commercial demonstration scale (65 tons/day, 2 MWe) using a fast internally circulating fluidized bed (FICFB) gasifier operating on forest wood over the past 10 years with high reliability and safety, with as much as 7000 hrs/year power production (80 percent availability) as shown in Fig 3. The system produces 2 MWe from a biomass thermal input of 8 MW for an electrical efficiency of 25 percent. With the inclusion of waste heat recovery of 5 MW for district heating, an overall energy efficiency of 80 percent is obtained with the Gussing DFB design.

The Gussing fluidized bed gasifier operates on olivine bed material, a naturally occurring mineral composed of Mg, Fe, and SiO_2. Olivine in natural formations includes trace amounts of chromium. Through attrition, chromium will appear in the ash eliminating the possibility of recycling the ash. For application to California agricultural biomass this is a significant environmental issue. The potential fertilizer would also bring in additional revenue if it were sold. The Gussing DFB system is being deployed in Europe at a 2-3 MWe scale with wood feedstock. This technology, however, cannot be deployed for either wood or agricultural biomass in California because of more restrictive emission standards than in Europe and the necessity of disposal of the ash from the gasification process which cannot be recycled back to agriculture.

West Biofuelshas developed over the last three years a BCHP system using a dual fluidized bed (DFB) gasifier (4 ton/day, wood feedstock, 100 kWe power) at an industrial-agriculture research facility in Woodland, CA. This facility has been operated over the last two years to evaluate gasification of biomass feedstock, develop gasifier bed materials, and develop emission controls for power production to meet CARB standards. A schematic of the West Biofuels DFB gasifier is presented in Fig. 2(b).

Figure 142: Schematic of (a) Gussing Renewable Energy America fast circulating fluidize bed (FCFB) gasifier and (b) West Biofuels' (DFB) dual fluidized bed gasifier.

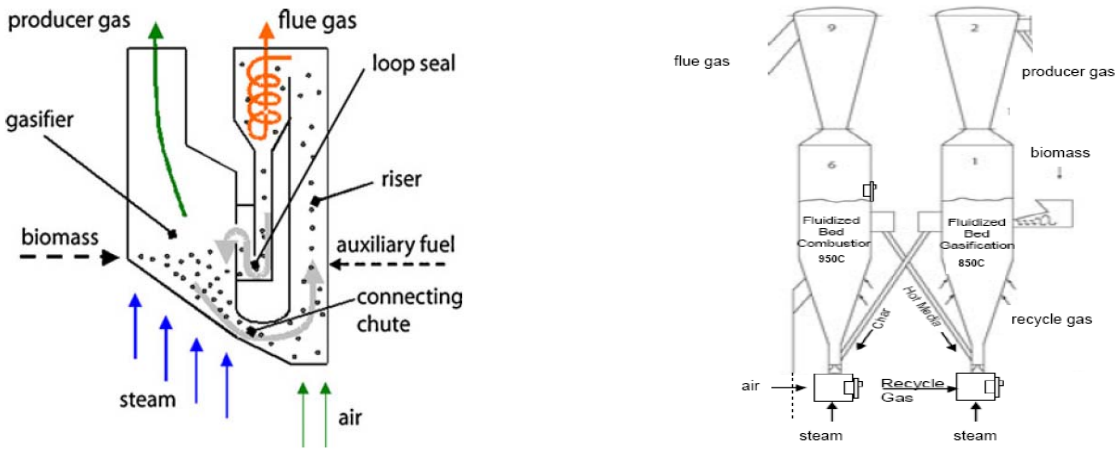

(a) (b)

Figure 143: Gasifier and engine availability history for Gussing BCHP operations 2002-2011

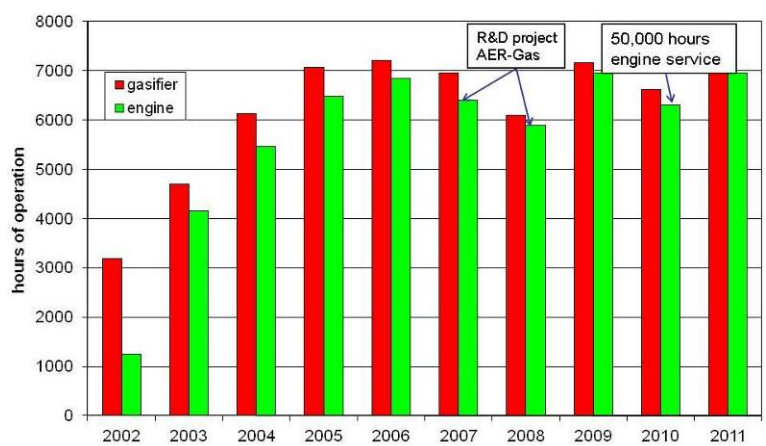

A comparison of the measured gas composition produced from the two DFB gasifier designs is presented in Table I. The Gussing design produces gas with a 20 percent higher heating value with higher H_2 and lower CO and also has lower tars than the West Biofuels design. However, using three-way-catalyst emission control, the West Biofuels system has much lower engine emissions of NOx and CO than the Gussing system. The Gussing system has an oxidation catalyst producing a 90 percent reduction of CO (300 ppm) and no control of the NOx (354 ppm) both far in excess of CARB standards.

West Biofuels has demonstrated the production of clean ash using an inert bed material, based on an engineered ceramic 300-400 micron particle, which can be used to replace the olivine bed material in the Gussing gasification process shown in Fig. 2a. In addition, West Biofuels, in collaboration with the University of California, has demonstrated as indicated in Table I, superior emissions control that can meet CARB standards using the DFB design in Fig. 2b.

The proposed BCHP technology combines technologies developed by West Biofuels (bed material producing clean ash and emission controls) and Gussing Renewable Energy America (superior gas quality, reliability, and safety) to provide BCHP operational performance, environmental compliance, and techno/economic analysis with the goal of demonstrating a robust, efficient, and an environmentally sound BCHP system that can be commercially deployed in the agricultural processing sector in California. A rendering of the BCHP system being developed is shown in Fig. 4.

Table 36: Producer gas properties from West Biofuels' (DFB) Dual Fluidized Bed Gasifier and from Gussing Renewable Energy's Fast Circulating Fluidized Bed (FCFB) Gasifier.

Gas Composition	West Biofuels (DFB) Dual Fluidized Bed Gasifier	Gussing Renewable Energy – (FCFB) Fast Circulation Fluidized Bed Gasifier
H_2	21.6%	40 %
CH_4	9.9 %	10 %
CO	30.2 %	22 %
CO_2	26.0 %	20 %
N_2	10.2%	3%
Tars (mg/m^3)	2000	25
H_2/CO Ratio	0.72	1.8
HHV (MJ/Nm^3)	10.5	12.1
NO_X (ppm)	7.3 (three-way catalyst)	354 (no control)
CO (ppm)	7.7 (three-way catalyst)	300 (with oxidation catalyst)

These BCHP technologies are being brought together in a Emerging Technologies Demonstration Project where West Biofuels is currently developing a 250 kW electric, 6 ton/day input BCHP demonstration project with the following objectives:

Qualify the use of almond biomass feedstock for BCHP operations (Target: Establish that 1.5 million tons of available almond biomass is feasible for gasification including shells, tree removal, and pruning wood)

Demonstrate emission controls for BCHP technologies that meet California Air Resources Board and Regional Air District Standards (Targets: NOx emissions < 0.07 lbs/MW-hr; CO emissions below 0.10 lbs/MW-hr; VOC emissions < 0.02 lbs/MW-hr).

Demonstrate an ash byproduct suitable for recycling as fertilizer back to agriculture (Targets: chromium composition in ash byproduct is less than 500 mg/kg; composition of other compounds below California non-hazardous ash standards)

Demonstrate electrical efficiency and heat recovery guidelines for BCHP that can be used by the California utilities to develop incentive and interconnection programs for BCHP technologies in the agricultural and food processing sector (Targets: Overall electrical efficiency of 22 percent; Combined heat and power efficiency of 65 percent)

Develop a techno/economic model for commercialization of BCHP to include a carbon and material life cycle analysis (Targets: Installed cost for commercial system less than $4000 per kWe; Minimum acceptable rate of return of 12 percent for potential commercial projects; Carbon emissions that are 70 percent less than conventional power and heating at an agricultural processing facility)

Figure 144: Rendering of commercial BCHP facility supplied by West Biofuels and Gussing Renewable Energy America

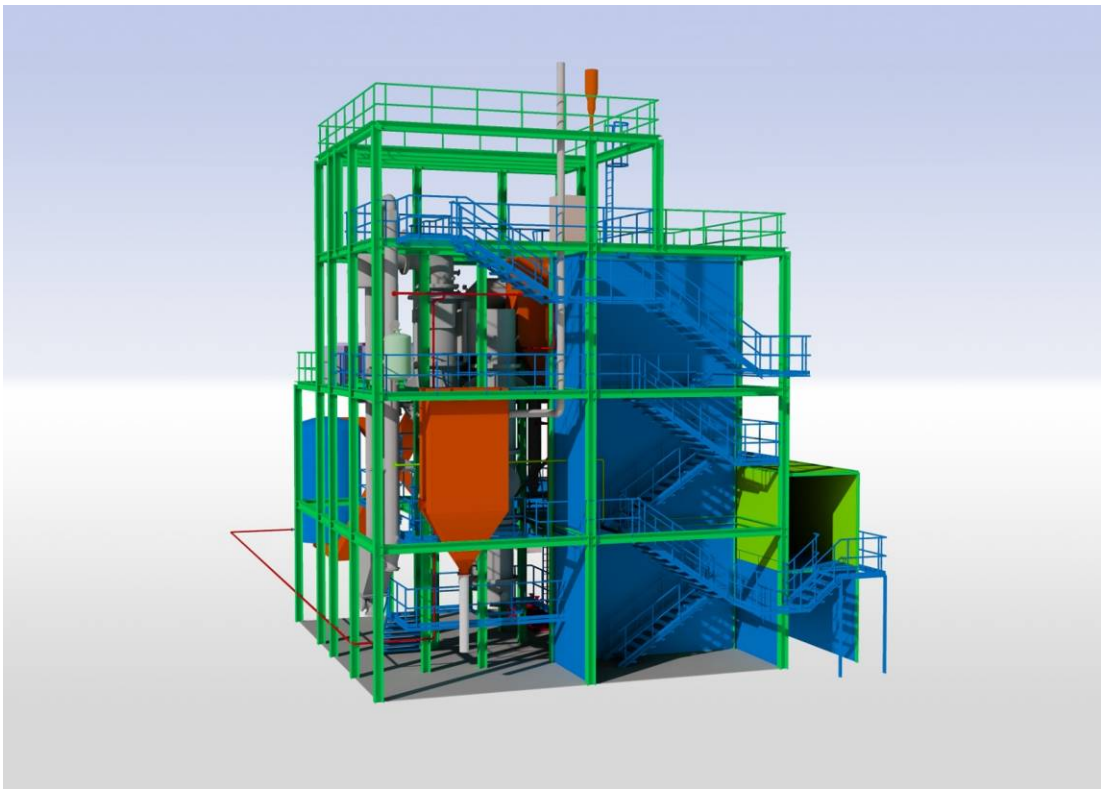

24.2 Production Facilities and Key Suppliers

West Biofuels has been developing facilities and suppliers capable of implementing BCHP projects in California and North America. Facilities include a fabrication warehouse in Woodland, California that is currently 18,000 SF and can be expanded to 54,000 SF as needed. This facility currently houses the Woodland Biomass Research Center and the BCHP demonstration plant. The facility is fully equipped with heavy equipment needed for assembly, refractory liner production, and light welding and fabrication. In addition the following key capabilities and suppliers are being developed by West Biofuels to support commercial projects.

- Vessels and Piping: All vessels and piping in the BCHP system including the gasifier and the gas handling systems are atmospheric pressure vessels designed to be constructed out of standard sized steel parts, flanges and gaskets that are available in the general marketplace. Each vessel can be produced by a number of identified suppliers who will be selected on a project-by-project basis through a competitive bidding process.

- Refractory: The main reactor systems require the installation of layered refractory to support the high temperatures and wear of the fluidizing media. This requires

specialized expertise which has been developed by West Biofuels. It is anticipated that refractory installation will take place at the West Biofuels facility in Woodland for the first commercial projects. West Biofuels will always supervise this process.

- Gas Scrubbers and Filters: There are several vendors that have been identified that can provide media scrubbers and filter systems required in the commercial plants. Suppliers will be selected on a project-by-project basis through a competitive bidding process.

- Compressors, Sensors, and Base of Plant Systems: Powered equipment required to operate the plant is all specified to be off-the-shelf within standard operating ranges available in the commercial marketplace. It is anticipated that this equipment can be supplied by a number of vendors to be selected by the main contractor for any given project.

- Controls: The system is controlled by a set of proprietary algorithms developed by West Biofuels. The control system is micro-computer based and involves variable frequency drives for each motorized sub-system. Sensors provide pressure, temperature and flow feedback to the control system.

- Structures and Foundations: Structures and foundations are likely to be project specific depending on earthquake and other structural and site requirements of any given project. Each project will involve a construction contractor that will be responsible for building the structural support system required by local codes. It is anticipated that this contractor will be hired in a competitive bidding process.

- Generator Set: The spark ignition gas engine and generator system will be supplied as a package system by commercial engine vendor. The project team has identified several potential suppliers for this key sub-system. Below are three potential suppliers that are being considered with some key capabilities described.

    - Guascor – This manufacturer appears to offer the lowest cost system integrating combined heat and power and has a presence in California on projects involving waste gas. The company has experience operating engines on producer gas in Europe. They offer engines in the 0.6 – 2.5 MW range as needed by the typical BCHP project.

    - Caterpillar- This supplier has the largest regional vendor support and service network in California and much of North America. They offer a number of engine generator models in the range required for BCHP projects. This manufacturer has limited experience with wood gas but has experience with other waste gas.

    - GE Jenbakker – This vendor has extensive experience with wood gas and in particular the fluidized bed system in Austria being used for the BCHP system. These engines have proven life expectancy on producer gas supplied by this gasifier system. The operating costs could be higher for these engines, but this needs to be factored in with life expectancy.

- Emissions and Engine Controls: The engine will be operated with control algorithms and emissions catalyst systems developed at the Woodland Biomass Research Center. It

is anticipated that a third-party vendor will be selected to support this part of the BCHP system. Potential vendors include several

- Engine Fuel and Emissions Engineering – This vendor has experience with engine and emissions control systems. In particular, EF&EE has experience with optimizing spark ignition engines on waste gas for optimum power generation and ultra-low emissions.
- Clean Air Systems – This vendor has a range of emissions control offerings and capabilities to support commercial projects. We believe this vendor can supply and support projects using producer gas.

24.3 Production Costs and Investment

Previous studies by West Biofuels and the UC project team have shown that at an installed cost of $3.5-$5.0 Million per MW, the BCHP system can be a cost effective form of power generation for many biomass energy projects in California and North America. This economics of any commercial project is dependent on project specific costs (feedstock, expendables, labor, etc.) and project specific returns (displaced power, displaced heat, value of ash, etc.). The analysis shows that a number of feasible projects are possible in this target cost range. Internal analysis by West Biofuels has shown that the BCHP system can be supplied for this cost with a modest technology license fee of 10 percent included in the cost.

The investment required to get the BCHP technology off the ground in California and North America include the cost of the demonstration project in Woodland, California the investment cost for the first commercial plant. The demonstration plant has a cost of $5 million and is being funded by West Biofuels, Gussing Renewable Energy America, and other partners with help from grant funding from California Energy Commission and University of California Discovery Grant Program.

Currently West Biofuels and Gussing Renewable Energy America are seeking Project Investment partners in a flagship commercial BCHP facility. Below is an example terms summary for a commercial project for a BCHP Facility supplied to a Project Investor entity.

Terms Summary (Example Only)

West Biofuels and Gussing Renewable Energy America (WB/GREA) are willing to license the Biomass Combined Heat and Power (BCHP) technology to the Project Investor (Project) entity in accordance with some simple but important terms and conditions. These include a License Fee to be paid by Project to WB/GREA and WB/GREA will provide to Project a scalable base design of the gasification plant that will be customized to suit the specific project specifications. The design and construction of the gasification plant can only be performed by approved engineers and contractors who are certified and supervised and/or managed by WB/GREA to perform such work.

The additional terms and conditions (T&Cs) are subject to change and revision after more accurate data is provided on the quality and quantity of the feedstock and WB/GREA has completed revised simulation modeling using the feedstock which is required for the final design. The following T&Cs provide an overview of the technology performance and cost estimates for the gasification plant based on the information provided by Project to date.

Ownership – We understand the plant would be owned by and licensed to Project.

Plant Capacity - We understand that 50 tonnes per day of dry biomass feedstock will be provided for the plant. All metals, glass, other inert materials and hazmats will be removed from the feedstock material. The remaining carbonic material will be shredded to be suitable feedstock for the plant.

Performance Specifications: The general specifications for a 50 tonne per day BCHP plant will be as follows:

Biomass thermal capacity entering (input performance)	*9.6 MW*
Biomass input (dry)	*2100 kg/h*
Producer gas volumetric flow	*2776 Nm³/h*
Producer gas mass flow	*2376 kg/h*
Utilizable volume of producer gas	*1776 Nm³/h*
Utilizable mass of producer gas	*1556 kg/h*
Utilizable calorific value of producer gas	*1.48 MW*
Achievable electric output	*~ 2.4 kW*
Thermal efficiency based on producer gas only	*74%*
Total thermal efficiency	*89%*
(with waste heat used for district heating systems)	

Warranties and Guarantees: The performance of the Hofbauer gasification plant with the associated equipment will be guaranteed by Gussing Renewable Energy GmbH (parent company of GREA, GREG) subject to specific terms and conditions. This warranty will be subject to the following:

1. Construction of the plant is performed by a GREG certified contractor who has been trained in Austria or at an alternative GREG approved facility;

2. Once built, the plant is commissioned by GREG and other personnel with Hofbauer gasification plant certification;

3. The plant is then operated by certified operators who have Level 3 or higher certification in boiler engineering and who have received specific training in Austria or at an alternative approved facility;

4. The plant is operated in a true manner to be effective and profitable; and

If the plant does not operate according to its specifications and the warranty terms are activated GREG has the right to purchase and remove the plant at a mutually agreeable discount rate of the construction cost.

5. The construction management company hired to fabricate the plant shall provide warranties and guarantees for the performance of their work which would typically cover structures, piping, electrical services, control systems, pumps and blowers, heaters, compressors and associated equipment. The performance of the engine generator on the producer gas will be provided by the engine system supplier manufacturer subject to their specific terms and conditions. Should an ORC system be used Project would have to secure manufacturer warranty separately for its energy yield, if a guarantee over the 2.4MW is required. We suggest it should be feasible to combine the Engine Generator, ORC, and GREG warranties, to provide a 3.4MW combined minimum electrical output warranty.

Schedule: In terms of construction timing, following completion of a formal contract, we suggest allowing six to eight months for testing the feedstock, modeling the feedstock functions for the gasification chamber, design modifications in accordance with modeling results according to the feedstock characteristics and twelve months for construction and commissioning of the plant. Note that this time line could be shorter and it does not include time set aside for permitting and government approvals which would be the responsibility of Project.

Operator Training: WB/GREG will provide operator training in Woodland, CA, USA and Gussing, Austria and during commissioning of the plant. Only certified operators are permitted to operate the plant and all guarantees and warranties are null and void if the plant is not operated by certified operators. Please note that all trainee operators should possess qualifications as a Boiler Engineer and the Lead Operator will need to possess, as a minimum, a Level 3 Boiler Engineers Certificate.

Cost Estimates: The price structure for the Hofbauer Gasification Plant and power generators is as follows:

One time "Right to Use" License Fee	*$1,000,000*
Capital cost estimate – Biomass gasification plant	*$10,000,000*
Capital costs estimate - Generator and ORC engines	*$4,000,000*
TOTAL	*$15,000,000*

The above costs do not include simulation modeling and engineering costs for revisions to the design specifically required for the feedstock characteristics to be carried out in California or Austria and nor do they include construction supervision costs required during fabrication and commissioning of the plant.

Contract Term: The projected life cycle for the main plant is 25 years but we recommend that it may be practical to extend it for a further 25 years of operation.

Operations and Maintenance: We recommend allowing $375,000 annually for plant operators and $350,000 for supplies and equipment maintenance as an average over this period. We will confirm these life cycle costs for the plant supplies and equipment maintenance during the technical feasibility assessment.

Operations Management: WB/GREA will provide operations management, working with Project, on a cost plus basis.

Closing: These are preliminary Terms and Conditions subject to change with additional information and may be revised following completion of a technical feasibility assessment which would include testing representative samples of the refuse derived biomass feedstock, conducting gasifier simulation modeling, preparation of the conceptual design of the selected plant and obtaining preliminary shop estimates for manufacturing, delivery and fabrication of the plant on site.

It is anticipated that additional commercial projects will develop during the construction of the demonstration and first commercial project, leading to a commercially viable venture funded by commercial projects by 2015. Therefore, the total investment required to get the BCHP technology to market is about $20 million including operation of the demonstration plant through 2015 plus the cost of the first commercial plant.

24.4 Implementation Plan

West Biofuels and Gussing Renewable Energy America are preparing for rapid commercialization of the BCHP technology in North America in conjunction with the construction of a demonstration plant in Woodland, CA. A scalable system design and project business plan are being developed that can be adapted to implement any commercial projects in California and North America involving the BCHP technology.

- Scalable System Design: This BCHP system design is in development for projects in the 1 – 100 MW Thermal (0.25 -25 MW Electric) range that is compatible with US standards.

This is based on an already completed design based on TUV standards for the European Union.

- Project Business Plan: A flexible plan that can be applied to any commercial project is in development with the following sections outlined below:
    - General Introduction
        - BCHP Technology
        - Overview of Operations
        - Company Overview
        - Contract Overview
    - Construction Plan
        - Detailed Description of System with Scaled Plans
        - Detailed Work Plan and Schedule
        - Nominated Contractors and Subcontractors
        - Outsourced Items To Be Bid, Process to Procure
        - Project Management Structure
        - Quality Assurance / Quality Control
        - Manufacturing and Equipment Guarantees
        - Contract Procedures
        - Contract Pricing
    - Operating Plan
        - Staffing Plan
        - Maintenance Plan
        - O&M Costs
        - Capital Plan – Capital Maintenance and Replacement
        - Insurance and Bonding
        - Performance Measures
        - Operator Training and Continuous Development
        - Work Safety Measures
        - Regulatory Reporting
        - Health and Safety Compliance
        - Dependencies on External Risks
        - Supplies Management
        - Contract Obligations

The construction of the demonstration plant is scheduled to begin in late-2012 and plant commissioning is expected by mid-2013. Demonstration plant operations including qualification of various biomass feedstocks for commercial partners have been scheduled through early 2015. The planning and design of first commercial facility will be concurrent with the construction and operation of the demonstration plant. The commissioning of the first commercial BCHP plant in North America is expected in 2014 or 2015.

Chapter 25: Summary and Recommendations

The goal of this research and development project to successfully demonstrate power generation from forest wood waste using the West Biofuels advanced thermochemical gasification process was accomplished through a series of technical tasks to provide the information necessary to evaluate the defined technical objectives. A summary of those tasks and associated recommendations are presented in this section.

25.1 Task 2.1 Producer Gas Purification System Design and Testing

A design review was conducted to evaluate gas scrubbing and purification systems for the removal of tars and contaminants in the producer gas generated from biomass gasification. Both a laboratory system and a pilot system for the West Biofuels gasifier were constructed. The laboratory gas cleaning system was designed primarily to remove particulate matter and tar. Particles larger than 20 microns are removed by cyclonic separation. A barrier filter removes particles greater than 1 micron. For tar removal, a packed-bed wet scrubber was designed to allow operation with different liquid solvents at variable flow rate. The scrubber contains a large reservoir for collection of condensables and for steam gasification. The laboratory system was constructed but delays in the installation and approval of a thermal oxidizer required fire safety systems at UC Davis prevented all but preliminary testing. The pilot gas purification system for the West Biofuels gasifier at the Woodland Biomass Research Center was built and tested continuously over the duration of the project with additional units added to improve gas cleaning. The final configuration consisted of two packed beds with water scrubbing followed by a charcoal filter to reduce the condensable tars with drop tanks and filters provide ahead of the SI engine/generator.

The recommended gas cleaning design includes a PM removal system specifically designed for the system gas flow and temperature and consisting of a cyclone followed by a ceramic candle filter module. Also to be included is a chilled solvent packed-bed scrubber for final drying and light tar removal. As with the initial design, the first packed bed scrubber is recommended to use an organic solvent (e.g., biodiesel) to better enable disposal through the combustor.

25.2 Task 2.2 Producer Gas SI Engine/Exhaust Gas Cleanup.

This task was originally intended to use a laboratory engine at the UC Berkeley and synthetic produce gas produced from reforming methanol to develop and test a fuel/air ratio controller and exhaust gas cleanup system. To replace and update the equipment UC Berkeley required additional time and funds which would have a negative effect on the progress of tests on the generator set at the Woodland site. It was concluded that the Task 2.2 could be effectively performed on the Waukesha Engine Generator at the Woodland Biomass Research site operating on producer gas from the West Biofuels gasifier to accomplish this task.

A fuel air ratio controller for engine operation based on throttling the air to the Waukesha engine was developed in conjunction with the installation of three-way automotive catalyst technology. Both lambda sensors and direct nitric oxide sensors were used in both single and

dual catalyst configurations to successfully remove NOx and CO from the engine emissions to meet the Yolo County AQMD RULE 2.32 for the emissions regulation.

25.3 Task 2.3 Power Generation from the Gasification of Wood Waste.

A Waukeshar H-2475G engine/generator set capable of 200 KWe when operated on natural gas as installed at the Woodland Biomass Research Center to operate on producer gas from the West Biofuels dual fluidized-bed gasifer. The engine generator was expected to generate 100-150 kWe when operated on producer gas from the gasification of wood. Power from the system was routed to a programmable load bank (1.4 to 140 KWe) that could be used from agricultural processing. The West Biofuels gasification facility cannot be operated continuously but is an intermittent technology demonstration facility. Also, the lack of a net-metering program for biomass power generation with the local utility (Pacific Gas and Electric Co) precluded a grid connection. The engine/generator was extensively instrumented and the exhaust emission monitored with both EPA approved continuous emission analyzer and more advanced GC and FTIR gas analysis instruments. Power generation from the gasification of wood waste with the West Biofuels gasifier was demonstrated at the 100 kWe level with both NOx and CO levels below 8 ppm using three-way catalyst technology adapted to the system Future engine/generator system designs should focus on lean burn engines to increase efficiency and power specific emissions. Lean burn engine exhaust provides the opportunity to evaluate other emission control technologies such as selective catalytic reduction (SCR) using urea injection.

25.4 Task 2.4 Combustion Properties and Chemical Mechanism for Producer Gas

An advanced chemical kinetic mechanism (43 species and 470 reactions) for the combustion of producer gas was developed and validated on laboratory experiments to predict auto-ignition, extinction properties, and laminar burning velocities for producer gas with varying composition. A skeletal chemical kinetic mechanism (15 species and 18 reactions) and a reduce chemical kinetic mechanism with 5 global reactions were also developed for use in direct engine simulation codes to predict performance and combustion emission

25.5 Task 2.5 Technology Transfer Activities

To communicate the development of the technologies investigated in this project, faculty, staff, and students at the University of California San Diego, Davis, and Berkeley have provided to industry, government, educational institutions, and the professional engineering community information on the performance of the biomass energy system that was developed with the aid of PIER sponsorship and in collaboration with other sponsors including the UC Discovery Pilot Program and an industrial sponsor, West Biofuels, LLC. This information was communicated through presentations to these entities and through written publication. In addition, through the University of California educational function both undergraduate graduate students, and post-doctoral scholars were exposed to critical issues associated with biomass energy production through associated research projects.

25.6 Task 2.6 Production Readiness Plan

This research and demonstration project at the Woodland Biomass Research Center (WBRC) has demonstrated that synthetic gas produced from biomass gasification can be used in conventional spark-ignited engines by implementing gas cleanup technology and a successful

engine control strategy for ultra-low emissions. To bring this technology to the marketplace, the entire package of a biomass gasifier, gas conditioning, and low-emissions engine generator will be commercialized together as a biomass combined heat and power (BCHP) system. West Biofuels, the commercial partner of UC San Diego on this project, has been working on implementing BCHP technology in California and North America. To become established in the marketplace and attract conventional investment and project financing, West Biofuels has teamed with companies with commercially proven technologies for each step of the process. Previous studies by West Biofuels and the UC project team have shown that at an installed cost of $3.5-$5.0 Million per MW, the BCHP system can be a cost effective form of power generation for many biomass energy projects in California and North America. The economics of any commercial project is dependent on project specific costs (feedstock, expendables, labor, etc.) and project specific returns (displaced power, displaced heat, value of ash, etc.). The analysis shows that a number of feasible projects are possible in this target cost range. Internal analysis by West Biofuels has shown that the BCHP system can be supplied for this cost with a modest technology license fee of 10 percent included in the cost. A new demonstration plant at the Woodland Biomass Research Center incorporating technologies developed in this project is scheduled to begin construction in 2012 and commissioned in 2013 in partnership with Gussing Renewable Energy American with matching funds from West Biofuels and the University of California Primary funding for the project is from the California Energy Commission Emerging Technology Demonstration Grant Program II (PON-11-501).

25.6.1 Technical Performance Objectives

The following for primary technical objectives were defined as bench marks for the performance of the biomass gasification power generation system developed in this PIER sponsored projection:

1) Achieve minimum gasification efficiency of 75 percent on a LHV basis using an advanced thermochemical gasification process.

A biomass rate (wood pellets) of 3 tons(wet)/day produced 68 scfm of producer gas. The lower heating value (LHV) of the gas is 52 percent of the lower heating value in the biomass. If all volatiles would be converted to producer gas then 69 percent of the biomass energy could be converted to producer gas. The present results are lower for two reasons. First, some of the gas was oxidized with oxygen above the fluidized bed to increase the temperature and reduce the tar content. Therefore, some of the gas was converted into CO_2 and H_2O and the energy content was lowered. Without this step, 58 percent of the biomass would have been converted to producer gas. Second, some gas (O_2 and air) entered into the gasifier from the combustor through the downcomer connected to the regeneration section of the gasifier. At the same time, not all of the volatile fraction of the biomass might have been converted and some was moved over to the combustor. This explains the remaining difference between the 58 percent and 69 percent conversion. Since the gasification process in general only converts the volatile fraction of the carbon in the biomass the maximum conversion for the wood biomass could only be 69 percent conversion. However, the 31 percent of the energy is not lost. The energy in the fixed carbon is used in the combustion regenerator to produce the necessary heat for the endothermic gasification process and can be recovered as waste heat and has been demonstrated in an integrated co-gen gasification system to contribute to an overall energy utilization of 80 percent.

2) Tar/contaminant gas cleaning of producer gas with a minimum efficiency of 96 percent.

Using the gas scrubbing and cleaning system developed for the West Biofuels gasification system (Task 2.1.7) the efficiency of the tar removal system is illustrated in Table 1 The measured reduction in tar species is 76 percent. It should be noted that these species are never released since they are either burned in the internal combustion engine or combustion flare if maintained at high temperature. At lower temperature then will condense on filters.

Table 37: Tar species before and after gas cleaning system.

	Pre Scrubber (mg/m^3 Producer Gas)	Post Scrubber (mg/m^3 Producer Gas)
Naphthalene	16272.8	4325.7
Acenaphthylene	2014.9	426.9
Fluorene	560.4	0.0
Anthracene	1049.7	270.3
Phenanthrene	346.0	0.0
Fluoranthene	538.5	0.0
Pyrene	429.8	0.0
Sum of compounds	21212.2	5022.9

To improve the performance of tar removal additional technical approaches are being developed to include higher operating temperature for the gasification process, catalytic bed materials, organic scrubbing liquids instead of water, and a regenerative catalytic reformer system developed by the National Renewable Energy Laboratory (Golden, Co) that will remove the tars listed in Table 1 by 99 percent for not only power production but provides the potential to use catalytic synthesis of the producer gas to produce fuel and chemicals.

3) Using an internal combustion engine fueled by producer gas a minimum thermodynamic efficiency of 30 percent.

The gasifier integrated with the SI engine/generator was operated over a power range from 40 to 100 kWe with different gasifier operating conditions. To minimize tar production and exhaust emissions it was necessary to operate the gasifier at 3 tons/day instead of the maximum 5 tons/day. The thermodynamic efficiency and operating characteristics are summarized in Table 2. The efficiency that was obtained was 16 percent since only about 40 percent of the capacity of the engine was used due to throttling of the gas and a large parasitic load of almost 60 kW. With full load the efficiency could be expected to be 25 to 30 percent. To obtain better efficiency either a smaller engine matched to the lower volumetric output of the current gasifier or improved energy content of the producer gas from the gasification process to better match the engine is required. In future development both improved producer gas properties and a lean burn engine would provide higher efficiency.

Table 38: Engine operating parameters and emissions.

Producer gas flow to engine	54	scfm
Exhaust flow	180	scfm
Power generated	42	kWe
Engine efficiency	16	%
NO	8	ppmv
CO	8	ppmv
NO emissions	0.16	lb/MWhr
CO emissions	0.15	lb/MWhr

4) Internal combustion engine exhaust cleanup will be below the Yolo County AQMD RULE 2.32 for the emissions regulation for NOx (2.1 lbs/MW-Hr) and CO (42.5 lbs/MW-Hr).

At optimized operating conditions the spark ignited (SI) engine used to generate electrical power produced 8 ppm of NO and CO with emission control adapted from automotive catalyst technology developed in Task 2.2. The emission levels correspond to 0.16lb/MW-hr for NO and 0.15 lb/MWhr for CO. These levels are well below the Yolo county requirements for small power production and are approaching the general more restrictive California Air Resources Board and Regional Air District Standards (Targets: NOx emissions < 0.07 lbs/MW-hr; CO emissions below 0.10 lbs/MW-hr) for non-attainment districts. Both improved engine efficiency and better operating characteristics of the gasification process should provide sufficient improvement for the emission control technology to meet the higher CARB standards.

25.6.2 Economic Performance Objectives:

1) A capital cost below $1500/kW at a production scale of 100 units.
The technical objective of $1500/KWe for a production scale of 100 units does not seem attainable with the current gasification technology and market. It is expected that to become established in the marketplace and attract conventional investment and project financing a commercial entity such as West Biofuels teamed with companies with commercially proven technologies for each step of the process can produce a BCHP system for many biomass energy projects in California and North America at an installed cost of $3.5-$5.0 Million per MW. This cost could be reduced with larger scale production, but typically power projects of this type are not produced an assembly line production system. A more realistic cost approaching $3 Million per MWe at large scale production may be attainable. With increased renewable power standards, higher retail power costs, and greenhouse gas cap and trade policy in California the expected cost of $3.5-$5.0 Million per MW should be economically viable.

2) Operating costs below $.06/kW-Hr to including variable feedstock cost.
The economic performance of a 3 MWe gasification co-generation power plant with a capital cost of $2..9M/MWe and a feedstock cost of $2/ton is shown in Figure 1 (R. Cattolica, et al). The critical element in the feasibility of an operating cost of $0.06/kW-Hr is the value of the recoverable waste heat sales which is tied to the cost of natural gas. The breakeven point in terms of the net present value (NPV) of the project for natural gas price of $4.5/MMBtu is $79/MW-Hr or $0.079 kW-Hr. The value of the waste heat at $4.5/MMBtu is worth $0.03 kW-hr so that without waste sales the breakeven price of the power sales would need to be $0.109/kW-Hr. The effect of feedstock cost (shown in Figure 2) is important but not as critical as capital costs, plant scale, and the value of the waste heat. As the feedstock cost changes from

$0 to $20/ton the effect on the cost of electrical sales changes by about $0.034/kW-Hr. From this analysis a target price of below $0.6/kW-Hr is only reachable with the inclusion of waste heat sales. For internal use by a feedstock supplier with waste heat processing needs such as agricultural processing in the California almond industry or wood mill co-generation that pay both retail power and natural gas prices a much value of sales is justified and could provide a substantial NPV.

Figure 145: Sensitivity of project returns to power prices and waste heat prices.

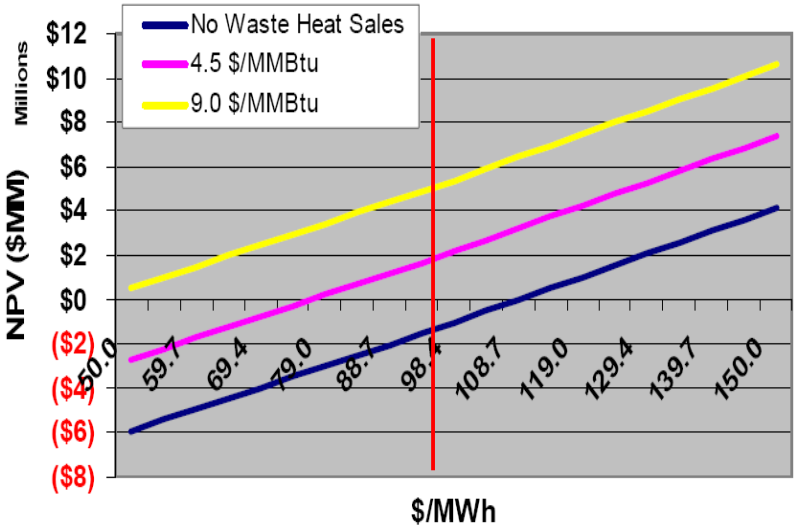

Figure 146: Sensitivity of project returns to feedstock costs with no waste heat sales.

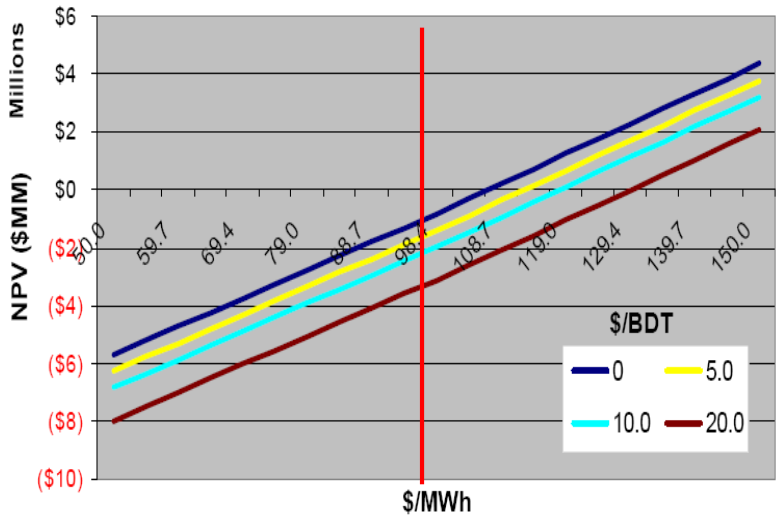

25.7 Benefits to California

In the state of California, renewable power standard requires 33 percent of the power to be generated from renewable sources by 2020. The peak power generation from biomass in the state of California occurred in the year 1992, which was 7,362 GWh.[1] The power generation from biomass has reduced by 25 percent to 5,575 GWh in the state of

California in this decade.[1,2] In the report on the roadmap for the development of biomass in California published by California Energy Commission (CEC) in 2006,[3] 32 million bone dry tons (BDT) per year of sustainable biomass feedstock is available for the production of energy in California as shown in Figure 1. The 32 million BDT/year biomass can produce 4,650 MW of electricity as shown in Table 1. This data shows that renewable energy from biomass could provide as much as a significant role in meeting the renewable power requirement in California.

Figure 147: Gross annual biomass production in California and feedstock amount estimated to be available for sustainable use for renewable energy.[6] BDT = bone dry tons.

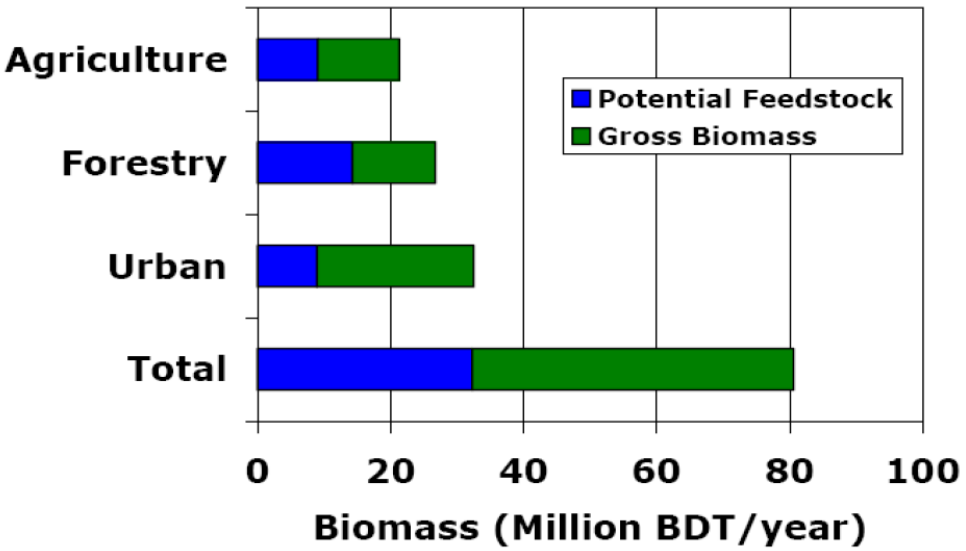

Table 39: Electricity and heat that can be produced from California biomass feedstock.[6] BDT = bone dry tons, CHP = combined heat and power, TWh = terawatt-hour, MWe = megawatt electric.

Category	Biomass (million BDT/year)	Energy in Product (Trillion BTU/year)	Total Capacity
Electricity	32	118	4,650 MWe

The international energy agency (IEA) has estimated the cost of electricity from 10 MW-30 MW power plants running on 100 percent biomass using integrated gasification combined cycle (IGCC).[4] Assuming the biomass cost of $3/GJ and the capital cost of $2,500-$5,500 per kW, the cost of electricity is $0.11-$0.13 per kWh. This cost of electricity from biomass gasification in the IEA report is consistent with the costs projected in the CEC report published in 2006.[4] These cost estimates exceed the economic performance target of $0.06 per kWh set for this project. However, if the economic value of the waste heat from the advanced thermochemical gasification of the biomass is used in a combined heat and power system (CHP) by at least half and as much as two-thirds to get to the performance target.

Power generation from renewable sources such as biomass which is "carbon neutral" will lower the greenhouse gas emissions for power generation in comparison to natural gas power production. Combined heat and power production from biomass can displace natural gas for power and heat production and eliminate the correspond carbon dioxide greenhouse gas. In table 3 the power and heat production from the gasification of 1,000,000 tons/year of biomass is presented showing a displacement of natural gas in the amount of 30,188 mmcf, and 1,896,755 tons CO_2/year. These displacements have the potential of being increased by a factor of at least 30 if the available biomass in California is used to produce combined heat and power.

Table 40: Biomass production of heat and power and the displacement of natural gas and associated carbon dioxide.

Biomass (tons/year)	Power Production (MWe/year)	Heat Production (MWth/year)	Natural Gas displacement ($mmft^3$)	Carbon Dioxide Mitigation (tons/year)
1,000,000	145		10,062	632,252
		290	20,125	1,264,503
Total			30,188	1,896,755

REFERENCES

Bergman, Patrcik C. A., van Paasen, Sander V.B., Boerrigter, Harold, The novel "OLGA"technology for complete tar removal from biomass producer gas, 2003, available at: http://www.ecn.nl/fileadmin/ecn/units/bio/Overig/pdf/Olga4.pdf

Billet, R., Packed Towers in Processing and Environmental Technology, translated by Fullarton, J., VCH Publishers, Germany, 1995.

Bolhar-Nordenkampf, M., K. Bosch, R. Rauch, S. Kaiser, H. Tremmel, C. Aichernig and H. Hofbauer (2002). Scale-up of a 100kWth pilot FICFB-gasifier to a 8 MWth FICFB-gasifier demonstration plant in Güssing, Austria. 1st International Ukrainian Conference on Biomass For Energy September 23-27, 2002, Kiev.

CEN (2006). Biomass gasification - Tar and particles in product gses- Sampling and analysis, European Committee for Standardization. Technical Specification CEN/TS 15439.

Dayton, D, Review of the Literature on Catalytic Biomass Tar Destruction: Milestone Completion Report. 33 pp.; NREL Report No. TP-510-32815, 2002.

Evans, R.J.; Milne, T.A. 1997. "Chemistry of Tar Formation and Maturation in the Thermochemical Conversion of Biomass," in *Developments in Thermochemical Biomass Conversion, Vol. 2*. Edited by A.V. Bridgwater and D.G.B. Boocock. London: Blackie Academic & Professional, pp. 803–816.

Gebhard, S. C., D. Wang, R. P. Overend and M. A. Paisley (1994). "Catalytic conditioning of synthesis gas produced by biomass gasification." Biomass and Bioenergy**7**(1-6): 307-313.

Gil, J., Corella, J., Aznar, M. P. & Caballero, M. A. Biomass gasification in atmospheric and bubbling fluidized bed: Effect of the type of gasifying agent on the product distribution. Biomass and Bioenergy, vol. 17, 1999, 389-403.

GKN, Filter Elements: High porosity sintered materials, GKN Sinter Metals Filters GmbB, Germany, 2002.

Griskey, R., Transport Phenomena and Unit Operations: A Combined Approach, John Wiley & Sons, 2002.

Hasler, P., and Nussbaumer, T., "Gas cleaning for IC engine applications from fixed bed biomass gasification." Biomass and Bioenergy, 16(6), 385-395, 1999.

Knoef, H. A. M. (2005) Handbook of Biomass Gasification. Pyne and GasNet, BTG biomass technology group, Enschede, The Netherlands.

Howard, J.R., Fluidized Bed Technology: Principles and Applications, Taylor & Francis, 1989.

IEA (1998). Meeting on Tar Measurement Protocol, Brussels, Thermal Gasification Task.

ropera, F. P., Dewitt, D. P., Fundamentals of Heat and Mass Transfer, 5th Edition, John Wiley & Sons, 2002.

Jenbacher Annex 20 Special Gas Limits, Wood gas I & II.

Jenbacher (2008). Fuel gas quality - Special gases. Technical Instruction No. 1000-0302.

Jenkins, B. M. (2005). EBS 216 Lecture Notes. University of California, Davis, Biological and Agricultural Engineering.

Jenkins, B.M., Baxter, L.L, Miles Jr., T.R. Miles, T.R., Combustion properties of biomass, Fuel Processing Technology, vol 54, 1998, pg. 17–46.

van Kasteren, J.M.N., Dizdarevic, D., van der Waall, W.R., Guo, J., Verberne, R., "Bio-ethanol from Syngas", Eindhoven University of Technology (TU/e), Telos Ingenia Consultants & Engineers, September 2005.

Kister, H. Z., Distillation Design, McGraw-Hill, 1992.

Koch-Glitsch, Intolox Packed Tower Systems: Metal Random Packings, Bulletin KGMRP-1 2M0303B, 2003, available at: www.koch-glitsch.com

Leith, D. and Licht, W., 1972. Collection efficiency of cyclone type particle collectors, a new theoretical approach. In: *A.I.Ch.E. Symp. Series: Air-1971*.

Meister, B. C., R. B. Williams and B. M. Jenkins (2005). Utilization of Waste Renewable Fuels in Boilers with Minimization of Pollutant Emissions- Laboratory Scale Gasification Screening Experiments, CEC-500-2005-160. University of California, Davis.

Milne, T. A., R. J. Evans and N. Abatzoglou (1998). Biomass gasifier "tars": their nature, formation and conversion, NREL/TP-570-25357. Golden, CO, NREL**:** 204.

Morf, P. O. (2001). Secondary reactions of tar during thermochemical biomass conversion., Eidgenoessische Technische Hochschule Zuerich (Switzerland). Dissertation.

Opdal, O. A., Skreiberg, O., "Production of synthetic biodiesel via Fischer-Tropsch synthesis", Norwegian University of Science and Technology, December 2006.

Brage, C., Q. Yu, et al. (1997). "Use of amino phase adsorbent for biomass tar sampling and separation." Fuel 76(2): 137-142.

CEN/TS, Biomass gasification—Tar and particles in product gases—Sampling and analysis. 2006. European Committee for Standardization (CEN). Available from British Standards Institute. www.bsiglobal.com/bsonline

Cui, H., Turn, S.Q., Keffer, V., Evans, D., Tran, T., and Foley M., (2010) "Contaminant Estimates and Removal in Product Gas from Biomass Steam Gasification", Energy Fuels, vol. 24, pg. 1222–1233.

Hansen, C. M., 2007, Hansen solubility parameters: a user's handbook, 2nd Edition, CRC Press: Boca Raton.

Hansen and Beerbower, Solubility Parameters in Kirk-Othermer Encylopedia of Chemical Technology, Supplemental Volume, 2nd Edition, edited by Standen, A., Interscience, NY 1971, pp 889-910.

Hildebrand, J. H., Prausnitz, J. M., and Scott, R. L., (1970) Regular and Related Solutions: the solubility of gases, liquids, and solids, Van Nostrand Reinhold Co., NY.

Levin, M., Redelius, P., Determination of Three-Dimensional Solubility Parameters and Solubility Spheres for Naphthenic Mineral Oils, *Energy & Fuels,*2008**,** *22* (5), 3395-3401.

Lindvig, T., Michelsen, M.L., Kontogeorgis, G.M., A Flory–Huggins model based on the Hansen solubility parameters, Fluid Phase Equilibria, Volume 203, Issues 1-2, 1 December 2002, Pages 247-260.

Segarceanu, O., Leca, M., "Improved method to calculate Hansen solubility parameters of a polymer", Progress in Organic Coatings, Volume 31, Issue 4, August 1997, Pages 307-310 .

Meister, B. C., R. B. Williams, and B. M. Jenkins (2005). Utilization of Waste Renewable Fuels in Boilers with Minimization of Pollutant Emissions- Laboratory Scale Gasification Screening Experiments, CEC-500-2005-160. University of California, Davis.

Boerrigter, H., M. Bolhar-Nordenkampf, E. P. Deurwaarder, T. Eriksson, J. W. Konemann, R. Rauch, S. van Paasen and J. Palonen (2006). *Olga Optimum- Improving the economics of integrated biomass gasification plants by extension of the functionalities of the OLGA tar washer,* ECN-E--06-048.

Ningbo T.C.I. Co., LTD. Image retrieved 10 May, 2012 from: http://www.rubbersealing.com/TCI/goods-78-HY-PAK+pall+ring.html

Bergman, P.C.A., S. van Paasen, and H. Boerrigter, eds. The novel "OLGA" technology for complete tar removal from biomass producer gas.Pyrolysis and Gasification of Biomass and Waste, ed. A.V. Bridgwater. 2003, CPL press: Newbury, UK. 347-346.

Boerrigter, H., van Paasen, S.V.B., Bergman, P.C.A., Könemann , J.W., Emmen, R., Wijnands, A., "OLGA tar removal technology", ECN-C--05-009, 2005.

Brage,C, Yu, Q., Chen, G., Sjöström, K. Use of amino phase adsorbent for biomass tar sampling and separation, Fuel, Volume 76, Issue 2, January 1997, Pages 137-142.

Devi, L., Ptasinski, K.J., Janssen, F.J.J.G., A review of the primary measures for tar elimination in biomass gasification processes, Biomass and Bioenergy, Volume 24, Issue 2, February 2003, Pages 125-140.

Jenkins, B.M., Baxter, L.L, Miles Jr., T.R. Miles, T.R., Combustion properties of biomass, Fuel Processing Technology, vol 54, 1998, pg. 17–46.

Kiel, J.H.A, "Gas-cleaning: the achilles heel of biomass gasification", 12th European Conference and Technology Exhibition on Biomass for Energy, Industry, and Climate Protection, June 17-21, 2002, Amsterdam, the Netherlands.

Milne, T. A., Evans, R.J., Abatzoglu, N., "Biomass gasifier "tars": their nature, formation and conversion", NREL/TP-570-25357. Golden, CO, 1998.

Scahill, J., Biomass Thermochemical Conversion. Biofuels Workshop - 2009 Integrated Energy Policy Report, Sacramento, CA, California Energy Commission.

Stassen, H. E. M. (1993). Strategies for upgrading producer gas from fixed bed gasifier systems to internal combustion engine quality. Biomass gasification: hot-gas clean-up. R. G. Graham and R. Bain, IEA Biomass Gasification Working Group

Stevens, D. J. 2001. Hot Gas Conditioning: Recent Progress with Larger-Scale Biomass Gasification Systems. NREL/SR-510-29952. Golden, CO: National Renewable Energy Laboratory.

Bridgwater, A. V. (1995). "The technical and economic feasibility of biomass gasification for power generation."Fuel 74(5): 631-653.

Boerrigter, H., van Paasen, S.V.B., Bergman, P.C.A., Könemann , J.W., Emmen, R., Wijnands, A., "OLGA tar removal technology", ECN-C--05-009, 2005.DahlmanFileter Technology, OLGA Tar Removal – Biomass gasification to electricity and more, Technical Information Paper, www.olgatechnology.com, Spring 2008.

Food and Agriculture Organization of the United Nations, (1987), Simple Technologies for Making Charcoal, Forest Industry Division, ISBN 92-5-101328-1.

Gil, J., Corella, J., Aznar, M. P. & Caballero, M. A. Biomass gasification in atmospheric and bubbling fluidized bed: Effect of the type of gasifying agent on the product distribution. Biomass and Bioenergy, vol. 17, 1999, 389-403.

Haufbauer and Knoef, H. A. M. (2005) Handbook of Biomass Gasification. Pyne and GasNet, BTG biomass technology group, Enschede, The Netherlands.

Herguido, J., Corella, J.,GonzBlez-Saiz, J. Steam gasification of lignocellulosic residues in fluidized bed at small pilot-plant scale. Effect of the type of feedstock. Ind. Eng. Chem. Res. 1992, vol. 31,1274-1282

Hermann, H., Reinhard, R., Klaus, B., Reinhard K., Christian, A., "Biomass CHP Plant Güssing – A Success Story", Expert Meeting on Pyrolysis and Gasification of Biomass and Waste; October 2002, Strasbourg, France.

Knoef, H. A. M. (2005) Handbook of Biomass Gasification. Pyne and GasNet, BTG biomass technology group, Enschede, The Netherlands.

Mayerhofer, M., Mitsakis, P., Meng, X., de Jong, W., Spliethoff, H., Gaderer, M. (2012) "Influence of pressure, temperature and steam on tar and gas in allothermal fluidized bed gasification", Fuel, Available online 30 April 2012.

T.A. Milne, R.J. Evans, Biomass Gasification ''Tars'': Their Nature, Formation and Conversion. NREL, Golden, CO, USA, Report no. NREL/TP-570-25357, 1998.

Narv, P.I. ,Orpso, A., Aznar, M.P., Corella, J. (1996). Biomass gasification with air in an atmospheric bubbling fluidized bed. Effect of six operational variables on the quality of produced raw gas, Industrial and Engineering Chemistry Research 35 (7) (1996) 2110 – 2120.

Narváez, A. Orio, J. Corella and M.P. Aznar, Biomass gasification with air in a bubbling fluidized bed.Effect of six operational variables on the quality of the produced raw gas.*Ind. Eng. Chem. Res.***35** 7 (1996), pp. 2110–2120.

Pan, Y.G , Roca, X., Velo, E., Puigjaner, L. (1999). Removal of tar by secondary air in fluidised bed gasification of residual biomass and coal, Fuel, Volume 78, Issue 14, November 1999, Pages 1703-170.

Phuphuakrat, T., T. Namioka, et al. (2011)."Absorptive removal of biomass tar using water and oily materials."Bioresource Technology 102(2): 543-549.

Rabou, L.P.L.M., Biomass tar recycling and destruction in a CFB gasifier, Fuel, Volume 84, Issue 5, March 2005, Pages 577-581.

I. Goekalp and E. Lebas. Alternative fuels for industrial gas turbines (aftur). Applied

Thermal Engineering, 2004:1655–1663, 24.

Acharya C, Lane A, Krause T (2006) Kinetic Study of the steam reforming of isobutene using a Pt-CeO_2-Gd_2O_3 Catalyst. Catalyst Letters Vol. 106, Nos 1-2.

Boyce, (2008) Design of a Methanol Reformer with the Purpose of Testing Syngas on a CFR Engine Master of Science Thesis, Department of Mechanical Engineering, University of California Berkeley CA.

Perez-Hernandez R, Guitierrez-Martinez A, Gutierrez-Wing CE (2007) Effect of Cu Loading on CeO_2 for Hydrogen production by oxidative steam reforming of methanol. Instituto Nacional de Investigaciones Nucleares, Carr. Mexico-Toluca S/N La Marquesa, Ocoyoacac, Edo. De Mexico C.P. 52750, Mexico.

Shiozaki R, Hayakawa T, Liu Y, Ishii T, Kumagai M, Hamakawa S, Suzuki K, Itoh T, Shishido T, Takehira K (1999) Methanol decomposition to synthesis gas over supported Pd catalysts prepared from synthetic anionic clays. Catalyst Letters 58, pp 131-140.

[1] Thermochemical Ethanol vial Indirect Gasification and Mixed Alcohol Synthesis of Lignocellulosic Biomass. S. Phillips et al.; National Renewable Energy Laboratory, Technical Report NREL/TP-510-41168, April 2007.

[2] I. Goekalp and E. Lebas. Alternative fuels for industrial gas turbines (aftur). Applied Thermal Engineering, 2004:1655–1663, 24.

[1] I. Goekalp and E. Lebas. Alternative fuels for industrial gas turbines (aftur). Applied Thermal Engineering, 2004:1655–1663, 24.

[2] Y. Lafay, B. Renou, G. Cabot, and M. Boukhalfa. Experimental and numerical investigation of the effect of h2 enrichment on laminar methane-air flame thickness. Combustion and Flame, 153:540–561, 2008.

[3] K. Seshadri and F. A. Williams. Laminar flow between parallel plates with injection of a reactant at high Reynolds number. International Journal of Heat and Mass Transfer, 21(2):251–253, 1978.

[4] H. Pitsch. Entwicklung eines Programmpaketes zur Berechnung eindimensionaler Flammenam Beispiel einer Gegenstromdiffusionsflamme. Master's thesis, RWTH Aachen, Germany, 1993.

[5] N. Peters. Flame calculations with reduced mechanisms - an outline. In N. Peters and B. Rogg, editors, Reduced Kinetic Mechanisms for Applications in Combustion Systems, volume m15 of Lecture Notes in Physics, chapter 1, pages 1–13. Springer-Verlag, Heidelberg, 1993.

[6] The San Diego Mechanism. http://maeweb.ucsd.edu/combustion.

[7] M. Frenklach and D.E Bornside. Shock-initiated ignition in methane-propane mixtures. Combustion and Flame, 56:1–27, 1984.

[8] L. J. Spadiccini and M. B. Colket. Ignition delay characteristics of methane fuels. Progress in Energy and Combustion Science, 20:431–460, 1994.

[9] C. M. Vagelopoulos and E. N. Egolfopoulos. Direct experimental determination of laminar flame speeds. Proceedings of the Combustion Institute, 27:513–519, 1998.

[10] S. C. Li and F. A. Williams. NOx formation in two-stage methane-air flames. Combustion and Flame, 118:399–411, 1999.

[11] R. Seiser and K. Seshadri. The influence of water on extinction and ignition of hydrogen and methane flames. Proceedings of the Combustion Institute, 30:407–414, 2005.

[12] R. W. Schefer. Hydrogen enrichment for improved lean flame stability. International Journal of Hydrogen Energy, 28:1131–1141, 2003.

[13] G. Yu, C. K. Law, and C. K. Wu. Laminar flame speeds of hydrocarbon + air mixtures with hydrogen addition. Combustion and Flame, 63:339–347, 1986.

[14] C. M. Vagelopoulos and F. N. Egolfopoulos. Laminar flame speeds and extinction strain rates of mixtures of carbon monoxide with hydrogen, methane, and air. Proceedings of the Combustion Institute, 25:1317–1323, 1994.

[15] M. Fairweather, M. P. Ormsby, C. G. W. Sheppard, and R. Wooley. Turbulent burning rates of methane and methane-hydrogen mixtures. Combustion and Flame, 156:780–790, 2009.

[16] F.H.V. Coppens, J. De Ruyck, and A. A. Konnov. The effect of composition on burning velocity and nitric oxide formation in laminar premixed flames of $CH_4 + H_2 + O_2 + N_2$. Combustion and Flame, 149:409–417, 2007.

[17] W. R. Anderson, N. Ilincic, N. E. Meagher, K. Seshadri, and J. A. Vanderhoff. Detailed and reduced chemical mechanisms for the dark zones of double base and nitramine propellants in the intermediate temperature regime. In 32nd JANNAF Combustion Subcommittee Meeting, volume 1 of CPIA Publication Number 638, page 197, Huntsville, Alabama, October 1995.

[18] P. Saxena and F. A. Williams. Testing a small detailed chemical-kinetic mechanism for the combustion of hydrogen and carbon monoxide. Combustion and Flame, 145:316–323, 2006.

[19] T. Shimizu, F. A. Williams, and A. Frassoldati. Concentrations of nitric oxide in laminar counterflow methane/air diffusion flames. Journal of Propulsion and Power, 21:1019–1028, 2005.

[20] M. M. Y. Waly, S. C. Li, and F. A. Williams. Experimental and numerical studies of two-stage ethane-air flames. Journal of Engineering for gas Turbines and Power, 122(4):651–658, 2000.

[21] B. Varatharajan and F. A. Williams. Ethylene ignition and detonation chemistry, part 1: Detailed modeling and experimental comparison. Journal of Propulsion and Power, 18:344–351, 2002.

[22] M. M. Y.Waly, S. C. Li, and F. A.Williams. Structures of non-sooting counterflow diluted acetylene-air flames. Proceedings of the Combustion Institute, 28:2005–2012, 2000.

[23] B. Varatharajan and F. A. Williams. Chemical-kinetic descriptions of high-temperature ignition and detonation of acetylene-oxygen-diluent systems. Combustion and Flame, 124:624–645, 2001.

[24] M. V. Petrova and F. A. Williams. A small detailed chemical-kinetic mechanism for hydrocarbon combustion. Combustion and Flame, 144:526–544, 2006.

[25] S. C. Li and F. A. Williams. Experimental and numerical studies of two-stage methanol flames. Proceedings of the Combustion Institute, 26:1017–1024, 1996.

[26] S. C. Li and F. A. Williams. Formation of NOx, CH_4, and C_2 species in laminar methanol flames. Proceedings of the Combustion Institute, 27:485–493, 1998.

[27] P. Saxena and F. A. Williams. Numerical and experimental studies of ethanol flames. Proceedings of the Combustion Institute, 31:1149–1156, 2007.

[28] P. Saxena. Numerical and experimental studies of ethanol flames and autoignition theory for higher alkanes. Ph.D thesis, University of California at San Diego, Department of Mechanical and Aerospace Engineering, La Jolla, CA 92093, 2007.

[29] R. J. Kee, F. M. Rupley, J. A. Miller, M. E. Coltrin, J. F. Grcar, E. Meeks, H. K. Moffat, A. E. Lutz, G. Dixon-Lewis, M. D. Smooke, J. Warnatz, G. H. Evans, R. S. Larson, R. E. Mitchell, L. R. Petzold, W. C. Reynolds, M. Caracotsios, W. E. Stewart, P. Glarborg, C. Wang, O. Adigun, W. G. Houf, C. P. Chou, and S. F. Miller. Chemkin collection, release 3.7.1. Technical report, Reaction Design Inc., San Diego, CA, 2003.

1. R. Cattolica, R. Herz, J. Giolitto, and M. Summers "Economic Analysis of a 3 MW Biomass Gasification Power Plant," ES2009-90374, 3rd International Conference on Energy Sustainability , ASME, San Francisco, CA, July 19-23, 2009

2. R. Cattolica, B. Jenkins, R. Dibble, and D. Taylor, "Dual Fluidized-Bed Gasification of Biomass for the Production of Power and Liquid Fuels, TCbiomass2009 – International Conference on Thermochemical Conversion Science, Chicago, Illnois, Sept. 16-18, 2009.

3. A. Didwania, R. Cattolica, and K. Mandich, "CFD Simulation Scale-up of a Dual-Fluidized Bed Gasifier for Biomass," 7th International Conference on CFDi n the Minerals and Processing Industries," CSIRO, Melbourne, Australia, December 9-11, 2009.

4. U. Niemann, C, Di Norscia, and K. Seshadri "Combustion of Mixtures of Producer Gas and Methane in Nonpremixed Flows", 2009 Fall Technical Meeting of the Western States Section of the Combustion Institute, Paper # 09F-13, University of California at Irvine, Irvine, CA, October 26-27, 2009

5. P. Saxena and K. Seshadri, "The Influence of Hydrogen and Carbon Monoxide of Structure and Burning Velocity of Methane Flames', 2009Fall Technical Meeting of the Western States Section of the CombustionInstitute, Paper # 09F-86, University of California at Irvine, Irvine, CA, October 26-27, 2009

6. C. Acharya and R. Cattolica, "Catalytic and non-catalytic steam and autothermal tar reforming of simulated biomass gasification producer gas," 239th American Chemical Society, San Francisco, CA , March 21-25, 2010.

7. R. Cattolica, "Dual-fluidized Bed Gasification for Biomass from the Production of Power and Liquid Fuels," Bioenergy , Australia 2010, December 8-10, Sydney, Australia December 16-18,2010.

8. R. Seiser, R. Cattolica,. A. Van Blarigan, R. Dibble, M. Summers, C. Liao, "Emission Reduction of SI-Engine Fueled by Biomass Gasifier," TCbiomass2011 – International Conference on Thermochemical Conversion Science, Chicago, Illnois, Sept. 27-30, 2011

10. C. Liao, M. Summers, C. Acharya, D. Backhouse, R. Seiser, R. Cattolica, R. Herz, and A. Didwania, " Simulation Analysis and Validation of a Pilot-Scale Dual Fluidized Bed Biomass Gasification," TCbiomass2011 – International Conference on Thermochemical Conversion Science, Chicago, Illnois, Sept. 27-30, 2011

11. R. Cattolica, B. Jenkins, R. Dibble, and M. Summers, "Collaborative Research on Biomass Gasification and Conversion Technology at the Woodland Biomass Research Center, TCbiomass2011 – International Conference on Thermochemical Conversion Science, Chicago, Illnois, Sept. 27-30, 2011

12. R, Seiser, U. Niemann, K. Seshadri, and R, Cattolica, "Experimental and Computational Studies of Combustion of Mixtures of Producer Gas and Methane in Nonpremixed Flows", 7th U.S. National Technical Meeting of the Combustion Institute. Georgia Institute of Technology, Atlanta, GA March 20-23, 2011

13. R. Seiser, K, Seshadri, U. Niemann, and R. Cattolica, "Non-Premixed and Premixed Combustion of Mixtures of Producer Gas and Methane", 2012 Spring Technical Meeting of the Western States Section of the Combustion Institute, Paper # 12S-52, Arizona State University, Tempe, Arizona, 2012

Cattolica, et. al. 2009. Economic Analysis of a 3 MW Biomass Gasification Power Plant. Paper no. ES2009-90374 pp. 385-392. ASME 2009 3rd International Conference on Energy Sustainability collocated with the Heat Transfer and InterPACK09 Conferences (ES2009), July 19–23, 2009 , San Francisco, California, USA.

West Biofuels. 2012. "Demonstration of Advanced Biomass Combined Heat and Power Systems in the Agricultural Processing Sector." Proposal for PON-11-051 - Emerging Technologies Demonstration Grant Program. California Energy Commission.

Gussing Renewable Energy America. 2012. Beecher Bay Zero Waste Project Business Plan. GREA Internal Document.

R. Cattolica, R. Herz, J. Giolitto, and M. Summers "Economic Analysis of a 3 MW Biomass Gasification Power Plant," ES2009-90374, 3rd International Conference on Energy Sustainability , ASME, San Francisco, CA, July 19-23, 2009

1. California Electrical Energy Generation, 1995 to 2004. Total Production By Resource Type. California Energy Commission www.dof.ca.gov/HTML/FS_DATA/stat-abs/tables/j11.pdf.

2. California Electrical Energy Generation, 1997 to 2007. Total Production By Resource Type. California Energy Commission www.dof.ca.gov/HTML/FS_DATA/stat-abs/documents/J11.pdf

4. A Preliminary Roadmap for the Development of Biomass in California. *California Energy Commission Report CEC-500-2006-095-D*, December 2006.

5. Biomass for Power Generation and CHP. *IEA Energy Technology Essentials ETE03 OECD/IEA 2007*, January 2007.